High Resolution Structural Studies of Membrane Proteins Using Solid State NMR

Lubica Aslimovska

Thesis submitted to the

Board of the Faculty of Biological Sciences

in partial fulfilment of the requirements for the

Degree of Doctor of Philosophy

at the University of Oxford

Christ Church

2007

Abbreviations and Symbols 6
Acknowledgements 8
Abstract 10
Chapter 1 Introduction 12
1.1 Studying Biological Macromolecular Structures 12
1.2 The Importance of Membrane Proteins 13
1.3 The Challenge of Studying Membrane Proteins 13
1.4 Secondary Structure 15
1.5 Introduction to G-Protein-Coupled Receptors 16
1.5.1 Metabotropic glutamate receptors 18
1.5.2 The brain and putative taste mGluR4 receptors 18
1.5.3 Glutamate-binding sites in mGluR1 20
1.6 Nuclear Magnetic Resonance 23
1.7 Introduction to Principles of NMR 28
1.7.1 Spin and magnetic moment 28
1.7.2 NMR interactions 30
1.8 Basic Solid-State NMR Techniques 32
1.8.1 Magic angle spinning 32
1.8.2 Cross polarisation 36
1.8.3 Proton decoupling 38
1.8.4 Recoupling methods 39
1.8.5 Solid-state NMR of quadrupolar nuclei 40
1.8.6 Static NMR experiments of oriented samples 41
1.9 Aims and Objectives 43
Chapter 2 Metabotropic Glutamate Receptor 4: Ligand Studies by Solid State NMR, Homology Modelling, Cloning and Expression 46
2.1 Introduction 46
2.1.1 Ligand studies by solid state NMR 46
2.1.2 Homology modelling of the ligand binding domain of mGluR4 47
2.1.3 Molecular biology of mGluR4 48
2.2 Materials and Methods 50
2.2.1 Solid state NMR of the ligand 50
2.2.1.a ^{13}C and ^{15}N CP MAS solid-state NMR of L-glutamic acid 50
2.2.1.b ^{17}O Solid-state NMR of L-glutamic acid 51
2.2.2 Homology modelling of the ligand binding domain of the taste mGluR4 52
2.2.2.a Model generation 53
2.2.2.b Model validation 53
2.2.3 Molecular Biology of mGluR4 54
2.2.3.a Cloning and expression of the taste mGluR4 LBD 54
2.2.3.b Expression of the taste mGluR4 LBD in *E. coli* 56
2.2.3.c Small scale taste mGluR4 LBD purification 57
2.2.3.d Protein detection 57
2.2.3.e Molecular biology of the full length mGluR4 60
2.2.3.f Expression of the full length mGluR4 62
2.2.3.g Molecular biology of the of brain mGluR4 LBD 62

2.2.3.h Expression of the brain mGluR4 LBD 71
2.2.3.i Periplasmic isolation 72
2.2.3.j Western blot analysis 72
2.3 Results and Discussion 73
2.3.1 Ligand studies by solid state NMR 73
2.3.1.a ^{13}C CP MAS solid-state NMR of L-glutamic acid 73
2.3.1.b ^{15}N CP MAS solid-state NMR of L-glutamic acid 74
2.3.2 Homology modelling 75
2.3.2.a Model generation and validation 75
2.3.2.b Visual assessment of models 78
2.3.3 Molecular biology of mGluR4 80
2.3.3.a Molecular biology of the full length mGluR4 83
2.3.3.b Molecular biology of the ligand binding domain of brain mGluR4 84
2.3.3.c Periplasmic expression of mGluR4 85
2.3.3.d Molecular biology of the ligand binding domain of the putative taste receptor 87
2.4 Conclusions 89
Chapter 3 Refolding of mGluR4 92
3.1 Introduction 92
3.1.1 Expression of protein into inclusion bodies 92
3.1.2 Characteristics of protein aggregates in inclusion bodies 93
3.1.3 Preparing purified and denatured protein 93
3.1.4 Characteristics of protein aggregates in IBs 94
3.2 Materials and Methods 96
3.2.1 Extraction of IBs 96
3.2.2 Denaturation of the IBs 98
3.2.3 Screening for optimal folding conditions 99
3.2.4 Measuring refolding 99
3.2.4.a Scale-up of the refolding reaction 100
3.2.4.b Ni- affinity purification of refolded mGluR4 100
3.2 Results and Discussion 102
3.2.1 Extraction and denaturation of IBs 102
3.2.2 Screening for optimal folding conditions 103
3.2.3 Measuring refolding 103
3.3 Conclusions 112
Chapter 4 Solid State NMR Studies of Selectively Labelled Bacteriorhodopsin 113
4.1 Introduction 113
4.1.1 The Importance of Sample Preparation for Solid State NMR 114
4.1.2 Different Sample Forms Used for Solid State NMR 114
4.1.3 Alternative means of sample preparation- Lipodisqs™ 118
4.1.4 Introduction to the Structure and Function of the Purple Membrane and Bacteriorhodopsin 119
4.2 Materials and Methods 122
4.2.1 Bacteriorhodopsin production 122
4.2.2 Preparation of 3D crystals 123

4.2.2.a Monomerisation of bR and crystallisation trials of monomeric, delipidated bR 123
4.2.2.b Crystallisation trial of bR in DMPC/CHAPSO bicelles 124
4.2.3 Alternative means of sample preparation- Lipodisqs™ 126
4.2.4 Solid state NMR 126
4.2.4.a Experiments acquired on a 800 MHz proton frequency Varian/Magnex Spectrometer 126
4.2.4.b Experiments acquired on a 500 MHz proton frequency Varian/Magnex Spectrometer 127
4.2.5 Transmission Electron Microscopy 128
4.2.6 Static ^{31}P solid state NMR experiments acquired on a 400 MHz proton frequency Bruker Spectrometer 128
4.3 Results and Discussion 129
4.3.1 Crystallisation trials of bR 129
4.3.2 Solid state NMR experiments of ^{15}N Met labelled bR 131
4.3.3 Studies of alternative means of sample preparation for solid state NMR 133
4.4 Conclusions 135
Chapter 5 Solid State NMR of U- ^{15}N, ^{13}C, ^{2}H Labelled Bacteriorhodopsin 138
5.1 Introduction 138
5.2 Use of Deuteration in NMR 140
5.2.1 Use of deuteration in solution state NMR 140
5.2.2 Use of deuteration in solid state NMR 140
5.2.3 Effects of deuteration on CP-efficiency 141
5.3 Introduction to NMR Spectroscopy Assignment of Proteins 142
5.3.1 Residue type assignment 145
5.3.1.a Two dimensional dipolar assisted rotational resonance 145
5.3.1.b 2D Radio frequency-driven dipolar recoupling (RFDR) 146
5.3.2 Site-specific assignment 147
5.4 Materials and Methods 149
5.4.1 Preparation of deuterated U- ^{13}C, ^{15}N labelled bacteriorhodopsin 149
5.4.1.a Strain of *H. salinarium* used and growth conditions 149
5.4.1.b Choosing the optimal labelling medium and cell growth conditions 150
5.4.2 Media preparation 152
5.4.2.a Celtone media preparation 152
5.4.2.b Silantes media preparation. 153
5.4.2.c Peptone media preparation. 153
5.4.3 Growth, purple membrane isolation and purification 154
5.4.4 Crystallisation of fMLF model peptide 154
5.4.5 Solid state NMR spectroscopy - acquisition parameters 156
5.4.5.a 1D ^{13}C CP MAS spectra 156
5.4.5.b 2D ^{13}C-^{13}C DARR homonuclear experiments of highly deuterated U-^{13}C, ^{15}N bR recorded on a 500 MHz spectrometer 157
5.4.5.c 2D ^{13}C-^{13}C DARR experiments of the fully protonated U-^{13}C, ^{15}N bR sample on the 800 MHz spectrometer 157

5.4.5.d 2D ^{13}C-^{13}C DARR with 3 ms and 13 ms mixing time of highly deuterated U-^{13}C, ^{15}N labelled bR recorded on at 800 MHz 158
5.4.5.e 2D ^{13}C-^{13}C DARR with 13 ms mixing time of 50% deuterated U-^{13}C, ^{15}N labelled bR sample recorded at 800 MHz 159
5.4.5.f 2D ^{13}C-^{13}C RFDR homonuclear experiment of the model compound fMLF 159
5.4.5.g 2D RFDR of 100% deuterated U-^{13}C, ^{15}N labelled bR sample 160
5.4.5.h 2D RFDR with 2ms of the 50% deuterated U-^{13}C, ^{15}N labelled bR sample. 160
5.4.5.i 2D ^{13}C-^{15}N NCA heteronuclear correlation experiment 161
5.4.5.j 2D ^{15}N-^{13}C NCO heteronuclear correlation experiments 162
5.4.6 Data processing 163
5.5 Results and Discussion 163
5.5.1 Preparation of deuterated U- ^{13}C, ^{15}N labelled bacteriorhodopsin 163
5.5.2 Solid State NMR Experiments 168
5.5.2.1 Effects of deuteration on solid state NMR spectra 168
5.5.2.2 Assignment studies of bacteriorhodopsin 178
5.5.3 Conclusions 191
Chapter 6 Conclusions 194
Appendix 198
References 199

Abbreviations and Symbols

1D, 2D, 3D	One-dimensional, two-dimensional, etc
Å	Angstrom (1 Å =0.1 nm)
AA	amino acid
B_0	static external magnetic field
bR	bacteriorhodopsin
CP	cross-polarisation
CP MAS	cross-polarisation magic angle spinning
CSA	chemical shift anisotropy
CV	column volume
CW	continuous wave
DARR	dipolar-assisted rotational resonance
DMPC	1,2-dimyrisotyl-*sn*-glycero-3-phosphocholine
DNA	deoxyribonucleic acid
EDTA	ethylenediaminetetracetic acid
EV	elution volume
FID	free induction decay
FT	Fourier transform
γ	gyromagnetic ratio
GPCR	G-protein coupled receptor
iGluR	Ionotropic glutamate receptor
IPTG	Isopropyl- β -D-thiogalactoside
mGluR	Metabotropic glutamate receptor
HEPES	4-(2-hydroxyethyl-1-piperazine ethane sulphonic acid)
Hz	Hertz
IBs	inclusion bodies
kDa	dalton x 10^{-3} (atomic mass unit)
LBD	ligand binding domain
LBR	ligand binding region
MAS	magic-angle spinning
MBP	maltose binding protein
mM	molar x 10^{-3}
MSG	monosodium glutamate
ms	milliseconds
M_w	molecular weight
nm	nanometer
ω_o	precession frequency
ω_r	rotor spinning frequency
NMR	nuclear magnetic resonance
OD	optical density
PAGE	polyacrylamide gel electrophoresis
PDB	protein data bank
PM	purple membrane
PMSF	phenylmethylsulphonyl fluoride

ppm	parts per million
ps	second x 10^{-12}
rpm	rotations per minute
rf	radio frequency
REDOR	rotational-echo-double-resonance
RT	room temperature
SDS	sodium dodecyl sulphate
SS NMR	solid state nuclear magnetic resonance
SW	spectral window
τ_r	rotational correlation time
T	absolute temperature
T_1	longitudinal relaxation time
T_2	transversal relaxation time
TM	transmembrane
7TMD	seven transmembrane domain
TPPM	two-pulse phase modulation
XiX	X inverse x

Abstract

NMR crystallography is a new and developing area. Unlike solution state NMR, solid state NMR has the potential for structural studies of large, motionally restricted biological macromolecules, such as proteins in crystals which may, or may not, diffract. However, finding the best and the most useful sample form and geometry is still a major obstacle to rapid progress. Little has been reported about protein sample preparation for any class of protein for NMR crystallography, mainly since the availability of NMR labelled proteins is still not routine, especially for eukaryotic membrane proteins.

The amino acid L-glutamate is the major excitatory neurotransmitter in the brain. Details of glutamate binding to any of its main brain or sensory receptors are not well resolved at the atomic level. In an effort to resolve the glutamate binding mechanism by solid state NMR methods, full-length taste and brain mGluR4 were expressed in *E. coli*, but proved to be toxic for the cells. The ligand-binding domains (LBD) of mGluR4, with various fusions for the periplasmic expression and with various fusions for expression in the cytoplasm therefore, were used.

Solubilisation and then purification of the LBD from inclusion bodies is still under way, no crystals of mGluR4 for NMR were, therefore, grown. Initial NMR spectra of labelled ^{13}C, ^{15}N and ^{17}O glutamate have been recorded to verify sensitivity requirements. Using homology modelling, a model for the truncated version of the ligand binding domain of mGluR4 has been constructed as a basis for designing solid state NMR experiments to probe the ligand binding site in the receptor.

Bacteriorhodopsin is a large membrane protein and a model for G-protein coupled receptors (GPCRs). Spectra of bacteriorhodopsin produced in *H. salinarium* in purple membrane are reported here and compared to spectra of the protein crystallised from bicelles. Optimal conditions for producing spectra suitable for spectral assignment are reported as an initial step towards spectral resolution. Three differently labelled samples of bacteriorhodopsin were prepared to test the applicability of the various assignment strategies and the effects of deuteration on quality of solid state NMR spectra of a large, crystalline membrane protein.

Publications:

Varga, K., Aslimovska, L., Parrot, I., Dauvergne, M-T., Haertline, M., Forsyth, T. and Watts, A. (2007) NMR Crystallography: The effect of deuteration on high resolution ^{13}C solid state NMR spectra of a 7-TM protein **Biochimica et Biophysica Acta** (in revision)

Aslimovska, L., Varga, K., Watts, A. (2007) Preliminary steps towards assignment of U-^{13}C, ^{15}N labelled bacteriorhodopsin by solid state NMR (in preparation)

Posters presented:

Alimovska, L., Varga, K., Parrot, I., Dauvergne, M-T., Haertlein, M., Forsyth T. and Watts, A. (2007) High resolution ^{13}C solid state NMR spectroscopy of a 7-TM protein: the effect of deuteration on U-13C, 15N labelled bacteriorhodopsin EBSA Congress, London

Aslimovska L., Menhert, T., Varga, K. and Watts, A. (2005) Solid state NMR study of bacteriorhodopsin crystals NMR Summer School Les Houche, France

Chapter 1 Introduction

1.1 Studying Biological Macromolecular Structures

Protein structure determination is one of the primary goals in biophysics research because knowledge of the 3D molecular structure of proteins leads to a mechanistic understanding of biological function. The number of structures deposited in the Protein Data Bank (PDB), a web based single worldwide database of 3D biological macromolecular structures [28], grows exponentially every year since the first two structures were deposited in 1972. The majority, now 32 000 in number, of the structures have been solved by X-ray crystallography (85%) and solution NMR (15%). However, 99.8 % come from soluble proteins and only 0.2 % are of membrane proteins.

Membranes play a vital role in both the structure and function of living cells. They serve not only to compartmentalize the cell, but also regulate the passage of information and material in and out of these compartments. Integral membrane proteins are tightly associated with the lipid bilayer, which forms the structural component of biomolecules and are only released in the presence of membrane disrupting agents such as detergents.

Most of the structural information regarding integral membrane proteins has been inferred through functional analysis, a variety of biophysical techniques, chemical labelling and site

directed mutagenesis. The most common biophysical techniques to probe membrane protein structures include X-ray crystallography, solution NMR, solid state NMR, electron paramagnetic resonance (EPR), electron microscopy and atomic force microscopy (AFM) [17].

1.2 The Importance of Membrane Proteins

Integral membrane proteins play a crucial role in many cellular processes, acting as channels, pumps, receptors and enzymes. Membrane proteins are estimated to constitute a third of the human genome [29], but proteomically they represent only about 1-2% of cellular protein. So far, we only have 20-30 unique crystal structures of integral membrane proteins. Some of them, for example the G-protein coupled receptors (GPCRs), are a specific family of membrane proteins which are thought to consist about 1% of the genome and represent primary receptor targets for drug discovery [30]. A better understanding of their structure and workings would help drug design and development, their use in bionanotechnology and in better understanding of cell function.

1.3 The Challenge of Studying Membrane Proteins

Membrane proteins in general, present particular difficulties in the determination of high-resolution structural studies by conventional biophysical techniques such as solution NMR and X-ray crystallography, since they are difficult to express and purify and are not readily soluble in aqueous solution. In addition, they are especially difficult to crystallize, thus only a few (80) crystal structures are available [31]. Solution NMR has limitations in the study of insoluble macromolecules and large (radius r) complexes, due to their slow tumbling rate $1/\tau_r \propto r^3$.

Although there are some notable accomplishments in assignments (e.g. KcsA [32]) and structure determination of small membrane proteins such as β-barrel proteins [33-39] synthase subunit c [40] and crambin [41], these are limited to (M_r<14kDa) small membrane proteins. Solid state NMR spectra are more complex than solution NMR spectra because the full effect of anisotropic or orientation-dependent interactions are observed in the spectra, effects which are averaged out in solution for small molecules due to rapid random tumbling.

Large membrane proteins are often difficult to keep solubilised and at a sufficiently high concentration (>mM) to obtain spectra with a high signal-to-noise ratio and resolution. In these cases the lipid bilayer is absent, or at best replaced by micelle detergent.

Solid state NMR is emerging as a promising alternative technique which allows for the study of membrane proteins in various membrane mimic environments, including detergent microcrystals, precipitates, bicelle-protein suspensions, nanodiscs, or embedded in the native membrane [42, 43].

Integral membrane proteins are stable in the membrane, and there has been increasing evidence that lipid species play an important structural, stability and functional role [44]. Some of these lipids may have relevance to the function of the protein [45-47], whereas others promote the formation of highly ordered crystals [48-51]. The purification of integral membrane proteins requires that they must be extracted from the membrane and rendered water-soluble. After detergent solubilisation membrane proteins often become unstable and quickly lose activity. Once the membrane proteins are purified, solid state NMR is a good biophysical method to

study them. General introduction to the principles underlying nuclear magnetic resonance spectroscopy in general is given in Section 1.6, the underlying principles of this biophysical method are described in Section 1.7 and the basic solid state NMR experiments that will be used are introduced in Section 1.8

1.4 Secondary Structure

Secondary structure defines the way in which a protein primary sequence is folded. Most frequently, integral membrane proteins are structured into α-helices and β-sheets linked by loops. In X-ray crystallographic studies, these secondary structure elements are often well resolved since they are relatively rigid, whereas loops are relatively mobile.

In solid state NMR studies, there is a strong correlation between protein secondary structure and NMR chemical shifts [52-54]. All resonances from α helices or β sheets have severe spectral overlap, due to their close chemical similarities. Mixed secondary structure elements facilitate assignments in structural studies since chemical shift will resolve the secondary structural features from each other. Thus, proteins of mixed secondary elements are more accessible for NMR studies. Protein stability (folding/unfolding) can be monitored by observing chemical shift perturbations of specific resonances - a shift usually indicates a change in the secondary structure [52, 54, 55]. Broadening of line widths is also a general indication of denaturation or conformational changes.

1.5 Introduction to G-Protein-Coupled Receptors

G-protein coupled receptors (GPCRs) are integral membrane proteins which function as receptors in diverse stimulus-response pathways. They share a common structural motif of seven putative transmembrane α-helices from computer-aided predictions, connected by three intracellular and three extracellular loops. Two cysteine residues found in two extracellular loops are conserved in most GPCRs, form a disulfide. Most GPCRs respond to the binding of a ligand and undergo multiple conformational changes upon agonist binding [56]. The binding of an extracellular signal (ligand) to the receptor triggers a cascade of intracellular responses. There are a wide variety of specific ligands, which range from photons, Ca^{2+} ions, and small organic molecules to complex polypeptide hormones and different effectors (adenyl cyclase and cGMP phosphodiesterase). GPCRs have very diverse physiological functions, affecting almost all aspects of cellular function. Nearly half of them serve as sensory receptors, e.g. olfactory receptors which bind odorants and pheromones, or retinal and opsins which convert incoming photons of light into a chemical message. GPCRs play an important role in intracellular communication between cells of the immune system, are involved in behavioural and mood regulation, and regulate both the sympathetic and parasympathetic nervous systems. In spite of their importance, little high resolution structural information is available for GPCRs and only rhodopsin has a crystal structure solved [57].

GPCRs are classified into several subfamilies made up of several families, depending on the type of ligand they bind and sequence variation. Aside from sequence variation, GPCRs differ in the length and function of their N-terminal extracellular domain, their C-terminal

intracellular domain and their loops. Figure 1.1 shows the three main GPCR families. Family 1 consists of receptors for odorants; small ligands including rhodopsin and β-adrenergic receptors where the binding sites are localised within the seven transmembrane region; receptors for peptides and glycoprotein hormone receptors characterised by a large extracellular domain. Family 2 GPCRs bind high molecular weight hormones and Family 3 contains the mGluRs and the Ca^{2+} sensing receptors [58].

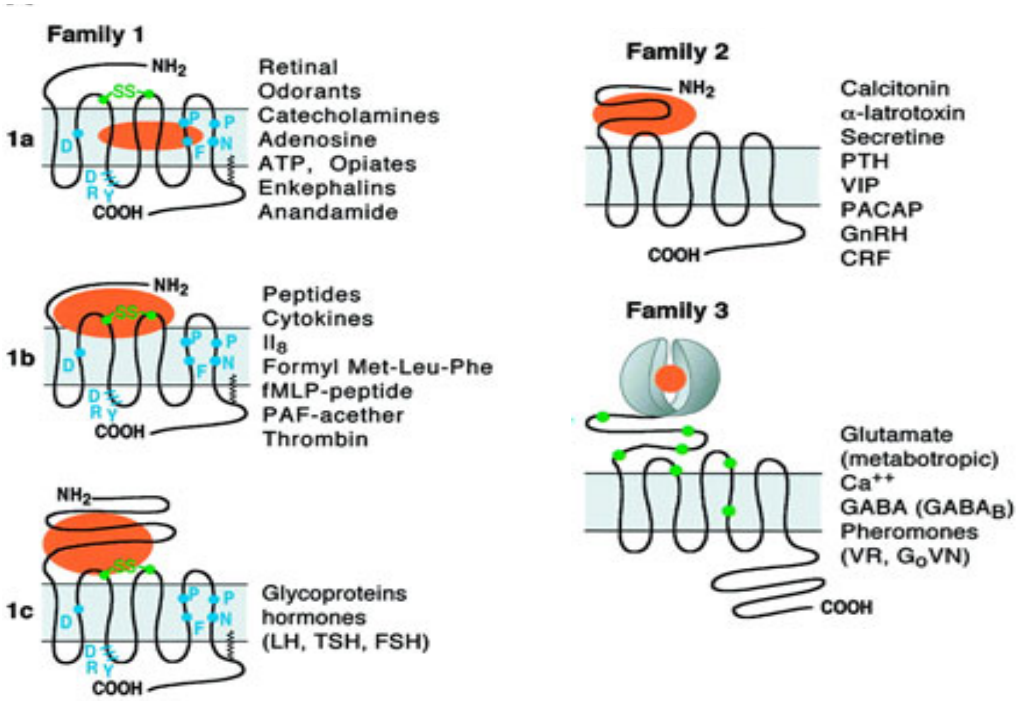

Figure 1.1 Classification of GPCRs. The three main families of GPCRs with their topography and conserved amino acids highlighted, adapted from [5].

The GPCR in this study, metabotropic glutamate receptor 4 (mGluR4), is a member of family 3 and is discussed in detail below, after a general introduction of metabotropic receptors.

1.5.1 Metabotropic glutamate receptors

Metabotropic glutamate receptors (mGluRs) are G-protein coupled receptors which are activated by glutamate, a major excitatory neurotransmitter, through a metabotropic process, unlike the ligand-gated cation channels termed ionotropic glutamate receptors (iGluRs) which are activated upon glutamate binding [59]. mGluRs are 7 transmembrane (TM) G-protein coupled receptors (GPCRs), with a large extracellular region of more than 500 amino acids [9] in which the ligand binding domain is located (Figure 1.2). To date, 8 subtypes of mGluRs have been characterised and each mGluR subtype is coupled to a G protein. There is a stretch of around 70 amino acids with 9 cysteines at the C terminus of the mGluR extracellular region, which is conserved among all mGluR subtypes [60]. mGluR4 together with mGluR6, mGluR7 and mGluR8, constitute the group III subclass of mGluRs.

1.5.2 The brain and putative taste mGluR4 receptors

The brain metabotropic glutamate receptor 4 subtype (mGluR4) is a presynaptic receptor that modulates neurotransmitter release. The umami receptor is a GPCR, and the term umami is used for the taste that the glutamate moiety in monosodium L-glutamate (L-MSG) elicits. This compound is found naturally in protein-rich and other foods. In taste receptors, molecular, physiological and behavioural evidence suggests that a receptor similar or identical to mGluR4 is involved in taste transduction of L-glutamate. mGluR4 is expressed in rat taste buds, and stimulating rat taste buds with glutamate triggers a signalling cascade where cellular cAMP is decreased and this alters membrane conductances. The findings suggest that the transduction of L-glutamate is mediated by an mGluR4-like receptor, however, some questions remain. For

example, 1-3 mM glutamate is required to elicit taste, whereas mGluR4 binds glutamate in the micromolar range [61], and the umami taste receptor is not blocked by a known antagonist of mGluR4. This casts some doubt on the proposed role of mGluR4 as a taste receptor. Since the ligand binding region of mGluR4 is of interest, the ligand binding domain of mGluR1, an mGluR4 homologue will be discussed in the next section. The ligand binding domain of mGluR1 has been resolved by x-ray crystallography [9].

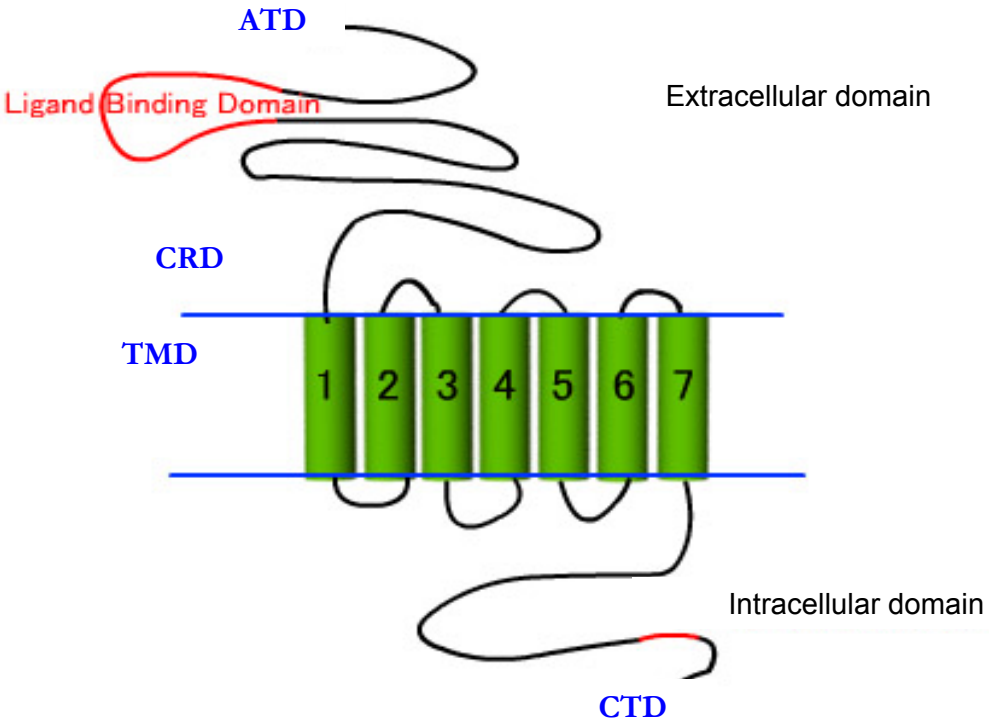

Figure 1.2 Topology of an mGluR. mGluRs have an extracellular region which contains the subunit where the ligand binds, called the amino terminal domain (ATD) that is relatively large (600 amino acids), a cysteine rich domain (CRD), a transmembrane domain (TMD) and an intracellular region called the carboxy terminal domain (CTD) [12].

1.5.3 Glutamate-binding sites in mGluR1

Five crystal structures of the ligand binding region (LBR), residues 33-522 of rat mGluR1 are available [9, 62] (Table 1). Two structures are ligand free, one has glutamate bound to the receptor; and in another an agonist is bound, and the last structure has a glutamate and a gadolinium ion (Gd^{3+}) both bound to the LBR [63].

Table 1 Different mGluR1 crystal structures of LBR of mGluR1 and their respective PDB IDs

Crystal Structure of Metabotropic Glutamate Receptor Subtype1	PDB file name
Complexed with glutamate	1EWK
Ligand free form I	1EWT
Ligand free form II	1EWV
Complexed with glutamate and Gd^{3+}	1ISR
Complexed with an antagonist	1ISS

Biochemical and structural studies have revealed that the mGluR1-LBR is a homodimer. Each protomer consists of two lobes, LB1 and LB2 (Figure 1.3) connected by a hinge region, giving rise to a closed and open form [64]. The glutamate binding site in mGluR1 is thought to contain 13 amino acid residues shared between the LB1 and LB2 domains of the protomer. The ligand binding domain exists in a dynamic equilibrium between the activated state and the resting state, which have different dimer crystal structures [64].

The interaction of glutamate with LB1 is initiated mainly through hydrogen bonds (Figure 1.4), and with LB2, binding is through hydrogen bonds and salt bridges. Cation-π interaction with Tyr236 is also thought to contribute to stabilising the binding. Seven invariant residues which may contribute to ligand binding are conserved in the whole mGluR family (Arg 78, Ser 165, Thr 188, Asp 208, Tyr 236, Asp 318 and Lys 409) [9].

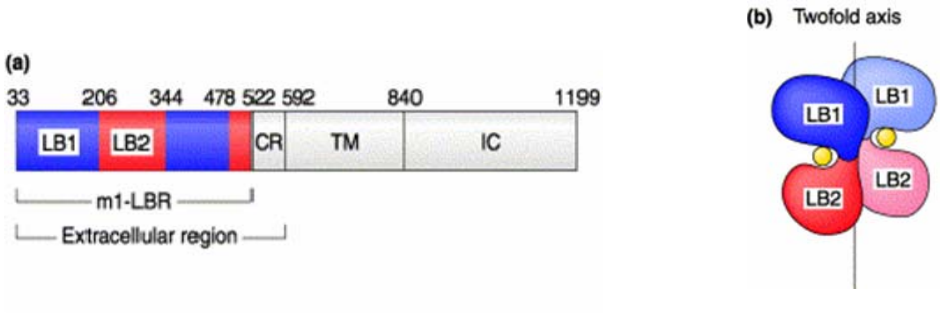

Figure 1.3 The LB1 and LB2 domains which constitute an LBR, are coloured blue and red, respectively. Numerical positions of the primary amino acids are indicated a). Spatial arrangements of a dimer of the LBR of mGluR1. The 2 protomers are distinguished by dark and light colouring. The yellow spheres indicate the ligand, glutamate b) [3].

The space between LB1 and LB2 (Figure 1.3) undergoes a change between the free form I and the glutamate-bound form. Upon glutamate binding the distance between LB1 and LB2 is reduced by more than 20 Å. The crystal structure of the glutamate bound form to LBR of mGluR1 is shown in Figure 1.4, and a schematic representation of the amino acids in the binding site in the closed and open form of the protomer is shown in Figure 1.5.

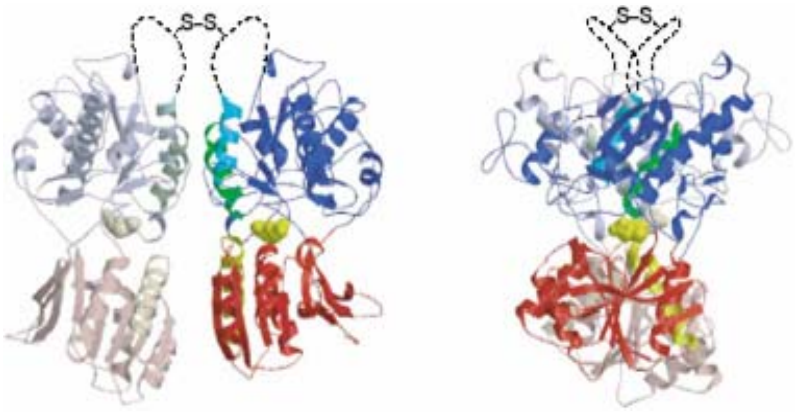

Figure 1.4 Crystal structure of glutamate bound form of the ligand binding region (LBR) of mGluR1. Two orthogonal views are shown here. The bound glutamate is shown in yellow space-filled model and the disordered region that contains the potential inter-protomer disulphide bridge is represented with dotted lines [9]. The blue and the red colour match the two protomers that comprise the LBD.

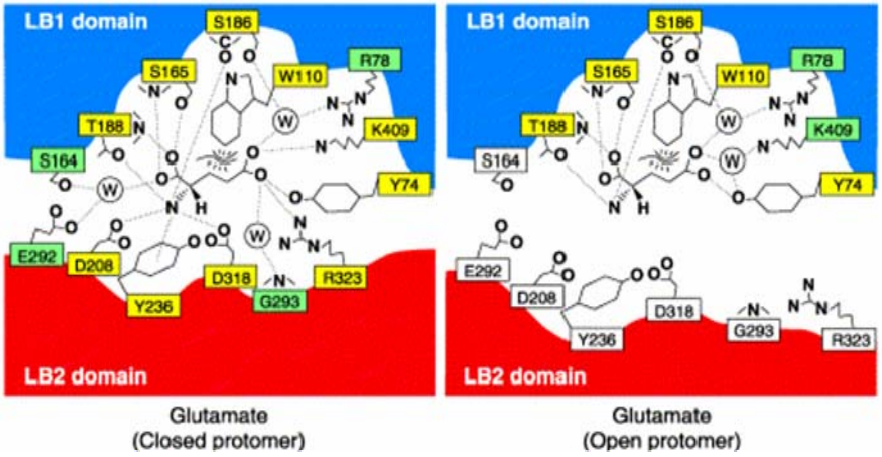

Figure 1.5 Schematic representation of the recognition of glutamate observed in the closed and open protomers of mGluR1. Yellow boxes represent the residues that form direct contacts and green boxes represent the residues that form water mediated interactions with the ligand. The water molecules are shown as the circled W. The ligands are recognised via polar interactions [3]. The blue and the red colour are as in Figure 1.4.

1.6 Nuclear Magnetic Resonance

Nuclear magnetic resonance (NMR) spectroscopy can provide atomic resolution structures of biological molecules such as proteins [65]. The nuclear spin is associated with a magnetic moment and defines the basic resonance frequency. The exact resonant frequency depends on the chemical environment of each spin. As a result, the NMR spectrum of a protein will show signals with slightly different frequencies (called chemical shifts). The use of NMR spectroscopy in biological research has a long and successful history. Most of these NMR studies have been performed in solution and were conducted primarily for structure elucidation of biomacromolecules of M_w < 30 kDa.

More recently, solid-state NMR spectroscopy has been used to provide high-resolution structural information of selected parts of biomolecules forming micro-crystalline or lyophilised powders [66-70]. It can also be used to give detailed structural, dynamic and electronic information about drugs and ligands while constrained at their site of action in membrane embedded receptors at near physiological condition (natural membrane fragment or reconstituted complexes) [71-74]. Furthermore, solid-state NMR can be used to provide structural information about the conformation of peptides [75-79], and the oligomers they form in biological membranes [80] as well as characterise small molecules in the solid-state and help drug development [81].

Over the past few years, the remarkable advances in solid-state NMR (SSNMR) approaches have contributed significantly to the characterisation of membrane protein and amyloid system structure and function [82-86] X-ray crystallography requires high quality crystals and is a long range method more suited to determining structures of large complexes, while solution state NMR being a short-range method, is ideal for smaller proteins. In addition, there is often overlapping and overcrowding of information in NMR spectra and simplification is required.

In contrast, in most solids, fast molecular tumbling is absent and anisotropic interactions like chemical shift anisotropy (CSA), dipolar interactions and, for spins >1/2, quadrupolar couplings, lead to resonance broadening. To overcome this problem, two general approaches for obtaining high resolution solid state NMR spectra have been developed. The first approach relies on oriented samples such as membranes layered on glass slides (Figure 1.6) [3, 87].

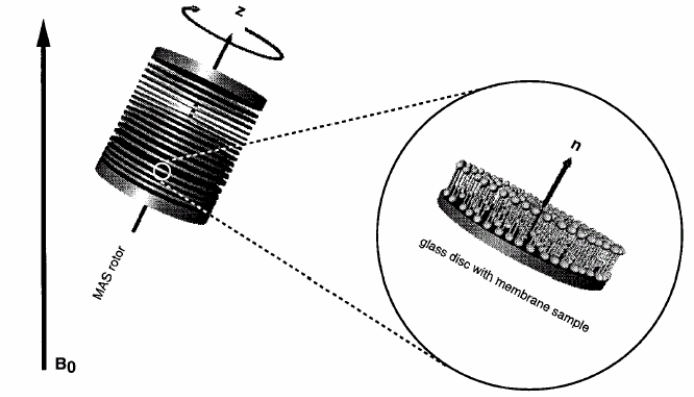

Figure 1.6 Membranes layered on glass slides and packed into a MAS rotor (MAOSS) [3].

Orientational restraints are derived from dipolar couplings and chemical shift interactions, whose values depend on the alignment of the molecule relative to the external magnetic field. For example polarisation inversion spin exchange at the magic angle (PISEMA) is an experiment on oriented samples. Here, the orientation of secondary structure elements is studied by exploiting ^{15}N chemical shift anisotropy in labelled peptides [88, 89]. The second approach for obtaining high-resolution spectra is the magic-angle spinning (MAS) technique, where the spectral resolution is improved by mechanically rotating the sample at the 'magic' angle that is around an axis that is tilted 54.7 º relative to the external magnetic field [13, 90, 91]. MAS can be applied to random dispersions of molecules.

MAS NMR applied to oriented and non-oriented samples produces sufficiently resolved spectra and allows the detection of the isotropic chemical shift. Analysis of chemical shift differences in solution and solid-state may provide structural information about the contact interface or, in the case of ligand-receptor binding studies, to probe the binding sites.

In solid state NMR no maximum molecular weight limit exists for the complex to be studied, and it can be used to supplement other techniques as long as site-specific labelling is possible. Recoupling methods can be used to determine distances to sub- Å resolution. The chemical shifts yield electronic detail at precise locations. Anisotropic details are accessible in ordered systems and provide orientational description at a molecular and atomic level. Dynamic information over a ps-ms time scale range can be obtained. Dynamics and motion are crucial to function [92]. Recently, a great variety of techniques have been developed: for resonance

assignments RFDR, SPC5 etc, for torsion angle measurements DQ coherence, for distance measurements RR, REDOR, ^{13}C and ^{1}H Spin Diffusion, DARR, etc.

Even when a crystal structure is available, the ligand (if present) is resolved from residual electron density after backbone refinement. Only one membrane protein bound to the ligand has been resolved by X-ray crystallography, the P-type Ca^{2+}-ATPase in its E1 state bound to calcium, and in its E2 state in the absence of Ca^{2+} but in the presence of the potent inhibitor thapsigargin (Figure 1.7) [4]. Solid state NMR methods can give a more direct approach to ligand-receptor interactions [93, 94].

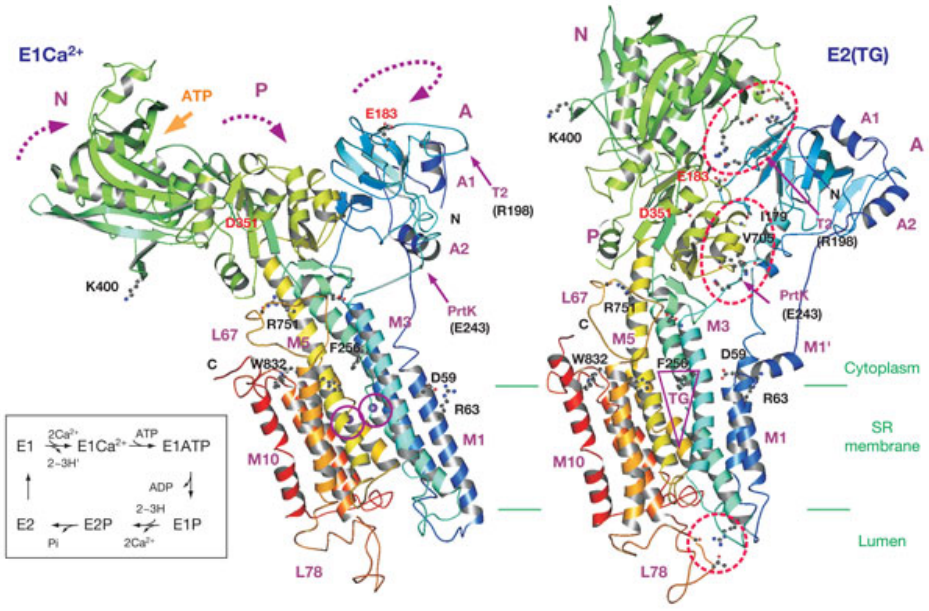

Figure 1.7 Ribbon representation of a sarcoplasmic reticulum Ca^{2+} ATPase in the Ca^{2+}-bound state ($E1Ca^{2+}$) and in the absence of Ca^{2+} but in the presence of thapsigargin labelled TG[4].

Some examples of solid state NMR being applied to membrane receptor-ligand interactions are bacteriorhodopsin [95], rhodopsin [72, 96], the H^+/K^+-ATPase - a gastric peptic ulcer target [18], nicotinic acetylcholine receptor (nAchR) [97] , neurotensin [98], and other membrane proteins. In addition, protein-membrane complexes are generally too large to tumble sufficiently rapidly to produce the averaging effects required for high-resolution NMR structure determination. Solid state NMR does not require isotropic tumbling and is therefore applicable to these systems where M_w>30kDa.

In the nicotinic acetylcholine receptor, a ligand-gated ion channel recognised as a target for a range of neurological diseases, direct observation of the agonist in its binding site in the membrane bound to a functional nicotinic acetylcholine receptor was studied [98]. For the ATP-driven cation pump, Na^+/K^+-ATPase, which binds cardiac glycosides such as oubain, detailed structural information about the inhibitor has been obtained using high resolution SS NMR methods to measure inter-atomic distances within the molecule at its pharmacological site of action [71]. Cross polarisation magic angle spinning (CP MAS) and rotational echo double resonance (REDOR) NMR experiments have been performed to determine the complete structure of the bound inhibitor of the imidazopyridine class of gastric proton pump inhibitors Figure 1.8 [74, 99].

In addition, SS NMR is used to probe dynamics of both lipids and proteins, using ^{31}P, ^{2}H and ^{13}C nuclei [100]. In particular wide-line static ^{2}H SS NMR [101] can be used to probe the mobility of the inhibitor. In this technique narrow lines correspond to highly mobile inhibitor and broad powder pattern are ascribed to a motion-restricted inhibitor.

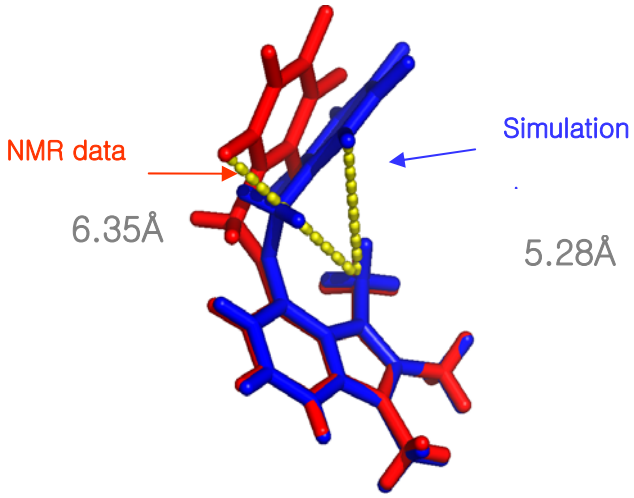

Figure 1.8 Three dimensional structure of the first drug at a membrane target binding site as resolved using solid state NMR. The reversible inhibitor TMPFIP using distance measurements (REDOR) and simulation using a docking algorithm to compare with experimental data [18].

Here, it was proposed to use SS NMR to determine distance constraints on the glutamate bound to the receptor. The method lends itself to studying the conformation of the ligand before and after binding to the receptor, as well as the conformation of the receptor itself, both with and without ligand.

1.7 Introduction to Principles of NMR

1.7.1 Spin and magnetic moment

Some nuclei possess an intrinsic property, angular momentum, called spin. Nuclear magnetic resonance (NMR) exploits the properties of these spins as non-perturbing probes to determine the magnetic environment of a nucleus. The response of a spin to the local environment can provide an insight into bond angles, internuclear distances and the orientation of nuclei with

respect to the external applied field [102]. The nuclear spin (**I**) can be related to a nuclear magnetic moment (μ) by

$$\mu = \gamma I$$

where γ is the gyromagnetic ratio. The gyromagnetic ratio is characteristic of each nuclear isotope. When nuclei exist in different electronic environments they will show NMR signals with slightly different frequencies. The values for the gyromagnetic ratio of the most commonly used nuclei in biological NMR are given in Table 2.

Table 2 Nuclei important for NMR spectroscopy of biological molecules and the nuclear properties of these nuclei [1].

Nucleus	Spin quantum number, I	Magnetic moment, μ (units, of μ_N)	Natural abundance (%)	Quadrupole moment, Q (e x 10^{-28} m^2)	Relative Sensitivity
^{1}H	½	2.79	99.99		1.00
^{2}H	1	0.41	0.015	0.003	0.0096
^{13}C	½	0.70	1.1		0.016
^{14}N	1	0.40	99.6	0.02	0.001
^{15}N	½	-0.28	0.37		0.001
^{17}O	5/2	-1.89	0.04	-0.004	0.029
^{19}F	½	2.62	100		1.00
^{31}P	½	1.31	100		1.00

1.7.2 NMR interactions

When a nuclear spin is placed in a magnetic field B_0, the spin precesses around the field with a precession frequency ω_o. The precession frequency is called the Larmor frequency and is given by:

$$\omega_0 = -\gamma B_0$$

where B_0 is the applied magnetic field and γ is the gyromagnetic ratio.

The complete spin Hamiltonian (H) for a nuclear spin is given by.

$$H = H_Z + H_{CS} + H_D + H_J + H_Q$$

Where H_Z is the Hamiltonian of the Zeeman interaction which describes the interaction between a nuclear spin I and the external magnetic field B_0, and determines the resonant portion of the NMR spectrum.

$$H_Z = -\gamma B_0 I_{JZ}$$

where I and B_0 are vectors.

Transitions between the Zeeman state are induced by an oscillating magnetic field B_1 which is induced by applied radiofrequency (RF) pulse.

The remaining terms of the Hamiltonian give rise to the characteristic features of an NMR spectrum. These are the chemical shift Hamiltonian H_{CS}, the dipolar Hamiltonian H_D, the J-coupling Hamiltonian H_J and the quadrupolar coupling Hamiltonian H_Q.

The chemical shift Hamiltonian can be written as

$$H_{CS} = \gamma \mathbf{I} \sigma B_0$$

where σ is the shielding tensor that describes the effect of the electronic distribution around the nuclear spin. Because the electronic distribution is not isotropic, the chemical shift interaction depends on the orientation of the nucleus with respect to B_0.

The dipolar Hamiltonian H_D describes the through-space coupling between two nuclear spins $\mathbf{I}_I$ and $\mathbf{I}_J$

$$H_D = \mathbf{I}_I \mathbf{D} \mathbf{I}_J$$

where **D** is the dipolar coupling tensor, which describes how the field due to the spin **I** varies with the orientation of the I-J internuclear vector in the applied field (θ_{IJ}). The dipolar coupling has an r^{-3} distance dependence, where r is the internuclear distance which provides the origin of distance restraints in NMR.

J-couplings are dipolar couplings that are mediated through bonds by the electrons. In the solid-state J-couplings are much smaller than the dipolar interactions and are often masked by line-broadening or other information.

The quadrupolar coupling Hamiltonian H_Q is non-zero only for nuclei with spins greater than ½, and is proportional to the electric-field gradient tensor V.

1.8 Basic Solid-State NMR Techniques

In solution NMR, all anisotropic interactions are averaged out because molecules in solution isotropically tumble faster than the frequency of the interactions. Solid state NMR on the other hand, includes the anisotropic interactions and is a powerful technique because the spectra contain significant structural information. Protons are not the preferred nuclei for observation in solid state NMR because they are involved in a strong dipolar coupled network of spins, resulting in broadened spectra. In protein solid state NMR, structural details are primarily obtained from the low-γ and dilute I=1/2 spins i.e. ^{13}C and ^{15}N. The detection of low abundance ^{13}C and ^{15}N and ^{2}H nuclei usually requires isotope enrichment for sensitivity enhancement. To further increase the sensitivity and resolution of solid-state spectra, MAS is combined with high-power proton decoupling [103] and cross-polarisation (CP) [104, 105].

1.8.1 Magic angle spinning

Magic-Angle spinning (MAS) as demonstrated first by Andrew and Lowe [106, 107] is an essential technique in solid-state NMR for obtaining high resolution spectra. The technique

leads to a significant simplification of solid-state NMR spectra by reducing the powder pattern to an average isotropic value where the observed signals are narrowed (Figure 1.9).

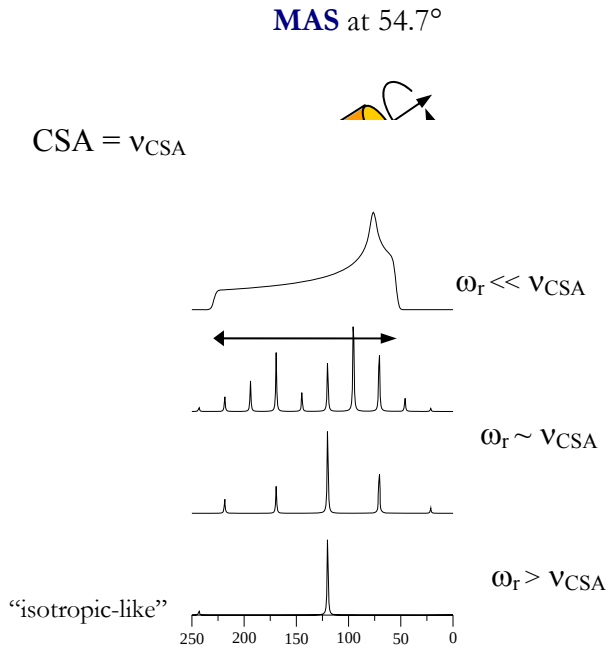

Figure 1.9 Solid state ^{15}N-NMR spectra of glycine illustrating the effects of solid state magic angle spinning (MAS) NMR to study biomolecules. Without MAS, broad unresolved resonances result from the chemical shift anisotropy (ν_{CSA}) and a typical powder pattern (upper slide) spectrum is obtained [13]. In MAS NMR the rotor is set at the 'magic angle' which is 54.7° with respect to the z axis of the static magnetic field. As the spinning frequency (ω_r) is increased, the broad powder spectrum breaks into narrow resonances at the isotropic chemical shifts and sets of rotational side bands spaced by the spinning frequency (the next two spectra below the powder spectrum). When the MAS frequency is much larger than the breadth of the chemical shift anisotropy, only the isotropic resonance is observed (the bottom spectrum). Spectra were acquired on a 500 MHz Infinity Plus spectrometer, with a 4 mm double resonance MAS probe at room temperature.

The method consists of rapidly spinning the sample container (rotor) into the spinning module of the probe shown in Figure 1.9 about an axis of 54.74°, the magic-angle, with respect to the

static field B_0. Chemical shielding, dipolar and quadrupolar interaction both contain a $(3\cos^2\theta-1)$ dependent term with respect to the magnetic field. In solution, rapid isotropic tumbling (if the tumbling rate is $\tau_r^{-1} >> \nu_{CSA}, \nu_D$) averages this spatial component to zero, while in the case of solids, another way to average this angular component is to average it mechanically.

The rate of MAS (ω_r) must be greater than or equal to the magnitude of the anisotropic interaction to average it to zero (i.e. most anisotropic interactions with a magnitude below the frequency of spinning of the sample are averaged). This leads to a decrease in the sideband intensities, and an increase in the centre band intensity because the isotropic shift interactions and the isotropic J-couplings are left, giving high-resolution solid-state NMR spectra similar to those seen in solution NMR. The disadvantage is that the spectrum loses all the molecular geometry information.

The MAS technique is of limited use for "high-gamma" nuclei like protons and fluorine, which can have dipolar coupling in excess of 100 kHz, where such high spinning rates cannot be achieved. If the sample is spun at a rate less than the magnitude of the anisotropic interaction, a manifold of sidebands becomes visible, which are separated by the rate of spinning (in Hz). However, analyses of the residual sidebands pattern can also provide valuable orientational information.

A **B**

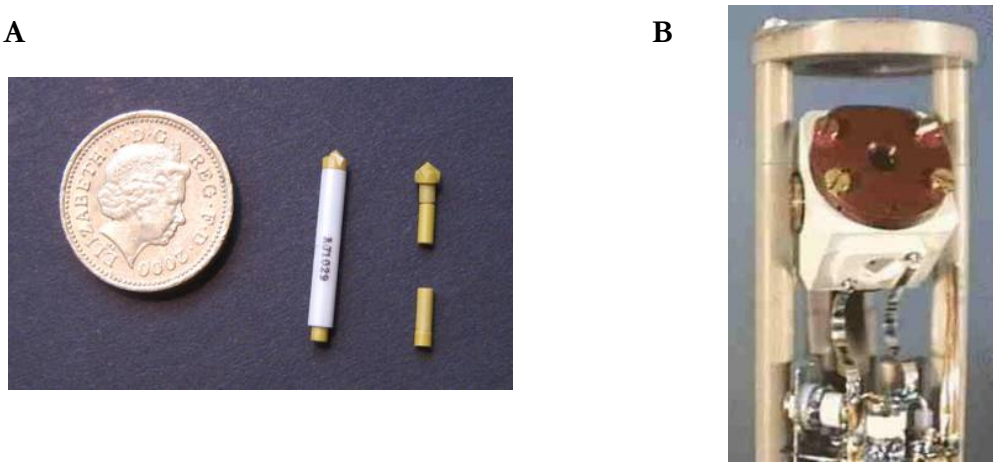

Figure 1.10 A) Magic angle spinning (MAS) rotor B) A spinning module (Stator) of a Varian MAS probe. MAS solid-state NMR samples are loaded into zirconium rotors with various diameters. In figure A, a Varian rotor of 3.2 mm outer diameter is shown in the middle. The components of the rotor are displayed on the right. From top to bottom: drive-tip, spacer, end-cap. A British one pound coin is shown (left) for size reference. B) The rotor is mechanically rotated in the probe-spinning module by blowing high-pressure compressed air or nitrogen gas at the drive tip, while the rotor floats on a bearing air. The maximum rotation frequency for a 3.2 mm standard wall Varian rotor is currently 25 kHz. The spacer and end-cap seal the rotor and hold the sample in place. This rotor can hold up to 15 µl of sample [15, 24].

Practically, the samples are often finely powdered, crystalline or for membrane proteins reconstituted in lipid bilayers (i.e. large size and slow tumbling rate) and packed tightly into the rotor, which are then spun at rates from 1 to 35 kHz, depending on the rotor size and type of experiment being conducted.

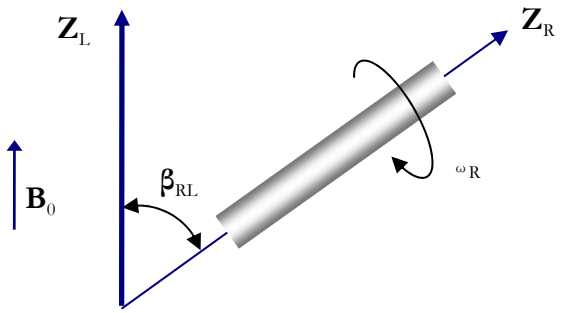

Figure 1.11 Schematic diagram for magic angle spinning (MAS). Z_L is z-axis of laboratory frame which is aligned with the external magnetic field B_0 and a rotor is spinning at ω_R around z-axis of rotor frame which is tilted by the magic angle β_{RL}. Taken from [11].

1.8.2 Cross polarisation

The sensitivity of rare spin species (S-spins) with low gyromagnetic ratio, such as ^{13}C and ^{15}N can be enhanced by transferring magnetisation from abundant spin species (I-spins) with high gyromagnetic ratio, such as ^{1}H, ^{19}F and ^{31}P [104, 105]. In a CP experiment, the field strengths are set to the Hartmann-Hahn condition (Figure 1.12). Polarisation is transferred when a spin-lock field is applied to I and S simultaneously, called the contact time.

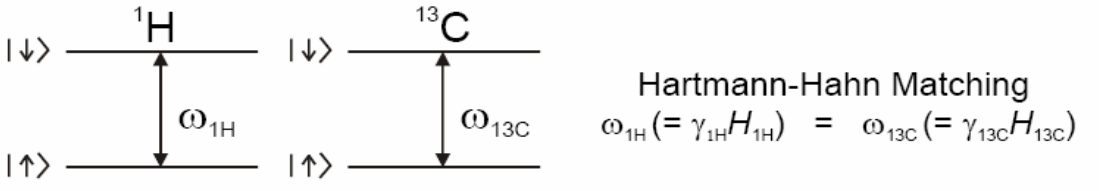

Figure 1.12 The classic Hartmann-Hahn condition for a non-spinning sample that allows transfer of polarisation from ^{1}H to low-γ nucleus such as ^{13}C. For a spinning sample the MAS frequency has to be taken into account and the matching condition becomes: $\omega_{1H} - \omega_{13C} = \pm n \omega_r$

$$\gamma B_{rf} +/- n\omega_r$$

Where n= 1, 2

$$|\gamma_I B^I_{rf}| = |\gamma_S B^S_{rf}|$$

where B^I_{rf} and B^S_{rf} are rf fields applied to spin I and S, respectively and γ_I and γ_S. The standard pulse program for a CP experiment is shown in Figure 1.13 with a ^1H excitation 90º- pulse and then magnetisation transfer from ^1H to the low frequency channel (e.g ^{13}C or ^{15}N) by the matched pair of CP pulses. In the presence of molecular motion or with increasing spinning frequency, problems in establishing and maintaining the Hartmann-Hahn matching condition can be encountered. Recently, it has been shown that a ramped pulse on one of the channels improves signal stability, compensates for B_1 inhomogeneity and increases sensitivity [108, 109]. The signal enhancement in CP is due to two factors. First, the larger gyromagnetic ratio of protons (e.g γ_H is 4 times bigger than γ_C) creates a larger ^1H polarisation which is transferred to the low-γ nucleus. Second, the repetition time of the experiment is determined by the shorter ^1H relaxation time relative to low-γ spins and hence the experiment repetition rate can be increased.

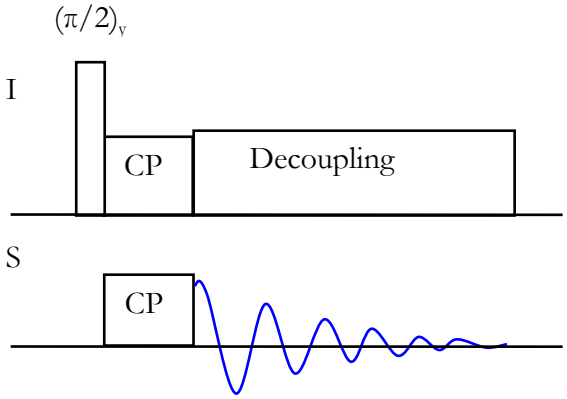

Figure 1.13 Standard CP pulse sequence with decoupling scheme during the signal acquisition

1.8.3 Proton decoupling

The ^{1}H nucleus has a large gyromagnetic ratio and almost 100% natural abundance (Table 2). Especially in biomolecules, there are a huge number of protons and their spin interactions with the other low γ nuclei such as ^{13}C and ^{15}N complicate the spectrum. ^{1}H decoupling therefore is necessary to remove residual ^{1}H-^{13}C dipolar couplings under MAS and ^{1}H-^{13}C residual J-couplings, which are not averaged with the sample spinning at the magic angle. Decoupling field strengths of 80-100 kHz are now commonly used. The simplest decoupling method involves continuous *rf* irradiation of fixed phase during the acquisition of the FID and is called continuous wave (CW) decoupling [103]. Recently, more sophisticated methods have been introduced, which significantly improve the decoupling efficiency [110]. Two-pulse phase modulation (TPPM) consists of two π pulses and their rapid phase switching. Experimentally it was found that TPPM decoupling is very sensitive to the parameter setting of the two values, the pulse length and the phase angle [111]. There is also X inverse-X (XiX) decoupling

scheme, which is a simple high-decoupling scheme that improves decoupling compared to other available sequences such as CW and TPPM. It consists of continuous irradiation of the protons with pulses of equal width τ_p and with a phase difference of 180°. For XiX, the performance depends only on the pulse width τ_p in units of the rotor period, $\tau_r=1/\omega_r$ [112].

1.8.4 Recoupling methods

The dipolar coupling between nuclei in specific sites in solids is an important structural parameter due to its r^{-3} dependence, where r is the internuclear distance, but it is reduced dramatically by rapid MAS. However, these interactions contain valuable structural and dynamic information. This information can be brought back by employing so-called 'recoupling methods' to recover the dipolar interactions lost during MAS. Different techniques have been developed for recoupling dipolar interactions, which are based on the application of *rf* pulses to disrupt the averaging due to samples rotation. These techniques can be separated into two general categories: techniques that recouple dipolar couplings between homonuclear spins such as dipolar recoupling at the magic angle (DRAMA) [113] and radiofrequency driven recoupling (RFDR) [114] and techniques that measure dipolar couplings between heteronuclear spins (rotational-echo double resonance) REDOR and CP between $^{13}C/^{15}N$. The application of homonuclear dipolar correlation spectroscopy on uniformly ^{13}C-labelled systems is important for assignment strategies in solid-state NMR. ^{13}C-homonuclear correlation experiments are used for the identification of amino-acid side-chains. 2D and 3D heteronuclear experiments like NCO, NCA, NCOCX, NCACX, on the other hand, have become very important for sequential assignment information.

1.8.5 Solid-state NMR of quadrupolar nuclei

Quadrupole nuclei have a spin >1/2 and an asymmetric distribution of nucleons which give rise to a non-spherical positive electric charge distribution. The asymmetric charge distribution in the nucleus is described by the nuclear electric quadrupole moment, eQ, which is an intrinsic property of the nucleus and is the same regardless of the environment. Quadrupolar nuclei interact with electric field gradients in the molecule, which are spatial changes in electric field in the molecule. The magnitude of the quadrupolar interaction is given by the nuclear quadrupole coupling constant, which accounts for both the intrinsic property of the nucleus and for its environment.

The double orientation rotation (DOR) technique is a solid-state NMR technique which is used for studying half integer quadrupole nuclei. This technique removes quadrupole interactions that are not removed by MAS. Consequently, narrower lines can be obtained and different sites can be resolved more easily and with greater accuracy. However it is an extremely difficult technique to implement and narrowing of the lines removes useful information. The limited spinning rates and large coil-part of the experiment mean that strong dipolar coupling to hydrogen/protons cannot be completely removed. As a result spectrum with O-H ^{17}O peaks are broadened to the extent that they are not seen.

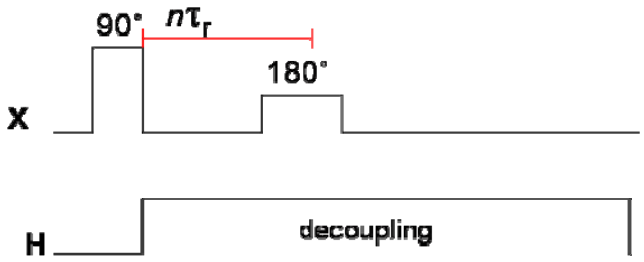

Figure 1.14 Schematic representation of Oldfield echo two pulse sequence, where n is an integer and τ_r is a rotor period combined with the XiX decoupling sequence.

Oldfield [115] introduced a technique, using standard equipment, originally proposed for second order powder pattern lineshapes for low γ nonintegral spin quadrupole nuclei. The Oldfield echo (Figure 1.14) uses the full phase-cycling rules to provide a 16-step sequence that removes unwanted signals and probe-ringing from the two pulses. When the echo signal is measured the probe has had time to recover, and hence the echo contains only signals from the sample that is being measured. This technique combined with high speed MAS and very strong decoupling effectively produces high resolution quadrupole spectra.

1.8.6 Static NMR experiments of oriented samples

Static solid-state NMR spectroscopy on macroscopically oriented lipid bilayers is an alternative approach to structural and functional elucidation of structure of membrane-bound peptides and proteins [116-121]. By aligning the sample on a solid support that has itself a specific direction with respect to the external magnetic field, orientationally dependent parameters like the chemical shift anisotropy of appropriate nuclei is determined to give direct molecular

structure for specifically introduced nuclei such as ^{2}H which shows quadrupolar anisotropy, or ^{13}C, ^{31}P, or ^{15}N which show chemical shift anisotropy and dipolar coupling for each labelled position [122].

Static ^{31}P NMR can be used to probe lipid alignment and membrane morphology. It is a highly sensitive method to characterize the degree of alignment and functional integrity of the bilayer lipids by probing the phospholipids [123]. Biological alignment takes advantage of the natural liquid crystalline arrays of certain membranes. The CSA tensor is axially symmetric for phospholipids undergoing fast rotation around an axis perpendicular to the bilayer plane [124]. For randomly, unoriented multilamellar bilayer dispersion, a broad spherically averaged powder spectrum is obtained. For a specific phospholipid in an oriented bilayer, the ^{31}P NMR spectrum consists of a single resonance line whose frequency ν_{CSA} increases with the angle θ between the membrane normal and the magnetic field. The static ^{31}P NMR spectra of lipids are governed by the asymmetric electronic distribution around the phosphate group within the lipid. The orientation dependence of ^{31}P spectra oriented lipid bilayer systems can be seen in Figure 1.16.

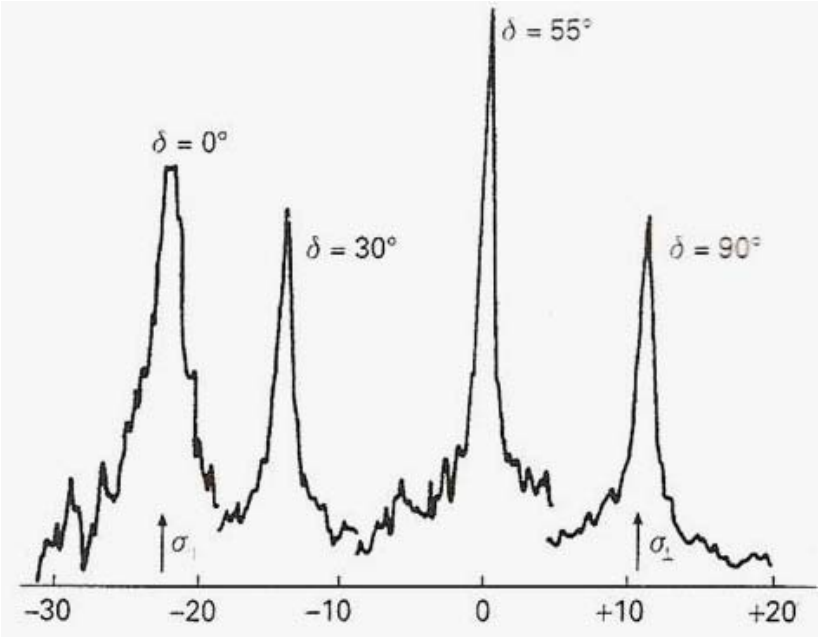

Figure 1.16 Orientational dependence of ^{31}P NMR spectra (at 36.4 MHz) of planar multi-bilayers of phosphatidylcholine, where δ is the angle of the applied field with respect to the membrane normal at T=77°adapted from [10]

1.9 Aims and Objectives

The main aim of the thesis is to resolve methodologies suitable for the study of crystalline membrane proteins by solid-state NMR, with mGluR4 and bacteriorhodopsin as case studies for NMR crystallography.

For the mGluR4 protein

It was planned to express and purify the active ligand-binding domain of mGluR4 in *E. coli* in sufficient amounts that will enable the ligand receptor interactions to be probed to high

resolution using solid-state NMR. Another aim was to crystallise the protein and examine the effects of crystallisation on ^{13}C NMR linewidths.

A homologue, mGluR1 has been crystallised and its structure resolved by x-ray crystallography [9]. A homology model was built based on the mGluR1 sequence and molecular dynamics simulations performed to support the NMR studies. Structural information, such as the conformation and the orientation of the bound-ligand obtained from NMR experiments should provide a detailed view of the ligand binding site.

Another aim was to characterise the ligand and assign its resonances using solid-state NMR to permit assignment of the resonances for glutamate when bound to mGluR4.

For the bacteriorhodopsin protein

Three dimensional (3D) crystals of bR have been produced in the context of solid state "NMR crystallography" and the effect it has on the quality of the spectra on the selectively ^{15}N labelled bacteriorhodopsin investigated. The ultimate goal of the bR crystallisation trials described was to produce highly homogeneous three dimensional bR crystals for MAS NMR and compare their resolution with the resolution of the purple membrane which is a natural 2 dimensional (2D) crystal. Alternative means of sample preparation like Lipodisqs™, which may find application for preparing samples for solid state NMR of strongly hydrophobic peptides, was studied by transmission electron microscopy in order to determine the diameter and the homogeneity. ^{31}P static solid state NMR was used to study the orientation of Lipodsiqs™ in a magnetic field.

One aim of this study is to investigate whether an improvement of spectral resolution in solid-state NMR ^{13}C linewidths could be achieved by deuterating U-^{13}C, ^{15}N bacteriorhodopsin. Three differently uniformly labelled bacteriorhodopsin samples were prepared: fully deuterated U-^{13}C, ^{15}N, 50% deuterated U-^{13}C, ^{15}N and fully protonated U-^{13}C, ^{15}N. Effects of deuteration on the quality of solid-state NMR spectra will be examined.

Another aim of the study of U- ^{13}C, ^{15}N labelled bR, was to establish the feasibility of sequential, site specific assignment of uniformly ^{13}C, ^{15}N labelled protein bacteriorhodopsin (bR) in the purple membrane using solid state NMR. Bacteriorhodopsin is a 248 amino acid, mostly α-helical 7 transmembrane protein consequently resonance assignment is expected to be challenging, but a prelude to studies on GPCRs and other polytopic membrane proteins.

Chapter 2 Metabotropic Glutamate Receptor 4: Ligand Studies by Solid State NMR, Homology Modelling, Cloning and Expression

2.1 Introduction

This chapter describes the steps undertaken to lay the groundwork necessary for studying ligand-receptor binding studies by solid state NMR of a novel protein. The chapter contains three parts: the first reports on the ^{13}C, ^{15}N and ^{17}O solid state NMR characterisation of the ligand for the mGluR4 receptor: L-glutamic acid. The second part of this chapter describes the building of a homology model to predict the structure of mGluR4, since there is no structural information available for it. The third part is concerned with the cloning and expression of mGluR4 in *E. coli,* in order to obtain sufficient amounts of functional receptor for solid state NMR studies. Clones of the full length receptor and the ligand binding domain for different expression pathways with different fusion tags were examined.

2.1.1 Ligand studies by solid state NMR

Before ligand bound to receptor studies could be attempted, it was necessary to study the ligand alone. This assists with assignment and characterisation of the spectra of the ligand-receptor complex later on in the studies. Details about the ^{13}C and ^{15}N CP MAS NMR

technique used is described in Chapter 1. A more detailed description of ^{17}O solid state NMR, which is of particular interest to ligand-binding studies, is given here.

^{17}O is the only NMR-active oxygen isotope, with spin I = 5/2. It possesses a quadrupole moment which leads to significantly broadened lines from solids and the fast relaxation time makes it unsuitable for solution state NMR. In addition it has a low natural abundance (0.037%) [125] which makes its use relatively uncommon. The advent of higher magnetic fields, faster MAS and techniques for improving resolution, has made the use of ^{17}O solid-state NMR more accessible. ^{17}O has been used in the study of biological materials in addition to the traditional inorganic materials such as glasses and zeolites [126, 127]. ^{17}O -NMR study of ^{17}O-labelled biomaterials is very sensitive to changes in the bonding environment, in particular H-bonding, which is important in ligand binding [128].

2.1.2 Homology modelling of the ligand binding domain of mGluR4

The structure of mGluR4 has not been resolved yet by any structural method. In the absence of high resolution structural data, model building on the basis of the known 3D structure of homologous proteins is a useful method to obtain structural information. Comparative or homology modelling combines the sequence of a macromolecule of unknown structure with the template [129] of one or several other homologous macromolecules, whose structures serve as starting points for the unknown structure. Homology modelling is considered to be one of the most accurate prediction methods [130, 131] and is useful for planning labelling schemes and experiments.

In this case, the homologous protein on which the mGluR4 homology model is going to be predicted is the ligand binding domain of mGluR1. There are several structures of mGluR1 available that have been resolved by x-ray crystallography. mGluR1 shares 30% sequence identity with mGluR4 which is sufficient for predicting an mGluR4 homology model. The next step in homology modelling is to align the template and the target sequence. Several models are generated by MODELLER, a program used for homology and comparative modelling and the models are validated by one of the softwares programs available.

2.1.3 Molecular biology of mGluR4

The mGluR4 receptors, both the brain and putative taste receptor, were described in Chapter 1. At the beginning of the study the focus was on the putative taste receptor, which is a truncated version of the brain mGluR4. The putative taste receptor shares the same amino-acid sequence as the brain mGluR4 receptor, except for the first 265 amino acids at the N-terminal which are missing from the taste receptor. The schematic representation of the modular parts of the putative taste and the brain mGluR4 compared to the brain mGluR1 receptor can be seen in Figure 2.1. Although the expression of taste- and brain-mGluR4 mRNAs in same tissue have been demonstrated, the expression of the putative taste mGluR4 protein in taste tissues is not conclusive. Consequently, the focus here was broadened to the brain mGluR4 receptor, which is a receptor for L-glutamic acid, a major excitatory neurotransmitter in the central nervous system. It is the binding site of glutamate which is the focus of the NMR study.

In order to study ligand-receptor conformational changes by solid state NMR, the ligand binding domains (LBD) of mGluR4 alone will be sufficient, since they retain the ligand-binding capacity and ligand selectivity comparable to the full length receptor [132].

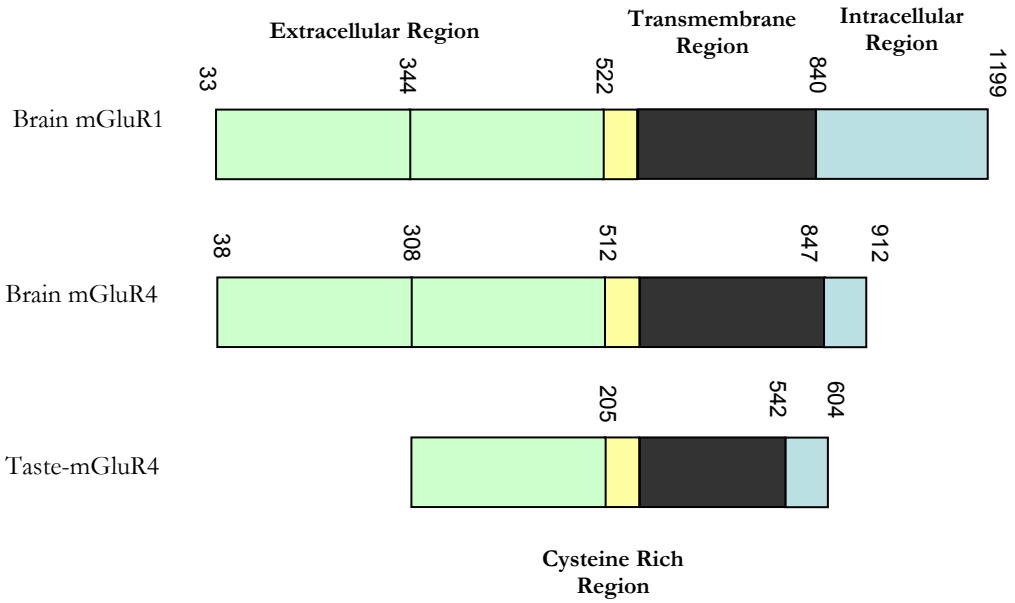

Figure 2.1 Modular parts of mGluR1 and mGluR4. The beginning of the domains are denoted by the number of the residue. The mGluR receptors consist of extracellular domain, cystein rich domain, transmembrane region and an intracellular C-terminal domain.

However, the full length mGluR4 receptor including the transmembrane and intracellular region is of interest as well. Hence, the LBD and the full length mGluR4 receptors of both the brain and the putative taste receptor will be cloned and their expression attempted in *E. coli.*

The disulfide bridges present in the LBD are predicted to make this protein insoluble in *E. coli,* due to the reducing nature of the cytosol in *E. coli.* Different fusion tags at either the N or the

C terminus to keep the protein soluble will be used as well as different cloning strategies, such as expression in the cytoplasm or periplasm, which is more favourable for disulfide bridge formation will be tried to overcome this problem and are discussed in the Materials and Methods section.

Expression of a full length active GPCR, the neurotensin receptor, in *E. coli* has been achieved in this laboratory [133]. The same cloning strategy will be applied to the full length mGluR4 receptor in order to obtain soluble, functionally active mGluR4 in *E. coli.*

There are three aims of this study. The first aim is to study the ligand of mGluR4- L-glutamic acid by solid state NMR, the second is to build a homology model which will be used for planning the labelling schemes of the protein and planning of the solid state NMR experiments. The third aim is to obtain sufficient amounts of functional receptor in *E. coli* for ligand binding and high resolution structural NMR studies of the receptor.

2.2 Materials and Methods

2.2.1 Solid state NMR of the ligand

2.2.1.a ^{13}C and ^{15}N CP MAS solid-state NMR of L-glutamic acid

One dimensional (1D) spectra were obtained using cross polarisation-magic angle spin (CP-MAS) SS NMR at a field of 9.4 T in a 4 mm standard rotor, on a ^{13}C uniformly labelled L-glutamic acid (BDH Chemicals) and ^{15}N uniformly labelled L-glutamic acid. The sample was spun at a frequency of 7 kHz. The experiments were carried out at room temperature (RT).

For the ^{13}C CP MAS experiment the contact time during CP was 2.5 ms. Pulse delay was 2 seconds and 1756 scans were collected. The spectral width was 50 kHz. ^{13}C frequency was 100.0575 MHz. Proton decoupling during acquisition was 70 kHz and 1024 data points were collected.

For the ^{15}N CP MAS crystallised ^{15}N labelled L-glutamic acid was packed into a 4 mm standard rotor. MAS frequency was 7 kHz and the experiment was carried out at RT. Contact time during CP was 2 ms. Proton decoupling during acquisition was 70 kHz. 5000 scans were collected. The L-glutamic acid was crystallised by V. Lemaitre.

2.2.1.b ^{17}O Solid-state NMR of L-glutamic acid

An ^{17}O solid-state NMR spectrum of L-glutamic acid was recorded at a Larmor frequency of 81.370 MHz and a spinning rate of 20 kHz. A Varian/Chemagnetix Infinity spectrometer was used, which was equipped with a 14.1 Tesla (600 MHz for ^{1}H) wide-bore magnet and a Varian 3.2-mm-rotor MAS probe. High-power ^{1}H decoupling, B1 was approximately 130 kHz, using the XiX scheme [134]. It was necessary for the magic angle to be as accurate as possible because echo and ^{1}H decoupling produce very high quality second-order quadrupolar line shapes [135]. The spectrum was referenced to distilled water at 0 ppm. ^{17}O uniformly labelled L-glutamic acid was synthesised and prepared by V. Lemaitre [136].

2.2.2 Homology modelling of the ligand binding domain of the taste mGluR4

The first step in homology modelling is to select a template. Since 2000, the crystal structures of the ligand binding region (LBR) of mGluR1 (listed in Table 3) have been solved at different resolutions.

Table 3 Solved crystal structures of LBR of mGLuR1, their PDB file names, resolution and date of deposition

Crystal structures of mGluR1	PDB ID	Resolution (Å)	Deposited (year)	Reference
With glutamate	1EWK	2.2	2000	[95]
Ligand free form I	1EWT	3.7	2000	
Ligand free form II	1EWV	4	2000	
With glutamate and Gd^{+}	1ISR	4	2001	[96]
With an antagonist	1ISS	3.3	2001	[96]

The crystal structure of the LBR mGluR1 complexed with glutamate solved to 2.2 Å [62] was selected as a template for modelling studies because it shares more than 30% sequence identity and the crystallographic data is with the best resolution. The next step in homology modelling is to align the template and the target sequence. Good sequence alignment is very important in generating a satisfactory homology model. The sequence identity between the template and the target is 30.02%, and sequence homology 64.39%.

2.2.2.a Model generation

MODELLER builds a model using distance and dihedral angle restraints on the target sequence derived from its alignment with the template 3D structure. MODELLER requires two types of input, the sequence alignment between the target and a template sequence and the structural data of the template protein in the PDB format.

2.2.2.b Model validation

In order to refine this group of models, the candidates were evaluated using parameters provided by PROCHECK, ProSa 2003 and Accelerys DS ViewPRo 5.0. PROCHECK is used to check the model stereochemistry. G factor is a log-odds score based on the observed distribution of the parameters taken into account by PROCHECK. These parameters include main chain bond length and bond angles; the distribution of φ, ψ and χ torsion angles. The G factor provides a measure of how normal, or alternatively unusual, the stereochemical properties are. Ideally, the G factor value should be above -0.5. Models with values for the G factor below -1.0 may need further investigation [137].

Another software program used to validate the models was ProSa 2003, a successor of Prosa II. It is software that allows analysis of three-dimensional structure of proteins. The program generates scores reflecting the quality of the structure. Z-score is a parameter generated by ProSa 2003 that indicates the quality of the protein structure and is based on water soluble proteins, not transmembrane proteins. For native folds, there is a correlation between the Z-score values and the sequence length.

2.2.3 Molecular Biology of mGluR4

The aim of this section is to describe the cloning and expression of several different mGluR4 constructs in *E. coli* with the aim to obtain large quantities of functional protein sufficient for structural studies. mGluR4 contains 2 disulfide bridges, a cysteine-rich domain and GPCR expression in general is challenging.

The first clone was of the LBD of the putative taste receptor, it was assumed that it might be soluble in *E. coli* since it is the soluble part of the protein, and it is a small fragment, however it resulted in insoluble protein. The focus then was broadened to the brain mGluR4, and strategies for improving the solubility of the protein in *E. coli* were looked into and they are described after the cloning and expression tests of the putative LBD. The cloning and expression of the putative taste LBD was done entirely by me, whereas the cloning and expression for the brain mGluR4 were discussed with Dr Simon Ross and he carried out the cloning and expression of the constructs.

2.2.3.a Cloning and expression of the taste mGluR4 LBD

The *E. coli* vector pCR T7 /NT-TOPO was chosen for the expression of the 'taste' ligand binding domain because of the size of the gene of interest, the ease and efficiency of cloning associated with this vector, the His-tag which allows affinity purification, the Express tag which aids specific detection with monoclonal antibodies and the T7 promoter.

The truncated version of mGluR4 was amplified using a AmpliTag® polymerase supplied in a GeneAmp High Fidelity PCR kit (Applied Biosystems). Details of the concentration of the reagents and the cycling parameters are listed in Table 4.

Table 4 Components of the PCR reaction and the cycling parameters

Component	Final concentration
Forward primer	300 nM
Reverse primer	300 nM
$MgCl_2$	2.5 mM
dNTP	200 µ M
Enzyme	2.5 Units
Buffer (x10)	x1
DNA template	100ng

Step	Temperature (˚C)	Times (sec)	Cycles
Initial denaturation	94	120	1
Denaturation Annealing Extension	94 61 72	15 30 105	30
Final extension	72	300	1

The PCR product was cloned into a pCR T7 /NT-TOPO vector (Invitrogen; Figure 2.2.). A 50 µl aliquot of chemically competent *E. coli* cells, strain-BL21 (DE3), was taken out of the -80 ˚C storage and thawed on ice. 1 µl of the ligation mixture was added to the cells and left on ice for 30 minutes. The cells were heat-shocked at 42 ˚C for 30 seconds, transferred into 250 µl SOC medium, which is a nutritionally rich bacterial growth medium used to maximise transformation efficiency and incubated for 1 hour at 37 ˚C. The culture was plated onto agar containing ampicillin (50 µg/ml) and left overnight at 37 ˚C.

Successful cloning and correct orientation of the insert were checked by double restriction digests with *Bam*HI and *Eco*RI Figure 2.17, and double checked by DNA sequencing with T7 forward and reverse primers.

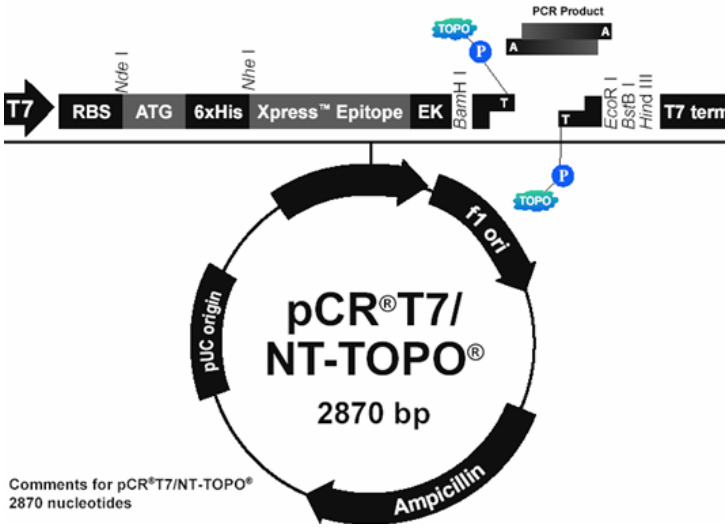

Figure 2.2 Map of the expression vector pCR T7/NT-TOPO. This vector contains a gene conferring Ampicillin resistance for bacterial selection. A T7 promoter is included as is the 6 His tag which allows detection and purification, and Express tags which is used for detection purposes [6].

2.2.3.b Expression of the taste mGluR4 LBD in *E. coli*

Starter cultures for expression of the LBR of the putative taste mGluR4 were set up by inoculating 5 ml LB containing ampicillin (50μg/ml) with the correctly oriented clones and were grown overnight. They were transferred into 50 ml LB containing ampicillin (50μg/ml). The cultures were grown at 37˚C in a 200 rpm shaker until they reached OD600 of ~0.5 at which point expression was induced by addition of IPTG to a final concentration of 1mM.

After four hours induction, the cells were collected by centrifugation (3000 rpm; 20 m; 4˚C). Samples were taken at each stage for analysis by SDS-PAGE.

2.2.3.c Small scale taste mGluR4 LBD purification

The cell pellet was lysed in buffer containing 10 ml 50 mM Tris-HCl (pH 8), 100 mM NaCl and 1 mM β-mercaptoethanol containing EDTA-free protease inhibitor cocktail (Roche), and then disrupted by sonication on ice. The cell lysate was centrifuged (120 000g; 4˚C; 40 m) to isolate inclusion bodies. The supernatant was loaded onto an equilibrated 2 ml Ni2+-NTA-Agarose column (Qiagen) and the pellet was dispersed in the lysis buffer containing 6M GuHCl and then shaken overnight (200 rpm, at 4˚C) and centrifuged again at (120 000 g, 4˚C, 40 minutes). After centrifugation the supernatant was loaded onto the Ni2+-NTA-Agarose column. The column was washed three times with three column volumes lysis buffer containing 5 mM imidazole. The protein was eluted in 200 mM imidazole.

2.2.3.d Protein detection

In order to detect the protein, the samples were separated by SDS-PAGE (Tricine 10-20% gels, Invitrogen, Novex). Two methods for protein detection were used: Coomassie brilliant blue staining and Western blot. Western blotting allows detection of epitope-tagged proteins in complex mixtures such as cell extracts and is more specific than Coomassie staining [138]. The anti-Express antibody (Invitrogen) was used to detect the truncated LBR of mGluR4. In *E. coli* there are histidine rich proteins, which reduce specificity of detection.

In Western blotting the electrophoretically separated proteins were transferred onto nitrocellulose membranes in a semi-dry system with transfer buffer. The membranes were blocked with 0.05% Tween/PBS (PBS-T) containing 5% non-fat milk for 1 hour at RT, followed by incubation with 1:5000 dilution of peroxidase-conjugated monoclonal mouse anti-Express IgG (Invitrogen) in 5% non-fat milk-PBS-T. After the incubation with the antibody the membranes were washed in 5% non-fat milk PBS-T 3 times for 5 m and 3 times for 15 m in PBS/T. ECL detection reagents (Amersham Pharmacia Biotech) were added to membrane for 1 minute and results were visualised by autoradiography. This clone resulted in an insoluble protein.

Alternative cloning strategies were looked into, because they can affect the choice of vector due to the need for restriction site and reading frame compatibility. Many pET vectors from Novagen share common restriction site configurations, which will make it possible to clone the target gene into several vectors with a single preparation of the insert. The reason the pET vectors were chosen is because these vectors can enhance solubility and or folding in one of three ways: 1) provide for fusion to a polypeptide that itself is highly soluble [e.g. glutathione-S-transferase (GST), thioredoxin (Trx), maltose binding protein (MBP)], 2) provide for fusion to an enzyme that catalyzes disulfide bond formation (e.g. Trx, DsbA, DsbC), or 3) provide a signal sequence for translocation into the periplasmic space (pelB, DsbA, DsbC). An alternative strategy to obtain active, soluble proteins is to use vectors that enable export into the periplasm, which is a more favourable environment for folding and disulfide bond formation. For this purpose vectors carrying signal peptides are used. DsbA and DsbC are periplasmic enzymes that catalyse the formation and isomerisation of disulfide bonds in pET-

39b (+) and pET40b (+). The His-tag sequence is very useful as a fusion partner for protein purification, and is optional in the pET vectors.

Several constructs with different fusion tags were made of the full length and LBD of both the rat putative taste receptor and the brain mGluR4 receptors. Since more than 16 clones were prepared, they are numbered for ease of reference and summarised in Table 5. Clones 4-8 are clones of the full length mGluR4s and 1-3 and 9-16 are clones of the ligand binding domain of mGluR4.

Table 5 Summary of the clones of mGluR4 prepared, the target sequence, the *E. coli* vector used, the fusion tags and the destination of the expressed protein.

Clone No	mGluR4 target sequence	Vector	Fusion Tags	Destination of Expressed Protein
3	Taste LBD	pCR T7/NT-TOPO	His6, Express	Cytoplasm
4	Full length receptor	pNTR1	MBP, TrxA, His10	Cell membrane
5	Full length receptor	pNTR1	MBP, His10	Cell membrane
6	Full length receptor	pNTR1	MBP	Cell membrane
7	Full length receptor	pNTR1	MBP, TrxA	Cell membrane
8	Full length, no C-terminal	pNTR1	TrxA, His10	Cell membrane
9	Brain LBD	pET-22 b(+)	His6	Cytoplasm
10	Brain LBD	pET-32 b(+)	TrxA	Cytoplasm
11	Brain LBD	pET-39 b(+)	DsbA, His6	Periplasm
12	Brain LBD	pET-40 b(+)	DsbC, His6	Periplasm
13	Brain LBD	pET-22 b(+)	His6	Cytoplasm
14	Brain LBD	pET21MBP	MBP	Cytoplasm
15	Brain LBD	pNTR1	MBP	Periplasm
16	Brain LBD	pNTR1	MBP	Periplasm

2.2.3.e Molecular biology of the full length mGluR4

Since the putative taste LBD of mGluR4 resulted in insoluble protein it was decided to use cloning strategies which will enhance solubility of the protein in the cytoplasm of *E. coli* or Generation of expression constructs. The cloning strategy of the full length mGluR4 was based on the strategy of Grisshammer for cloning of the neurotensin 1 receptor (NTR1), with which maximum 800 neurotensin receptor binding sites per cell are achieved [139]. For this strategy, in Clone 4 the full length mGluR4 gene was amplified by polymerase chain reaction (PCR) with primers 5MGLUR4 and 3MGLUR4. The PCR product was digested with *Bam*HI/*Eco*RV and cloned into the *Bam*HI/*Sma*I site of pNTR1 (MBP-N10-Tev-rT43NTR-N5G3S-Tev-G3S-TrxA-H10) to replace the NTR1. (ATCTGAGGATCCAAGCCCAAGGGTCACCCCCACATGAA) and (GCGTGTGATATCCGATGGCATGGTTGGTGTAGGTGACGTA) respectively, between the MBP and thioredoxinA (TrxA) fusions (Figure 2.3). The vector contains a lac promoter which is a very low expression promoter [139].

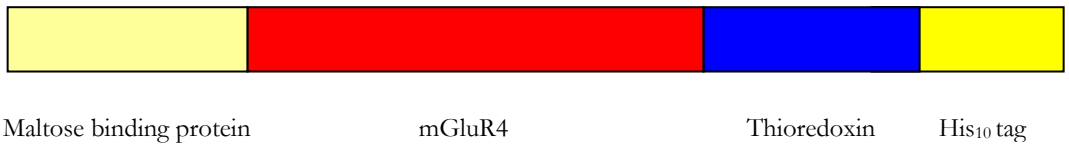

Figure 2.3 Schematic diagram representing the fusions used to express mGluR4 in the neurotensin vector

Another clone of the full length mGluR4 was Clone 5, in which mGluR4 with an N-terminal MBP and a C-terminal His tag fusion only has been cloned. The mGluR4 gene was amplified by PCR with 5MGLUR4 and 3MGluR4 primers, and like Clone 4 it was cloned into *Bam*HI/*Eco*RV site into pBluescript vector (Stratagene). pBluescript vector is a vector which is designed for propagation of the constructs and to simplify commonly used cloning and sequencing procedures. The fragment was digested from pBluescript with *Eco*RV and cloned in His-tag linker TGCATCACCATCACCACCATCACCATCACCATTAATAAGAT such that the stop codons are at the C-terminus. The fragment was cut out with *Sph*/*Hin*dIII and it replaced the *Bam*HI/*Sma*I fragment of construct 4.

Clone 6 is a clone of the mGluR4 receptor with an N-terminal MBP fusion and no c-terminal fusions. The mGluR4 gene was amplified by PCR using the 5MGLUR4 primer above and 3' primer 3GR4 (GCGTGTGATATCTCACTAGATGGCATGGTTGGTGTAGGTGACGTA) and cloned into the *Bam*HI/*Eco*RV site of pBluescript and then digested with *Sph*I/*Hin*dIII, the fragment was used to replace the *Sph*I/*Hin*dIII fragment in construct 4.

Clone 7 of the full length 'taste' receptor was cloned between MBP and TrxA fusion in the pNTR1. The gene was amplified by PCR with primers (5'-3') (ATCTGAGGATCCATGGGTTCTGATAGCTGGGGCTCCAAG) and 3MGLUR4 3' primer. It was cloned into the *Bam*HI/*Eco*RV site of pBluescript and then digested with *Bam*HI/*Sma*I and replaced the *Bam*HI/*Sma*I fragment of construct 4.

Clone 8 is a clone of mGluR4 with the C-terminal cytoplasmic domain removed, and the fragment was cloned between MBP and TrxA fusions in the pNTR1 vector. The gene was amplified with 5MGLUR4 and Terminated C-terminal primer (GCGTGTGATATCCGTTCTGCTCCGGGTGGAAGAGGATGATG), digested with *Bam*HI/*Eco*RV and cloned into the *Bam*HI/*Sma*I site of pNTR1 to replace the neurotensin 1 receptor.

2.2.3.f Expression of the full length mGluR4

Expression of clone 4 was tried in DH5α, BL21(DE3) and C43(DE3) competent cells. Methods of tighter induction control were looked into, which led to expression in Rosetta-gami 2 strain of competent cells. The Rosetta gammi competent cells are designed to enhance cytoplasmic disulfide bond formation and enhanced expression of eukaryotic proteins that contain codons rarely used in *E. coli*.

2.2.3.g Molecular biology of the of brain mGluR4 LBD

Several ligand binding domain (LBD) constructs were cloned and expressed in BL21 competent cells with rare tRNA plasmid.

Clone 9 is a clone of the LBD of the mGluR4 cloned into pET-22 b(+) (Figure 2.4) for export into the periplasm with no N-terminal fusion. The gene was amplified by PCR with full and 3prime primers (AGTACTGCGGATCCGAAGCCCAAGGGTCACCCCCACATGAA and

GATATCAAGCTTGGAGCGCGGCAGCTGCTGGCCAC) and cloned into the *Sma*I site of pBluescript. The clone was digested with *Bam*HI/*Hin*dIII and cloned into *Bam*HI/*Hin*dIII site of pET22b (+) (Figure 2.4) (Novagen) between the *Nde*I and *Hin*dIII. There was no N terminal fusion domain except for a few amino acids in order to take into account potential bacterial secretion inhibitory effect of positive charge in eukaryotic mGluR4 sequence within the first few amino acids after the signal peptide [140], and it contains a C-terminal His-tag. The full length ligand binding domain has a lot of positive charges at the beginning of the sequence; consequently the signal from the mRNA was omitted. The clone starts with the first amino acid of the protein sequence. It is homologous to the crystal structure of mGluR1 [141].

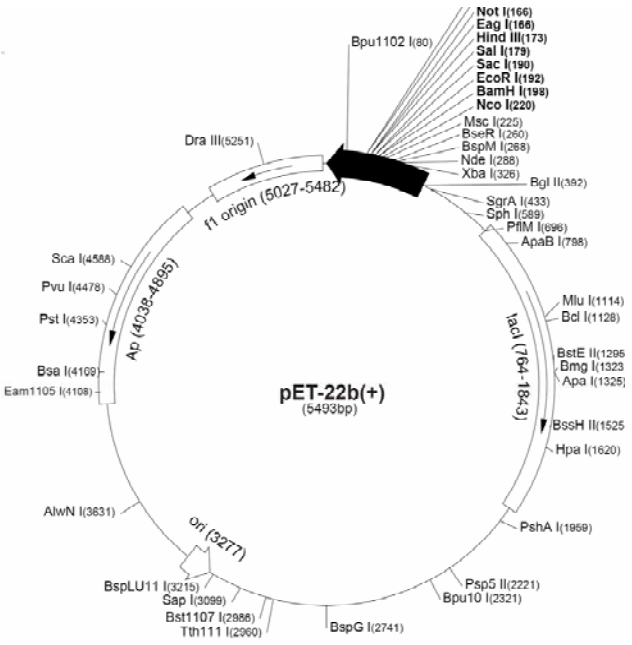

Figure 2.4 Vector map of pET22b (+) from Novagen. The pET22b (+) vector carries an N-terminal *pelB* signal sequence for potential periplasmic localisation, plus an optional C-terminal His tag [2].

Clone 10 is a clone of the ligand binding domain of mGluR4 cloned into pET32 (+) (Figure 2.5) for cytoplasmic expression with an N-terminal TrxA fusion. The mGluR4 gene was amplified with the Full and 3' primers (AGTACTGCGGATCCGAAGCCCAAGGGTCACCCCCACATGAA and GATATCAAGCTTGGAGCGCGGCAGCTGCTGGCCAC) and cloned into the *Sma*I restriction site of pBluescript. It was digested with *Bam*HI/*Hin*dIII and cloned into *Bam*HI/*Hin*dIII cloning site of pET32b (+).

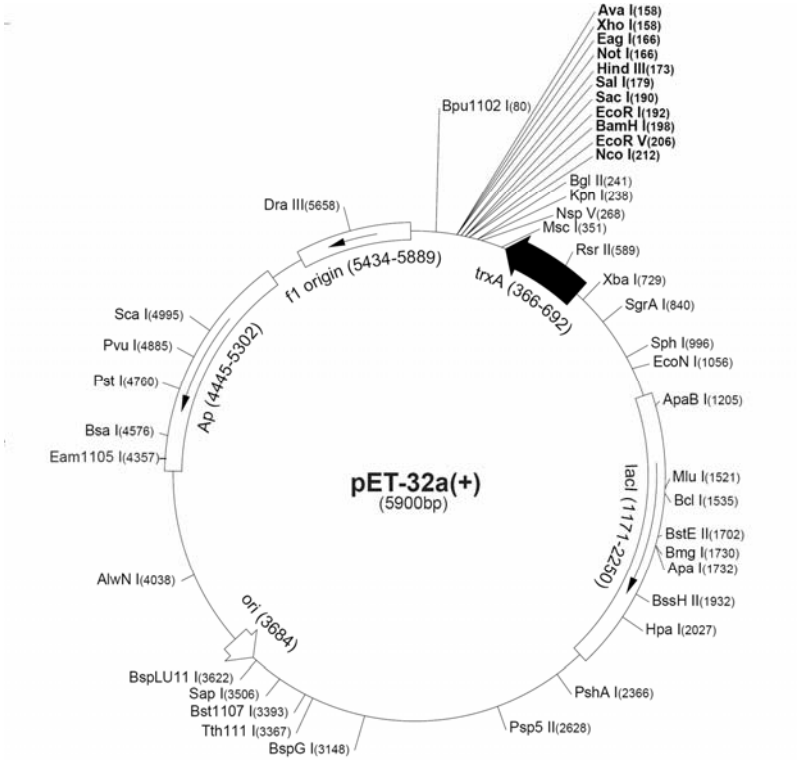

Figure 2.5 Vector map of pET-32a(+) (Novagen). This vector is prepared for high-level expression of polypeptides fused with the 109 amino acid thioredoxin (Trx) protein which aids solubilisation of proteins. Fusion proteins also contain cleavable His-tag [2]. The map of pET-32b(+) is the same as pET-32a(+) with the exception that pET-32b(+) is 5899 base pairs

Clone 11 is a clone of the mGluR4 ligand binding domain cloned into pET39b (+) vector for export into the periplasm of E.coli with a DsbA N-terminal fusion and C-terminal His-tag. The disulphide bond protein –DsbA can promote disulphide bonding and is exported via the co-translational export pathway. It may counteract any blocking of export due to rapid folding of the protein on the cytoplasmic side of the membrane. The mGluR4 gene was amplified by PCR with the Full and 3' primers (AGTACTGCGGATCCGAAGCCCAAGGGTCACCCCCACATGAA) and (GATATCAAGCTTGGAGCGCGGCAGCTGCTGGCCAC) and cloned into *Sma*I site of pBluescript. The fragment was digested with *Sca*I/*Hind*III and cloned into the *Sca*I/*Hin*dIII cloning site of pET39b (+) vector (Figure 2.6).

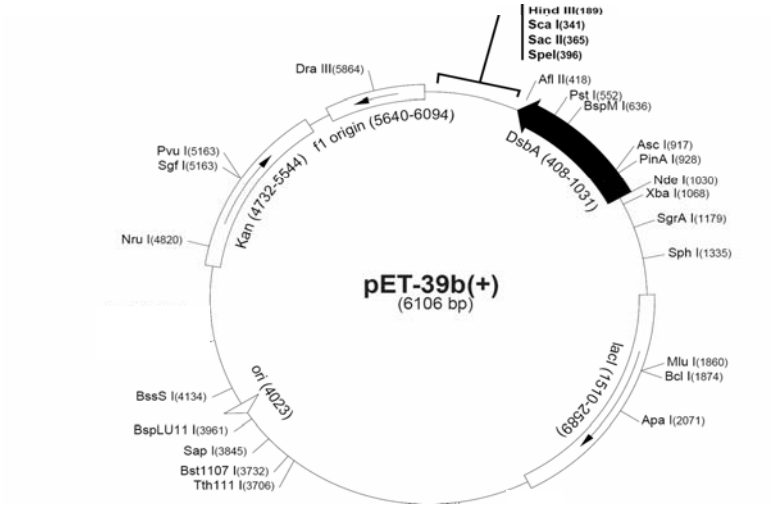

Figure 2.6 Vector map of pET-39b (+) from Novagen [2]. Vector pET-39b(+) is designed for expressing DsbA fusion proteins.

Clone 12 is a clone of mGluR4 ligand binding domain cloned into pET40b (+) for export into periplasm and contains a DsbC N-terminal fusion with C-terminal tag. mGluR4 was amplified with Full and 3' primers (AGTACTGCGGATCCGAAGCCCAAGGGTCACCCCCACATGAA) and (GATATCAAGCTTGGAGCGCGGCAGCTGCTGGCCAC) and clone into *Sma*I site of pBluescript. The fragment was digested with *Sca*I/*Hin*dIII and clone into the *Sca*I/*Hin*dIII cloning site of pET40b (Figure 2.7). In construct 12, pET40 vector was used which contains the DsbC N-terminal fusion with C-terminal His-tag. This fusion promotes rearrangement of incorrectly folded disulphide bonds and when attached to ScFv antibodies, can promote their correct folding and solubility [142].

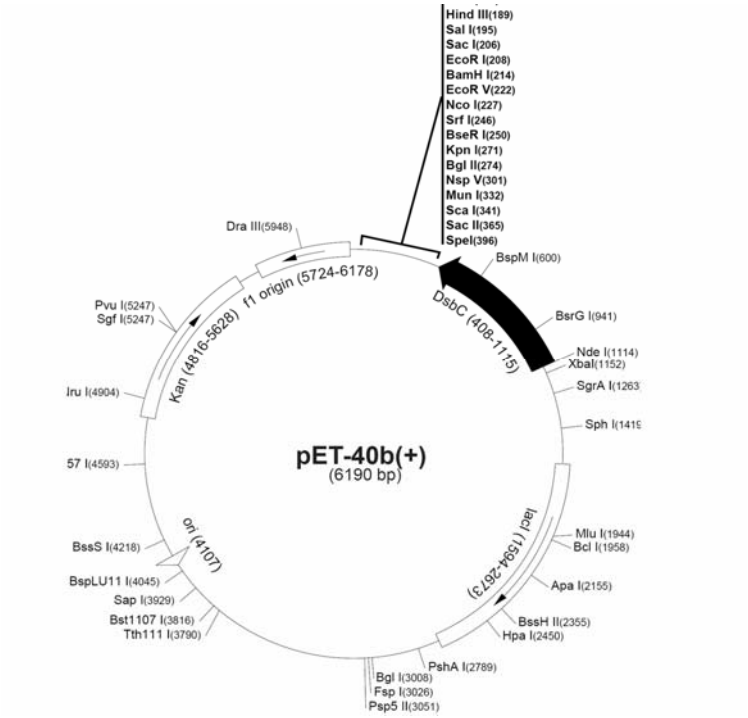

Figure 2.7 Vector map of pET-40b(+) (Novagen) [2]. The pET-40b(+) vector is designed for expression of DsbC fusion proteins.

Clone 13 is a clone of mGluR4 ligand binding domain with fusion tags cloned behind a T7 promoter for cytoplasmic expression in the pET-22b (+) vector. mGluR4 gene was amplified by PCR with new Full primer (AGTACTCATATGAAGCCCAAGGGTCACCCCCACATGAA) and 3' primer and digested with *Nde*I/*Hin*dIII, subsequently cloned into the pET-22b (+) (Figure 2.4) *Nde*I/*Hin*dIII site.

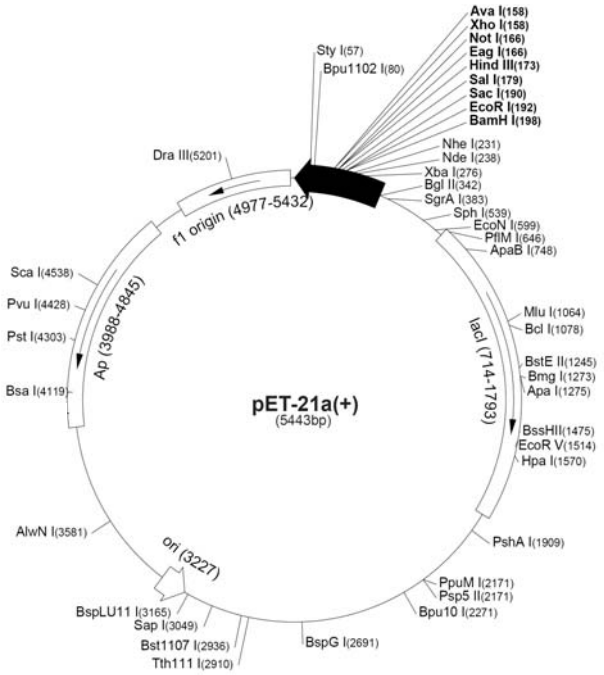

Figure 2.8 Vector map of pET-21a(+) from Novagen. pET-21a(+) carries an N-terminal T7 tag sequence plus an optional C-termianl His-tag. A C-terminal His-tag is available [2].

Clone 14 is a clone of mGluR4 ligand binding domain cloned behind a T7 promoter for cytoplasmic expression with an MBP N-terminal fusion in the p-ET21MBP vector. mGluR4 was amplified with Econde 5' primer (GAATTCCATATGAAGCCCAAGGGTCACCCCCACATGAA) and 3' newsal3 primer (GGTACCGTCGACGATCTTATCGTCGTCATCCTTGTAATCGTCGGAGCGCGGCA GCTGCTGGCCAC), digested with *Sal*I/*Eco*RI and cloned into the *Sal*I/*Eco*RI site of p-ET21MBP vector from Nie and colleagues [143].

Clone 15 is a construct of the mGluR4 ligand binding domain cloned behind the MBP fusion in the pNTR1 vector, so that it is exported as an N-terminal fusion with MBP into the periplasm from a lac promoter. mGluR4 was amplified with 5MGLUR4 and 3primenewsal3 primers, digested with *Kpn*I/*Bam*HI and cloned into *Bam*HI/*Kpn*I site of pNTR1 vector to replace the neurotensin 1 receptor.

Clone 16 is a clone of the mGluR4 ligand binding domain cloned behind the MBP fusion in the nts1 backbone vector so it is exported as an N-terminal fusion with MBP into the periplasm from a lac promoter with an increased hydrophobic signal peptide. The cloning strategy was the same as for construct 15 except that the signal peptide was altered using the primer CCTCGCATTATTCGCATTAATGCTGATGATGTTTTCCGCCTCGGCTCTCG.

Exporting the LBD behind a weak promoter (clone 15) was also tried. The same construct was used with a more hydrophobic signal peptide (clone 16) to try and divert the construct into the co-translational export pathway in case the protein was getting blocked in the membrane due to premature cytoplasmic folding [144].

Plasmids (10 ng) were amplified by PCR with Phusion polymerase from NEB. Volume of the total PCR reactions was 50 µl. The PCR parameters for the LBD of brain mGluR4 are listed in Table 6 below, the PCR reactions for the other clones were similar to this one, the only difference was the length of the extension time which depends on the number of base pairs that need to be amplified and the annealing temperature which depends on the melting temperature of the primers. The number of cycles was constant.

Table 6 Typical PCR parameters used for amplifying DNA fragments. The length of the annealing or extension cycles were modified depending on the length of the DNA amplified.

Step	Temperature (˚C)	Times (sec)	Cycles
Initial denaturation	98	30	1
Denaturation Annealing Extension	98 68 72	15 30 105	22
Final extension	72	300	1

The ligation reactions were carried out by running 5 µl of the completed PCR reaction on an agarose gel. The band was cut out and purified with a Qiagen PCR kit, the fragment was isolated. Ligation of the fragment to pET 22-b(+) was achieved with a NEB ligase. (30 ng) of backbone vector and twice as many molecules for the insert were used. The ligation reaction was left to incubate overnight at 14 °C.

Correct amplification and ligation were confirmed by DNA sequencing and expressed in BL21- Codon Plus (DE3)-RIL from Stratagene with 1 mM isopropyl-beta-D-thiopyranoside (IPTG) at 37ºC. This particular strain of competent cells was used due to its suitability for the T7 RNA polymerase promoters for high-level expression. The BL21-CodonPlus expression strains naturally lack the Lon protease, which can degrade recombinant proteins. They are deficient for the OmpT protease and contain a colE1 compatible, pACYC-based plasmid

which contains extra copies for rare tRNAs in *E.coli* such as argU, ileY leuW. In addition, BL21-CodonPlus (DE3)-RIL cells contain a gene that encodes endonuclease I (endA), an enzyme that rapidly degrades plasmid DNA isolated by most miniprep procedures, has been inactivated in these cells. There was no expression of this construct in either BL21 or C43. The rare codons AGG and AGA comprise 2% and 4%, respectively, of the arginine codons of *E. coli* K-12, and their cognate tRNAs are sparse. High AG content interferes with expression because frame shift can occur.

2.2.3.h Expression of the brain mGluR4 LBD

Cultures were grown in 2x YT medium supplemented with the appropriate antibiotic for each vector and grown until A_{600} ~1. Induction was initiated with the appropriate level of IPTG. After 4 h incubation at 37 °C cells were harvested for analysis.

For the periplasmic expression cells were transformed by electroporation. The vector carrying the mGluR4 sequence was introduced into the host cells by applying an electric pulse of 1.450 Volts during 6.5 ms. The sample was then quickly placed in LB media containing 10 mM $MgCl_2$ and shaken for 1 h at 37 °. Aliquots of the cultures were plated on agar plates supplemented with 1% glucose, 75 μg/ml streptomycin, 34 μg/ml chloramphenicol and 100 μg/ml ampicillin. The next day, starter cultures were prepared by inoculating 15 ml LB media supplemented with 2% glucose and the appropriate antibiotics and shaken at 180 rpm in an orbital shaker at 37 °C. Once grown the starter cultures were transferred into 500 ml 2xYT media flasks supplemented with antibiotics and 0.2% glucose. The OD of the growing cultures were checked regularly and when they reached OD600 of 0.5, were induced with 0.25

mM IPTG and the temperature was decreased from 37 °C to 20 °C and the cultures were left overnight.

2.2.3.i Periplasmic isolation

Once the cells reached an OD600 ~2, the cells were harvested by centrifugation (6000 g, 15 min, 4 °C). The supernatant was removed and the cells were washed and resuspended into 6 ml of 10 mM Tris, 150 mM NaCl, pH 8.0. The prep was centrifuged (6000 g, 15 min, 4 °C), the supernatant removed and the pellet was resuspended in 8 mM Tris, 3 mM EDTA, 20% sucrose and 20 µl of 1mg/ml lysozyme was added and 0.6 ml of ice cold water were added. The solution was left at RT for half an hour, then centrifuged (10000 g, 45 min, 4 °C) and the periplasmic fraction is in the supernatant, whereas the cytoplasmic fraction is the pellet.

The periplasmic fraction was collected and centrifuged (100 000 g, 30 min, 4 °C) in order to remove remaining pieces of membrane and cell debris. Samples were taken from each fraction for Western blot analysis.

2.2.3.j Western blot analysis

4-12% Tris-Glycine (Invitrogen) SDS-PAGE was conducted on the samples of the soluble and insoluble parts of the cytoplasmic and periplasmic fractions. The proteins were transferred onto a nitrocellulose membrane and Western blotted.

2.3 Results and Discussion

2.3.1 Ligand studies by solid state NMR

2.3.1.a ^{13}C CP MAS solid-state NMR of L-glutamic acid

In Figure 2.9 the ^{13}C CP MAS spectrum of crystallised L-glutamic acid is shown. Resonances of the two carboxyl carbons and the Cβ-Cγ carbons respectively are very close to each other. It may be necessary to use higher magnetic field, higher MAS frequency and high proton decoupling power to resolve fully these two peaks.

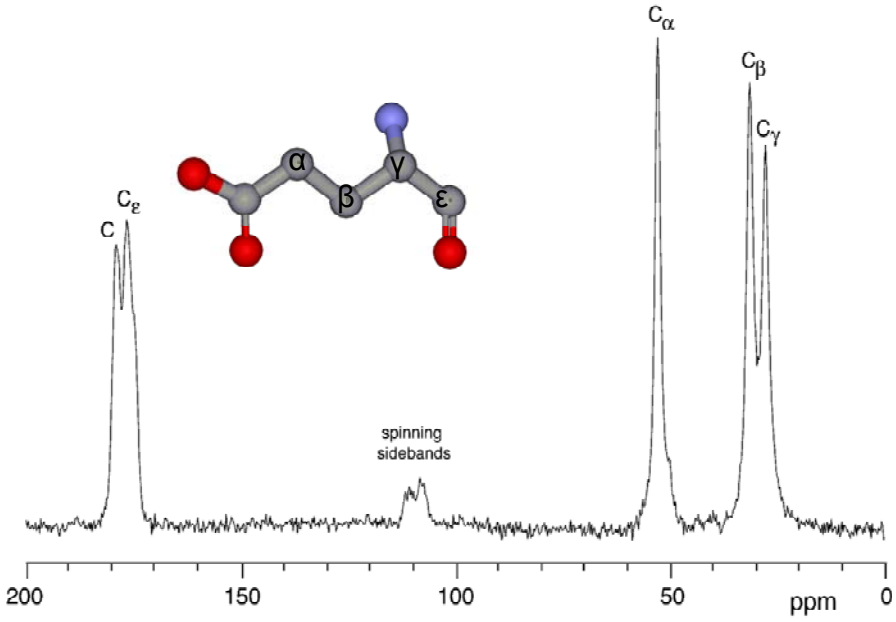

Figure 2.9 ^{13}C CP-MAS natural abundance spectrum of crystallised L-glutamic acid (BDH Chemicals) recorded on a 400 MHz Varian/Magnex spectrometer. The CP-MAS experimental conditions were ω_r= 7 kHz, contact time 2.5 ms. Proton decoupling during acquisition was 70kHz, 2.0 s pulse delay time and 1023 complex date points were obtained, 1755 scans were collected, resolution 124 Hz. Resonances of the two carboxyl carbons and the C_β and C_γ carbons respectively are very close due to the symmetry of the molecule

2.3.1.b ^{15}N CP MAS solid-state NMR of L-glutamic acid

The ^{15}N CP MAS spectrum of ^{15}N labelled L-glutamic acid is shown in Figure 2.10. There is only one ^{15}N resonance. The chemical shift is very sensitive to the local environment of the nucleus, when the ligand will be bound to the receptor; a shift of the ^{15}N chemical shift is expected, due to changes in local environment.

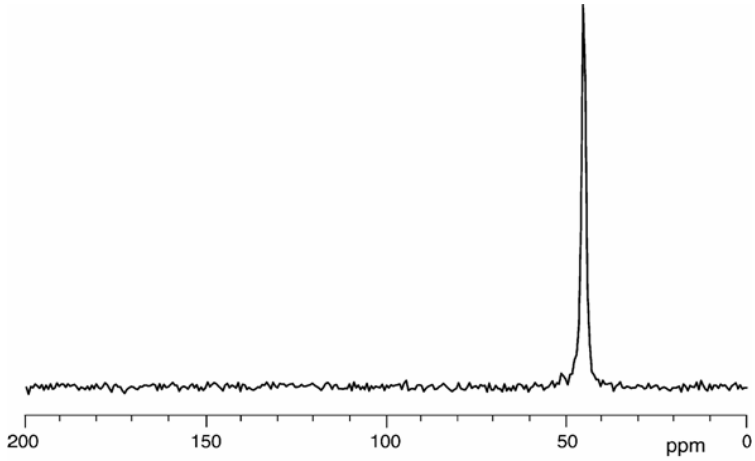

Figure 2.10. ^{15}N CP-MAS spectrum of crystallised ^{15}N uniformly labelled L-glutamic acid. Experimental conditions were: ω_r= 7 kHz, 2.0 ms contact time, 5000 scans, resolution 106 Hz, 2048 complex data points

The ^{17}O solid-state NMR spectrum from L-glutamic acid shown in Figure 2.11 contains two main resonances. Each resonance is composed of two strongly overlapping lines. There is a large increase in the resolution of the spectrum by employing the Oldfield echo coupled with strong decoupling. The spinning speed of 20 kHz can be identified from the spinning side bands. The assignment of the spectrum is shown in different colours. Although all 8 sites cannot be resolved completely, inspection of the spectrum shows that the oxygens occupy four

pairs of very similar sites. Higher resolution techniques than MAS are necessary to reveal the differences. The ability to resolve the different sites and detect bonding changes suggests ^{17}O solid-state NMR can be used for biochemical investigation on ligand-receptor interaction as planned here, and shown for a membrane embedded peptide [128].

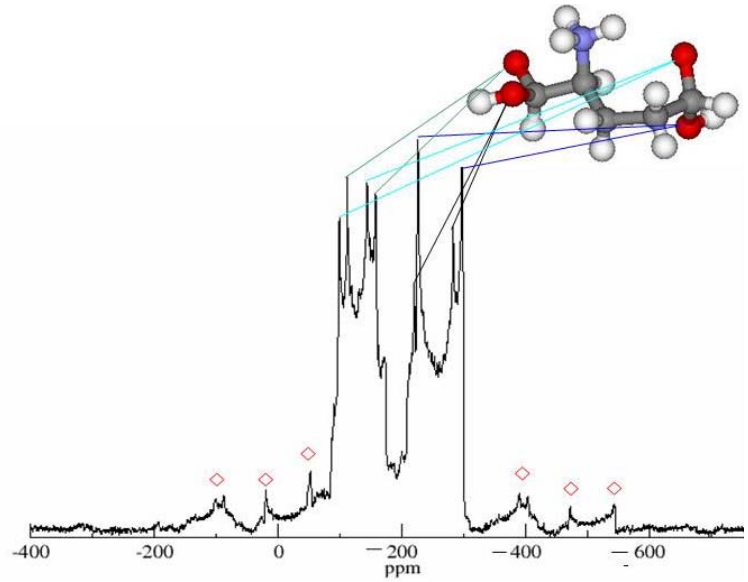

Figure 2.11 ^{17}O MAS NMR (14.1 T) spectrum of L-glutamic acid hydrochloride. MAS at 20 kHz, proton XiX decoupling during acquisition was 130 kHz, 20000 acquisitions were recorded, the pulses were 50 µs apart with an echo period of one rotor period. The XiX-scheme decoupling utilised 1.85 rotor periods and for the 90° pulse ~ 120 kHz was used and for the 180° ~16 kHz. The spectrum contains 20Hz exponential broadening and represent spinning side-bands

2.3.2 Homology modelling

2.3.2.a Model generation and validation

The sequence alignment, which was performed by Clustal X [145] and the results are shown in Figure 2.12. The structural data from the template in a PDB form, file name 1EWK was used

to predict the mGluR4 homology model. Initially, 20 models were constructed for the truncated extracellular region of mGluR4 using MODELLER [130].

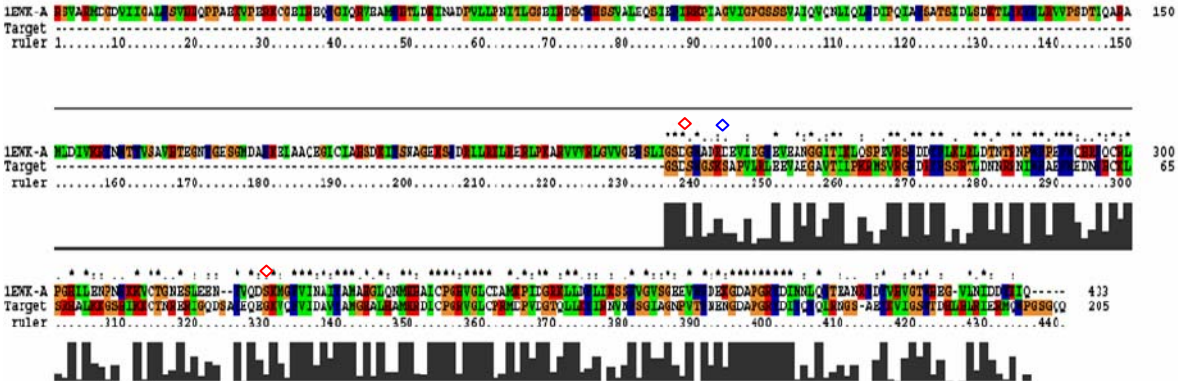

Figure 2.12 Sequence alignment of the LB regions of mGluR4 with mGluR1. Heights of the bars show the magnitude of homology. The alignment was realised by CLUSTAL X. The red square represents the conserved amino acids in the ligand binding site and the blue square represents the mutated residue involved in binding the ligand.

The Z-score of the generated models is -5.17 to -5.39 (Table 7). Because the template is 183 amino acids long, the Z value should be between -4.5 to -8. The homology models are within the observed range of values. Low Z-score of a model means that the model has a good quality of protein structure. Zp is a Z-score of protein and Z_1 is Z-score of fragment of low energy found in the protein. Zp-comb is the overall Z score and for the models.

Table 7 Z-scores of the chosen models

mGluR4 homology model number	Zp-combined
6	-5.22
15	-5.39
18	-5.17

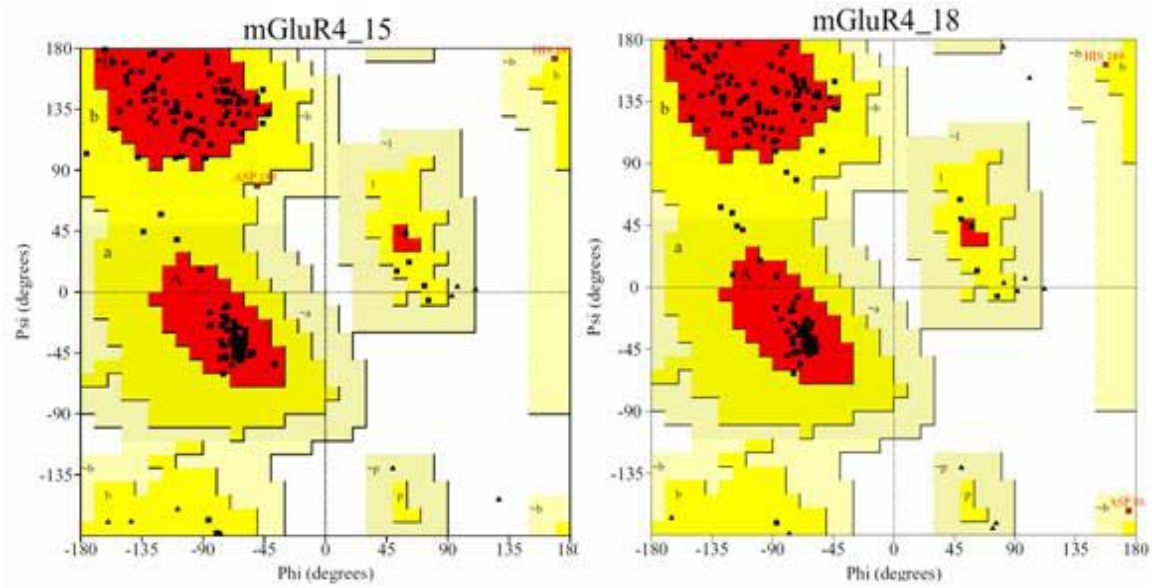

Model	mGluR4_15	mGluR4_18	mGluR4_6
Core	89.3%	89.8%	90.4%
Allowed	9.6%	9.0%	9.0%
Disallowed	0.0%	0.0%	0.0%
Bad contacts	2	3	5
G Dihedral angles	0.02	0.00	0.01
G covalent	-0.20	-0.18	-0.21
G overall	-0.06	-0.06	-0.07

Figure 2.13 Ramachandran plot of the mGluR4 LBR homology model. Glycine residues are shown as triangles; all other residues are represented as squares. No residues are found in the disallowed regions and the residues have about 90 % of the phi and psi backbone torsion angles within the most favoured region. A single letter code identifies which region of the Ramachandran plot the residue is in. For end residues and glycines this assignment does not apply.

Considering the results of several evaluation programs, model 15 shown in Figure 2.14 was chosen as the final model for the truncated LBR of mGluR4 based on homology with mGluR4.

The Ramachandran plot of the predicted models (Figure 2.13) after energy minimisation was calculated with PROCHECK and revealed a rather good stereochemistry, judging by the values of the torsion angles.

2.3.2.b Visual assessment of models

Visual inspection was performed using the graphic viewers PyMol and Accelerys DS ViewPro 5.0. Direction of the residues especially those surrounding the binding site were examined.

Table 8 Comparison of values for the stereochemical parameters and G factors given by PROCHECK for the homology models of the truncated of LBR of mGluR4

Model	Core	Allowed	Disallowed	Bad contacts	G Dihedral angles	G covalent	G overall
mGluR4_15	89.3%	9.6%	0.0%	2	0.02	-0.20	-0.06
mGluR4_18	89.8%	9.0%	0.0%	3	0.00	-0.18	-0.06
mGluR4_6	90.4%	9.0%	0.0%	5	0.01	-0.21	-0.07

Models were selected according to their low G factors, low disallowed positions of the amino acid residues and high percentage of amino acids in the allowed region. They were also checked for the position of bad contacts. The model with the lowest G factor value was not chosen as the best model because it contained a lot of bad contacts (Table 8). Bad contacts are defined as any pair of non-bonded atoms that are at a distance of ≤ 2.6 Å from one another.

For the other models a check was made to ensure that the bad contacts were not in the binding site.

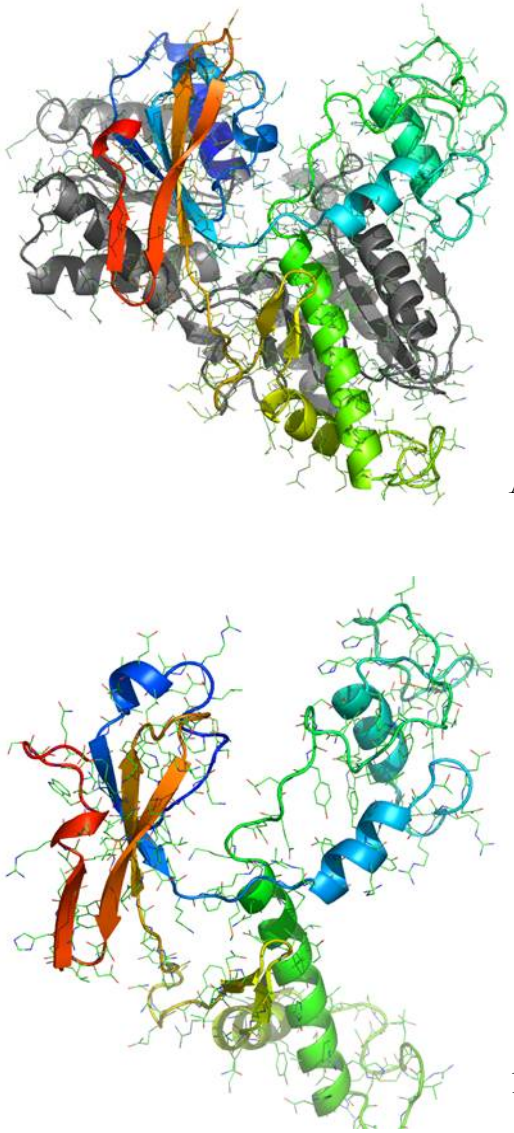

Figure 2.14 Three dimensional side view of A the LBR of the putative mGluR1, the template. The structures represented with grey colour are the truncated residues. B the truncated LBR of mGluR4 homology model generated by MODELLER6v2. The figure was generated by PyMol.

Once ss NMR data for ligand-bound structure (distances and conformation) is obtained, it could be used to refine the ligand, receptor and the ligand-receptor structure. The 3D model allows investigation of the binding pocket and which residues interact with the ligand. Once the key residues are identified, based on the mGluR1 studies and NMR data, further research can be done on which part of the residues interacts and what type of interaction is involved. Glutamate is a negatively charged amino acid so the receptor likely has a positively charged residue which has been confirmed with analysis of the sequence alignment. Residue K409 has a positive charge, which interacts with the oxygen from glutamate in mGluR1 and probably a hydrogen bond interaction involved which should be visible by SS NMR. In the taste mGluR4 nine out of fourteen residues that are important in ligand binding are truncated. Two conserved residues in all mGluRs, D318 and K409, have not been removed by truncation. However, in mGluR4 residue R323 has been substituted with K323. This mutation may contribute to the lower affinity of the putative taste GluR4 for the ligand compared to the brain mGluR4.

2.3.3 Molecular biology of mGluR4

The mGluR4 protein is a structurally uncharacterised member of the metabotropic glutamate receptor family. Structural studies by solid state NMR require high amount of protein, in the mg range. This section presents and discusses the results of cloning and expression studies of mGluR4. The cloning of the full length and the LBD of mGluR4 was done by Dr Simon Ross, after the cloning strategy was discussed. The results of only the putative taste mGluR4 will be presented here. The clones of the LBD will be discussed only, since all produced insoluble protein.

The full length mGluR4 protein was expressed in the neurotensin receptor plasmid. Depending on the growth conditions varying degrees of degradation were seen. Expression yield was increased by co-expressing a plasmid which provides rare bacterial tRNAs. At that stage expression was very toxic and inhibited cell growth when induced. The temperature was reduced down to as low as 15 °C to reduce toxicity, using none or low amounts of inducer but the result was the same in that a plateau of expression was reached which then stopped the cell growth. The level of protein expression was very low. The full length protein was detectable using anti His-tag antibodies. The expression of the 'taste' version of mGluR4 between the maltose binding protein (MBP) and TrxA fusions in the pNTR1 vector was also tried. It resulted in same low level expression. The TrxA tag was taken off the C-terminus of the full length mGluR4 construct and replaced with no tag or His-tag to no great effect on the overall expression levels of the protein.

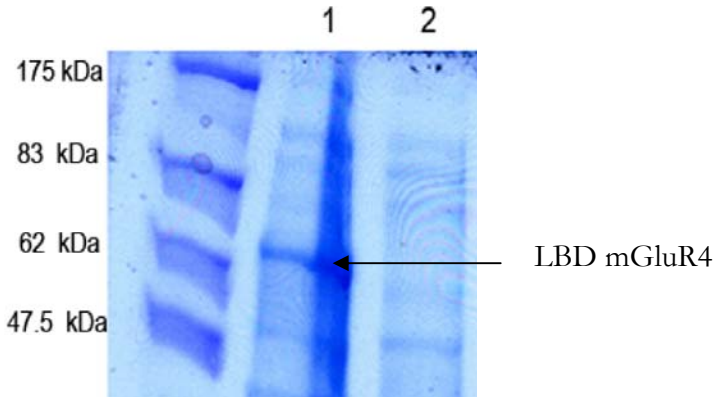

Figure 2.15 Coomassie stained SDS-PAGE of the brain LBD mGluR4 in pET22 Novagen vector expressed in Rosetta-gami 2 cells. The receptor was in lane 1, which is the insoluble fraction, whereas lane 2 is the soluble fraction. The cells were induced overnight at 25 °C with 0.02 mM IPTG.

The LBD of mGluR4 with various fusions to control expression in the cytoplasm or periplasm were used (Figure 2.15). For the expression in the cytoplasm, Origami™ competent cells were used. For expression in the periplasm mGluR4 was expressed as a fusion protein in *E. coli* BL21(DE3)RIL competent cells (Stratagene) from the pNTR1 vector. Chaperon proteins are required to ensure that the refolding of mGluR4 will take place. Therefore, pTum4 helper plasmid was used, which codes for 4 established periplasmic molecular chaperones and folding catalysts: the thiol-disulfide oxidoreductases DsbA and DsbC that catalyse the formation and isomerisation of disulfide bridges and the petydil-prolyl cis/trans isomerase with chaperone activity, FkpA and SurA. Another helper plasmid was introduced into the competent cells, pRARE plasmid which contains the genes that encode transfer RNA for the rare codons in *E. coli*: AGA, AGG (Arg), GGA (Gly), AUA (Ile), CUA (Leu), CCC (Pro). Two controls were used to check that the protein was expressed in the periplasm.

The most promising result was obtained with clone 15. In this clone mGluR4 is ligated into the pNTR1 vector with an MBP fusion at the N-terminus and a membrane-targeting signal peptide targets it in the periplasm. The pNTR1 has the *lac* promoter which is a weak promoter. pTUM4 for expression of chaperones and pSC101 (streptomycin alternative to the pRARE plasmid for rare tRNA, different selection gene and origin of replication had to be considered) were transformed into the competent cells. The presence of pTUM4 seemed to make a big difference.

The Western blot (Figure 2.16) indicated that the protein gets into the periplasmic space but the protein could not be isolated and purified.

For the cytoplasmic expression constructs with MBP and TrxA were made, which resulted in insoluble mGluR4. The yeast *Pichia pastoris* was used to express the full length mGluR4 without success, possibly due to codon incompatibility of the recombinant mGluR4 with the host *P. pastoris*. The cloning and expression of mGluR4 in *P. pastoris* was attempted by L. Grgic from Roslyn Bill's group at Aston University, Birmingham.

2.3.3.a Molecular biology of the full length mGluR4

The mGluR4 was amplified by PCR using gene-specific primers. The gene was cloned into the pNTR1 vector. The expression of mGluR4 protein was tested in DH5α, BL21(DE3) and C43(DE3) and analysed by Western blot analysis with an antibody derived against the hexa-histidine tag. Only in C43(DE3) competent cells with pREP-4 plasmid expression could be detected with anti-MBP antibody. The transformation of the clone repeatedly resulted in many small and few large colonies. Toxicity was reduced by adding 0.2% glucose to the 2 YT media [146]. Addition of 0.2% glucose prevented the appearance of two different size colonies. No large colonies were observed, only small uniform colonies.

Due to codon bias when expressing heterologous proteins in *E. coli*, in this case arg and agg codons which code for arginine are rare in *E. coli* [147], codon usage of the rat mGluR4 gene had to be optimized. Plasmid pRARE2 which encodes tRNAs for mammalian codons that rarely occur in *E. coli* was used. It enhanced the expression level of the protein in C43 (DE3) competent cells which was limited by codon usage and it restored it in Rosetta 2 (Novagen) cells. The expression level improved with supplementation of rare tRNAs, but it made the

increase in concentration of the protein toxic for the cell. The cells stopped growing when induced with higher concentrations of IPTG. Toxicity was troubleshooted by addition of 2% glucose and varying the temperature (15º, 20º and 25 ºC) during expression. Samples were taken at 4, 5, 20 and 40 h after induction and different IPTG concentrations 5, 35 and 250 μM were tested.

The use of benzyl alcohol in order to induce chaperon networks was tested to improve expression [148]. PMSF in growth media was used to try and stop degradation but there was no positive effect. Induction at OD600 0.9 for 4 h was tried. Different carbon sources were not tested. 2 YT media with 0.2% glucose was used only [146]. Optimal yield was achieved by leaving the colonies uninduced overnight. The level of expression was $1/25^{th}$ of the neurotensin receptor expression, which was too low to obtain enough material for a binding assay. The expression of the full length putative 'taste' mGluR4 was also tried between the MBP and TrxA fusions in the same plasmid resulting in the same low level expression yield.

2.3.3.b Molecular biology of the ligand binding domain of brain mGluR4

Construct 13, a clone of the LBD with no fusion tags, was insoluble when expressed in the cytoplasm. The protein obtained from this clone was used for *in vitro* refolding trials. In construct 14, the mGluR4 LBD was cloned behind MBP and expression was tried in the cytoplasm using the same vector used for successful expression in the cytoplasm of *E. coli* of a LBD of a class C GPCR [143]. Induction at 37 °C with 0.1 mM IPTG resulted in expression of insoluble protein. Lower IPTG concentration was tried (0.05 mM) at 20 °C in Rosetta-gami (DE3)pLysS competent cells from Novagen. These cells contain rare tRNA plasmid and allow

disulphide bond formation in the cytoplasm. Another strain of competent cells that was tried for expression was BL21(DE3)RIL from Stratagene, which contain 3 rare tRNAs (arginine, isoleucine and leucine). The constructs were all again insoluble. Construct 14 was expressed in C43(DE3) with pRARE2, but it resulted in insoluble protein.

The expression of the LBD constructs was also tried in BL21 cells with pSC based rare tRNA plasmid with and without sorbitol and pTUM4 [149]. Plasmid pTUM4 expresses 4 established periplasmic chaperons and folding catalysts: the thiol-disulfide oxidoreductase DsbA and DscC that catalyse the formation and isomerisation of disulfide bridges and the peptidyl-prolyl cis/trans isomerases with chaperon activity, FkpA and SurA. A combination of Dsb co-expression and sorbitol has been shown to enhance soluble expression of Dsb co-expression of scFv antibodies in *E. coli* [150]. pTUM4 at 20 °C and 0.25 mM IPTG had dramatic effect on the solubility of the products with the majority in the soluble fraction, but degradation was present. When only the periplasmic proteins were isolated, it was found that the large majority of the product remained associated with the membrane. Purifying the periplasmic protein on His-tag column was tried, but the eluate showed many bands on a gel.

2.3.3.c Periplasmic expression of mGluR4

The periplasmic expression of the LBD of mGluR4 requires helper plasmid which provides tRNAs and chaperone proteins, which are not native in the host cell. The periplasmic and cytoplasmic fractions had to be separated carefully for analysis of their contents.

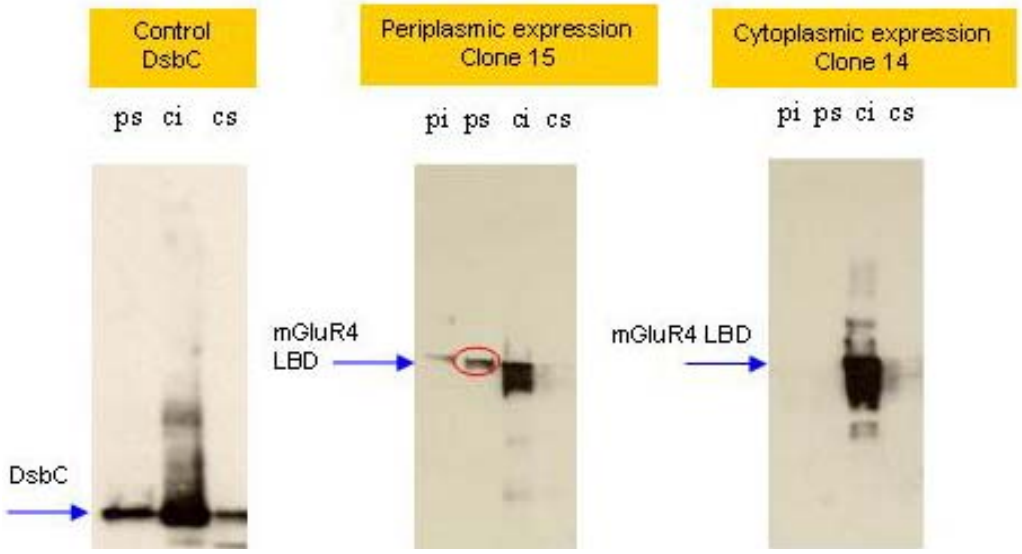

Figure 2.16 Western blot of expression of the molecular chaperone DsbC, clone 15 - the periplasmic construct of mGluR4 LBD coexpressed with DsbC and clone 14 - the cytoplasmic construct of mGluR4 LBD expressed without DsbC. The control of DsbC expression only indicates that the DsbC was expressed in the periplasm and that the soluble periplasmic fraction (ps) was successfully isolated from the soluble and insoluble cytoplasmic fractions (denoted ci and cs, respectively). The receptor was found in large quantities in the insoluble cytoplasmic fraction as well as in small amount in the periplasmic insoluble fraction (pi). The expression of clone 14- the cytoplasmic construct of mGluR4 LBD, resulted in solely insoluble protein in the cytoplasmic fraction and it shows that no mGluR4 was exported to the periplasm without the helper plasmids which codes for DsbC. The expression of the periplasmic construct of mGluR4 LBD-clone 15 did produce receptor in a soluble state in the periplasm (circled in red), and a small fraction was present in an insoluble state in the periplasm, however most of it was insoluble in the cytoplasm.

In Figure 2.16, Western blot analysis of two clones of mGluR4 LBD: clone 15 and clone 14 and a control in which the chaperone DsbC is expressed on its own are shown. The same figure shows the isolated soluble and insoluble fractions of the cytoplasm and periplasm of *E. coli* in which clone 15 was expressed. In the control, DsbC was transported to and expressed in the periplasm, although high concentration of the protein was found in the insoluble fraction of the cytoplasm. In addition the control confirms that the periplasmic isolation was efficient.

The control in which only the cytoplasmic construct of mGluR4 was expressed confirms that mGluR4 cannot be exported to the periplasm without helper plasmids. A fraction of the expressed mGluR4 was found as soluble protein in the periplasm but a large part remained in the cytoplasm. It seems that the transport mechanism across the inner membrane of *E. coli* becomes saturated before all the expressed mGluR4 is transported to the periplasm. Improving the transport to the periplasm and increasing the yield of soluble mGluR4 LBD will constitute future work for this project.

2.3.3.d Molecular biology of the ligand binding domain of the putative taste receptor

The DNA agarose gel (Figure 2.3) showed two inserts, the upper one, 2.8 kbp corresponds to the size of the vector and the lower one, ~620 bp corresponds to the size of the insert. The Coomassie stained gel showed an over-expressed band of the right size, which was not present in the negative control (Figure 2.18). The negative control consisted of cell lysate from BL21(DE3) grown under the same conditions, but without the gene.

The Western blot Figure 2.19 confirmed a band of the right size (30 kDa), and a band with a smaller intensity which corresponds to a dimer.

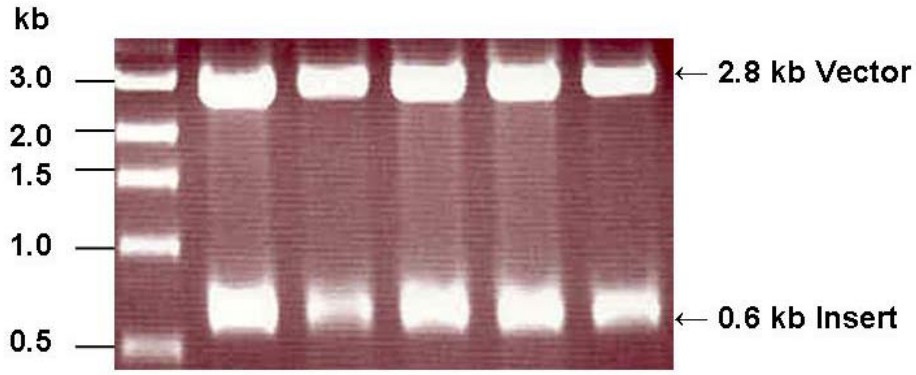

Figure 2.17 Agarose gel showing the results from the double digest with *Bam*HI and *Eco*RI of pCR T7 /NT-TOPO containing the ~618 base pairs long truncated version of the extracellular soluble part of mGluR4, from minipreped plasmid DNA. The first lane on the left is a 1 kb DNA (New England BioLabs).

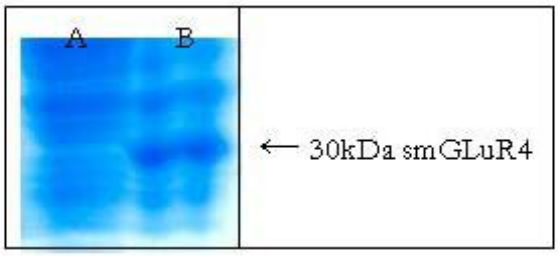

Figure 2.18 Coomassie stained SDS-PAGE gel of cell lysates of BL21(DE3) *E. coli* strain. Detection of the truncated ligand binding domain was done by Coomassie brilliant staining. Sample A is a negative control, BL21(DE3) without the plasmid. Sample B is the cell lysate of BL21(DE3) expressing the soluble domain of mGluR4 taste LBD. The overexpressed mGluR4 (30 kDa) is seen as a darker band where as in the negative control it is missing.

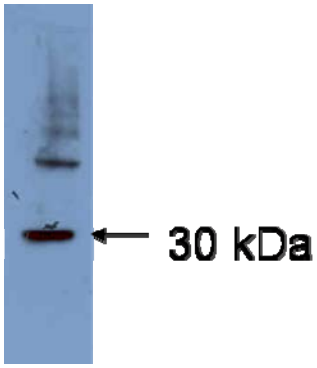

Figure 2.19 Western Blot using monoclonal anti-Express antibody (Invitrogen) shows a protein of 30 kDa, which corresponds to the protein of interest. Band of higher molecular weight (about 60 kDa) are possible dimers, and subsequent higher bands must be multimers of the protein. The Express epitope is very specific for the Express tag.

2.4 Conclusions

A homology model of the LBD of mGluR4 was constructed based on the crystal structure of the closed confirmation of the LBD of mGluR1 bound to glutamate (pdb code: 1ewk). This structure was chosen because the protein was going to be cloned, expressed and then studied by solid state NMR bound to the ligand. Distance measurement of a small molecule bound to a receptor is limited by the strength of the dipolar coupling, therefore distance range that can be covered is 1-15 Å [151]. Modelled structures can be useful for identifying suitable sites for NMR labels, either by giving the distance between the nuclei or by predicting which residues will be involved in the binding site. The homology model of the mGluR4 LBD was eventually going to be refined with experimental data.

The L-glutamic acid was characterised by ^{13}C, ^{15}N and ^{17}O MAS solid state NMR. Even if the receptor protein cannot be obtained in isotope-labelled form, it will still be possible to study

ligand-binding to the receptor [43]. Advantage can be taken of the high sensitivity of the isotopic NMR resonance frequency to local structure, like Cα and Cβ chemical shifts $\delta_{C\alpha}$ and $\delta_{C\beta}$ which are particularly sensitive to the protein backbone conformation [152, 153] and may be used to obtain conformation-dependent chemical shifts in the solid-state. The natural abundance of ^{13}C is about 1%; consequently it can be used combined with a few labelled sites for one-dimensional cross polarisation. If the protein can be obtained in isotope-labelled form either selectively or uniformly, the studies can be extended to the structure of the protein itself.

The LBR of the brain and taste mGluR4 have been cloned successfully and its expression yielded relatively high amounts of LBR mGLuR4. Despite cloning several clones of the LBD of mGluR4 with various fusions to improve solubility and aid refolding most of the clones resulted in insoluble protein.

The full length of the brain and taste mGluR4 protein were expressed in the neurotensin receptor plasmid-pNTR1 the expression was toxic consequently the level of expression was very low. Removal of the TrxA tag from the C-terminus of the full length mGluR4 construct and replaced with no tag or His-tag to no great effect on the overall expression levels.

Even expression in specifically tailored competent cells to aid insoluble proteins did not make a difference. In *E.coli* the yield of the LBD of mGluR4 was always high, but the protein was in most cases insoluble. The most promising result was obtained with the periplasmic construct for which the Western blot indicated that the protein is transported into the periplasmic space

but the protein could not be isolated and purified. Preparation of inclusion bodies and screening for optimal refolding conditions is described in the next chapter, Chapter 3.

The yeast *Pichia pastoris* was used to express the full length mGluR4 without success, possibly due to codon difference of the recombinant mGluR4 with the host *P. pastoris*.

Chapter 3 Refolding of mGluR4

3.1 Introduction

3.1.1 Expression of protein into inclusion bodies

Successful expression and purification of proteins in an active form is essential for structural and biochemical studies. General expression systems on the basis of host used are bacterial, insect, yeast, and mammalian. Bacterial expression systems are often used because they deliver the highest protein yield per volume of culture. *E. coli* remains the first host choice for expression due to its speed, simplicity [154] and usability such as for NMR labelling. However, due to high-level expression and simple protein folding machinery, proteins obtained from bacteria are typically found to be insoluble, forming dense aggregates of misfolded polypeptide termed inclusion bodies (IBs) [155]. Inclusion body proteins are devoid of biological activity and need elaborate solubilisation, refolding and purification procedures to recover functionally active product [156-158]. Although protein expression in the form of IBs is often considered undesirable, their formation can be advantageous because the protein is expressed in high yield, more than 30% of the total protein content of the cell in some cases, and the IBs can be isolated easily from the cell due to differences in their size and density. They are less susceptible to proteolytic degradation by proteases and are more homogenous which reduces the number of purification steps to recover pure protein.

3.1.2 Characteristics of protein aggregates in inclusion bodies

IBs are found both in the cytoplasmic and periplasmic spaces of *E.coli* during high-level expression of heterologous protein. Non-native proteins, especially highly hydrophobic ones, are more prone to accumulation in IBs [159].

Proteins having disulfide bonds are expected to form IBs as the bacterial cytosol is reduced and inhibits formation of disulfide bonds. Inclusion bodies have higher density (~1.3 mg ml^{-1}) than many of the cellular components [159-161], thus they can be easily separated by high-speed centrifugation after cell disruption. IBs, despite being dense particles, are highly hydrated and have a porous architecture [160, 162]. They contain very little host protein, ribosomal components or DNA/RNA fragments [163, 164]. Their formation in *E. coli* is reported to be due to an unbalanced equilibrium between aggregated and soluble protein [165]. Significant features of protein aggregates in IBs are the existence of native-like secondary structure of the expressed protein and resistance to proteolytic degradation. Purification of the IBs can be achieved by washing with detergents, low concentrations of salt and urea [160, 166, 167]. The presence of contaminating proteins reduces the refolding yield of denatured proteins, isolation and purification of IBs to homogeneity before solubilisation improves the recovery of bioactive protein from IBs [154].

3.1.3 Preparing purified and denatured protein

Methods for preparing denatured protein involve isolation of inclusion bodies, with removal of contaminants, followed by solubilisation with a denaturant [154]. IBs are usually released

mechanically or chemically from the cell, followed by a centrifugation or filtration. There is increased evidence that contaminants present in preparations of IBs can significantly reduce refolding yield [168]. Good cell breakage is important and washing the pellet to get a homogeneous preparation. Generally if there is good expression, and in some instances if the inclusion preparation consists of 50% or more of the protein of interest; than an inclusion body preparation can be used directly for refolding trials.

A combination of enzymatic and mechanical disruption of harvested cells, enzymatic digestion of DNA, treatment with Triton -X 100 and centrifugation are used to harvest the IBs. Following preparation of pure IB paste, IB solubilisation is usually conducted in concentrated denaturant which can be urea, guanidium chloride or detergents [169].

The aim of this chapter is to describe the isolation of the insoluble LBD of the brain and taste mGluR4 of clones 3 and 13 from the previous chapter. Another aim is to describe the solubilisation of the IBs and the refolding screening of these two proteins using a commercially available kit with 96 refolding conditions and the scale-up of the refolding conditions.

3.1.4 Characteristics of protein aggregates in IBs

In general, IBs are solubilised by use of a high concentration of denaturants such as urea or guanidium hydrochloride, along with a reducing agent or detergents such as SDS, N-cetyl trimethyl ammonium chloride and sarkosyl (sodium N-lauroyl sarcosine). Additional reducing agents like β-mercaptoethanol, dithiothreitol or cysteine are also often used for solubilisation of IB proteins. These agents maintain cysteine residues in a reduced state and thus prevent non-

native intra- or inter-disulfide bond formation in highly concentrated protein solutions [159]. Chelating agents like EDTA are frequently used in the solubilisation buffer to prevent metal-catalyzed air oxidation of cysteine. Solubilised proteins are then refolded by slow removal of the denaturant [156, 170]. In the case of proteins having multiple disulfide bonds, they need the presence of optimal concentrations of both oxidizing and reducing agents for the formation of disulfide bonds. Oxidation can also be achieved by adding a mixture of oxidized and reduced thiol reagents such as reduced/ oxidized glutathione (GSH/GSSG), DTT/GSSH, cysteine/cystine, and cysteamine/cystamine at a total 5-15 mM with a molar ratio of reduced to oxidized compounds of 1:1 to 5:1, respectively [170, 171]. Refolding is usually followed by purification to remove high molecular weight aggregates, along with contaminants. One of the reasons for poor recovery of refolded protein from solubilisation mixture is aggregation. Protein aggregation is a higher order reaction while refolding is a first-order reaction [172]. Unimolecular intrachain interactions promote the formation of the native state, while multimolecular interchain interactions increase with the concentration of the refolding protein and lead to misfolding and aggregation [173, 174]. Kinetic studies suggest that aggregation occurs very early during refolding through non-specific hydrophobic interactions [174].

Additives have been used such as L-arginine, low-concentration (1-2 M) urea or guanidine hydrochloride and detergents. These additives influence the stability and solubility of the unfolded protein [175]. Protein refolding using pulse renaturation, size-exclusion and adsorption chromatography has been used. Different dialysis and dilution methods have been used. Pulse renaturation consists of addition of small amount of solubilised protein in the renaturation buffer at successive intervals [176]. Protein concentrations in the range of 10-50 $\mu g\ ml^{-1}$ are typically used during refolding [175], [176].

There is no universal method for refolding and there are many factors to be considered in finding a suitable protocol. A simple, guaranteed method does not exist. If an effective refolding protocol is defined, scaling-up is the next step which may incur further changes in procedure.

3.2 Materials and Methods

3.2.1 Extraction of IBs

In this section the extraction of the brain and taste mGluR4 LBD IBs is described. The taste mGluR4 IBs were purified on a Ni-affinity column directly from the insoluble fraction of the cell lysate. The brain mGluR4 LBD IBs were extracted following the instructions from the Novagen Refolding Kit protocol.

For the brain mGluR4 LBD IBs, a cell pellet of cultures expressing the brain mGluR4 LBD, weighing 2.2 g was resuspended in 22 ml of resuspension buffer (50 mM Tris-HCl, 50 mM NaCl, 1 mM TCEP, 0.5 mM EDTA, and 5% glycerol, pH 8.0), and 20 µl per 1 g cell paste Benzonase (Novagen) was added to the lysate to reduce viscosity. The cells were sonicated (for 6 m; 10 s bursts; 20 s breaks; 4 °C). TritonX-100 was added to a final concentration of 1% (v/v) and stirred slowly (15 m; RT). The mixture was centrifuged (8000 x g; 15 m; 10 °C), the supernatant discarded and the pellet was washed by resuspending it in wash buffer (50 mM Tris-HCl, 50 mM NaCl, 1 mM TCEP, 0.5 mM EDTA, 5% glycerol and TritonX-100 pH 8.0) at a ratio of 10 ml buffer per 1 g original cell paste. The contents were centrifuged (8000 x g; 15 m; 10 °C) and the supernatant discarded. The wash step was repeated one more time. To

remove residual Triton-X 100, the pellet was resuspended in cell resuspension buffer at a ratio of 10 ml per 1 g cell paste and centrifuged (8000 x g; 15 m; 10 °C) and the supernatant discarded. The wash step was repeated one more time and the pellet was weighed. A sample (20 µl) of resuspended IBs was collected for SDS-PAGE analysis. The brain LBD IBs were used directly for screening since the IB prep consisted of more than 60% mGluR4 LBD as determined by SDS-PAGE analysis.

The putative taste LBD pellet was weighed and dissolved in denaturant buffer (0.1 M Tris, 6 M Guanidinium HCl, 20 mM DTT and 1 mM EDTA pH 8.0) and purified on a Ni- Affinity column to remove contaminants. The cell lysate was centrifuged (10 000 g; 15 m; 15°C), and the insoluble fraction was solubilised in a denaturant buffer containing 6M Guanidium HCl with 5 mM β-mercaptoethanol. The column was washed with 5 column volumes (cv) 20% ethanol, and then equilibrated with 5 cv of the denaturant buffer plus 5 mM β-mercaptoethanol. The sample was loaded onto the column and washed with 10 cv sample buffer plus 10 mM Imidazole. The bound protein was eluted in 5 cv elution buffer which was the same as the equilibration buffer containing 300 mM Imidazole. A second elution was done with elution buffer containing 500 mM Imidazole. The Ni-affinity purified IBs were dialysed out of the elution buffer overnight against MilliQ H_2O. The protein precipitated once the 6M Guanidium HCl was removed. The precipitate was centrifuged (25 000 x g; 40 m; 4°C). Both the isolated brain mGluR4 and purified taste mGluR4 were denatured in the same way described in the next section.

3.2.2 Denaturation of the IBs

Extracted IBs of brain mGluR4 LBD and Ni-affinity purified, precipitated IBs of taste LBD mGluR4 (0.5 g wet weight each) were dissolved in 10 ml denaturation buffer (50 mM Tris-HCl, 50 mM NaCl, 5 mM TCEP, 0.5 mM EDTA, 5% glycerol pH 8.0) separately and disrupted using a glass homogenizer. The sample was sonicated for (3 m) and then N-lauroylsarcosine was added (3% final concentration) and stirred at RT until the solution cleared. A centrifugation step followed (25 000 x g; 15 m; 4 °C), and 10-15 ml supernatants were dialysed against 2 L dialysis buffer (10mM Tris-HCl, 0.05 mM EDTA, 0.1 mM TCEP and 0.06% (w/v) N-lauroylsarcosine, pH 8.0) in order to remove the detergent. Snake skin pleated dialysis tubing (Pierce) with a 7 kDa molecular weight cut-off was used (even though the molecular weight of the protein is ~50 kDa); because the protein is assumed to be denatured (linear chain) and may pass through a larger molecular weight cut-off membrane, a lower molecular weight cut-off membrane is used. The dialysed sample was centrifuged (25 000 g for 15 m; 4 °C) to remove any aggregates.

The protein concentration was estimated either by A_{280} measurement, using the protein factor for this protein (1.169) which was calculated by entering the amino acid sequence of the protein into the ProtParam service on the ExPASy proteomics server [177] or by using a BCA Protein Assay Kit (Pierce). This commercial assaying kit was used because it is compatible with protein samples that contain up to 10 mM TCEP. mGluR4 (27 mg) was dissolved from 0.5 g Ni-affinity purified IBs wet weight. Solubilised IBs (56.3 mg) of the putative taste LBD were isolated. Samples were taken at each step of the procedure for SDS-PAGE analysis.

3.2.3 Screening for optimal folding conditions

Protein solution (50 µl 1 mg/ml) was added to each of the 96 wells of the iFOLD Protein Refolding plate (Novagen), a commercial refolding kit, which contained refolding buffer (450 µl) in each well with the exception of 2 wells which are reserved for controls. The IBs were mixed rapidly into the refolding buffers by pipetting up and down at least 10 times. The refolding 96-well plate was gently shaken overnight at room temperature. The components of the wells are shown in Figure 3.1. The buffer in all wells is 50 mM Tris and the ionic strength was 100 mM or 250 mM NaCl and as a detergent trap 12.5 mM β-Cyclodextrin is used. The redox reagents were 1 mM TCEP or 3.8/1.2 mM GSH/GSSG. As additives 20% (v/v) glycerol, 0.1% (w/v) PEG 6000, 500 mM L-Arg, 500 mM GuHCl, 1 mM $CaCl_2$/$MgCl_2$ or 1mM EDTA were tested.

3.2.4 Measuring refolding

Although no universal, accessible, high-throughput method is available to monitor protein refolding, sample absorbance at 340 nm (A_{340}) provides an initial screen for refolding efficiency. It is used as an indicator of the degree of aggregation in the solution as a result of turbidity.

Twenty-two conditions were chosen for further investigation by SDS-PAGE, mainly ones with low turbidity, but also a few with high aggregation to serve as negative controls. Refolding reactions (100 µl) were taken and alkylated and run on a SDS-PAGE gel. Samples were alkylated (100 mM alkylating reagent, iodoacetamide), and the reaction was incubated in a water

bath at 37 °C for half an hour. Alkylation allows the proteins to run on the gels with the same molecular weight as they would in solution [178].

3.2.4.a Scale-up of the refolding reaction

From the results from both the SDS-PAGE and the OD measurements several refolding conditions were scaled-up to 50 ml containing final concentration 0.1 mg/ml receptor. After refolding, the reactions were concentrated to 5 ml in 20 ml Vivaspin concentrators (5000 g, 4 °C). After concentration the receptor was dialysed overnight in binding assay buffer (30 mM HEPES, 110 mM NaCl, 5mM KCl, 1.2 mM $MgCl_2$ 6 H_2O, 2.5 mM $CaCl_2$, pH 8.0) [179] with a 10 kDa molecular cut off membrane [180]. After dialysis the samples were centrifuged (139 000 g; 1 h; 4 °C). Samples were taken at each step and analysed by Tris-Glycine SDS-PAGE.

3.2.4.b Ni- affinity purification of refolded mGluR4

Protein binding to Ni-affinity superflow beads (Qiagen) was checked. A bead volume of 175 µl was equilibrated with 50 mM NaH_2PO_4, 300 mM NaCl, 10 mM Imidazole pH 8.0, 5 bead volume (bv). The beads were separated by a short spin in a bench top centrifuge (13 000 x g; 1 m; RT) and the supernatant aspirated. The beads were incubated overnight at 4 ºC. The sample was then centrifuged (13 000 x g; 1 m; RT) and the supernatant removed and the beads were washed with 10 bv wash buffer (50 mM NaH_2PO_4, 300 mM NaCl, 20 mM Imidazole, pH 8.0). The sample was eluted in 2 cv, samples were taken at each step during the purification and separated on a Tris-Glycine 12 % SDS PAGE.

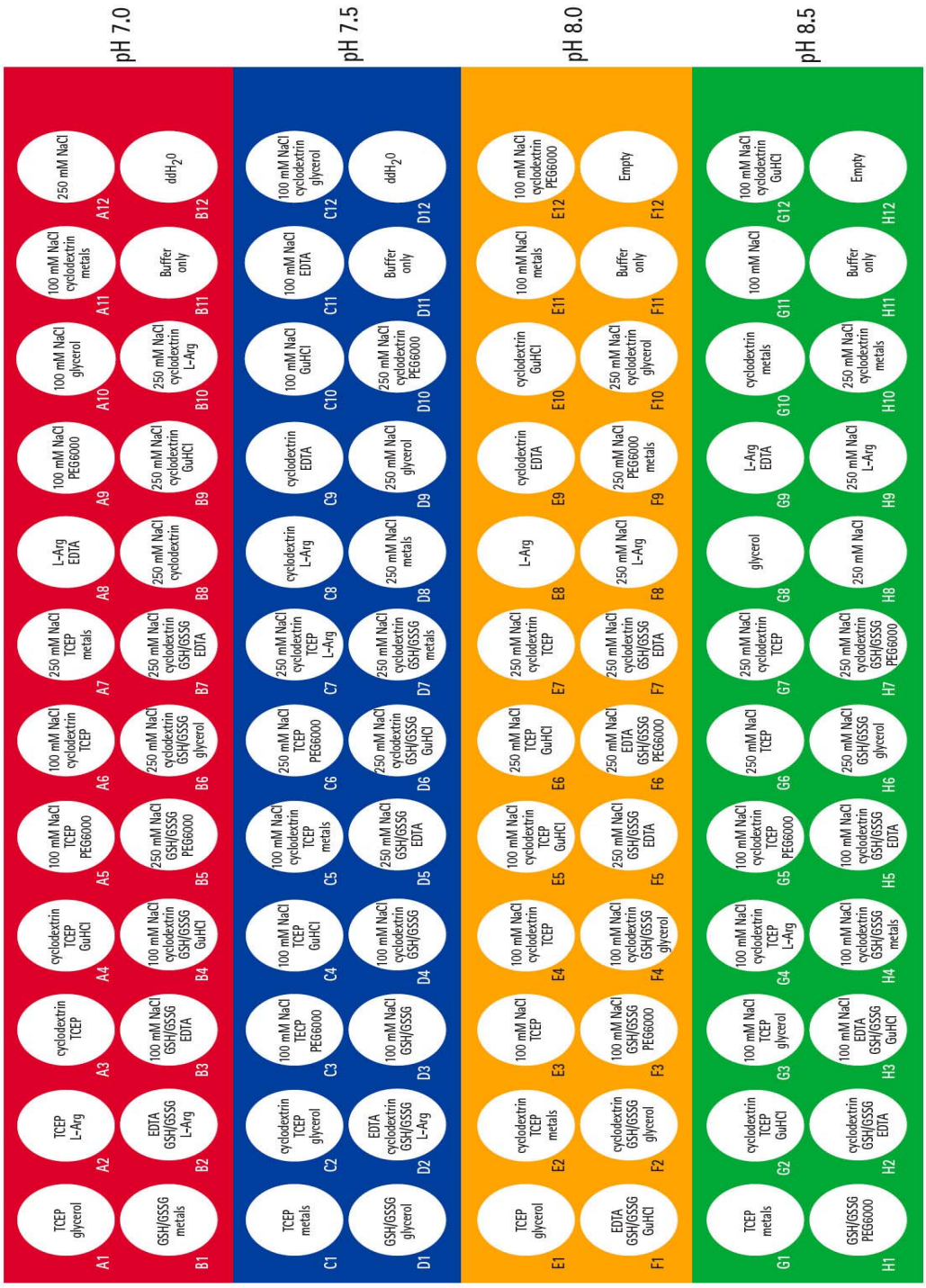

Figure 3.1 Components of the Novagen iFold Protein Refolding System and their concentrations and pH

3.2 Results and Discussion

3.2.1 Extraction and denaturation of IBs

From one litre culture of the brain and taste LBD of mGluR4 about 2.2-2.5 g of cell pellet was obtained. The protein was concentrated in the IBs and wash steps further remove contaminants. It was important for the IBs to be denatured thoroughly. Mechanical disruption of the cells with a glass homogeniser, followed by sonication was used to achieve the desired denaturation. The denaturant, in this case the detergent N-lauroyl sarcosine was removed by dialysis before the protein was added to the refolding buffer. The amount of protein was assessed by taking a A_{280} reading and using the protein factor for the brain mGluR4 LBD 1.469. From 0.5 g IB prep, 45 mg receptor was obtained (Figure 3.2).

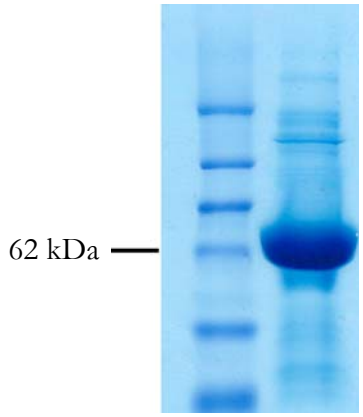

Figure 3.2 Inclusion bodies of brain mGluR4 LBD, isolated according to the Novagen iFold protocol. 1L cell culture produced 2.2 g of cell pellet and the isolated IBs from the cell pellet weighed ~ 1 g.

In Figure 3.2 the purity of the isolated brain mGluR4 LBD IBs, and be seen and Figure 3.3 shows the Ni-affinity purification steps of taste mGluR4 LBD analysed by SDS-PAGE. The

protein binds to the Ni-affinity column in the presence of 6M GuHCl and most impurities were seen to be removed with this step.

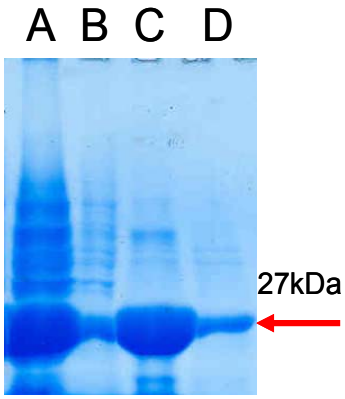

Figure 3.3 Coomassie stained SDS-PAGE gel of the Ni-affinity purification steps of taste mGluR4 LBD IBs. A) cell lysate B) the wash with 10 mM imidazole, C) 300 mM imidazole elution, and D) 500 mM imidazole elution.

3.2.2 Screening for optimal folding conditions

96 conditions were tested in a 96-well Novagen iFold refolding plate by adding 50 µl of the 1mg/ml receptor to each well of the plate. The state of refolding was followed by measuring A_{340}.

3.2.3 Measuring refolding

The extent of precipitation in the wells was estimated by measuring the A_{340} using dd H_2O as a blank. Smaller A_{340} values denote less precipitation. The A_{340} measurements of the taste mGluR4 LBD refolding screening are shown in Figure 3.4. Readings are represented in a bar chart for better visualisation in Figure 3.5. It seems that most of the taste mGluR4 LBD

protein stays in solution around pH 8.0 (Figure 3.5), which is the optimal pH for disulfide bond formation.

For the brain mGluR4 LBD the A_{340} measurements are shown in Figure 3.6 and in a form of a bar chart in Figure 3.7. It seems that for the brain mGluR4 LBD, the protein is most soluble in pH 8.5 (Figure 3.7).

Figure 3.4 A_{340} readings for each well of the plate from the iFold Refolding screen (Novagen) for the taste mGluR4 LBD to monitor aggregation of refolded mGluR4 at 22 °C. Green wells with A_{340} readings ≤0.02, white wells with A_{340} readings >0.02, orange wells with A_{340} readings >0.5

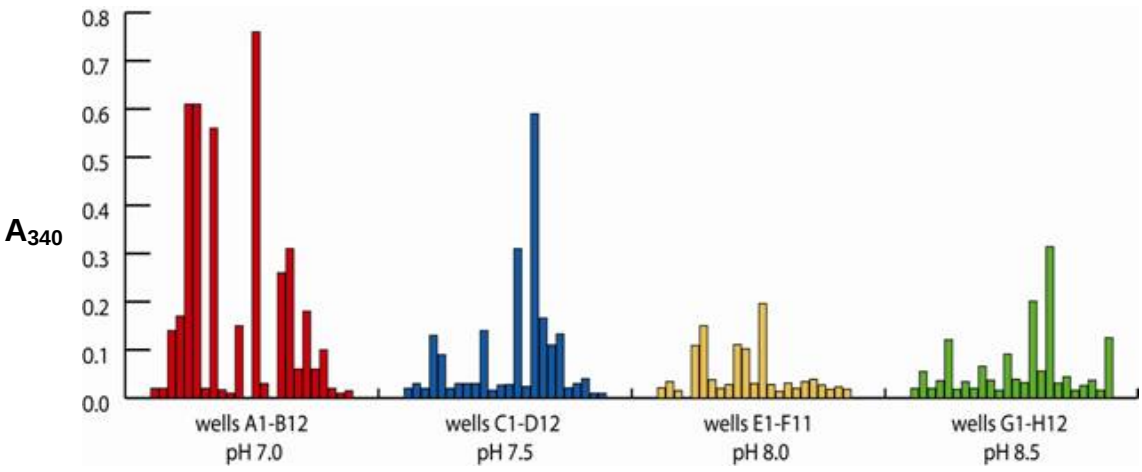

Figure 3.5 Aggregation of the taste LBD mGluR4 refolded at 22 °C determined by A340. The buffer contents of the wells can be seen in Figure 3.1.

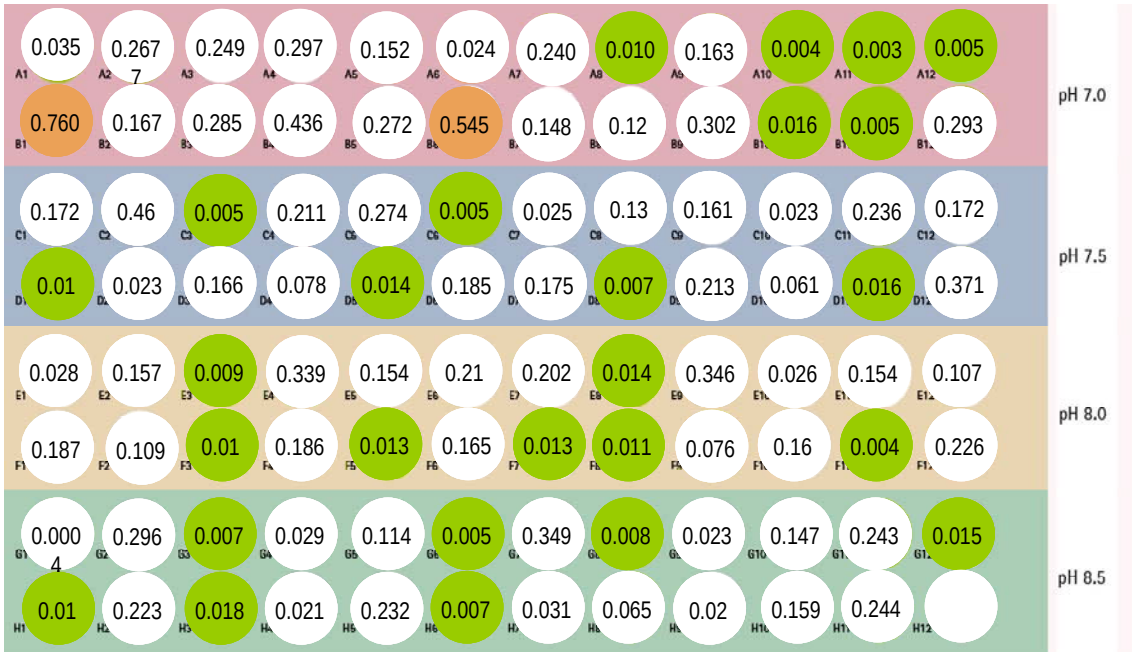

Figure 3.6 A_{340} readings of the iFold Refolding screen (Novagen) to monitor aggregation of refolded brain LBD mGluR4 at 22 °C

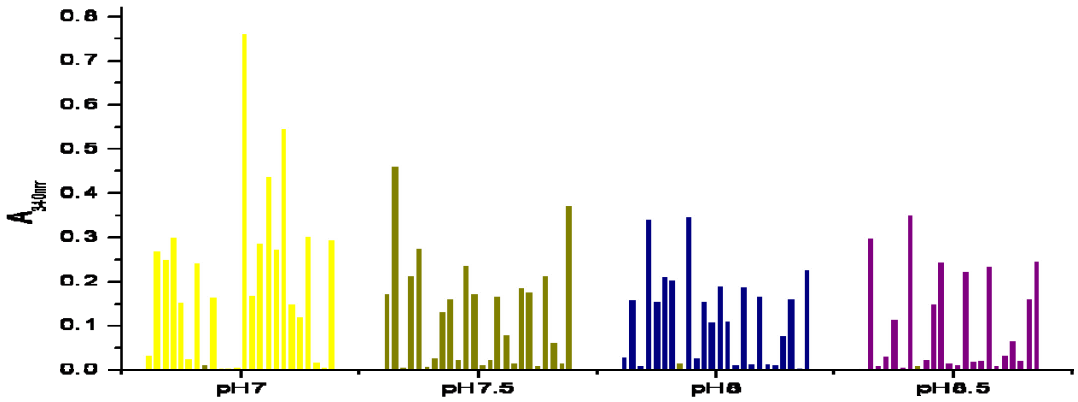

Figure 3.7 Aggregation of the brain LBD mGluR4 refolded at 22 °C determined by A_{340}. Buffer components are shown in Figure 3.1.

Next, 22 conditions were selected for further analysis. Results of the SDS-PAGE for the brain mGluR4 LBD can be seen in Figure 3.8 and for taste mGluR4 LBD in Figure 3.9.

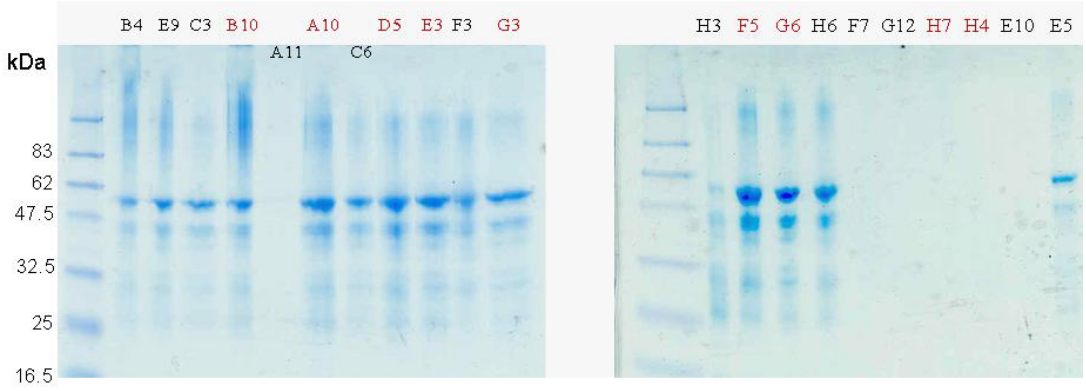

Figure 3.8 SDS PAGE of brain mGluR4 LBD (arrow shows expected M_w) IBs in 22 refolding conditions. 96 refolding conditions were tested on the Novagen kit. After OD measurements, 22 conditions were selected and run on a gel. The refolding conditions in which most protein is in solution were used for scaling up experiments by preparing the corresponding buffers in a larger volume.

Of the 22 conditions from the optimising of the taste mGluR3 LBD, 7 conditions were chosen where most of the protein was in solution. The 500 µl screen refolding reactions were scaled up to 20 ml Figure 3.10. Out of the 7 conditions 4 were narrowed down, and scaled up to 50 ml and analysed by SDS-PAGE (Figure 3.11).

From the gels, some conclusions could be drawn about the parameters that affect the solubility of this protein. For the taste mGluR4 LBD (Figure 3.8) the receptor precipitated in the presence of divalent cations (lanes 5, 8, 22), cyclodextrin (lanes 2, 7, 11, 19, 22) and PEG 6000 (lanes 9 and 12). pH 8.0 seemed to allow most of the protein to stay in solution, which is the optimal pH for the formation of disulfide bonds. Most of the protein stays in solution in refolding buffer containing 250 mM NaCl, GSH/GSSG 3.8 mM, 1 mM EDTA remains in solution. This agrees with the fact that there are two disulfide bridges and an oxido-reductive system is necessary for disulfide bond formation.

Ni-affinity purification of refolded taste LBD mGluR4 resulted in some bands purified, lanes 8-11 and 19-21 in Figure 3.12, however the amount of purified protein was low and it was not possible to repeat the Ni-affinity purification when the refolding reactions were scaled-up. In the flow through there was a smear at the higher molecular weight which indicates the protein is not properly solubilised

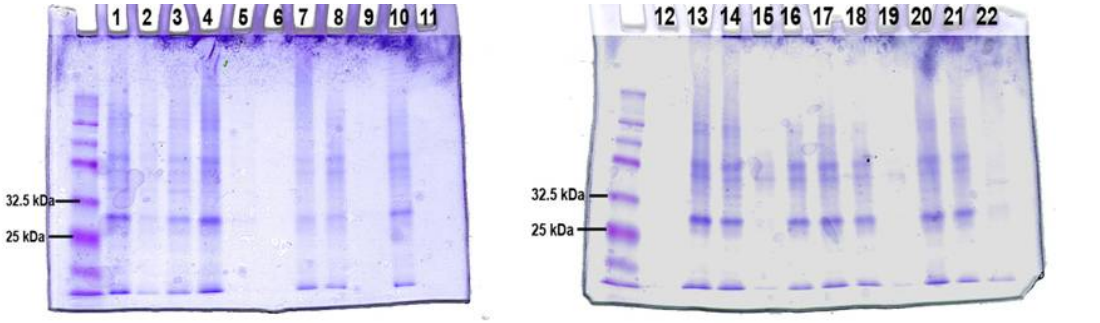

1	A2	TCEP, L-Arg pH 7.0
2	A6	100mM NaCl, cyclodextrin, TCEP pH 7.0
3	A7	250mM NaCl, TCEP, metals pH 7.0
4	A8	L-Arg, EDTA pH.7.0
5	B1	GSH/GSSG, metals pH 7.0
6	B3	100mM NaCl, GSH/GSSG, EDTA pH 7.0
7	B10	250mM NaCl, cyclodextrin, L-Arg, pH 7.0
8	C1	TCEP, metals, pH 7.5
9	C6	250mM NaCl, TCEP, PEG6000, pH 7.5
10	E3	100mM NaCl, TCEP pH 8.0
11	E4	100mM NaCl, cyclodextrin, TCEP pH 8.0
12	F3	100mM NaCl, GSH/GSSG, PEG6000 pH 8.0
13	F5	250mM NaCl, GSH/GSSG, EDTA pH 8.0
14	C7	250mM NaCl, cyclodextrin, TCEP, L-Arg pH 8.0
15	G1	TCEP, metals pH 8.5
16	G3	100mMNaCl, TCEP pH 8.5
17	G6	250mM NaCl, TCEP pH 8.5
18	G11	100mM NaCl pH8.5
19	E9	cyclodextrin, EDTA pH 8.0
20	A12	250mM NaCl pH 7.0
21	C11	100mM NaCl, EDTA pH 7.5
22	D7	250mM NaCl, GSH/GSSG, cyclodextrin, metals pH 7.5

Figure 3.9 Coomassie stained SDS-PAGE gel of taste mGluR4 LBD in 22 different refolding conditions from Novagen iFOLD Protein Refolding screening. The components of the refolding conditions are listed below the gels.

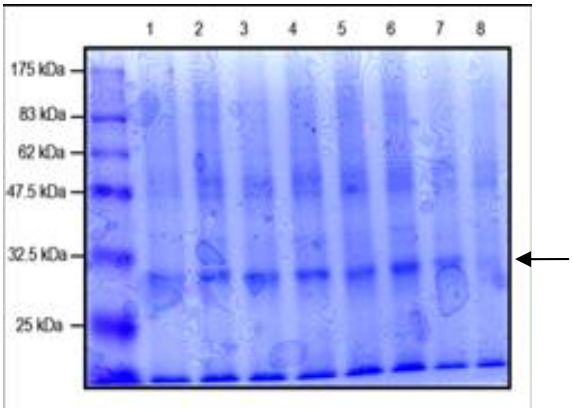

Figure 3.10 Coomassie stained SDS_PAGE gel of alkylated samples from a 20 ml scale up of refolding of taste mGluR4 LBD (arrow shows expected M_w) separated on Tris-Glycine 12% SDS-PAGE. 1. L-Arg, EDTA; 2. L-Arg, TCEP; 3. 250 mM NaCl, GSH/GSSG, EDTA; 4. 100mM NaCl, TCEP, EDTA, L-Arg; 5. 250 mM NaCl; 6. 250 mM NaCl, GSH/GSSG, EDTA, L-Arg; 7. 250 mM NaCl, TCEP; 8. IBs.

From the 50 ml scale up reaction for taste mGluR4 LBD, we were able to calculate how much protein remained in solution after removal of the denaturant. Five mg of protein was added at the beginning of the reaction. After concentration, dialysis and ultracentrifugation, 3.02 mg of protein that can be seen in lane D2 on the gel in (Figure 3.11) remained in solution, which corresponds to 60 % of the starting material.

The next step consisted of dialysing out the refolding buffers. The solutions turned cloudy after dialysis in assay buffer (30 mM HEPES, 5mM KCl, 100 NaCl, 1.2 mM $MgCl_2$, 2.5 mM $CaCl_2$ pH 8.0). Detergent precipitation was visible, possibly due to the low temperature, or mre likely due to the low ionic strength of the buffer. Components of other dialysis buffers that were tested are listed in Table 9. The protein precipitated in these dialysis buffers as well.

Table 9 Components of the buffers tested to transfer the protein from the refolding buffer by dialysis for the brain mGluR4 LBD

1 (pH 8)	2 (pH7)	3 (pH 8)	4-Assay buffer (pH 8)	5 (pH 8)	6 (pH 8)
20 mM Tris-HCl	20 mM Tris-HCl	20 mM Tris-HCl	30 mM hepes-sodium	buffer 4	buffer 4
150 mM NaCl	150 mM NaCl	150 mM NaCl	5 mM KCl	0.03% Brij 35	10% glycerol
1.2 mM $MgCl_2$	5 mM DTT	5 mM DTT	100 mM NaCl	5 mM DTT	
2.5 mM $CaCl_2$	0.03% Brij 35	0.03% Brij 35	1.2 mM MgCl2		
5 mM DTT		10% glycerol	2.5 mM CaCl2		
0.03% Brij 35					

For the brain mGluR4 LBD protein, the protein was mainly soluble in a buffer containing 100 mM NaCl and TCEP reducing reagent (Table 10). Divalent cations seemed to cause the protein to precipitate

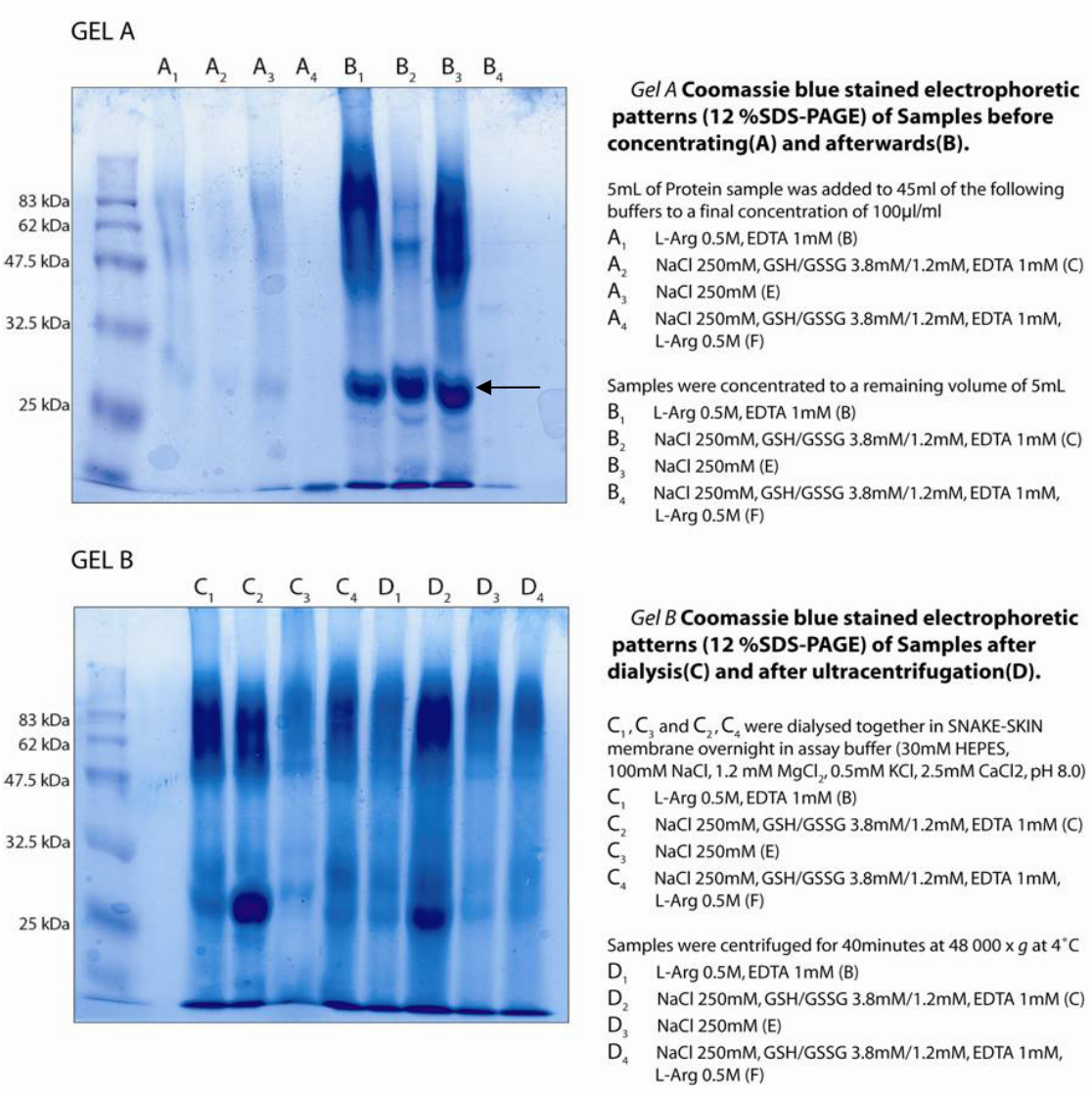

Figure 3.11 Scale-up of refolding reaction of taste mGluR4 LBD (50 ml). The arrow in gel A shows the expected M_w. The buffer was 50 mM Tris, the refolding was done at room temperature. Buffer 1 and 3 are at pH 7.0, Buffer 2 and 4 are at pH 8.0. All the samples were alkylated with 100 mM iodoacetic acid for 30 minutes at 37°C and treated with Strataclean beads before loading the gel.

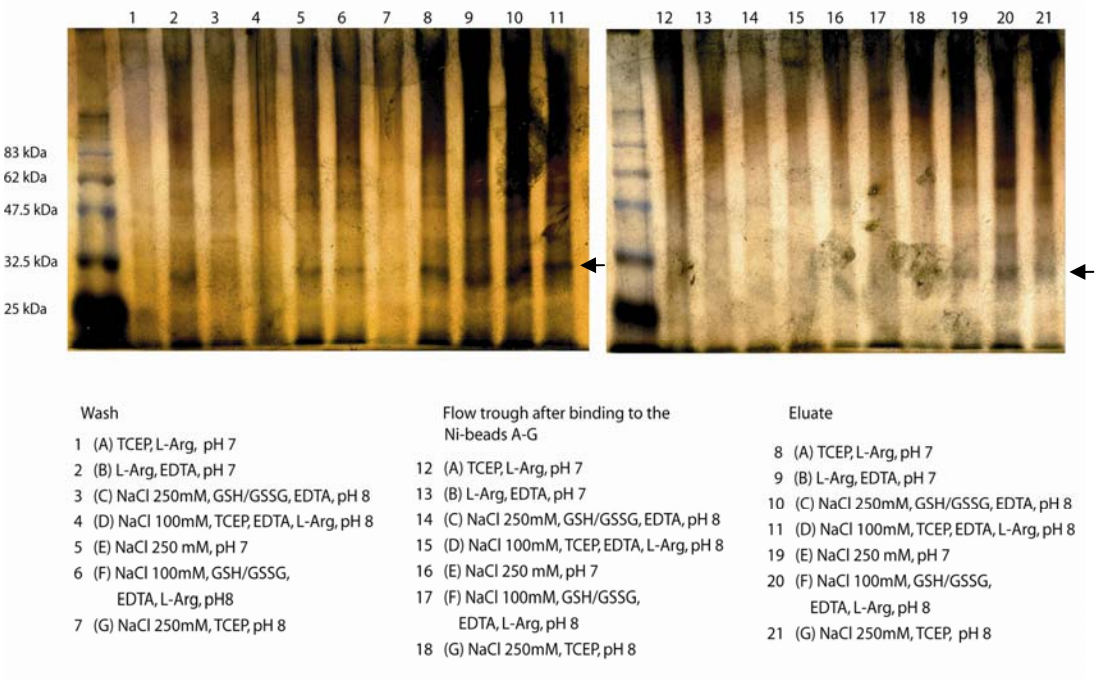

Figure 3.12 Silverstained protein SDS-PAGE gel of Ni-affinity purification of scaled-up of taste mGluR4 LBD (arrows show the expected M_w). The refolding buffer was 50 mM Tris, 1 mM TCEP, 3.8/1.2 mM, 500 mM L-Arg, 1 mM EDTA

Table 10 Refolding buffers which enhanced the solubility of the brain mGluR4 IBs. The turbidity of the protein was checked after a week.

Buffer name	Buffer Composition	Buffer pH	A_{340}	A_{340} (after 7 days)
A10	100 mM NaCl, 20% glycerol	pH 7.0	0.033	0.009
B10	250 mM NaCl, cyclodextrin L-Arg	pH 7.0	0.018	0.203
D5	250 mM NaCl, GSH/GSSG, EDTA	pH 7.5	0.017	0.001
E3	100 mM NaCl, TCEP	pH 8.0	0.000	0.258
F5	250 mM NaCl, GSH/GSSG, EDTA	pH 8.0	0.000	0.020
G3	100 mM NaCl, TCEP, 20% glycerol	pH 8.5	0.000	0.001
G6	250 mM NaCl, TCEP	pH 8.5	0.000	0.002

3.3 Conclusions

The isolation of IBs of brain mGluR4 LBD resulted in high purity of about 85% receptor of the total protein (Figure 3.2). From 1 L culture, ~ 200 mg of receptor in IBs was isolated for both the brain and taste mGluR4 LBDs, and about the same for the taste mGluR4 LBD. The refolding screening showed parameters which enhanced the solubility of the protein in the refolding buffer (Table 10) and the pH profile coincided with the optimal pH for disulfide bridge formation, around pH 8.0 (Figure 3.5) for the taste mGluR4 LBD and between pH 8.0 and pH 8.5 (Figure 3.7) for the brain mGluR4 LBD. The results were reproducible and repeated at least 3 times. There was protein in solution in the refolding buffer (Figure 3.8 and Figure 3.9), and it was possible to scale up the reactions (Figure 3.11). It was, therefore not possible to exchange the refolding buffer with an assay buffer, because the protein usually came out of solution once it was in the assay buffer, and whatever protein remained in solution precipitated during concentration. There was never enough protein after concentration to carry out ligand binding studies. It was therefore not possible to obtain enough soluble mGluR4 LBD outside the refolding buffer with the refolding conditions we used, hence preventing any attempts at crystallisation or NMR. The mGluR1 crystal structure was resolved using mGluR1 expressed in baculovirus, without the need for refolding. Other modification which could be included in this system are trying to refold the protein at a lower concentration than 100 μg/ml, and more detergents in the dialysis buffer.

Chapter 4 Solid State NMR Studies of Selectively Labelled Bacteriorhodopsin

4.1 Introduction

Chapters 4 and 5 are related; both chapters describe solid state NMR experiments carried out on bacteriorhodopsin (bR). This chapter reports on three dimensional (3D) crystallisation trials of bR in the context of solid state NMR sample preparation and its effect on the quality of the selectively ^{15}N labelled bacteriorhodopsin spectra. Chapter 5 presents the studies of uniformly ^{13}C, ^{15}N labelled bacteriorhodopsin with different levels of deuteration.

The ultimate goal of the bR crystallisation trials described in Chapter 4 is to produce highly homogeneous 3D bR crystals for MAS NMR crystallography experiments and to compare critically their resolution with the resolution obtained from the purple membrane, which is a natural two dimensional (2D) crystal. Another goal is to look into alternative means of sample preparation for solid state NMR. Nanodiscs called Lipodisqs™ are formed when a patented polyacrylamide polymer solution is mixed with a lipid solution. They are very robust and can solubilise very hydrophobic materials, thus Lipodisqs™ may find application in preparing solid state NMR samples of highly hydrophobic proteins, such as membrane proteins. Lipodisqs™ are visualised by transmission electron microscopy (TEM) to determine their shape and to

measure the diameter of the particles. ^{31}P static solid state NMR of the Lipodisqs™ has been performed in order to study their orientation in the magnetic field.

4.1.1 The Importance of Sample Preparation for Solid State NMR

Successful spectral assignment and determination of structural constraints in isotopically enriched materials (mostly ^{13}C, ^{15}N) is still limited by **resolution** and **sensitivity**. Sample preparation is perhaps the most important factor for obtaining high-quality protein spectra. The structural homogeneity of the sample determines line widths and hence affects spectral resolution. Peak doubling, unexpected multiplets and line broadenings, indicate structural heterogeneity. Different sample preparation conditions have been compared for solid state NMR spectral resolution [19, 181-186].

4.1.2 Different Sample Forms Used for Solid State NMR

There have been examples of solid state NMR studies of proteins as lyophilized powders, microcrystal precipitated by organic molecules, membrane proteins in membranes, and frozen protein solutions [17] (Figure 4.1).

In early studies, lyophilisation (freeze-drying), the simplest method of making a solid protein sample, was often used. Frozen or dried pellets cause signal broadening, with linewidths typically 1-2 ppm, which is not sufficient for most structural studies [182]. Both the freezing and drying steps may denature the proteins or alter their secondary structure. This is consistent with the observation that NMR lines of lyophilised proteins are usually

inhomogeneously broadened, but addition of cryoprotectant such as polyethylene glycol (PEG) or trehalose, have been found to improve protein line widths [19]. However, even if the protein backbone is correctly folded, the side chain conformations may be variable, resulting in sample heterogeneity.

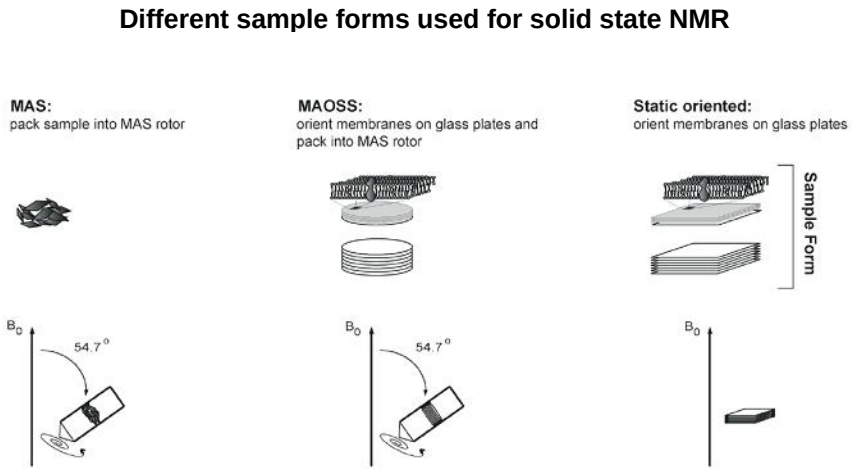

Figure 4.1 Sample preparation in different types of ssNMR: MAS, MAOSS and static NMR. Different nature and state of samples can be used for solid state NMR: membranes, membrane proteins in membranes or detergent micelles or bicelles, proteins in frozen solution, lyophilised or precipitated in microcrystalline form and insoluble proteins amyloid and prion proteins. Adapted from [15].

Great progress has been made by discovering that microcrystalline protein samples yield narrow resonance lines for soluble proteins [19, 25, 187]. There is accumulating evidence that protein precipitates, formed in a controlled manner, yield equivalent spectral resolution as medium or X-ray quality crystals [19, 182, 188]. The precipitating conditions can strongly influence the NMR line width – several precipitation conditions may have to be screened for a

high resolution NMR sample. For instance, ubiquitin can be crystallized both from polytheylene glycol (PEG) 8000 and 2-methyl-2,4-pentanediol (MPD), however the MPD-induced crystals have much narrower lines for natural abundance ubiquitin than for PEG-induced crystal formation [187].

For membrane proteins, there are only a few studies available on optimisation of sample preparation for solid state NMR study. Optimal sample preparation for membrane proteins seems to be different for each membrane protein with few generalisations. Detergent purified membrane proteins can be precipitated as microcrystals or reconstituted into lipid bilayers to form proteoliposomes or 2D crystals. The available, limited studies suggest that proteoliposomes yield the worst resolution spectra among these methods. Oschkinat and colleagues reconstituted the purified *E. coli* outer membrane protein G (OmpG) into *E. coli* total lipid extract in 1:2 and 3:2 (w/w) lipid-to-protein ratios to yield 2D crystals and proteoliposomes, respectively [186]. Spectra obtained from 2D crystals showed better resolved lines than spectra from proteoliposomes. In another study, Glaubitz and coworkers [185] report that microcrystalline diaglycerol kinase (DGK) yielded better resolution spectra than proteoliposomes. McDermott and colleagues [17] showed that U-^{13}C, ^{15}N KcsA potassium ion channel was precipitated by polyethylene glycol (PEG) in detergent micelles, where the linewidth of a single ^{13}C peak was about 80-100 Hz, similar to the linewidth of 2D crystals of OmpG [186] and of bacteriorhodopsin. Structural homogeneity of a sample is essential to achieve high resolution spectra.

Another concern when preparing samples for ssNMR is the dehydration of the sample. At high spinning rates and over time, water may escape from the sample through tiny holes around the spacers used in assembling the rotor. Various methods have been suggested to prevent dehydration, for instance an application of o-rings and thin film of a fluorotube wax [189].

In another study, NMR samples of solid Src homology domain (SH3) domain were generated in four different ways (denoted as I, II, III and IV), and their ^{13}C CPMAS spectra have been compared [19]. Sample I was lyophilised from an aqueous low salt solution, sample II was supplemented by a drop of water, resulting in a moist sample. Sample III was lyophilised from an ammonium sulphate solution, which additionally contained PEG 8000 and sucrose. The linewidths of the signals in 1D CP MAS ^{13}C spectra of these four preparations are decreased successively from sample I to IV, with the signals of the microcrystalline sample IV giving the best with respect to resolution. Thus the partial assignment of 2D ^{13}C-^{13}C RFDR spectrum of the microcrystalline sample was accomplished due to the sufficient resolution obtained. The further structural investigation and complete sequence assignment were eventually achieved on this microcrystalline high resolution sample (Figure 4.2) [19].

The prospect of studying proteins as precipitates is a particularly significant benefit for membrane proteins. The amphiphilic nature of membrane proteins implies that crystallisation is difficult and detergents have to be used to isolate and purify them. Since high X-ray quality crystals are not required for structural studies by NMR [190, 191], membrane proteins can be

studied in high resolution and under variable conditions precipitated in detergent micelles or bicelles by solid state NMR.

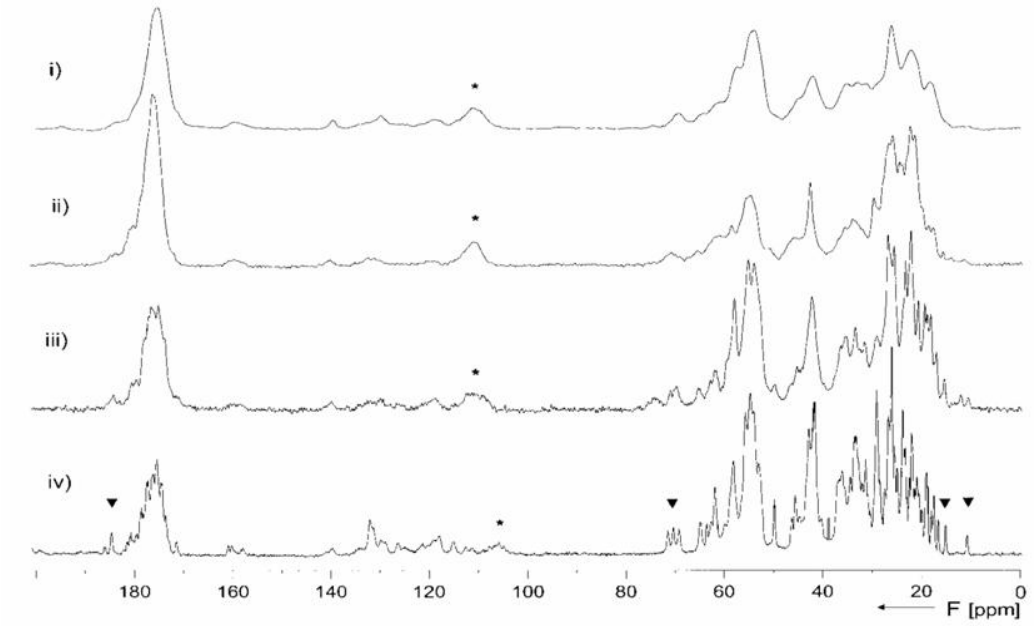

Figure 4.2 Four different U-^{13}C, ^{15}N enriched samples of the solid SH3, i) lyophilized from an aqueous low-salt solution, ii) supplemented by a drop of water, iii) lyophilized from a $(NH_4)_2SO_4$, PEG8000 and sucrose solution, iv) precipitated from a $(NH_4)_2SO_4$ rich solution by changing its pH [19].

4.1.3 Alternative means of sample preparation- Lipodisqs™

Lipodisqs™ are nanoparticles (Malceutics) and formed when mixing a polymer solution with a lipid solution. They are thought to mimic the natural lipoproteins. They form clear and colourless nanoemulsions as aqueous solutions or aqueous based gels. They are stable in aqueous solutions and gels in the pH 5.0 to 8.0 range. Lipodisqs™ can be freeze-dried after incorporation of an active compound, which can be strongly hydrophobic, and readily reconstituted. The materials are not very expensive, and Lipodisqs™ are effective at taking up

agents such steroids and hydrophobic peptides. This may be useful in preparing solid state NMR samples, but had not been characterised.

4.1.4 Introduction to the Structure and Function of the Purple Membrane and Bacteriorhodopsin

The purple membrane (PM) from the extreme halophilic archaeon *Halobacterium salinarium* is one of the best-characterised natural membranes [192, 193]. Under anaerobic conditions the archaea can exist by fermentation. When both oxygen and arginine are unavailable the archaeon synthesizes the purple membrane.

The PM is a two dimensional hexagonal crystal lattice in which the main constituent is bacteriorhodopsin (bR). Bacteriorhodopsin forms a trimer surrounded by archaeal lipids. The dry weight distribution of the membrane is 25% lipid and 75% protein [26]. About 90% of the total lipids in *H. salinarium* are polar lipids and are derivatives of a branched glycerol diether, 2,3-di-O-phytanyl-*sn*-glycerol, diphtytany phosphophatidylglycerolphosphate (DPhPGP) and a glycolipid sulphate (DPhGLS) [194].

Bacteriorhodopsin contains seven transmembrane α-helices and relatively short loops (Figure 4.3) and is bound stoichiometrically to the chromophore- retinal which is covalently bound to Lys216 by a Schiff base [193, 195, 196]. The composition and structure appears to be closely related to the visual pigments of higher animals.

The function of bR as a proton pump is based on a thermo-reversible all-trans to 13-cis photoisomerisation of the retinal moiety to which the transient deprotonation of the protonated Schiff base is connected. This initiates a thermal photocycle of events, resulting in the unidirectional transport of a proton across the membrane. The photocycle of the molecule is comprised of a number of intermediate conformations [197]. The proton motive force generated by this photocycle is used by the organism for the ATP synthesis required for its metabolism under nonrespiratory conditions (such as low oxygen) [198].

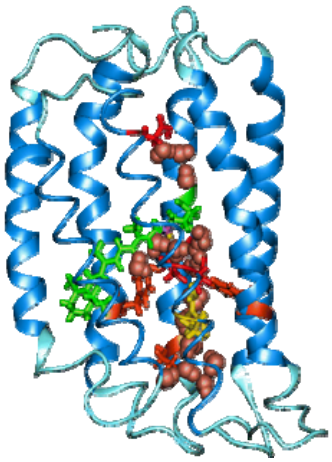

Figure 4.3 Three dimensional model of bacteriorhodopsin showing the trans-membrane region [20, 21]. The chromophore retinal is represented in green.

Bacteriorhodopsin is very stable in films, maintains structural and functional integrity under a wide range of pH, temperature, humidity or chemical environment [199]. It is easy to obtain large amounts (10s mg) of selectively/uniformly labelled bacteriorhodopsin [200].

Bacteriorhodopsin has been extensively studied by several spectroscopic methods not only to elucidate its biological activity, but also as a model for G-protein coupled receptors [201]. Because bacteriorhodopsin naturally forms a two dimensional crystal, the PM pellet gives reasonably narrow NMR signals in MAS spectra [202]. The aim of this chapter is to compare the resolution of 3D bR crystals with the resolution of 2D arrays of bR in purple membrane (MAS and MAOSS). The ultimate goal is to evaluate whether it is possible to generalise a method for membrane proteins sample preparation for solid state NMR.

PDB code	Method	Resolution (Å)	Residues in the model
1BRD	EM	3.5	8–32, 38–62, 74–100, 106–127, 137–157, 166–191, 202–225
2BRD	EM	3.5	7–227
1AT9	EM	3.0	2–231
2AT9	EM	3.0	6–227
1FBB	EM	3.2	4–227
1AP9	X-ray	2.35	7–225
1BRR	X-ray	2.9	3–232
1BRX	X-ray	2.3	6–152, 167–228
1C3W	X-ray	1.55	5–156, 162–231
1BM1	X-ray	3.5	7–227
1QHJ	X-ray	1.9	5–232
1E0P(A)	X-ray	2.1	5–232
1CWQ(A)	X-ray	2.25	2–239
1QM8	X-ray	2.5	2–230
1KGB	X-ray	1.81	5–156, 162–231
1IW6	X-ray	2.3	5–231
1KME	X-ray	2.0	5–231
1M0L	X-ray	1.47	5–156, 162–231

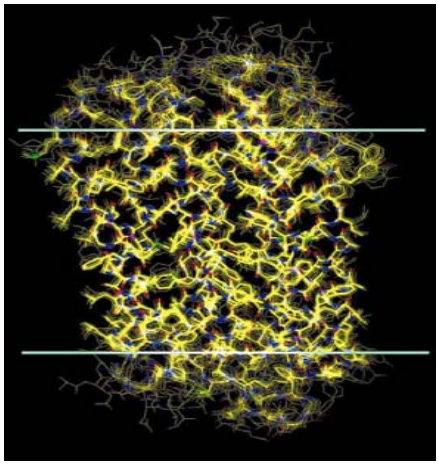

Figure 4.4 Bacteriorhodopsin is a well studied protein. Models for the ground state only of bacteriorhodopsin by EM or X-ray are summarised in table, and are adapted from [16]. There is a remarkable agreement among the different coordinate sets in the transmembrane region, but less so in the loop region.

4.2 Materials and Methods

4.2.1 Bacteriorhodopsin production

Halobacterium salinarium (S9) was cultured in a synthetic medium containing nutrients essential for normal growth [203]. ^{15}N-L-methionine (0.19 g/L) was added to the medium in place of the natural abundance L-methionine. With this method all 9 methionines can be labeled with minimal scrambling. The position of the 9 labelled methionines can be seen in Figure 1.4. After 5 days of incubation (110 rpm, 37 ° C, in the dark), when the OD_{660} has peaked, the cells were harvested and the purple membranes were purified according to the method of Oesterhelt and Stoekenius [204]. Samples containing purified purple membrane were washed in MilliQ water and resuspended in 20 mM Na_3Citrate buffer (pH 6.0).

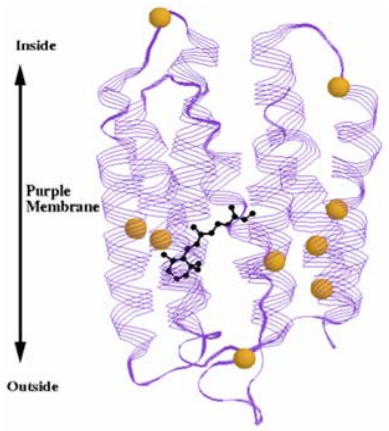

Figure 4.5 Bacteriorhodopsin 3D structure indicating the positions of the nine ^{15}N labelled methionine residues, with six located in the transmembrane helices (Met-20, Met-56, Met-60, Met-118, Met-145 and Met-209) the two in the loops (Met-68 and Met-163), and one (Met- 32) at the loop helix interface of helix A. The figure was generated using RASMOL with coordinates 2BRD from the Protein Databank, which is a structure of the protein embedded in the membrane [25-27]

4.2.2 Preparation of 3D crystals

Two different methods of producing 3D bR crystals were tested. One method involved the crystallisation of bR from a monomeric form with the archael lipid removed [205]. The other method utilised the crystallisation of bR from the PM from DMPC:CHAPSO bicelles according to the method of Faham and colleagues [206]. In this method the membrane protein is crystallized from the bilayer.

4.2.2.a Monomerisation of bR and crystallisation trials of monomeric, delipidated bR

Purple membrane suspension containing 3.6 mg of bR in 1 ml of 10 mM HEPES, 50 mM NaCl and 0.025% Na azide pH 7.0 was dissolved in 2 ml solubilisation buffer (1% Triton, 10 mM NaH_2PO_4, pH 5.6). The mixture was stirred overnight in an orbital shaker at 37 °C, protected from light. After ultracentrifugation (100 000 g, 20 m, 4 °C), the supernatant containing the monomeric bR, which is a lighter purple colour than the PM, was collected. The pellet, which contained the unsolubilised bR and denatured protein was removed. The solubilisation buffer was exchanged by binding the bR to a DEAE-Sephacel column, which was previously equilibrated with exchange buffer (1% DDM or OG, 10 mM NaH_2PO_4 pH 5.6). The bR was washed on the column slowly with the exchange buffer. The monomeric bR was eluted in high salt concentration elution buffer 1% DDM or OG, 500 mM NaH_2PO_4, pH 5.6. The eluate was dialysed overnight against low salt buffer (10 mM NaH_2PO_4 pH 5.6) and subsequently concentrated in an Amicon tube.

The concentration of the bR monomer was monitored by reading the absorbance at 552 nm, the wavelength at which the bR monomer absorbs [8]. Triton X-100 is a good solubilising detergent for membrane proteins, however bR-Triton X-100 complexes do not form crystals [205], so it is necessary to exchange the Triton with a different detergent. According to Schertler and colleagues [207], the best crystals can be obtained by using pipecolinic acid and benzamidine hydrochloride as amphiphiles.

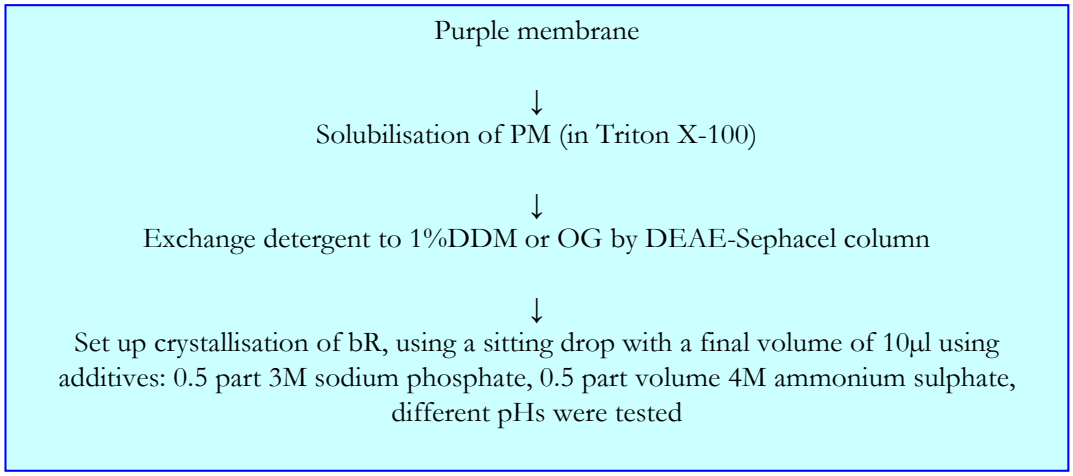

Figure 4.6 Outline of the crystallisation trial of the delipidated monomeric bacteriorhodopsin

4.2.2.b Crystallisation trial of bR in DMPC/CHAPSO bicelles

The other crystallisation method attempted utilised bicelles. The bicelles consist of long-chain phospholipids that form planar bilayers and short-chain lipids that "cap" the rim of the bilayer

made up of 3-(cholamidopropyl) dimethylammonium-2-hydroxyl-1-propane-sulfonate (CHAPSO) and 1, 2-dimyrisotyl-sn-glycero-3-phosphocholine (DMPC) (Figure 4.7).

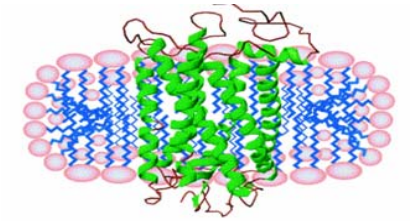

Figure 4.7 Schematic representation of DMPC:CHAPSO bicelle containing a protein molecule [17].

DMPC was purchased from Avanti Polar Lipids and CHAPSO was purchased from Sigma-Aldrich. 40%, 2.8:1 (DMPC:CHAPSO) bicelles mixture was prepared, and then mixed with the protein in a 4:1 (protein:bicelles) ratio. Crystals were grown by the hanging drop method in 1-2 weeks, by mixing 4 µl protein/bicelles mixture with 1.5 µl precipitant solution. The precipitant solution was used as mother liquor in the well.

Batch crystallisation method was tried as well; however the hanging drop method gave more uniform results and was easier to reproduce. The precipitant solution contained 2.45 M NaH_2PO_4 pH 3.7, 180 mM hexanediol, and 3.5% triethyleneglycol. The protein/bicelles mixture was kept on ice to ensure its fluidity and was homogenized by pipetting up and down. Crystal trays were kept at RT in the dark.

4.2.3 Alternative means of sample preparation- Lipodisqs™

Lipodisq™ samples were prepared by mixing a 2.5% polymer sample supplied by Malceutics Ltd was mixed with 2.0% DMPC (Avanti Polar Lipids) in 50 mM Tris HCl (pH 8.0) in a polymer: lipid weight ratio of 1.25:1. The mixtures had to be mixed for the Lipodisqs™ to form. Once formed the Lipodisqs™ were colourless and liquid.

4.2.4 Solid state NMR

For the ease of comparison, all the ss NMR experiments were performed at the same probe temperature of 253 K and MAS frequency of 10 kHz. Ramped-amplitude cross polarisation (CP) was performed with contact time always 1 ms and two pulse phase modulated [207] decoupling during the acquisition period. Dwell was 10 μs and spectral width 100 kHz in all four experiments. All the spectra were referenced externally to NH_4Cl [208].

4.2.4.a Experiments acquired on a 800 MHz proton frequency Varian/Magnex Spectrometer

One comparison of the spectra from the purple membrane and microcrystals was performed on the 18.8 T (800 MHz proton frequency) Varian/Magnex Infinity + solid-state NMR spectrometer in a 3.2 mm Balun probe. The pulse delay between transients was 2 s. The spectra were referenced to NH_4Cl at 39.27 ppm [208].

For the ^{15}N CP MAS spectrum of purple membrane (23 mg), the ^{1}H and ^{15}N field strengths were 57 kHz and 46-29 kHz during CP, respectively. TPPM proton decoupling of 74 kHz was applied during the 41 ms of ^{15}N acquisition. 24 k scans were collected. For the bacteriorhodopsin crystal spectrum, 24 mg of bR crystals were packed into a 3.2 mm thin wall rotor. The ^{15}N polarization was established using ramped-amplitude cross-polarization (CP) from proton to nitrogen with a contact time of 1 ms: the ^{1}H and ^{15}N field strengths were 57 kHz and 46-29 kHz during CP, respectively. TPPM proton decoupling of 80 kHz was applied during the 51.2 ms ^{15}N acquisition time. 28 k scans were collected.

4.2.4.b Experiments acquired on a 500 MHz proton frequency Varian/Magnex Spectrometer

The other set of purple membrane and bacteriorhodopsin crystals spectra comparison was carried out on a lower magnetic field 11.7 T (500 MHz proton frequency) Varian Infinity Plus spectrometer in a 4 mm APEX HX probe. Using Teflon spacers the sample was positioned in the centre of the rotor to achieve optimal field homogeneity. The acquisition time for both experiments was 51.2 ms, the dwell 10 μs and spectral width was 100 kHz. The pulse delay for these experiments was 4 s.

^{15}N-Met labelled bR crystals (60 mg) were packed into a 4 mm standard rotor. Proton decoupling during acquisition was 75 kHz. Resolution was 0.4 ppm. Proton 90 degree pulse on 497.91 MHz was 75.6 kHz. ^{1}H field strength during the tangent CP was 62 kHz, and the

field strength on ^{15}N 50.45886 MHz was 42-50 kHz. Proton decoupling during acquisition was 77 kHz. 32 k scans were acquired.

^{15}N Met labelled PM (18.9 mg) in Na citrate buffer pH 6.0 was packed into a 4 mm standard rotor. The experimental conditions for the 1D tangent shaped CP experiment were the same as for the bR crystals apart from the 90 degree pulse on ^{1}H was 83.3 kHz. ^{1}H and ^{15}N field strength during the tangent shape CP pulses were 64 kHz and 42-50 kHz, respectively. Proton decoupling of 75 kHz was used during acquisition.

4.2.5 Transmission Electron Microscopy

Lipodisq™ was adsorbed for 10s to parlodion carbon-coated grids rendered hydrophilic by glow discharged at low pressure in air. Grids were washed with tour drops of double-distilled water and stained with 2 drops of 0.75% uranyl formate. Images were recorded on Eastman Kodak Co. SO-163 sheet films with a Hitachi H-7000 electron microscope operated at 100 kV.

4.2.6 Static ^{31}P solid state NMR experiments acquired on a 400 MHz proton frequency Bruker Spectrometer

One dimensional ^{31}P spectra of Lipodisqs™ (with oriented lipids on glass slides parallel and perpendicular to the magnetic field) were recorded using a Hahn-echo pulse sequence under conditions of proton decoupling during the acquisition. The spectra were recorded on a 400 MHz Bruker spectrometer using a static probehead and 1028 scans were collected at room

temperature. The effect of higher temperature on the orientation of Lipodisqs™ was tested by repeating the experiment at 296 K.

4.3 Results and Discussion

4.3.1 Crystallisation trials of bR

The progress of 3D crystallisation of membrane proteins is generally slow and every protein requires different conditions for crystallisation. There are more parameters that have to be varied than with the soluble proteins, and integral membrane proteins generally do not form well-ordered crystals as readily as soluble ones. The goal of the work presented in this chapter was to produce three-dimensional crystals of bacteriorhodopsin and to compare by solid state NMR their resolution with the resolution of the purple membrane, which is naturally a 2D crystal. For 3D crystallisation, bR was solubilised into monomers which were used for crystallisation. The purity of the detergents has been reported to be important for crystal formation in this protocol [205]. Solubilisation and detergent exchange are also very important. However, the crystallisation trials of delipidated, monomeric bR did not result in 3D crystals, possibly because the detergent was not replaced completely, insufficient protein was present in the drops or impurities such as the dimeric or trimeric forms of bR, and lipid molecules might have interfered with the crystallisation. The monomeric bR in the sitting drops lost its purple colour after a few months, which indicates the protein became denatured.

The other crystallisation approach using bicelles, resulted in diamond-shaped 3D crystals that formed relatively quickly and reproducibly (Figure 4.8). The protein is thought to pack in layers inside the crystal and the packing within each layer remains the same [8] and the crystal appears to be stacked sheets of two-dimensional (2D) crystals. The sheet structures in the crystals are the same, but the way the sheets stack is thought to be different in each crystals. It has been suggested that there is a probability that crystal growth is nucleated by the formation of the 2D crystals onto each other. The bicelles method is based on the ability to control the liquid to gel phase transition.

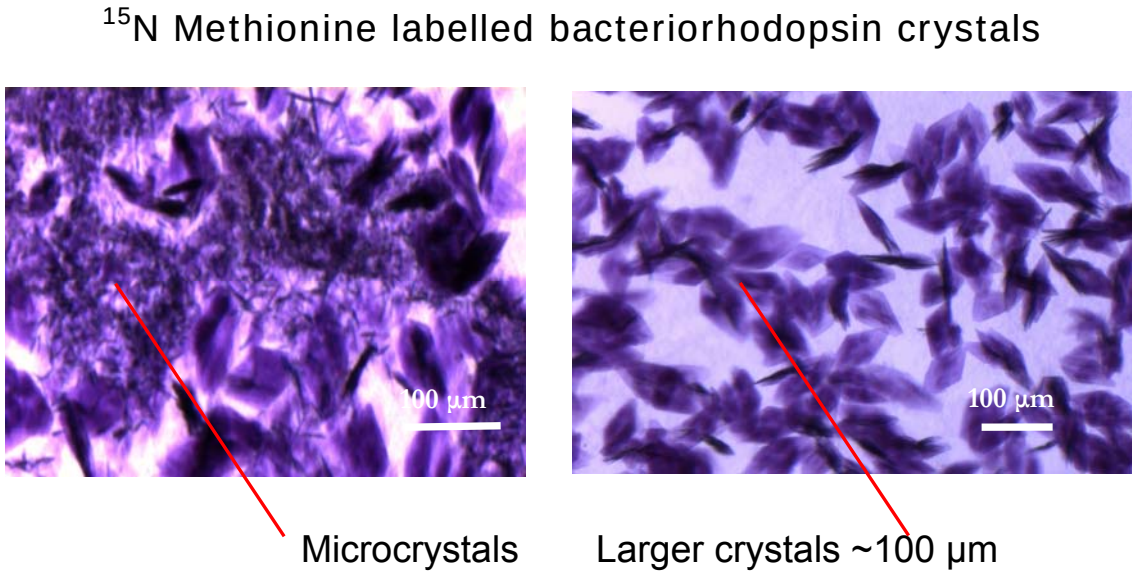

Figure 4.8 ^{15}N Methionine labelled bacteriorhodopsin three dimensional crystals, grown at room temperature in DMPC:CHAPSO bicelles [8]. The crystals are diamond-shaped. Small, microcrystals formed at the nucleation sites (left) and larger crystals (right) about 100 µm in length.

4.3.2 Solid state NMR experiments of ^{15}N Met labelled bR

1D ^{15}N CP MAS spectra were collected for both PM and the 3D crystallised bR on 500 MHz and 800 MHz Varian/Magnex Infinity + spectrometers. In the 1D ^{15}N spectra of ^{15}N-Met labelled bacteriorhodopsin collected on 500 MHz and 800 MHz Varian/Magnex Infinity + spectrometers (Figure 4.9 and Figure 4.10), at least six out of the nine methionine resonances are resolved in the 248 residue bR. In our hands PM seems to be more homogeneous. It was not possible to resolve all nine methionines.

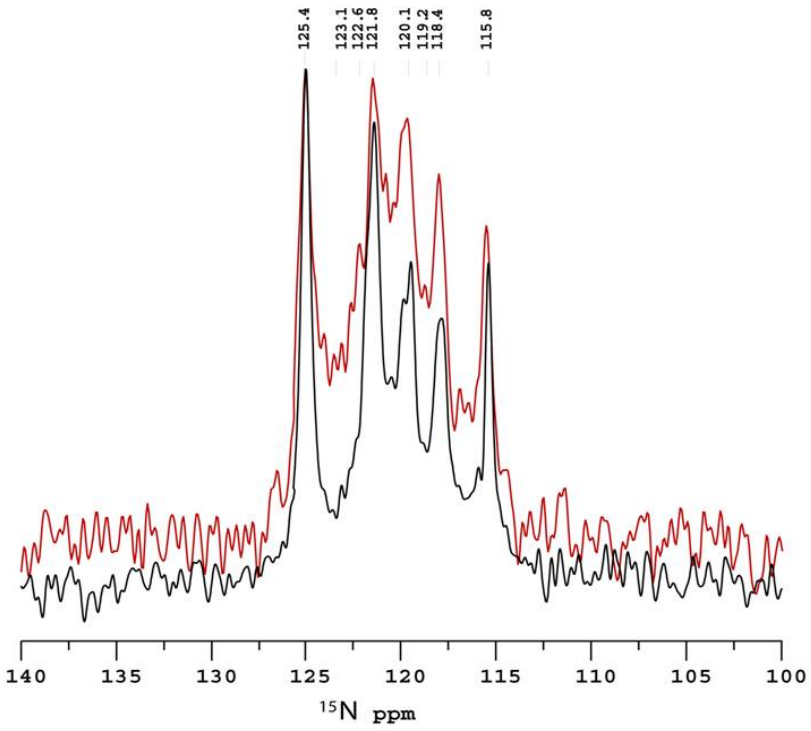

Figure 4.9 Overlay of 1D ^{15}N spectra of ^{15}N-Met labelled 23 mg purple membrane sample (black spectrum) and 24 mg bR microcrystal sample packed in a 3.2 thin wall rotor (red spectrum) collected in a 3.2 mm Balun probe on an 18.8 T Varian Infinity + solid state NMR spectrometer. Spinning frequency was 10 kHz and probe temperature 253 K. ^{1}H decoupling of 74 kHz was applied during the 41 ms ^{15}N acquisition. For more experimental detail see Material and Method section in this chapter.

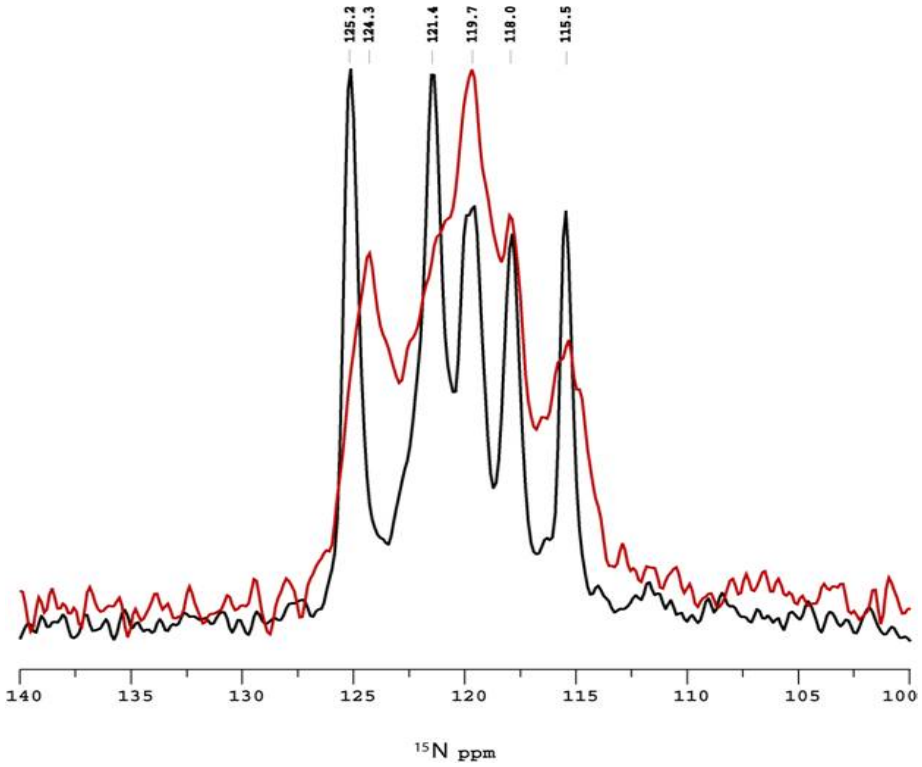

Figure 4.10 Overlay of ^{15}N CP MAS spectra of 18.9 mg purple membrane sample in Na citrate buffer pH 6.0 (black spectrum) 57344 acquisitions with the 59.8 mg microcrystal spectra of bacteriorhodopsin (red spectrum) 43008 acquisitions recorded on the 500 MHz Varian/Magnex Infinity + Spectrometer in a 4mm HX APEX probe. The probe temperature was 253 K and the MAS frequency was 10 kHz. The FID was acquired for 51.2 ms and 75 kHz TPPM proton decoupling was applied during acquisition.

In Table 11 chemical shifts of the samples collected on the 500 MHz and 800 MHz Vairan/Magnex Infinity + spectrometer were compared to chemical shifts resolved previously [22]. There is a general agreement of the chemical shifts that are fully resolved; however there are several unresolved resonances in our samples. Further orientation of the purple membrane on glass slides may improve resolution, but this was not tried.

Table 11 ^{15}N Chemical Shifts identified in the ^{15}N CP MAS spectrum of (±0.1 ppm). The chemical shift of the purple membrane sample we prepared (recorded on the 500 MHz and 800 MHz Varian/Magnex Infinity + spectrometers) match the chemical shift resolved previously [22].

Residue number	MAS (600 MHz) *Summurised*	MAS (800 MHz) Spectrometer Purple membrane	MAS (500) Spectrometer Purple Membrane
M118	125.3	125.4	125.2
M	123.0	Not observed	124.3
M32	122.2	Not observed	Not observed
M68	121.6	121.8	121.4
M163	Not observed	Not observed	Not observed
?	120.1	120.1	Not observed
?	119.7	Not observed	119.7
M145	118.3	118.4	118.0
M20	115.7	115.5	115.8

4.3.3 Studies of alternative means of sample preparation for solid state NMR

The Lipodisqs™ were visualised by transmission electron microscopy (TEM) in the Müller Institute for Structural Biology in the University of Basel by members of the group of Professor Engel in order to determine their shape and measure their diameter. The Lipodisqs™ were prepared in 50 mM Tris buffer (pH 8.0). Individual Lipodisqs™ can be recognised and are pointed with white arrows in the TEM micrograph in Figure 4.11. The preparation seems to be quite homogeneous; however the discs have a tendency to form aggregates. The frames of the enlarged areas in Figure 4.11 are 25.6 nm long.

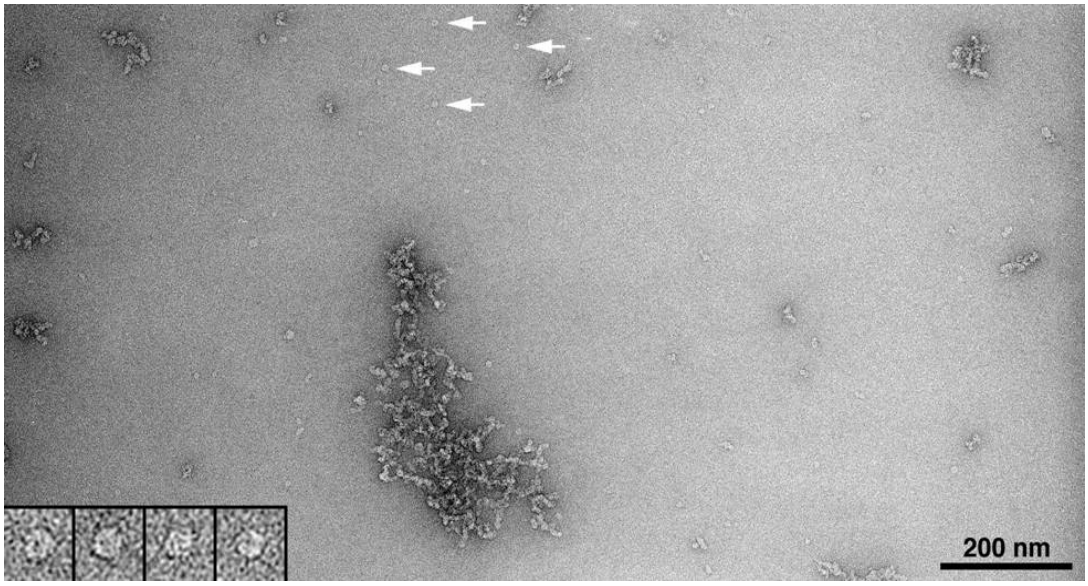

Figure 4.11 TEM micrograph of negatively stained Lipodisqs™ prepared in 50 mM Tris buffer with pH 8.0. This is a homogeneous particle population, with a diameter of about 11 nm. Individual Lipodisqs™ selected with the white arrows were magnified and are displayed in the gallery. The discs tend to form aggregates. The scale bar represents 200 nm, and the frame size of the magnified particles in the gallery is 25.6 nm. The TEM micrograph of our sample was taken in the Müller Institute for Structural Biology, University of Basel by Dimitrios Fotiadis in the Group of Andreas Engel.

It is of interest to find out whether the Lipodisqs™ orient in a magnetic field. Phosphorus-31 NMRspectra for Lipodisq™ shown in Figure 4.12 and Figure 4.13 respectively show that the Lipodisqs™ do not orient in the magnetic field. The narrow isotropic peak at 0 ppm is from the Lipodisqs™. Oriented egg phosphatidyl choline (PC) lipid bilayer was used as a control.

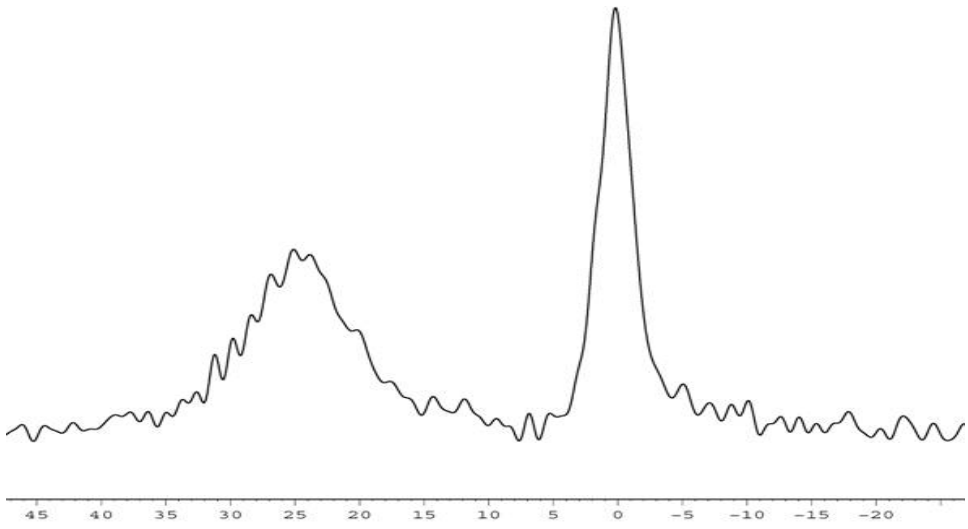

Figure 4.12 ^{31}P static NMR spectrum of Lipodisqs™ made of 20% DMPC and Lipodisq™ solution with 1.25:1 polymer:lipid weight ratio. The Hanh echo spectrum was taken on a 400 MHz Bruker Avance spectrometer in a static probe at 310 K. 1028 scans were collected. The Lipodisqs™ were placed in the coil of the static solid state probe against oriented lipid bilayer (Egg PC) for ease of comparison, where lipids are oriented parallel to the magnetic field at 25 ppm. The isotropic peak of Lipodisqs™ is at 0 ppm.

4.4 Conclusions

In our hands, PM seems to be more homogeneous than the 3D bR microcrystals. Thus, we proceeded with the purple membrane preparation for further experiments reported in Chapter 5. Inhomogeneity of 3D crystals could have been caused by one of several possibilities. For x-ray crystallography studies a single crystal of highest quality is picked, in our study many crystals were used indiscriminately. Other possibilities include using a different method for

harvesting the crystals and packing as an option, because the harvesting and packing might influence the integrity of the crystals. The crystallisation method can be further optimised towards obtaining homogeneous crystals for NMR. Crystals can be washed with the buffer of same concentration with a lower salt concentration, instead of MilliQ H_2O. Optimising batch crystallisation to produce more homogeneous crystals may improve the quality of the crystals.

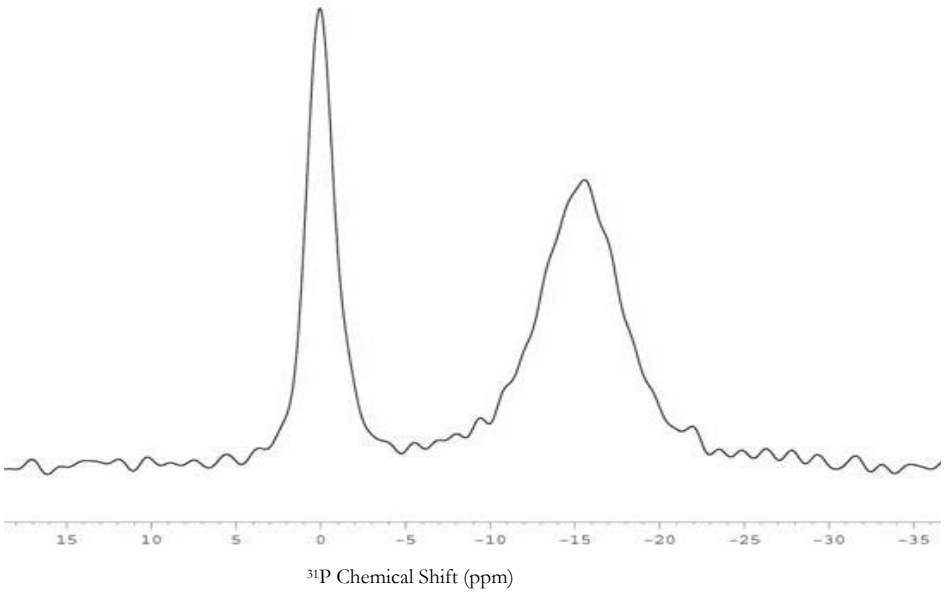

Figure 4.13 ^{31}P static solid state NMR spectrum of Hanh echo experiment of Lipodisqs™ made up of 100 µl 2% DMPC and 1.25:1 polymer:lipid weight. The spectrum was recorded on a 400 MHz Bruker solid state NMR magnet using a static probe. 1028 scans collected at 310 K against oriented lipid bilayer (Egg PC oriented with the bilayer normal perpendicular to the magnetic field, gives rise to the peak at -15 ppm) for ease of reference. The peak at 0 ppm is that of the lipodisq. This frequency indicated that the Lipodisqs™ have rapid isotropic motion. The effect of higher temperature on the orientation of Lipodisqs™ was tested (results not shown) by repeating the experiment at 296 K, but result were the same.

2D crystals in purple membranes are more suitable for solid state NMR studies than 3D bR crystals (under current crystallisation conditions), which could be due to different types of crystalline forms.

As an alternative mean of sample preparation TEM of negatively stained Lipodisqs™ revealed a homogeneous population of discoid particles with a great tendency to aggregate. The measured diameter of the particles was 11 nm. ^{31}P static solid state NMR studies of Lipodisqs™ revealed that the particles do not orient in a magnetic field without protein.

Chapter 5 Solid State NMR of U- ^{15}N, ^{13}C, ^{2}H Labelled Bacteriorhodopsin

Varga, K., Aslimovska, L., Parrot, I., Dauvergne, M-T., Haertline, M., Forsyth, T. and Watts, A. (2007) NMR Crystallography: The effect of deuteration on high resolution ^{13}C solid state NMR spectra of a 7-TM protein (in revision) BBA

5.1 Introduction

The assignment of integral membrane proteins by solid state NMR is still a difficult challenge, largely because of their size and difficulty in obtaining enough material. The main aim of the research reported in this chapter is to establish the feasibility of sequential, site specific assignment of uniformly ^{13}C, ^{15}N labelled bacteriorhodopsin (bR) in the purple membrane by solid state NMR crystallography. Bacteriorhodopsin is a 248 amino acid, mostly α-helical 7 transmembrane protein from *H. salinarium*. Prior to assignment studies optimal conditions for producing spectra suitable for spectral assignment were investigated by studying the effects of deuteration on the solid state NMR spectral resolution of large membrane proteins by deuterating a U-^{13}C, ^{15}N bacteriorhodopsin. Comparison of ^{13}C linewidths of highly deuterated - more than 50 %, 50% deuterated and non-deuterated U-^{13}C, ^{15}N labelled bR 2D crystals in purple membrane, its natural environment have been made and the sample with optimal deuteration level be used for protein assignment. Another aim is to find the best experimental methods for completing the assignment. The assignment work is still in progress. Further experiments, which would assist in confirming and completing the assignment, will be discussed.

The photoreceptor bacteriorhodopsin (bR) was chosen as a model system because of its stability; bR is stable at room temperature for extended periods of time. It is a tightly associated trimer and very well characterised structurally and functionally. Long sample life time and thermal stability make bR a suitable system for solid state NMR studies. Sample heating is another general consideration at MAS high frequency (~10 - 13 kHz). Even more importantly, hydrated protein samples which contain salt buffers are prone to heating caused by high *rf* power pulses, especially during long proton decoupling. Another reason for choosing bR is its availability and relative ease. For most membrane proteins, overexpression and purification is still a challenge, as discussed in Chapter 1. Bacteriorhodopsin is readily available from *H. salinarium* and the purification is well established [209]. It is possible to label uniformly the protein with ^{13}C, ^{15}N and ^{2}H [24]. In addition, bR has a secondary structure which resembles GPCRs; bacteriorhodopsin is an integral seven transmembrane protein in a mostly α-helical confirmation [27]. There is a strong correlation between protein secondary structure and chemical shifts, as discussed in Chapter 1. The feasibility of the resonance assignment on bR may be indicative of the feasibility of assignment techniques for other structurally unresolved receptors, including GPCRs.

Bacteriorhodopsin is therefore a very well studied membrane protein and the above mentioned characteristics make it an ideal system for study here. Three differently labelled samples of bacteriorhodopsin were prepared to test the applicability of the various NMR assignment strategies, and the effects of deuteration on a large membrane protein, for solid state NMR investigation.

5.2 Use of Deuteration in NMR

5.2.1 Use of deuteration in solution state NMR

Deuteration has been used routinely in solution NMR for ^{13}C, ^{15}N labelled protein assignment studies [210]. Deuteration of the non-exchangeable proton sites, except the H_N protons, improves the sensitivity of the experiment due to two effects: first, the nuclei, in particular the ^{13}C, relax more slowly thus allowing more magnetisation to be transferred between J-coupled nuclei; second, the slower relaxation of $^{1}H_N$ nuclei results in sharper, more intense lines in the observed spectrum. In addition, the slower relaxation of ^{13}C makes it possible to extend the length of the evolution period, thus to obtain higher resolution in the indirect dimension. The suppression of scalar couplings ($J_{H\text{-}H}$) further improves linewidths in solution NMR studies of membrane proteins, which routinely suffer from poor spectral resolution due to the large size of detergent micelle-protein complexes [211].

5.2.2 Use of deuteration in solid state NMR

In solid state NMR (ssNMR), deuteration has been mainly used as a tool to study protein and lipid dynamics [211]. Deuterium has a gyromagnetic ratio ~6.5 times lower than that of ^{1}H, which greatly reduces dipolar couplings. Deuterium has low natural abundance of 0.02 %. In deuterium NMR experiments, the quadrupolar interaction (~170 kHz) is much larger than the chemical shift anisotropy and homo- and heteronuclear dipolar couplings [211]. In ssNMR, deuteration is also used for the purpose of diluting ^{1}Hs to eliminate the strong ^{1}H homonuclear dipolar couplings, resulting in narrow ^{1}H lines without the need for multiple pulse ^{1}H homonuclear decoupling [212].

To date, only a few studies are available on the effect of deuteration on ^{13}C and ^{15}N linewidths of soluble, microcrystalline proteins [213-215], and none have been reported for membrane proteins [215-217]. Moreover, the findings from these studies are not consistent with each other. On the one hand, high resolution ^{13}C spectra which were obtained for ubiquitin, where the linewidths were found to be identical between the protonated and deuterated samples when proton decoupling was applied [215]. On the other hand, proton decoupling was not sufficient to achieve high resolution ^{13}C spectra for the SH3 domain, and deuterium decoupling significantly improved ^{13}C linewidths [217]. In another study, on the Crh receptor, deuteration did not improve ^{13}C linewidths relative to the protonated Crh, and the line broadening could not be recovered with ^{2}H decoupling [216]. Here, the effect of deuteration on line widths and spectral resolution of U-^{13}C, ^{15}N labelled bacteriorhodopsin was studied.

5.2.3 Effects of deuteration on CP-efficiency

The ^{13}C cross polarisation (CP) magic-angle spinning (MAS) NMR of deuterated proteins can be expected to be less efficient than for protonated proteins [218]. By diluting the ^{1}H pool there is less ^{1}H magnetisation available for CP, and therefore the ultimate enhancement of the ^{13}C signal will be lessened. Diluting the ^{1}H bath would also be expected to increase the ^{1}H T_1 time, requiring the recycle delay to be lengthened in any ^{13}C and ^{15}N observed CP MAS experiments. These potential drawbacks did not, in fact, present significant difficulties to ^{13}C CP MAS spectroscopy of some heavily deuterated proteins [215]. Reasonable CP efficiency was obtained for CO and Cα carbons in deuterated samples in the study of Morcombe and colleagues [215]. Deuteration has surprisingly little effect on both ^{1}H and ^{13}C longitudinal relaxation times. A comparison of ^{1}H decoupled ^{13}C line widths for Cα carbons in protonated and deuterated

ubiquitin by Morcombe and colleagues [215] discovered no statistically significant differences, and therefore deuteration decoupling was not deemed necessary .

Deuteration has, however, been found to provide significant advantages in many applications. By employing deuteration, the ^{13}C resolution in 2D and 3D experiments need not be limited by decoupler heating. If ^{1}H decoupling is not applied, the CO and deuterated Cα carbon line widths only increase by a modest 0.08 ppm at a MAS rate of 20 kHz [215]. Since deuteration also provides for very high resolution in the amide ^{1}H spectrum, this aspect can be taken advantage of in ^{1}H/^{15}N/^{13}C triple resonance experiments where the ^{1}H decoupling is critical for optimizing the ^{15}N resolution. Proteins that prove to be too sensitive to decoupler heating to be studied by the standard CP MAS methods, may also become accessible with extensive deuteration. Perdeuteration is also useful for correlation spectroscopy experiments and helps circumvent truncation problems by simplifying the spin system [215].

5.3 Introduction to NMR Spectroscopy Assignment of Proteins

For investigation of proteins by either solution or solid-state NMR spectroscopy, independent of whether structural or dynamic information is extracted from the spectrum, the resonance assignment of individual sites of the system is necessary [205]. Assignment of resonance peaks means correlation of the correct chemical shift of the observed resonances to the corresponding amino acid site in the protein. In solution NMR, multidimensional homonuclear and heteronuclear chemical shift correlation methods based on scalar couplings are used to transfer the coherence between spins and provide a basis for the resonance assignment of proteins.

Analogous correlation schemes can be employed when designing multidimensional magic angle spinning (MAS) experiments for the resonance assignment of solid proteins. With the MAS methods, the observed isotropic shift allows identification of the different amino-acid types by means of the characteristic side-chain correlation patterns, as in solution NMR. However, different from solution NMR, in solid-state experiments dipolar couplings are used for coherence transfer as well as the scalar couplings [65, 212, 219-223]. Under MAS, homonuclear and heteronuclear dipolar couplings can be reintroduced by various radio-frequency sequences [224].

One main difference between the solution and solid state NMR techniques is the type of spins usually observed. In solution NMR, assignment experiments involve proton detection, as well as ^{13}C and ^{15}N detection. In solid-state NMR ^{1}H detection is not routine because of strong dipolar couplings between protons which give rise to broad lines, even when using sophisticated resolution enhancement techniques combined with fast MAS of the currently highest available magnetic field (21.1 T). Since low-γ nuclei, such as ^{13}C and ^{15}N have smaller dipolar couplings and a larger chemical shift range, they give rise to much better resolved spectra and are the nuclei of choice for detection. A potential assignment strategy for solid state NMR involves ^{13}C and ^{15}N. First, ^{13}C resonances belonging to the same **residue type** are identified in 2D homonuclear ^{13}C correlation spectra [114, 225-228]. The second step of the assignment procedure concerns the sequential **site specific** assignment, that consists in correlating the side-chain signals to the backbone resonance in such a way that the sequential number can be assigned to the identified residue. For this purpose, heteronuclear ^{13}C, ^{15}N spectrum can be recorded where selective transfer between the ^{15}N backbone signal and the Cα or CO signals is

achieved. These experiments will be referred to as the NCA and NCO experiments in the text. A schematic diagram of the magnetization transfer and the pulse sequence of the NCA and NCO are shown in Figure 5.2.

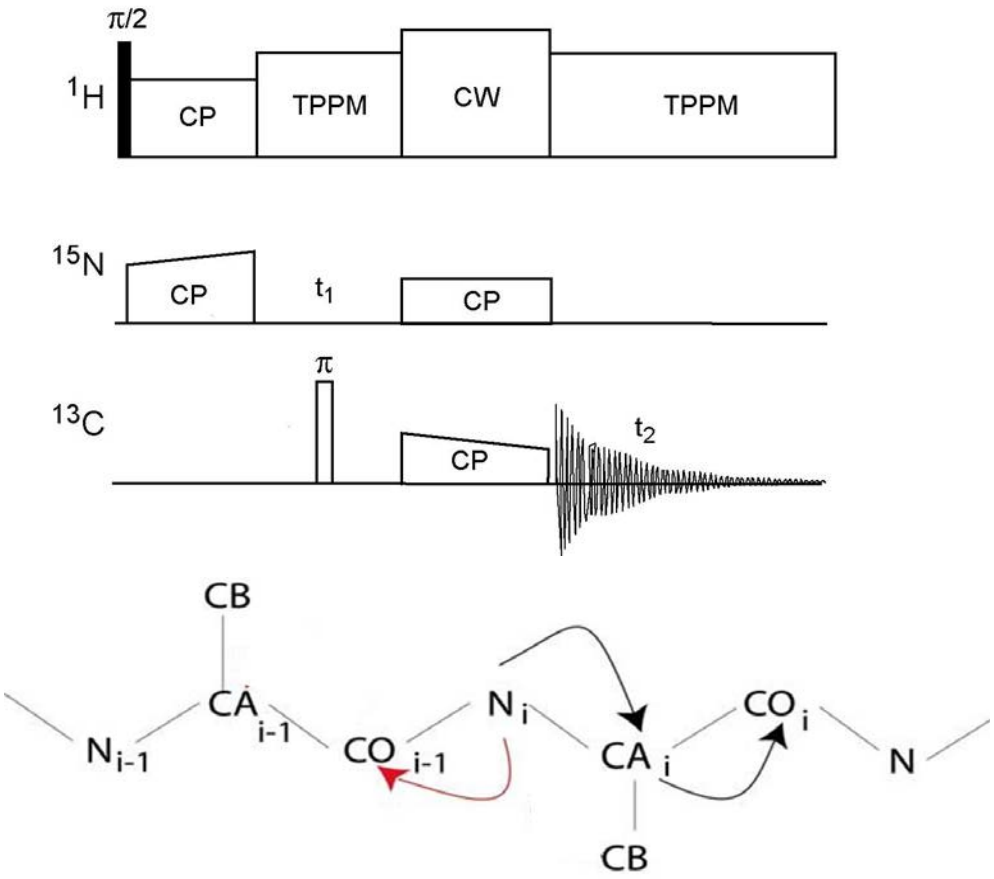

Figure 5.1 Schematic representation of the pulse sequence used for the 2D heteronuclear NCA and NCO correlation experiments and the magnetization transfer in these experiments. Heteronuclear decoupling can be achieved by the two pulse phase modulation (TPPM) [19] [25] decoupling method during evolution and acquisition, while continuous wave (CW) decoupling can be applied during the specific-CP step, which is indicated with red arrow. Magnetisation from the neighbouring protons is transferred to ^{15}N. With a second, selective CP the magnetization can further be transferred onto the neighbouring Cα indicated with a black arrow or CO indicated with a red arrow. If the resolution is good enough, sequential assignment for the backbone is possible based on the NCA and NCO spectra. However, for uniformly labelled large proteins the 2D NCA and NCO spectra are too congested to be able to resolve most of the peaks. Therefore, these spectra are often used as a preparation for 3D structure determination

5.3.1 Residue type assignment

5.3.1.a Two dimensional dipolar assisted rotational resonance

2D DARR (dipolar assisted rotational resonance) is a recoupling mechanism, which uses a combination of mechanical rotation of the sample and homonuclear dipolar coupling [229]. Magnetisation is exchanged when a spinning sideband of one spin overlaps with the isotropic resonance or sideband of another. Irradiation of the protons at the rotational resonance condition recouples the ^{13}C-^{1}H dipolar interaction, broadening the lines in the carbon spectrum.

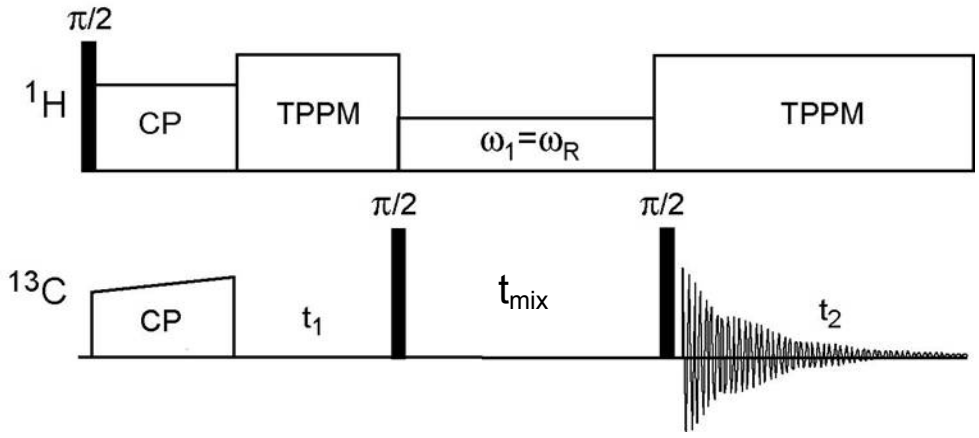

Figure 5.2 Pulse sequence for the 2D DARR ^{13}C-^{13}C correlation experiment. Following ^{1}H excitation, a ramped cross-polarisation between ^{1}H and ^{13}C creates an initial ^{13}C magnetisation. Following ^{13}C evolution, a 90° pulse on ^{13}C brings back the magnetisation along the z-axis. During the mixing time (t_{mix}) low proton field is applied and polarisation transfer between ^{13}C-^{13}C occurs in through proton dipolar couplings. A second 90° pulse on ^{13}C pushes the magnetisation in the x-y plane. During all evolution periods (t_1 and t_2), proton decoupling is applied, using the two-pulse phase modulation technique (TPPM) decoupling scheme.

The pulse sequence of DARR is shown in Figure 5.2. After cross polarization from proton magnetisations, longitudinal magnetisation of ^{13}C spin is obtained by a $\pi/2$ rf pulse. The length

of the mixing time determines the number of bond transfers of the magnetisation. In DARR, reintroduction of ^{1}H- ^{13}C dipolar coupling is utilised by continuous wave (CW) ^{1}H irradiation with the intensity satisfying the rotary resonance condition $\omega_1=n \times \omega_{R,}$ n=1 or 2, where ω_1 is the field strength of the recoupling ^{1}H pulse and ω_R is the rotor spinning frequency. Finally the magnetisations are converted to observable (-1)-quantum coherences by the last $\pi/2$ pulse on the ^{13}C channel. The DARR experiment is more effective than radio frequency driven recoupling (RFDR) (described next) at measuring long range, through-space correlations that carry the most information concerning structure, and DARR is less sensitive to inhomogeneous B_1 fields than RFDR [228, 230]. The DARR sequence has been reported to solve problems associated with dipolar truncation [231].

5.3.1.b 2D Radio frequency-driven dipolar recoupling (RFDR)

The second 2D type of ^{13}C-^{13}C homonuclear correlation experiment to be used here is radio frequency driven recoupling (RFDR) which is used for measuring ^{13}C-^{13}C through space correlations [229]. A rotor-synchronised sequence of π-pulses, which satisfies the echo condition ($t_{mix}=n*T_r$, where T_r is the rotor period and is equal to the inverse of sample rotation frequency), is applied to partially reintroduce dipolar coupling over the mixing time [229]. The pulse train, Figure 5.3, reintroduces the zero quantum (flip-flop) part of the dipolar coupling term of the spin Hamiltonian, allowing for magnetisation exchange between coupled spins. The exchange rate (t^{-1}) is relatively rapid. Drawback of RFDR is that the refocusing of the magnetisation for acquisition is sensitive to precise setting of the 180° pulses; as a result B_1 inhomogeneity causes significant dephasing of the signal when the sample is not constrained to

the centre of the rotor. The length of the mixing time and the observable distance is limited by the capabilities of the hardware and sample heating due to this requirement for high ^{1}H power.

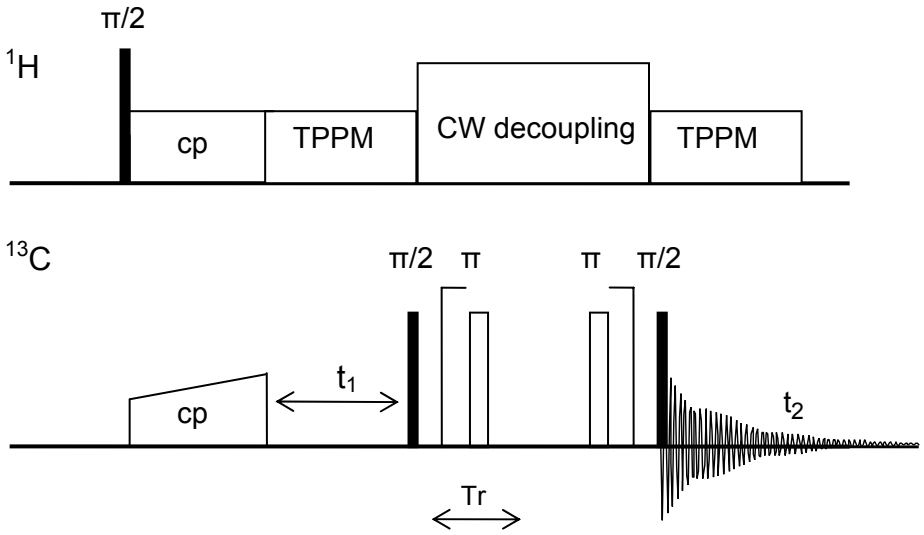

Figure 5.3 Schematic representation of the RFDR pulse sequence. The sequence begins with a CP using a ramped pulse on the ^{13}C channel. After the evolution period t_1, a 90° pulse moves the magnetisation along the z- axis where the mixing occurs with high power ^{1}H decoupling. In RFDR experiment, the mixing is driven by a train of rotor synchronised 180 ° pulses on the ^{13}C channel. Two pulse phase modulated decoupling is used during acquisition and evolution [23, 24].

5.3.2 Site-specific assignment

Site-specific assignments can be made based on 3D spectral assignments and backbone walk. In the 3D ^{15}N-^{13}C-^{13}C spectrum, the ^{13}C spectral congestion is relieved by the dispersion of the ^{15}N chemical shifts. Unique side-chain shifts can further improve resolution. 3D NCACX and NCOCX, where CX refers to any carbon, spectra can be acquired by the DCP-DARR sequence [114] which combines a selective double cross polarization (DCP) [232] sequence and DARR.

The double cross-polarisation sequence (DCP) can be used to selectively direct polarization from ^{15}N to ^{13}CA or ^{13}CO, which was then transferred to other ^{13}C nuclei by DARR. The polarization transfer scheme is shown in Figure 5.4.

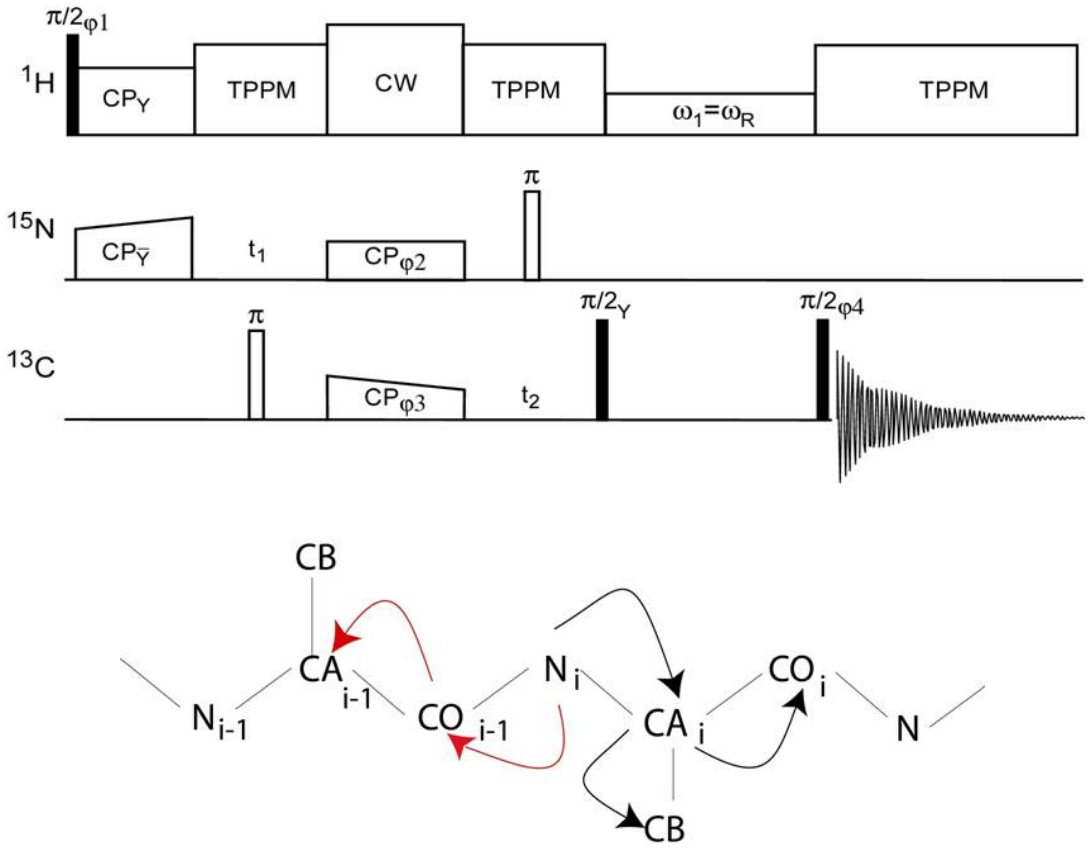

Figure 5.4 3D DCP-DARR pulse sequence and schematic representation of the polarisation transfer pathways on the backbone. The intra-residue transfer pathway (NCACX) is indicated with black arrows, and the inter-residue pathway (NCOCX) is indicated with red arrows [17].

5.4 Materials and Methods

5.4.1 Preparation of deuterated U-^{13}C, ^{15}N labelled bacteriorhodopsin

This section describes three differently labelled bacteriorhodopsin samples prepared, in order to study the effect of deuteration on solid state NMR spectra. The samples are all U -^{13}C, ^{15}N labelled with different deuteration levels: one is fully protonated, the other one is 50% deuterated and the third sample is heavily deuterated, grown in more than 50% deuterated media. There is one described method in the literature for deuterated U- ^{13}C, ^{15}N labelling of bR [24] using ^{2}H, ^{15}N or ^{13}C, ^{15}N-labelled media prepared from *Scenedesmus obliquus* algae and *Chenopodium rubrum* cell cultures respectively. Here two commercially available labelling media Silantes and Celtone were tested. Celtone was found to be better suited for Halobacterial growth. The growth conditions were further optimised and used for labelling. The testing, optimisation and labelling procedures are reported here.

5.4.1.a Strain of *H. salinarium* used and growth conditions

For the expression of bR the *Halobacterium salinarium* strain S9 was used. The S9 strain is a bacteriorhodopsin overproducer, it is a derivative obtained from a mutagenised culture of wild type R1 and is gas vacuole-deficient (Vac^-) which aids the isolation of cell membrane [233, 234] The comparison of the phenotypes of the wild type and the S9 strain can be seen in Table 12.

Halobacterial cells grow at temperatures as high as 57 °C, however evaporation of water becomes a problem at that temperature and therefore 37 °C is usually used [235]. Growth of Halobacterial cells is followed by measuring the absorbance of the cultures at 660 nm and

synthesis of purple membrane (PM) is measured by absorbance of the purple membrane fraction at 560 nm. A sharp increase in the synthesis of the PM occurs at the end of the exponential growth phase. Small differences in culture conditions may result in almost complete loss of purple membrane. This was taken into account when growing the uniformly labelled deuterated bacteriorhodopsin. Among other parameters, light and the O_2 tension in the culture medium are crucial [204]. Growth at low O_2 levels, 37 ° C and illumination favors bR production. In some cases, the purple membrane can represent as much as 50% of the total cell surface area in *H. salinarium* [236]. Synthesis of bacterioruberin may impinge on PM synthesis because bacterioruberins share common biosynthetic pathway with retinal [237]. Conditions which favoured bacterioruberin over bR production, such as aeration and insufficient amounts of vitamins like thiamine, folic acid and biotin, were avoided.

Table 12 Comparison of the wild type R1 and S9 *H. salinarium* strains phenotypes. S9 is a gas vacuole deficient (Vac^-), ruberin synthesising (Rub^+) and purple membrane overproducing (Pum^{++}) derivative of the wild type [14]

Strain	Phenotype	Source
Wild type (R1)	Vac^+ Rub^+ Pum^+	
S9	Vac^- Rub^+ Pum^{++}	W. Stoeckenius

5.4.1.b Choosing the optimal labelling medium and cell growth conditions

For the production of triple labelled (^2H, ^{13}C, ^{15}N) bR, two commercially available labelling media were compared: Celtone from (Spectra Isotope Laboratories) and Silantes media

(Silantes). The growth of *H. salinarium* in these labelling media was checked against the growth in the bacteriological peptone non-labelling media from Oxoid in which the cells grow optimally. *H. salinarium* grew better in Celtone medium than in Silantes, hence Celtone was used to optimise and prepare uniformly ^{13}C, ^{15}N labelled bR.

Comparison of growth of *H. salinarium* in Peptone (OxoidL37) and Celtone-CN was made using 25 ml volume cultures. The archaea grow exponentially at the same rate (results not shown here) until day 3. After day 3 the archaea in peptone medium continue to grow faster than the archaea in the hydrogenated Celtone medium. Effects of aeration, illumination, vitamins and minerals on growth were tested.

When the starter cultures were at the mid log phase, they were transferred into flasks containing 500 ml media and incubated in an orbital shaker at 37 °C for 10 days with a shaking speed of 110 rpm under illumination for about 5 days. Growth was monitored at OD_{660} and visual inspection of the pellet colour was used as an indicator of bR production. The cultures were harvested by centrifugation when the optical density at 660 nm had peaked. The growth of labelled medium was optimized and the highly deuterated CN-bR and 50% HDCN-bR were produced in the ILL-EMBL Deuteration Laboratory at the Partnership for Structural Biology in Grenoble, France.

5.4.2 Media preparation

5.4.2.a Celtone media preparation.

All three samples were U-^{13}C, ^{15}N labelled using the Celtone medium obtained from Spectra Stable Isotopes but with different level of deuteration. One sample was grown in fully protonated medium, the other one was grown in 50/50 mixture of H_2O/D_2O and the third one was grown in 50% deuterated medium dissolved in 100% D_2O. The procedure for preparation of all three differently labelled Celtone media was the same, the only difference is the use of the Celtone powder with the appropriate labelling scheme (Celtone-CN for the fully protonated, Celtone-dCN 50% for the 50% deuterated sample and Celtone dCN 97% for the fully deuterated) and the appropriate percentage of D_2O used to prepare the media (0% D_2O for the fully protonated, 50% D_2O for the 50% deuterated and 99.9% D_2O for the fully deuterated bR sample).

For volume of 500 ml cultures the following were weighed: 125 g NaCl, 1 g KCl, 10 g $MgSO_4$, 1.5 g sodium citrate ($Na_3C_6H_5O_7$) and 2.5 g of the appropriate Celtone powder (Celtone CN for the fully protonated, Celtone-dCN 50% for the 100% deuterated sample and Celtone dCN 97% for the fully deuterated) pH 6.46. The growth media were also supplemented with trace metals of $MnSO_4$ (0.3 μg/l), $FeCl_2*4H_2O$ (3.6 μg/l), $ZnSO_4*7H_2O$ (0.44 μg/l), and $CuSO_4*5H_2O$ (0.05 μg/l), and sterilised either by autoclaving or by heating to dissolve the salts and powder, and then passing through 0.2 μm Millipore filter.

5.4.2.b Silantes media preparation.

Silantes media was a ready made media provided by the supplier ready for testing, however 125 g of NaCl, 1 g of KCl, 10 g of $MgSO_4$, 1.5 g of sodium citrate ($Na_3C_6H_5O_7$) were also added and sterilised by filtering.

5.4.2.c Peptone media preparation.

For 1L Bacteriologial Peptone media (Oxoid) 250g NaCl, 20g $MgSO_4$ * $7H_2O$, 3 g of sodium citrate *$2H_2O$, 2 g of KCl, 0.2 g of $CaCl_2$ and 10g of Oxoid L37 peptone were weighed and dissolved in water. The growth media were also supplemented with trace metals of $MnSO_4$ (0.3 μg/l), $FeCl_2$*$4H_2O$ (3.6 μg/l), $ZnSO_4$*$7H_2O$ (0.44 μg/l), and $CuSO_4$*$5H_2O$ (0.05 μg/l) and the pH was adjusted to 7.4 with NaOH solution. The medium was sterilised by autoclaving. All the media and their labelling schemes used to produce labelled bR are listed in Table 13.

Table 13 Labelling media tested and used for deuteration and U ^{13}C, ^{15}N labelling of bacteriorhodopsin

Labelling Medium	% Isotopic enrichment	Supplier
Celtone-CN	^{13}C, >98% ^{15}N, >98%	Spectra Stable Isotopes
Celtone-dCN (50%) in 50% D_2O	^{2}H, 50% ^{13}C, >98% ^{15}N, >98%	Spectra Stable Isotopes
Celtone-dCN (>50%) in 99.9% D_2O	^{2}H, 50% ^{13}C, >98% ^{15}N, >98%	Spectra Stable Isotopes
Silantes	Natural abundance	Silantes
Bacteriological peptone	Natural abundance	OxoidL37

5.4.3 Growth, purple membrane isolation and purification

The cells were grown under illumination, in air-tight conditions, and the yield of purple membrane increased. Trace metals were also added to enhance cell growth: $MnSO_4$, $FeCl_2$ $*4H_2O$, $ZnSO_4$ $7*H_2O$, $CuSO_4$ $*5H_2O$.

The purple membrane was isolated as described in reference by Oesterhelt and Stoeckenius [204]. The sizes of the pellets are indicative of the yield of cells. Deuteration of bR increased the weight of the protein. The % of the sucrose gradient had to be altered from 25%-45% to 25%-70% to improve the purification step.

5.4.4 Crystallisation of fMLF model peptide

Met, Leu, Phe (fMLF) peptide is a model compound used for testing solid state NMR pulse sequences and optimising acquisition parameters. It was necessary to crystallise it before using it. The manufacture's protocol crystallisation was followed. Hence, 10mg 98% U-^{13}C, ^{15}N labelled fMLF with 40 mg natural abundance fMLF peptide from Cambridge Isotope Laboratories were dissolved in 12-20 ml isopropanol by stirring it at elevated temperature ~55 °C and sonication, for up to 20-30 minutes. The cycle of stirring it at elevated temperature and sonicating it for 20-30 minutes was repeated several times until the solution became clear. Once it was clear it was allowed to evaporate slowly. Complete evaporation occurred in about 1-3 days.

This preparation procedure resulted in 2 fractions, one that precipitated at the surface of the solution and another one that coated the walls of the vessels. The precipitate at the surface of the solution was collected and used for solid state NMR experiments. Great care was taken not to contaminate this fraction with the isoform precipitate which formed on the walls of the vessel.

5.4.5 Solid state NMR spectroscopy - acquisition parameters

5.4.5.a 1D ^{13}C CP MAS spectra

One set of one dimensional spectra were collected on an 800 MHz Varian/Magnex Infinity + spectrometer in a 3.2 mm HCN Balun probe, using 74 kHz proton decoupling during 30 ms acquisition. The MAS frequency was 10.776 kHz. 1024 transients were signal averaged with 4 s pulse delay. The spectral width was set to 100.00 kHz. ^{1}H-^{13}C cross polarisation (CP) was achieved with a 57 kHz ^{1}H and 39-55 kHz tangent ramped ^{13}C pulse 0.8 ms for the fully protonated, and 1.25 ms for the 50% deuterated and highly deuterated U-^{13}C, ^{15}N bR samples.

The other set of one dimensional spectra were collected on the 500 MHz Infinity Plus spectrometer in a 4 mm HXY Apex probe. MAS frequency was 11.574 kHz and the temperature was 263 K for all three 1D spectra. 1024 transients were signal averaged with 4 s pulse delay. The spectral width like for the 1D spectra collected on the 800 MHz was set to 100 kHz. Contact time during CP was 1.2 ms for the deuterated, 1.75 ms for the 50% deuterated and 0.8 ms for the fully protonated bR sample. The field strength of ^{13}C and ^{1}H were 46-36 kHz and 54 kHz respectively. Acquisition was 30 ms and proton decoupling during this period was 72 kHz.

CP build up curves were acquired by arraying the contact from 100 μs during to 3.5 ms in steps of 100 μs during a ^{1}H-^{13}C CP pulse at 58 kHz and 47 kHz (no ramp) for ^{1}H and ^{13}C respectively. The FIDs were collected for 20.0 ms.

5.4.5.b 2D ^{13}C-^{13}C DARR homonuclear experiments of highly deuterated U-^{13}C, ^{15}N bR recorded on a 500 MHz spectrometer

40 mg of highly deuterated U-^{13}C, ^{15}N purple membrane was packed into a 4 mm standard wall solid state NMR MAS rotor. 2D ^{13}C-^{13}C homonuclear correlation spectra (DARR) were collected on a Varian Infinity Plus 500 spectrometer (11.7 T) at -20 °C VT inlet gas temperature and at 11.548 kHz spinning frequency using a 4 mm HX Apex probe. The DARR mixing time was carried out with an n=1 rotary resonance condition for the protons, and a mixing time of 15 ms in order to identify 2-3 bond contacts. Cross polarization was achieved using a 50.1 kHz square ^{1}H pulse at 497.910 MHz and a 23.2-44.3 kHz tangent ramped ^{13}C pulse at 125.211 MHz for 1 ms. There were 2048 points and 840 points collected in direct and indirect ^{13}C dimensions for 29 ms and 12 ms, respectively. During acquisition, 70.4 kHz two pulse phase-modulated (TPPM) decoupling was applied on the ^{1}H channel. 32 scans were collected, using 3 s pulse delay. The spectrum was processed using sinebell apodisation function in both the direct and indirect dimensions. The carbon dimension was referenced externally using the ^{13}C adamantane methylene peak [236].

5.4.5.c 2D ^{13}C-^{13}C DARR experiments of the fully protonated U-^{13}C, ^{15}N bR sample on the 800 MHz spectrometer

Two dimensional (2D) ^{13}C-^{13}C homonuclear correlation spectra of bR were collected using the DARR pulse sequence [238] for 28 hours for each sample. The number of acquisitions was 32 for each FID with a 3 s pulse delay. The CP conditions were the same as for the 1D spectra described previously, acquired on the 800 MHz Varian/Magnex Infinity + spectrometer, in a 3.2 mm HCN Balun probe. During the 20.5 ms and 11.9 ms acquisition

time in the direct and indirect dimensions respectively, 74 kHz two-pulse phase-modulated (TPPM) [110] proton decoupling was applied. The dwell was set to 10.0 μs and 11.6 μs for the direct and indirect dimensions respectively. Homonuclear ^{13}C mixing was obtained with the n=1 rotary resonance condition on the protons for a 3, 15 ms and 30 ms mixing time. The spectra were apodised by cosine shifted sine bell function. The carbon dimension was referenced externally to DSS using the downfield ^{13}C adamantine methylene peak at 40.48 ppm [239].

5.4.5.d 2D ^{13}C-^{13}C DARR with 3 ms and 13 ms mixing time of highly deuterated U-^{13}C, ^{15}N labelled bR recorded on at 800 MHz

The 2D ^{13}C-^{13}C DARR experiments with 13 ms and 15 ms mixing time was performed at a field of 18.8 T on a Varian/Magnex 800 MHz Infinity Plus wide-bore solid state NMR spectrometer, equipped with a 3.2 mm triple resonance Balun probe operating at 799.16500 MHz and 200.96813 MHz for ^{1}H and ^{13}C. The 2D DARR spectrum with 13 ms mixing time was acquired with a MAS frequency of 8.33 kHz at 253 K probe temperature. 64 scans were acquired over 55 h total experimental time. There were 2048 points and 1024 points collected in the direct and indirect ^{13}C dimensions for 20 ms and 10 ms, respectively. During acquisition 71 kHz proton decoupling was applied. 64 scans were collected, using 3 s pulse delay.

The other 2D DARR spectrum with 15 ms mixing time was acquired at a 10.776 kHz MAS frequency. The apparent sample temperature was regulated to be 263 K. The experimental time was 28 h. The CP conditions were the same as for the 1D spectrum of the highly deuterated U-^{13}C, ^{15}N labelled. During the data acquisition periods of 20 ms and 12 ms in

the direct and indirect dimensions respectively, 74 kHz two-pulse phase-modulated (TPPM) [110] decoupling was applied on the ^{1}H channel. The dwell was set to 10.0 μs and 11.6 μs in the direct and indirect dimensions respectively.

5.4.5.e 2D ^{13}C-^{13}C DARR with 13 ms mixing time of 50% deuterated U-^{13}C, ^{15}N labelled bR sample recorded at 800 MHz

The experimental conditions were the same as for the fully deuterated U-^{13}C, ^{15}N labelled bR sample with 15 ms mixing time. The only difference is the contact time during CP was 1.25 ms HDCN-bR.

5.4.5.f2D ^{13}C-^{13}C RFDR homonuclear experiment of the model compound fMLF

Polycrystalline U-^{13}C, ^{15}N labelled fMLF (5.5 mg) was packed into a 4 mm standard rotor. The sample was prepared by diluting the U-^{13}C, ^{15}N labelled fMLF fivefold in natural abundance fMLF to reduce the influence of intermolecular dipole-dipole interactions. The sample was recrystallised by slow evaporation from isopropanol. The spectrum was recorded at 303 K probe temperature and MAS was 11.574 kHz. ^{1}H frequency was 497.9088 MHz and that of ^{13}C was 125.2128 MHz. Contact time during CP was 2 ms. The field strength of ^{1}H and ^{13}C were 68 kHz and 50 kHz respectively. Pulse delay between transients was 3 seconds. After the evolution period, the magnetisation was placed along the z-axis with a 50 kHz 90 degree pulse on the ^{13}C channel, and after the RFDR mixing time the magnetisation was returned to the x-y plane with another 50 kHz 90 degree pulse. During the mixing period (1.03 ms of 20 π pulses) continuous wave ^{1}H decoupling was implemented with the amplitude of 73 kHz. Dwell was 14.4 μs in both the direct and

indirect dimension. TPPM proton decoupling during evolution and acquisition was 71 kHz. Acquisition time was 14.74 ms. 16 scans were collected. 1024 and 512 points were collected in the direct and indirect dimensions, respectively.

5.4.5.g 2D RFDR of 100% deuterated U-^{13}C, ^{15}N labelled bR sample

100% deuterated U- ^{13}C, ^{15}N labelled purple membrane (40 mg) was packed in a 4 mm standard rotor. The 2D ^{13}C-^{13}C RFDR experiment with 2.25 ms mixing time was performed in a HXY probe on a 500 MHz Varian/Magnex Infinity + spectrometer at a temperature of 263 K. The ^{1}H and the ^{13}C frequencies were 497.9088 MHz and 125.210875 MHz respectively. MAS frequency was 11.574 kHz. The initial 90 degree pulse on ^{1}H was 76 kHz. 64 scans were collected with a pulse delay of 3 seconds. Dwell in the direct and indirect dimension, were 14.4 μs. Contact time for the ramped CP was 1.2 ms. The CP filed strengths for ^{13}C and ^{1}H were 53.2 kHz and 50.8 kHz, respectively. TPPM proton decoupling of 72 kHz was applied during evolution and acquisition. Acquisition time was 20.16 ms. Longitudinal magnetisation of the ^{13}C spin was obtained by a 90 pulse with 60 kHz field strength. The RFDR π pulses were set to 55.5 kHz. 1400 and 1024 points were collected in the direct and indirect dimensions respectively.

5.4.5.h 2D RFDR with 2ms of the 50% deuterated U-^{13}C, ^{15}N labelled bR sample

50% deuterated U-^{13}C, ^{15}N labelled bR in purple membrane in 20 mM Na citrate pH 6.0 containing 0.01% NaN_3. The experiment was performed on 500 MHz Varian/Magnex Infinity + solid state NMR spectrometer, in a 4 mm HXY probe. The probe temperature was set to 263 K. Spinning frequency of the rotor was 11.574 kHz. The ^{1}H and the^{13}C

frequency were 497.90625 MHz and 125. 2103575 MHz. Contact time during CP was 1.75 ms. Dwell 14.4 μs. Pulse delay was 3 seconds. Dwell in the indirect dimension was 14.4 μs. The 90° pulse on ^{1}H was 75.8 kHz. The CP conditions were the same as for the 100% U-^{13}C, ^{15}N deuterated bR sample. Acquisition time was 20.16 ms. TPPM proton decoupling in the direct and the indirect dimensions was during acquisition was 72 kHz. Decoupling during the mixing time was 72 kHz.

5.4.5.i 2D ^{13}C-^{15}N NCA heteronuclear correlation experiment

For the 2D heteronuclear NCA and NCO correlation experiments 28 mg of U- ^{13}C, ^{15}N labelled and >50 % deuterated purple membrane was packed into a 3.2 mm rotor. The 2D dipolar NCO and NCA correlation experiments were performed at 18.8 T using a wide-bore Varian 800 MHz Infinity Plus spectrometer. The spectrometer was equipped with a 3.2 mm T3 Balun probe. MAS frequency was 8.33 kHz at 253 K.

For the 2D ^{15}N-^{13}C NCA correlation spectrum of U-^{13}C, ^{15}N, ^{2}H enriched purple membrane the cross polarization unit contained a tangent shape spin-lock pulse on the ^{15}N nucleus with a frequency of 81.04842 kHz to broaden the CP matching profile at high MAS frequencies. A moderate proton RF power corresponding to a ^{1}H nutation frequency of 52 kHz was applied. The contact time during the second CP from ^{15}N with to ^{13}C with a Larmor frequency for the Cα 201.10985 mHz was 4 ms, during which the ^{15}N field strength was 22.6 kHz and the ^{13}C field strength was 12.8 kHz. Proton decoupling was achieved by use of the two-pulse phase modulation (TPPM) with a 70 kHz field strength .Over a 29 h total experimental time, 2048 and 180 points were recorded in the direct and indirect dimensions respectively. 192 scans with 3 ms pulse delay were collected.

5.4.5.j 2D ^{15}N-^{13}C NCO heteronuclear correlation experiments

For the 2D ^{15}N-^{13}C NCO correlation experiment of U-^{13}C, ^{15}N, ^{2}H enriched purple membrane a moderate proton RF power corresponding to a ^{1}H nutation frequency of 52 kHz was applied. The contact time during the second CP from ^{15}N to ^{13}C with a Larmor frequency for the CO 201.132969 MHz was 3.5 ms, during which the ^{15}N field strength was 20.9 kHz and the ^{13}C field strength was 25.0 kHz. Proton decoupling was achieved by use of the two-pulse phase modulation (TPPM) with 70 kHz field strength. Over a 30 h total experimental time, 2048 and 186 points were recorded in the direct and indirect dimensions respectively. 192 scans with a 3 ms pulse delay were collected. All the samples used in the study are listed in Table 14.

Table 14 Sample list of all the differently labelled purple membrane samples used in this study, the rotors they were packed in and the amount packed. The sample buffer was always 20 mM sodium citrate pH 6.0 with 0.01% NaN_3.

	Rotor Type	Sample	Sample weight
A	4 mm standard	U-^{13}C, ^{15}N > 50% Deuterated PM	40 mg
B	3.2 mm thin wall	U-^{13}C, ^{15}N > 50% Deuterated PM	28 mg
C	4 mm standard	U-^{13}C, ^{15}N 50% Deuterated PM	46 mg
D	3.2 mm thin wall	U-^{13}C, ^{15}N 50% Deuterated PM	30 mg
E	4 mm standard	U-^{13}C, ^{15}N 0% Deuterated PM	48 mg
F	3.2 mm thin wall	U-^{13}C, ^{15}N 0% Deuterated PM	24 mg

5.4.6 Data processing

All 1D spectra were processed by sineball square (cosine shifted) apodisation and zero filled to 16 K points before Fourier transform in Spinsight (Varian). Signal-to-noise and integral measurements were also carried out with Spinsight. All 2D solid-state data were processed with NMRpipe [240] software and subsequently analysed and assigned using the program Sparky, version 3.1 [241]. All DARR spectra were sine bell square apodised, then zero filled to 4 k points in both dimensions before being Fourier transformed. For the DARR spectrum of the fully deuterated sample in Figure 5.24 line broadening was applied as specified in the figure legend. One set of the heteronuclear correlation spectra were further processed by applying exponential line broadening in both the direct and indirect dimension. All data was zero filled once before being Fourier transformed.

5.5 Results and Discussion

5.5.1 Preparation of deuterated U-^{13}C, ^{15}N labelled bacteriorhodopsin

Celtone growth-media proved to be a better starting material for optimisation of deuteration and U-^{13}C, ^{15}N labelling of bR than Silantes labelling media. The culture grown in Celtone was compared to the ones in peptone media from Oxoid. There was no purple colour in the Silantes grown cultures which is indicative of poor bR production.

Test cultures of 100 ml Celtone medium were used. If the cultures were not sealed well, separation of the medium was observed. The flasks had to be air-tight. The yield of the fully deuterated sample was very low. Optimising the media for uniform labelling showed that adding $CaCl_2$ (0.2 g/L) improves cell growth yield by 20%. Addition of folic acid, biotin and thiamine to the cultures also improved growth.

For the bR cultures, cell growth rates were slower in D_2O than in H_2O. Illumination increased the bR production. Growth media had different colours which can be seen in Figure 5.5 and the OD_{660} readings of the cultures are listed in Table 15. The samples were centrifuged, and the size and the intensity of colour of the pellets can be seen in Figure 5.6. The U ^{13}C, ^{15}N, 50% ^{2}H labelled bR has higher molecular weight than unlabelled bR, therefore the sucrose gradient had to be modified for the purification of the deuterated samples. A sucrose solution with higher 25% - 70% percentage was used than for the protonated sample.

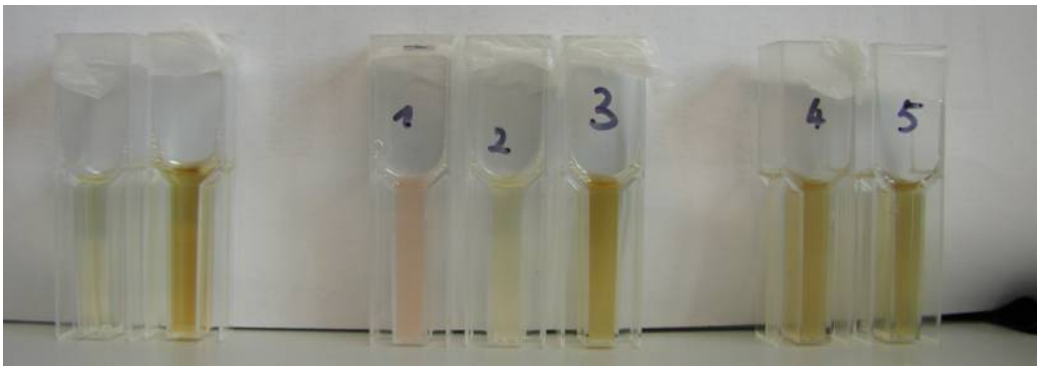

Figure 5.5 Different colour of the labelling media. The first 2 cuvettes are media alone. The other numbered cuvettes are *H. salinarium* grown in 1. Oxoid medium; 2. Oxoid medium; 3. H Celtone; 4. 50% d Celtone at 50% d Celtone

Table 15 OD_{660} reading of the different media after *H. salinarium* growth.

Tube Number	1	2	3	4	5
Media	Oxoid	Oxoid	H Celtone	50% deuterated Celton	50% deuterated
OD_{660}	1.40	0.35	0.47	1.05	0.55

Figure 5.6 Colour of the pellets from 1 ml of the cultures from Figure 5.5 after centrifugation. *H. salinarium* grown in peptone medium has the strongest purple colour and largest pellet. The pellet from 50% d Celtone at OD_{660} 1.05 in Eppendorf 4 is purple/brown colour. The brown colour of the pellet grown in Celtone medium is due to the medium which is dark brown.

The lag phase of *H salinarium* in fully deuterated Celtone was increased compared to *H salinarium* in fully protonated Celtone, however the growth rate stayed the same (results not shown). *H. salinarium* grew better in Celtone medium than Silantes, subsequently the optimisation of the yield of uniformly labelled bR was carried out on the Celtone medium.

H. salinarium (strain S9) was inoculated into Celtone medium (Spectra Stable Isotopes) with the appropriate isotopic enrichment Table 13. The pellets from 30 ml cultures after the final wash after sucrose gradient can be seen in Figure 5.7. Again the increase in the size of deuterated bR is observed. Hence, the 50 % deuterated U-^{13}C, ^{15}N PM migrated to the bottom of the 25-45% sucrose gradient. Figure 5.8 , whereas it was between the 45% and 60% sucrose band in the 25% to 70% sucrose gradient (Figure 5.8).

Figure 5.7 Harvested cell pellets from 30 ml bacteriorhodospin cultures from the three different growth media

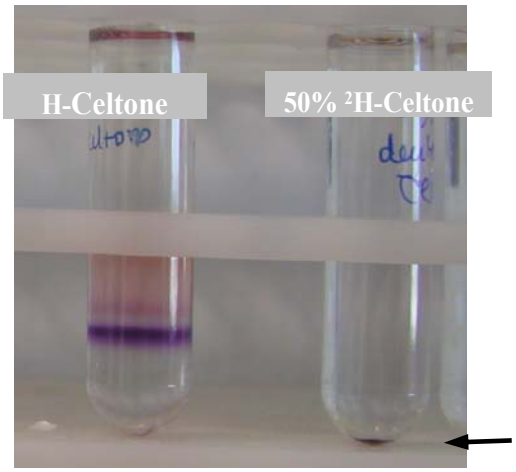

Figure 5.8 Isolation of 50% U-^{13}C, ^{15}N labelled bacteriorhodopsin on a 25%-70% sucrose gradient. The purple membrane appears as a purple ring at different positions on the same sucrose gradient after ultracentrifugation due to heavier molecular weight of the 50% deuterated bR. The fully protonated bR is lighter

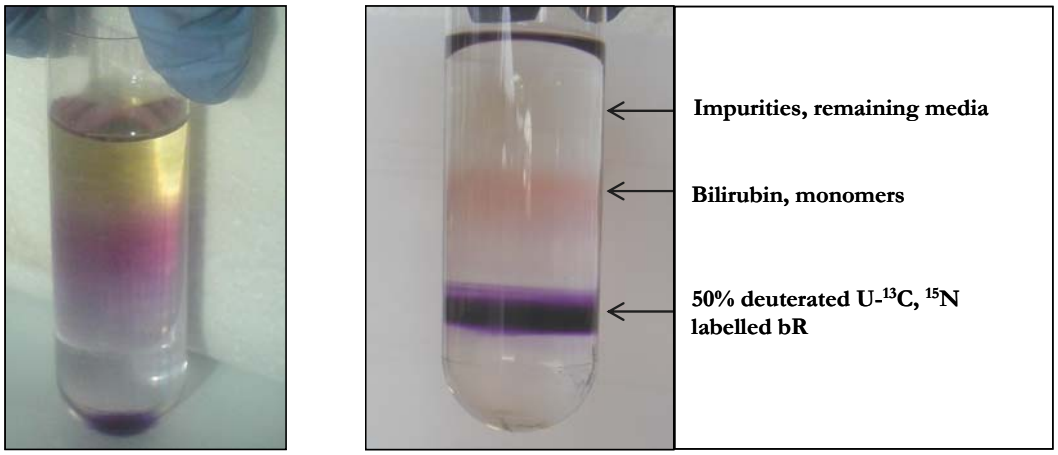

Figure 5.9 Purification of the 50% deuteration U-^{13}C, ^{15}N labelled purple membrane from *H. salinarium* on a sucrose gradient. After dialysis and centrifugation, the bR pellet was resuspended in MilliQ water and layered on top of a sucrose gradient. A part of the 50% deuterate bR was isolated by a 25% to 45% sucrose gradient (left). In this case, the membrane was at the bottom of the tube, whereas in the 25% to 70% sucrose gradient, it was located between the 45% and 60% sucrose solutions. The purification is more efficient with the 25%-70% sucrose gradient, thus this gradient was used for purification of the sample.

The yield for the three differently deuterated U-^{13}C, ^{15}N labelled bR samples per 1 L culture were: 17.3 mg fully protonated, 5.5 mg 50% deuterated bR and 3.75 mg >50% deuterated. To check for the purity of the isolated purple membrane, aliquots of each sample were run on a 12% Tris-Tricine SDS-PAGE Figure 5.11.

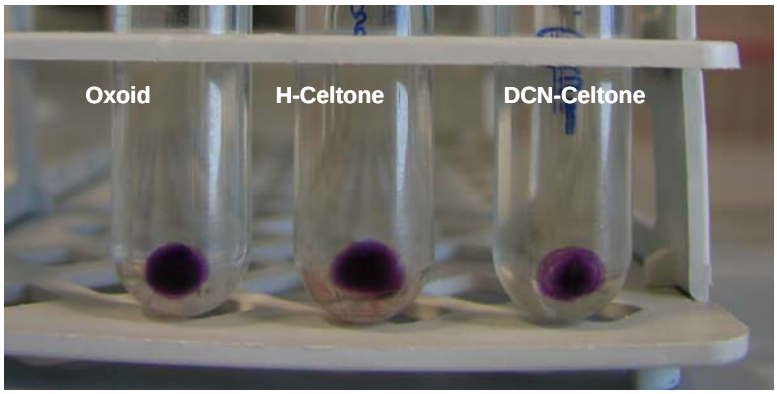

Figure 5.10 Isolated purple membrane from the sucrose gradient and washed in MilliQ H_2O from three different growth media.

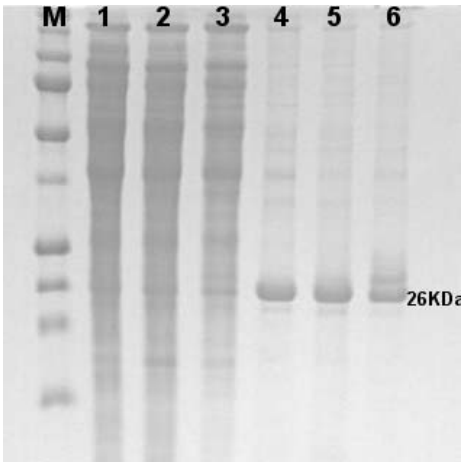

Figure 5.11 12% Tris-Tricine SDS-PAGE of purified bacteriorhodopsin: M: Biorad markers Samples: 1. From Oxoid non-labelling medium after the 0.1M NaCl dialysis, 2. From H Celtone after the 0.1 M NaCl dialysis 3. From 50% D2O-DCN celtone after the 0.1 M NaCl dialysis 4. From Oxoid medium after the sucrose gradient 5. From H Celtone after the sucrose gradient 6. From 50% D2O-DCN Celtone after the sucrose gradient

5.5.2 Solid State NMR Experiments

Three differently labelled bacteriorhodopsin (bR) samples were compared to find out which one is the most suitable for assignment. This is what is discussed in the first part of the section. In the next part, the preliminary results towards site-specific assignment will be presented.

5.5.2.1 Effects of deuteration on solid state NMR spectra

5.5.2.1.a Effects of deuteration on the linewidth of ^{13}C spectra

One set of the 1D spectra (A, B and C) shown in Figure 5.12 of the three bR with various deuteration levels samples was acquired at -10 °C on an 18.8 T (800 MHz for proton) Varian/Magnex Infinity + spectrometer. The other set (D, E and F) was acquired on an 11.7 T (500 MHz for proton) Varian/Magnex Infinity + spectrometer. Comparison of the

spectra of the differently labelled bR samples indicate that the fully protonated bR spectrum has the best resolution among the 1D spectra, which is particularly obvious in the spectra collected on the 800 MHz Varian/Magnex Infinity + spectrometer. The resolution of the deuterated 1D spectrum did not change when the temperature was varied from - 20 ° C to 20 ° C (data not shown).

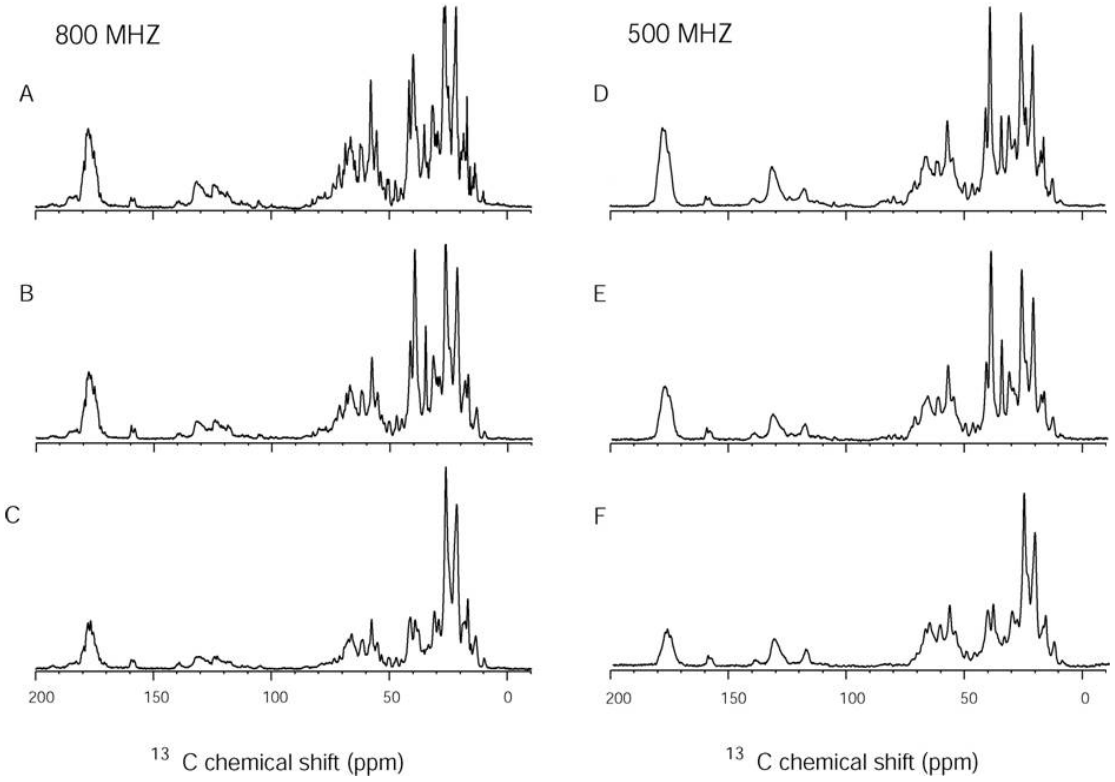

Figure 5.12 1D ^{13}C NMR spectra of fully protonated (A, D), 50% deuterated (B, E), and highly deuterated- (C, F) U-^{13}C, ^{15}N labelled bR, with 24-27 mg of purple membrane per sample fully hydrated in sodium citrate buffer (pH 6.0). The spectra were collected under very similar conditions, at -10 ^{o}C and at a spinning frequency of 10.776 kHz. Each spectrum was signal averaged by 1K scans with 74.0 kHz ^{1}H decoupling for 30 ms. Spectra A, B and C were collected on the 800 MHz Varian/Magnex Infinity + Spectrometer and D, E and F on the 500 MHz Varian/Magnex Infinity + Spectrometer.

1D solution state NMR spectrum of U-^{13}C, ^{15}N labelled bR in micelles by Patzelt and colleagues [7] is presented in Figure 5.13. The resolution of this spectrum is comparable with the resolution of the solid state NMR spectrum of U-^{13}C, ^{15}N labelled bR, in addition the signals from the detergents in the micelles is absent in the solid state NMR spectrum.

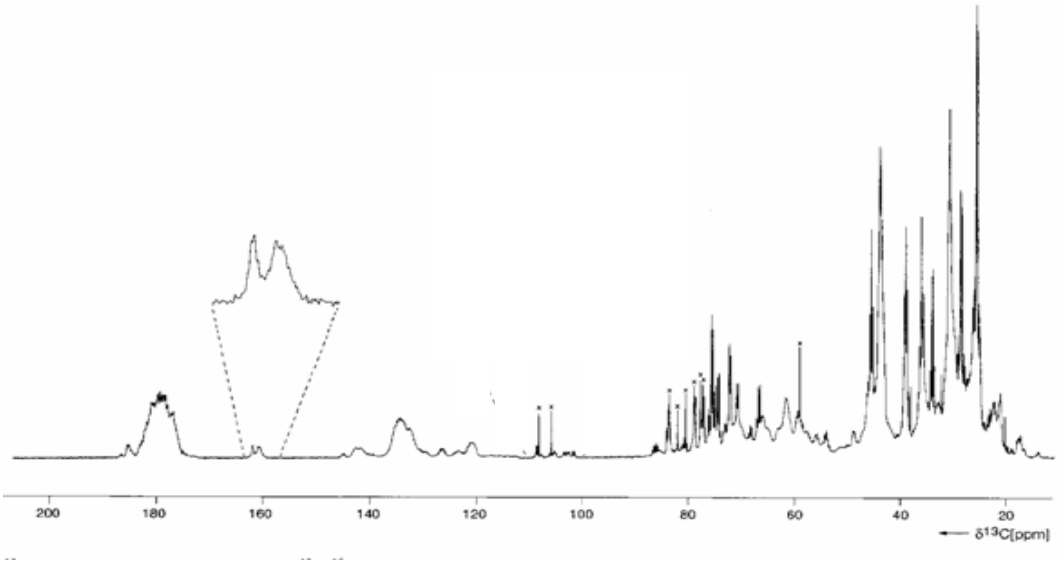

Figure 5.13 1D Solution state NMR 1D ^{13}C spectrum [7] of bacteriorhodopsin in micelles at 40 °C collected on a Bruker AMX600. The regions with the protonated Schiff base carbon (around 160 ppm) are shown in larger scale. The signals marked wih an x are due to detergent present in the micelles.

To investigate the origin of the broadening of the lines of the 1D spectrum, 2D ^{13}C- ^{13}C DARR spectra were acquired (Figure 5.14). The increased resolution of this method allows comparison of some specific individual resonances. Comparison of the 2D DARR spectra reveal that the individual peak resolution of the fully deuterated sample is similar to the protonated bR sample, however there was peak doubling, even tripling in the 50% and highly deuterated U-^{13}C, ^{15}N labelled bR. After collecting the 2D experiments, it was clear that the loss of resolution was due to peak doubling, which is particularly obvious in the case of isoleucine shown in Figure 5.15. In the deuterated sample many peaks are weak or

missing compared to the protonated. This could be due to low ^{1}H magnetisation source, dynamics and/or inefficient ^{1}H-^{13}C recoupling due to low ^{1}H pool.

The experiments were taken under very similar experimental conditions and the contours of spectra in Figure 5.14 were cut at the same level for ease of comparison. Bacteriorhodopsin contains 29 alanines, most of which have similar chemical shifts due to their backbone position. However, at least 6 alanine Cβ-Cα resonances which are shown in the enlarged regions (D, E and F) of Figure 5.14 can be clearly resolved in the fully protonated U-^{13}C, ^{15}N labelled bacteriorhodopsin. These 6 peaks can also be seen distinguished in the 50% and highly deuterated bR sample spectrum Figure 5.14 E and F. Although the peaks can be distinguished in the 50% and highly deuterated bR samples Figure 5.14 E and F, the resolution is greatly reduced due to peak multiplicity the peaks are at least doubled or even tripled. For the 50% deuterated sample, which was grown in 50/50 ^{1}H/^{2}H medium, this spectral multiplicity can be explained by the presence of ^{1}H-^{13}Cα coupled to $^{1}H_3$-Cβ, $^{1}H_2{}^{2}$H-Cβ, $^{1}H^{2}H_2$-Cβ, and $^{2}H_3$-Cβ.

5.5.2.1.b Effects of deuteration on spectral resolution

Even though the highly deuterated sample was grown in >50% deuterated medium, the residual protonation of the covalently, non-exchangeable protons are the source of the presence of multiple resonances. The reason for the missing alanine peaks in spectrum F in Figure 5.14 is probably due to interference of deuteration with protein dynamics. These are probably resonances situated in the loop region, based on their chemical shift [242], and may be cross polarised from the few ^{1}Hs in the protein and the buffer.

Another relatively well resolved region in the 2D DARR spectrum shown in Figure 5.15 is the isoleucine sidechain region (9-40 ppm). Peak doubling is also apparent in this region of the deuterated bR sample (blue spectrum). This is attributed to two very similar conformations of bR present in the native purple membranes within 0.2-0.3 ppm. The two forms are present in roughly equal percentages, based on the signal amplitude of the isolated peaks. The preparation of the purple membrane was similar for all the preparation studied; hence it is not clear as to what is the origin of the different isoforms.

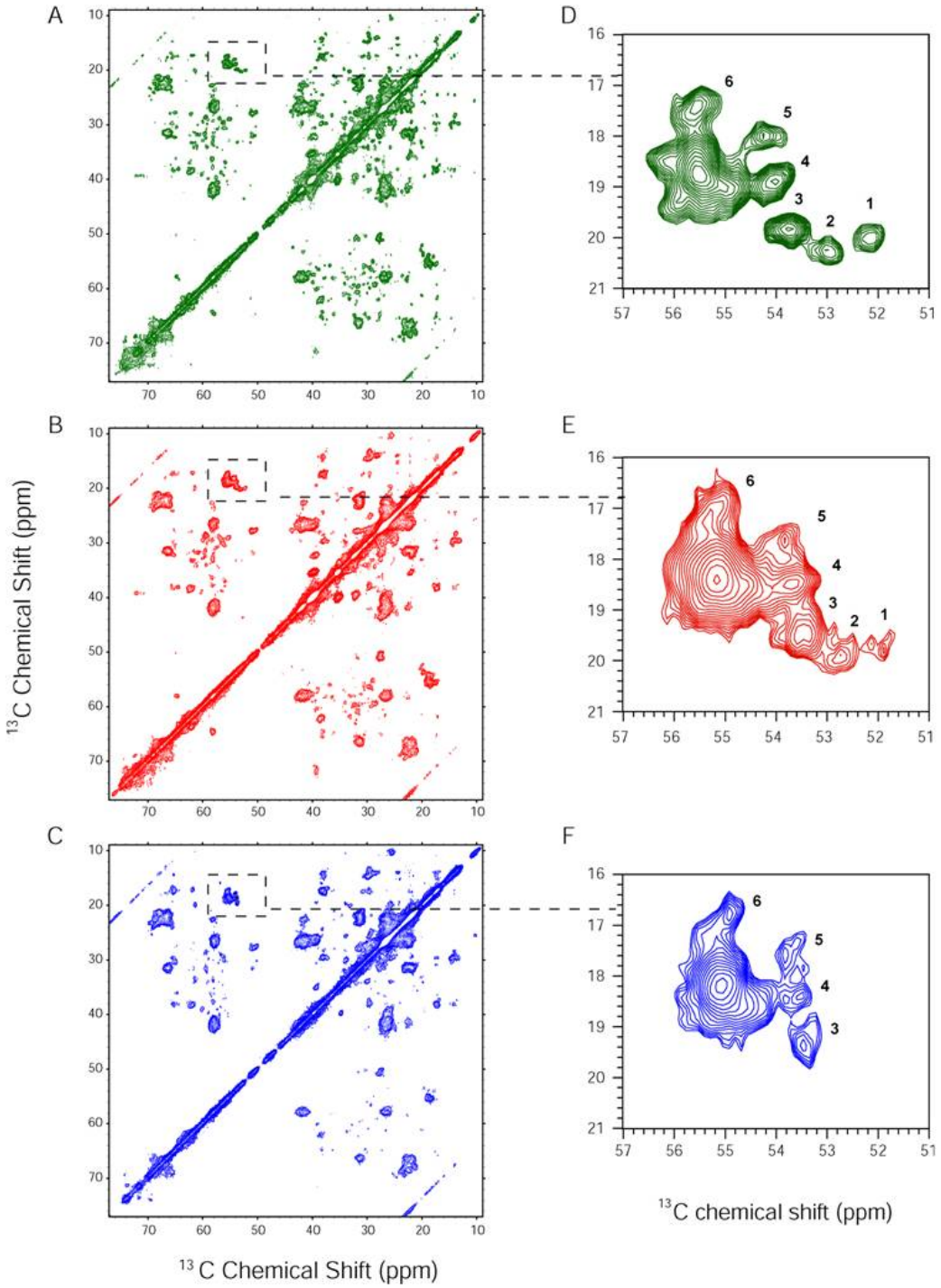

Figure 5.14 2D DARR 15 ms mixing time spectra of (A) highly protonated U-^{13}C, ^{15}N bR; (B) 50% deuterated U-^{13}C, ^{15}N bR and (C) fully deuterated U- ^{13}C, ^{15}N bR recorded on a 800 MHz Varian/Magnex Infinity + spectrometer. In the deuterated sample many cross peaks are weak or missing compared to the protonated. Detailed comparison of the 2D spectra reveals that the broadened 1D spectra of the deuterated sample is due to peak doubling, depicted in the enlarged area of alanine Cβ-Cα region. The alanine Cβ-Cα enlarged regions are of (D) fully protonated U-^{13}C, ^{15}N bR, (E) 50% deuterated U-^{13}C, ^{15}N bR and (F) highly deuterated U-^{13}C, ^{15}N bR 2D ^{13}C-^{13}C DARR spectra. The 6 resolved peaks of the fully protonated bR spectrum are numbered for easy comparison between the spectra. All three spectra were acquired under identical conditions for all parameters except for the contact time which was sample dependent. See materials and Methods section for further experimental details and the text for discussion.

The individual linewidths for the isoleucine $C_{\gamma 1}$, $C_{\gamma 2}$ and Cδ crosspeaks were estimated to be 0.5-0.55 ppm for both the highly deuterated and fully protonated bR samples.

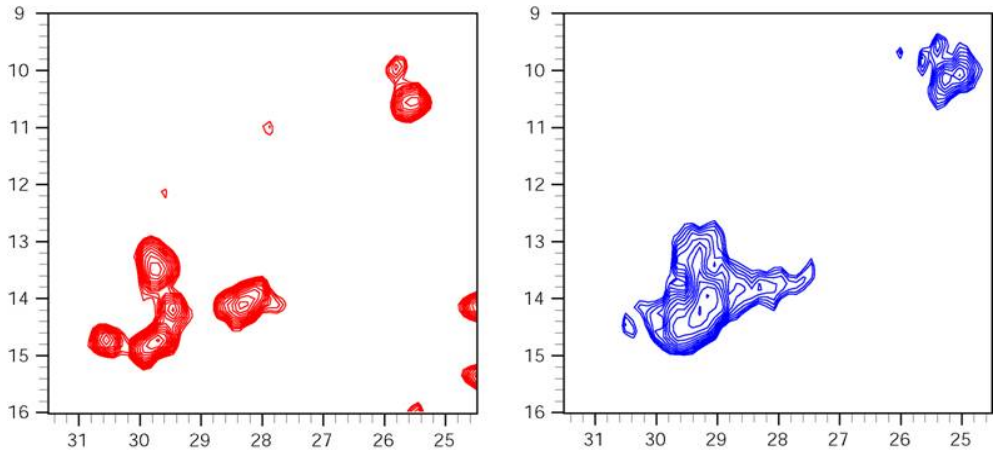

Figure 5.15 Peak doubling observed in the 2D DARR 15 ms isoleucine region of fully protonated (red spectrum) and highly deuterated (blue) U-^{13}C, ^{15}N labelled bR.

5.5.2.1.c Isotope effect

There is observable upfield deuterium isotopic shift of the ^{13}C resonances in the 50% and >50% deuterated sample compared to the protonated bR sample, of about 0.3-0.5 ppm depending on the number of deuterons attached to the ^{13}C (Figure 5.16). It is well known from solution state NMR studies that deuterium isotope effects in partially deuterated samples lead to multiple ^{13}C resonances, which could induce line-broadening. This line-broadening can be due to residual protonation which was observed for methyl groups, which may correspond to $^{1}H_3$-Cβ, $^{1}H_2{}^{2}H$-Cβ, $^{1}H{}^{2}H_2$-Cβ, and $^{2}H_3$-Cβ groups [216]. Carbon resonances were observed to be equally broadened in highly deuterated Cα and a shift of the isotropic ^{13}C frequencies of about 0.3 ppm per directly attached ^{2}H for deuterated sites, and assignments of the deuterated carbons that can be estimated from the assignments

made on protonated sample. These sizeable isotope shifts complicate the transfer of ^{13}C resonance assignment from a hydrogenated sample directly to spectra acquired for deuterated protein.

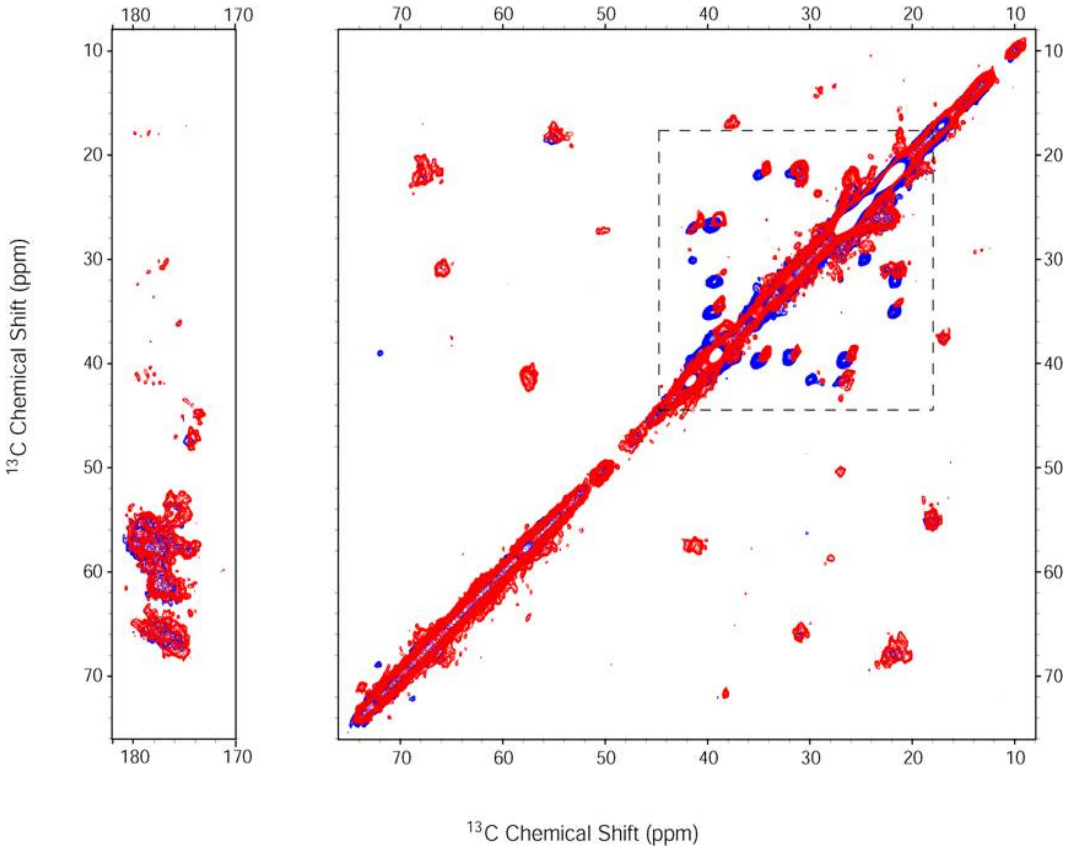

Figure 5.16 The deuterium isotope effect seen by overlaying the 2D RFDR 2 ms mixing time ^{13}C spectra of 50% deuterated (red) and highly deuterated (blue) taken on the 500 MHz Varian/Magnex Infinity + magnet. Upfield shift of ^{13}C spectrum of highly deuterated U-^{13}C, ^{15}N bacteriorhodopsin with respect to the 50% deuterated U-^{13}C, ^{15}N bR. The ^{13}Cβ resonances in the highly deuterated bacteriorhodopsin are shifted upfield by 0.3 to 0.6 ppm (selected in the box) depending on how many ^{2}H are attached to the ^{13}C, due to the ^{2}H isotope effect.

5.5.2.1.d CP efficiency in deuterated samples

One of the potential drawbacks of the highly deuterated sample is the low CP efficiency. All three bR samples were purified in protonated buffers which allow all the exchangeable

deuterons to be replaced with protons, about 25% of the total protons in the protein. Amide sites buried in the α-helical regions are not accessible to deuterium/proton exchange [243], hence only the loops are susceptible to exchange the deuterons with protons, which could in theory further decrease CP efficiency. Considering the above mentioned disadvantage, the CP efficiency of the highly deuterated U -^{13}C, ^{15}N bR sample was reasonably good compared to the protonated sample.

In order to compare numerically the CP-efficiency build up rate of the highly-deuterated U -^{13}C, ^{15}N bR sample and the fully-protonated U -^{13}C, ^{15}N bR sample, build up curves were plotted in Figure 5.17. The contact time during the ^{1}H-^{13}C CP was varied and plotted against the integral of the spectral intensity of CO, Cα and the sidechain regions. The fatty acid sidechains of the purple membranes are also uniformly labelled; consequently the presence of lipid signals in the sidechain region complicates the comparison of the CP efficiency. No ramp was used during the CP and the contact time was arrayed. The same matching condition was used for both the protonated and deuterated samples (5.4 x ω_r and 4.4 x ω_r) for the best match. The match conditions were similar for the different regions, however, they were not the same; hence the match condition was chosen to be closest to both Cα and CO signal. The build up curves Figure 5.17 show that the CP buildup was only slightly slower for the deuterated bR sample. The CP build up is fast for the Cα spectral region of the protonated sample (0.1 ms) and for the deuterated bR sample the buildup levels off after 0.4 ms contact time. The CO buildup levels off at 0.4 and 0.6 ms for the protonated sample. The sidechains reach maximum intensity at 0.3 ms for both samples. The curves were not corrected for relaxation. The above results imply that the

most deuterated sample does not require significantly longer contact time during CP when there is residual protonation present.

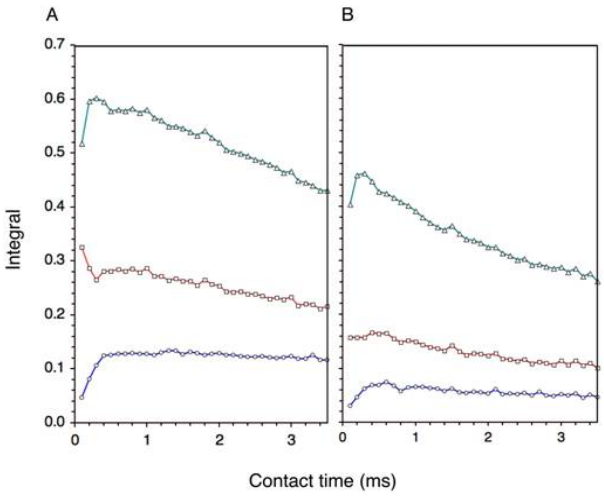

Figure 5.17 CP buildup curves for the fully protonated U-^{13}C, ^{15}N-bR (A) and highly deuterated U-^{13}C, ^{15}N-bR samples (B). The contact time was varied from 0.1 to 3.5 ms in steps of 0.1 ms and plotted vs. the integral of various regions of the spectra. The integrals of various regions of the 1D spectra were estimated by the program Spinsight to compare CP buildup: 164-189 ppm for CO (circles with blue line), 44-75 ppm for Cα (squares connected with red line), and 9-44 ppm for the protein sidechain region (triangles with green line), which includes the lipid fatty acid chains as well. The integrals of the 100% deuterated U-^{13}C^{15}N-bR sample were scaled to correct for a slight difference in sample amount (~11%).

For an estimation of the CP efficiency in the membrane samples, the largest integral from the CP buildup curve was picked. The comparison showed the CP transfer efficiency of the highly deuterated relative to the fully protonated bR sample was 56%, 51% and 77% for the CO, Cα, and the sidechains respectively.

The similarity in the CP efficiency for the CO spectral regions is consistent with the suggestion based on the 1D spectra of ubiquitin [215], the CO transfer magnetisation comes mainly from the H(N) protons. Based on the observation of the 2D ^{13}C-^{13}C DARR

spectra in Figure 5.14 most resonances present in the protonated spectrum are present in both (50% and >50%) deuterated bR spectra with 15 ms DARR mixing time. These observations imply that sufficient proton pool is present in the sample for both the ^{1}H-^{13}C CP and DARR mixing even in a membrane protein which was produced in a highly deuterated (>50%) crystalline membrane environment.

5.5.2.1.e Decoupling efficiency in deuterated samples

^{1}H decoupling on the fully protonated bR sample and deuterated sample was also investigated. Proton decoupling had less effect on the deuterated bR sample than on the protonated bR sample as judged from the 1D spectra where continuous wave decoupling was applied. The intensity of the Cα resonance group at 58.0 ppm for the fully protonated bR (at 57.7 ppm for the fully deuterated bR), was measured in the 1D spectra. When the decoupling decreased from 74.0 kHz to 43.0 kHz, for the fully deuterated bR sample, the intensity decreased only to 86% of the original value, while the intensity of the fully protonated dropped to 71%. Hence, the deuterated sample may be advantageous for samples for which the application of lower decoupling levels may be preferably for sample stability.

5.5.2.2 Assignment studies of bacteriorhodopsin

There are several types of 2D homonuclear ^{13}C-^{13}C correlation experiments commonly used in assignment strategies. Here we applied the dipolar assisted rotational resonance (DARR) [229] and radiofrequency driven recoupling (RFDR) [114]. The 2D ^{13}C-^{13}C homonuclear spectra of ^{13}C uniformly labelled proteins are often the first spectra collected for the resonance assignment procedure; they provide an indication of the feasibility of the

assignment as well as indication of protein secondary structure. The 2D spectra are relatively simple to set up and can be used to monitor protein stability when needed. DARR spectra with different mixing times give different information; short mixing times show short distance correlations and longer mixing times show long range correlations DARR spectra with different mixing times were collected.

5.5.2.2.a Assignment studies based on homonuclear 2D ^{13}C-^{13}C correlation spectra

Initially the two- dimensional (2D) solid-state ^{13}C-^{13}C homonuclear radiofrequency driven dipolar recoupling experiment (RFDR) on crystallised model compound N-formyl methionine-leucine-phenylalanine (fMLF) (Cambridge Stable Isotopes) model compound was conducted in order to test and optimise the experimental conditions and to demonstrate the assignment strategy that is being used for assignment of bR. fMLF is a tripeptide, which is a highly suitable model compound because it has only a few, well resolved peaks and gives crosspeaks with high signal-to-noise ratio. For the crystallisation protocol of fMLF see the Materials and Methods section of this chapter.

The 2D ^{13}C-^{13}C RFDR spectrum of the fMLF in Figure 5.18 shows the assignment strategy that is applied for the assignment of bR. The assignment is mainly based on the statistics on the ^{13}C chemical shifts derived by studies of proteins in solution [244] and can be used as a guide for the identification of the different amino-acid networks. Correlation pattern connectivies are shown for the leucine residue in Figure 5.18, where the cross peak which line up are connected with a black line.

As the first sample to be studied was the fully deuterated bR, the RFDR was used because it usually gives stronger crosspeaks in the CO region than the DARR sequence, see Figure 5.19. For the fully protonated sample the signal-to-noise of the CO region crosspeaks was high, therefore there was no need to use RFDR.

There are two problems associated with 2D methods of chemical shift resolution in biological solid-state NMR. One is the loss of signal due to the dephasing of magnetisation by inhomogeneous B_1 fields. The other problem is dipolar truncation, where a weak correlation between two spins is not observed if one or both of the spins is also strongly dipolar coupled to other spins [17]. The DARR experiment is more effective at measuring long range, through-space correlations that carry the most information concerning structure, and DARR is less sensitive to inhomogeneous B_1 fields than RFDR [105, 228]. The DARR sequence has been reported to solve problems associated with dipolar truncation [231].

Amino acid types and protein secondary structure elements are often confirmed in 2D DARR spectra as the initial step of the assignment process. ^{13}C chemical shifts in proteins are sensitive to backbone dihedral angles (ϕ,φ). ^{13}C shift deviation from random coil values is referred to as the secondary shift [152, 245]. Spera and Bax [152] showed that in peptides and proteins, the helical $^{13}C\alpha$ isotropic chemical shift is approximately +3 ppm higher than the random coil value, while for β-sheet conformation there is about -1 upfield shift.

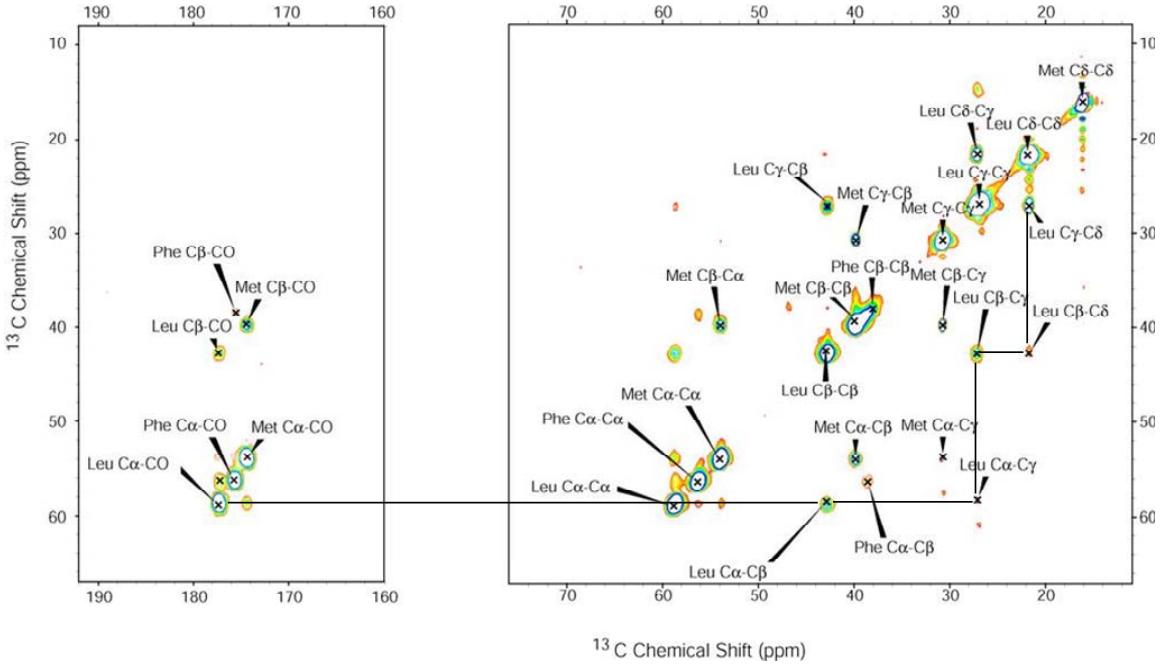

Figure 5.18 Assigned 2D ^{13}C-^{13}C RFDR with 1.03 ms mixing time spectrum of the U-^{13}C, ^{15}N labelled model compound fMLF obtained in a 4 mm standard rotor on a 500 MHz Varian/Magnex Infinity + spectrometer. The experiment was conducted at 303 K probe temperature and 11.574 kHz MAS frequency. Proton decoupling during evolution and acquisition was 71 kHz. Acquisition time was 14.74 ms during which 16 scans were collected with 3 s pulse delay. The 2D RFDR spectrum on the model compound MLF shows the assignment strategy that was going to be applied on bR. The assignment strategy is demonstrated on the leucine residue, where the crosspeaks which line up are connected with a black line.

Recent advances in protein assignment by solid state NMR initiated the comparison of solid state NMR chemical shifts to solution chemical shifts, and the evaluation of secondary shifts for solid state samples [208, 246]. The statistics for solid state chemical shifts are limited, since only a few proteins have been assigned, however it was reported for these proteins that the chemical shifts agree very closely between the solid state and solution assignments for the vast majority of the amino acids.

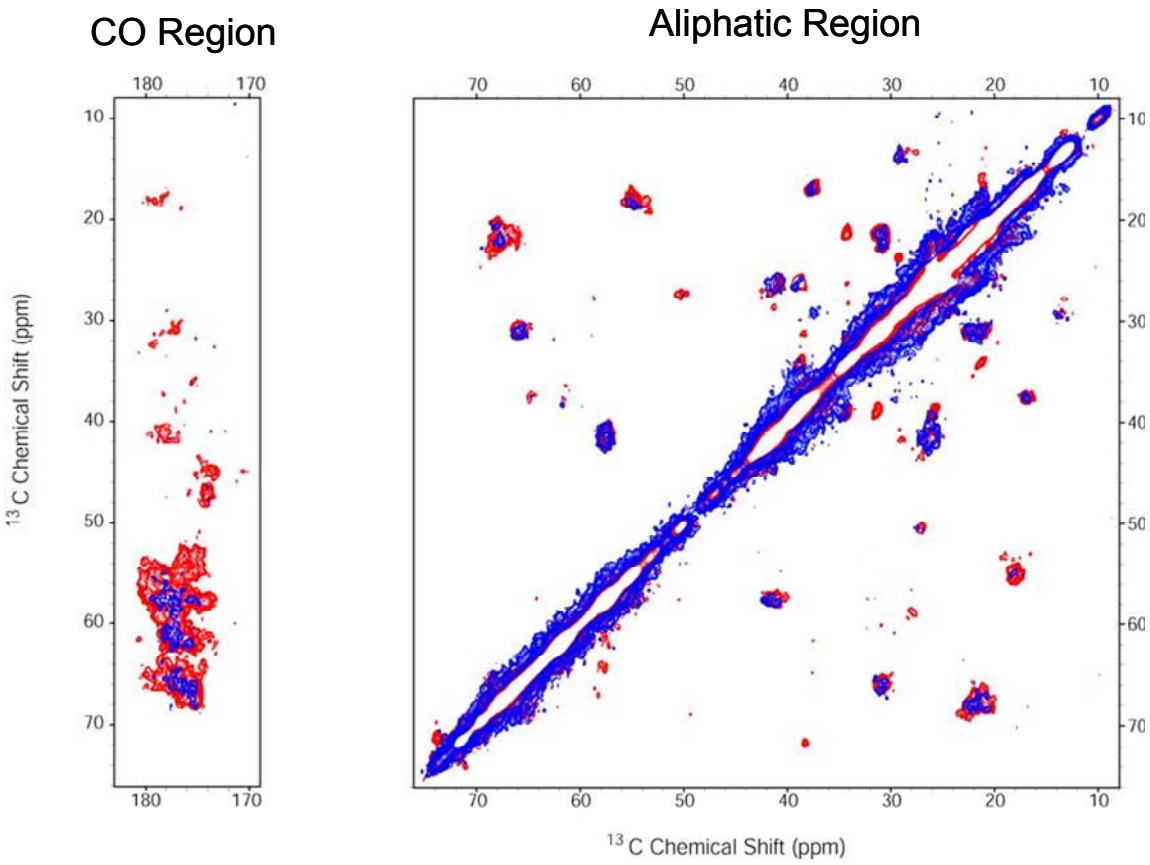

Figure 5.19 Overlay of 50% deuterated U ^{13}C, ^{15}N labelled bR 2D DARR 3 ms mixing time (blue) and 2D RFDR 2 ms mixing time (red) spectra taken on the 500 MHz Infinity plus spectrometer. The RFDR recoupling experiment is more efficient for CO-Cα magnetisation transfer.

Amino acid type identification was possible based on accumulated chemical shift statistics [244] and the DARR spectra of U- ^{13}C, ^{15}N labelled bR which exhibit mostly α-helical chemical shifts. One and two bond transfers are very strong in the DARR with 15 ms mixing time spectra of the fully protonated bR sample. Cross peaks are weaker in the deuterated sample, however with line broadening some 3 bond transfers show up as well in the deuterated sample (Figure 5.24). Since bacteriorhodopsin is a large, mostly α-helical protein (248 amino acids), there are a lot of cross peaks, thus the spectrum is very crowded. The same amino acid types have similar chemical shifts, which results in spectral overlap.

Peaks of certain amino acids based on the chemical shift and connectivity can be identified (Figure 5.21).

The 2D DARR spectrum of the fully protonated sample (Figure 5.21) has the highest resolution and implies that the sample is homogeneous, as discussed in section 5.5.2.1, which is an advantage for assignment. The observed ^{13}C linewidths of 0.5-0.55 ppm not only are consistent with the linewidths other studies of membrane proteins by solid state NMR are reporting [185, 186, 247, 248], but confirm that high-resolution solid state NMR spectra can be obtained for membrane proteins in their natural environment.

In the 2D DARR spectra in Figure 5.20 of 3 ms (red spectrum) and 15 ms (blue spectrum) mixing time of fully protonated sample collected on the 800 MHz Varian/Magnex Infinity + spectrometer are shown. In the DARR spectrum with 3 ms mixing time, mostly one bond transfers are visible, in the DARR spectrum with 15 ms mixing time, crosspeaks with even three bond transfers can be detected (Figure 5.20 spectrum D). Thus the 15 ms mixing time spectrum is much more crowded in the 20-25 ppm region (Figure 5.20 spectrum D), and the crosspeaks of the two or three bond transfers can overlap the one bond transfer crosspeaks. This is illustrated in Figure 5.20 C and D, which show the valine and proline Cα-sidechain and Threonine Cβ-Cγ correlations. In Figure 5.20 D (15 ms DARR mixing), the valine Cα-Cγ1 and valine Cα-Cγ2 peak group overlaps with the threonine Cβ-Cγ region. In Figure 5.20 C (3 ms DARR mixing) however, one bond threonine Cβ-Cγ transfers are observed. Thus, it is advantageous in the assignment process to the collect DARR spectra with different mixing times.

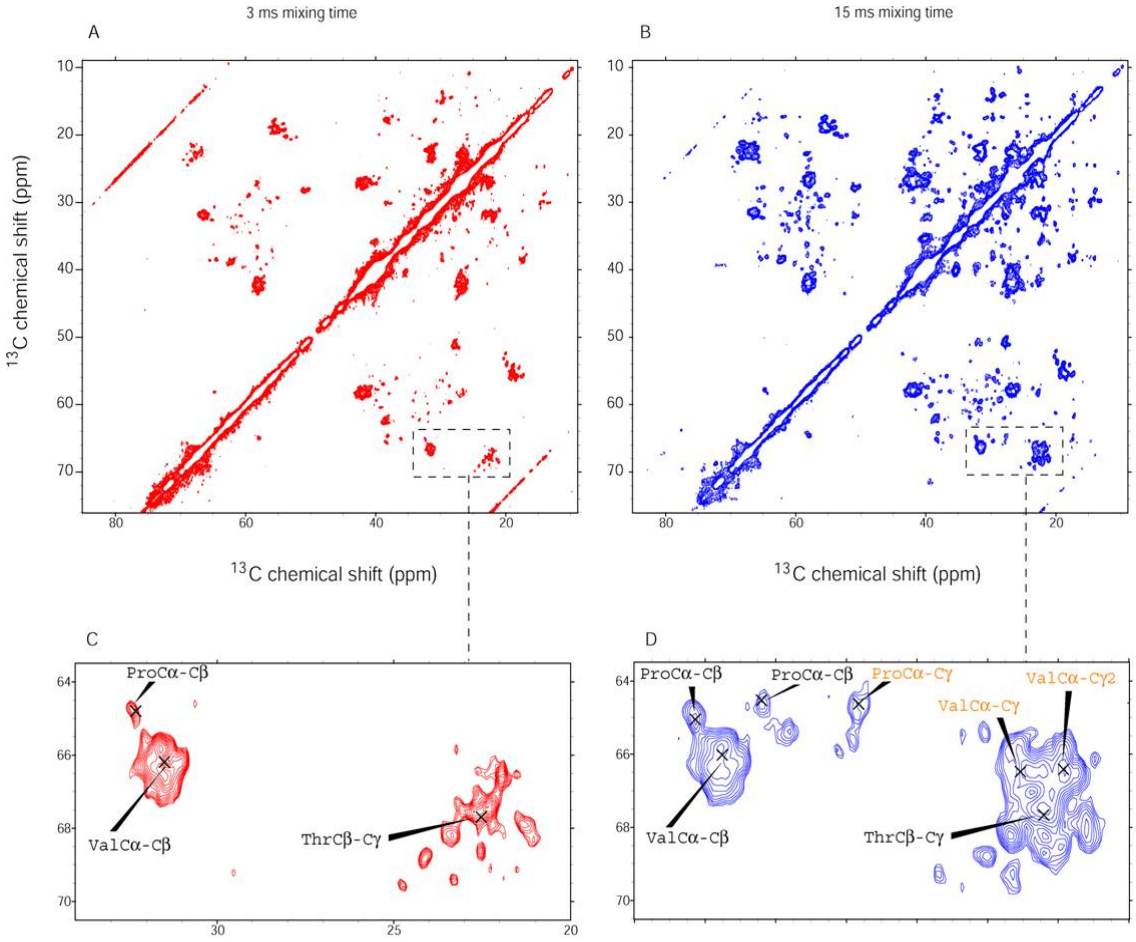

Figure 5.20 2D DARR spectra of 3 ms (red spectrum) and 15 ms (blue spectrum) mixing time of fully protonated sample collected on the 800 MHz Varian/Magnex Infinity + spectrometer. In the DARR spectrum with 3 ms mixing time mostly one bond transfers are visible, while in the DARR spectrum with 15 ms mixing time, crosspeaks with even three bond transfers can be detected. Thus the 15 ms mixing time spectrum is much more crowded, and the crosspeaks of the 2 or 3 bond transfers can overlap the one bond transfer crosspeaks. The two bond transfer peaks are coloured orange. This is illustrated in figure C and D, which show the valine and proline Cα-sidechain and Threonine Cβ-Cγ correlations. In figure D (15 ms DARR mixing), the valine Cα-Cγ1 and valine Cα-Cγ2 peak group overlaps with the Threonine Cβ-Cγ region. In figure C (3 ms DARR mixing) however, one bond Threonine Cβ-Cγ transfers can be observed.

In the aliphatic and carbonyl regions of the ^{13}C-^{13}C DARR spectrum of fully protonated U-^{13}C, ^{15}N labelled bR amino acid type assignments are shown Figure 5.21. Although site specific assignments cannot be made in a 2D ^{13}C-^{13}C spectrum the connectivities of many

residues peaks can be identified thus the amino acid type and the resonances which belong to the same amino acid can be identified. Isoleucine sidechains have chemical shifts which do not overlap with the other residues. For bR, the isoleucine sidechains have good chemical shift dispersion and many individual peaks can be resolved. Isoleucines are labelled by letters (eg. IleA – IleJ).

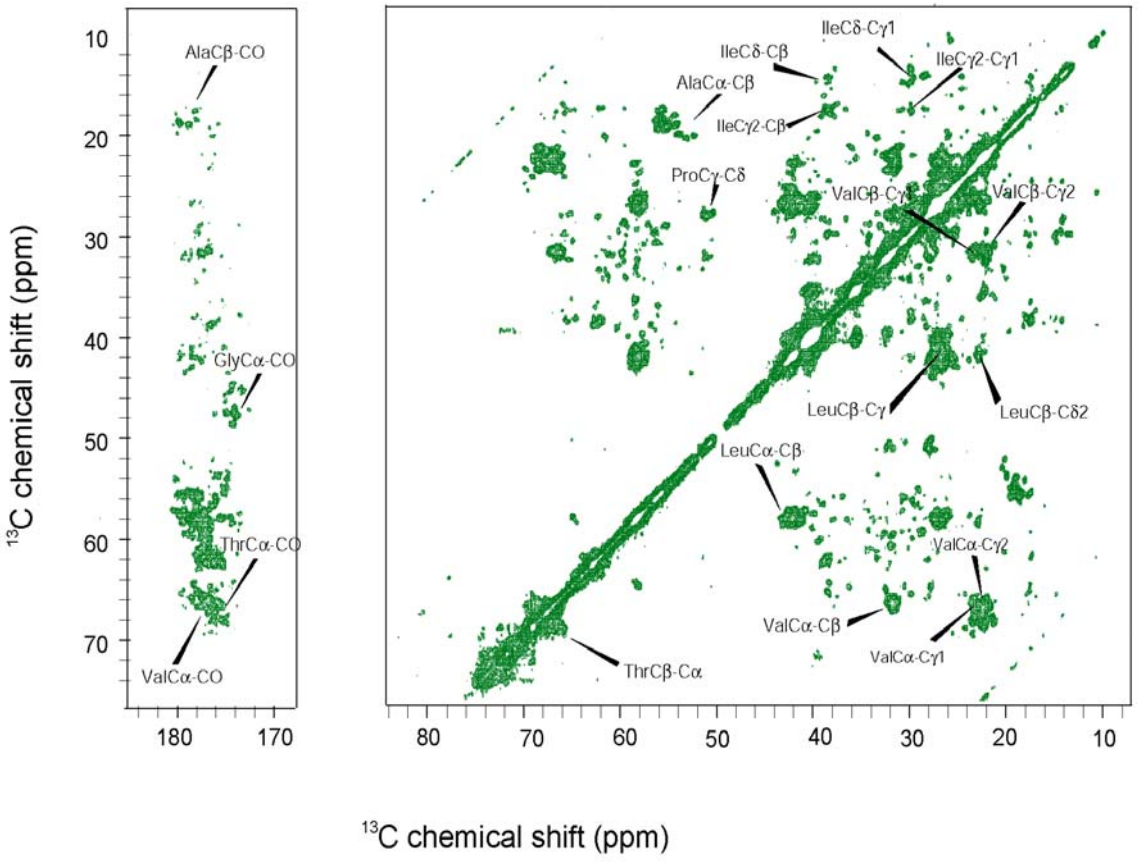

Figure 5.21 The aliphatic and carbonyl regions of a 2D DARR with 15 ms mixing time spectrum of a fully protonated U-^{13}C, ^{15}N recorded on the 800 MHz Varian/Magnex Infinity + Spectrometer at 263 K. The MAS frequency was 10.776 kHz. Amino peak clusters are present but there are many resolved peaks. The spectrum was processed with sine-bell apodisation function in both the direct and indirect dimensions.

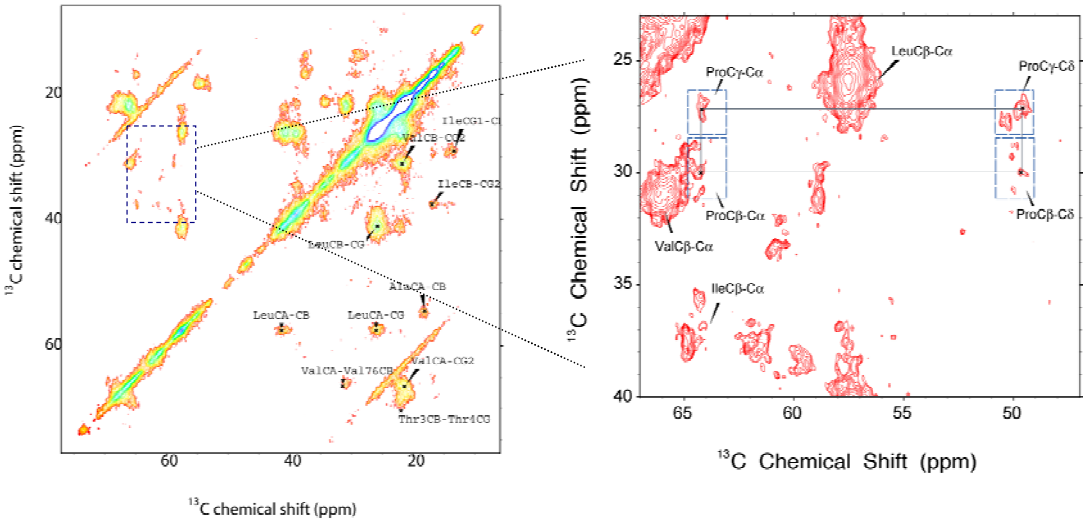

Figure 5.22 Proline connectivites in the aliphatic region of a 2D ^{13}C-^{13}C DARR spectrum of the highly deuterated U-^{13}C, ^{15}N bR. Proline peaks can be identified and partially resolved in the 2D ^{13}C-^{13}C DARR spectrum according to their characteristic chemical shift and connectivity. The aliphatic region of the DARR spectrum is shown on the left with the enlarged region (on the right) highlighted. 28 mg of purple membrane was packed into a 3.2 mm thin wall solid state NMR MAS rotor. The 2D ^{13}C-^{13}C homonuclear correlation spectra (DARR) were collected on a 800 MHz Varian/Magnex Infinity + spectrometer (at 18.8 T) at –20 ^{o}C VT inlet gas temperature and at 8.333 kHz spinning frequency using a 3.2 mm Balun probe. The DARR mixing was carried out with an n=1 rotary resonance condition for the protons, and a mixing time of 13 ms in order to identify 2-3 bond contacts. There were 2048 points and 1024 points collected in the direct and indirect ^{13}C dimensions for 20 ms and 10 ms, respectively. During acquisition 71 kHz proton decoupling was applied. 64 scans were collected, using 3 s pulse delay. The spectrum was processed using 30 Hz exponential line broadening in both the direct and indirect dimensions.

Spectra showing bond transfers can be seen in Figure 5.23. At least 10 out of 15 isoleucines can be assigned based on their connectivities. Solid state NMR chemical shifts of isoleucine are shown in Figure 5.23.

In spite of the lower resolution due to peak doubling and lower signal-to-noise ratio, it was possible to study amino acid connectivities in the fully deuterated bR sample (Figure 5.22 and Figure 5.24). The signal-to-noise ratio of these spectra was improved by alternative

processing scheme whereby exponential line broadening (also called exponential multiplication) was applied in each dimension. This type of processing can lead to loss of resolution for peaks with similar chemical shift due to line broadening, but it is extremely practical for the identification of isolated, otherwise weak or even unobservable peaks. In the case of the 2D DARR spectra of the highly deuterated sample line broadening had to be used to detect isolated peaks such as the isoleucines (Figure 5.22) and prolines (Figure 5.24).

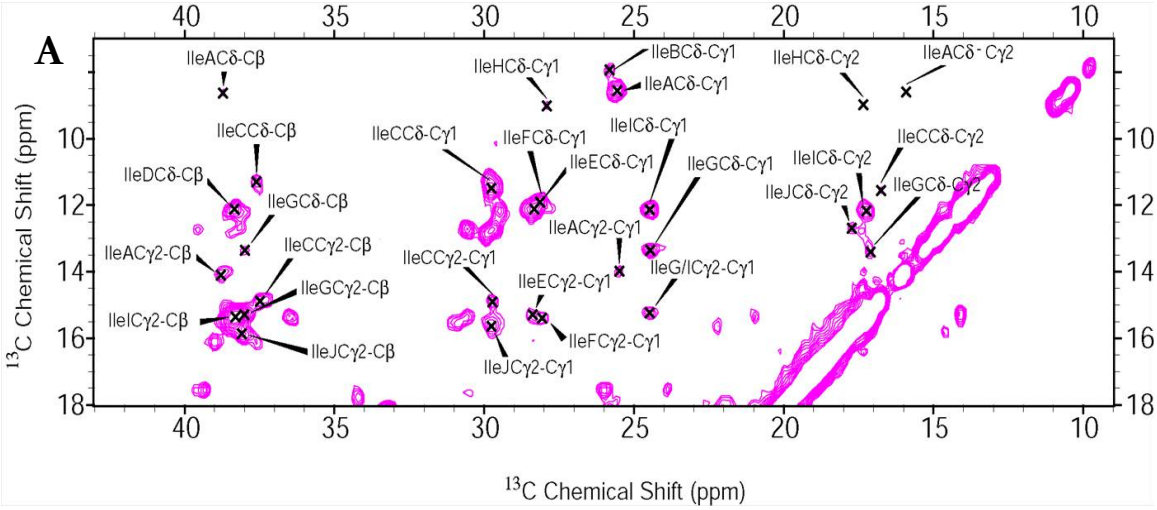

Figure 5.23 A) Connectivity of isoleucines a 2D DARR 15 ms mixing time spectrum of the fully protonated U-^{13}C, ^{15}N bR sample acquired on the 800 MHz Varian/Magnex Infinity + spectrometer. The bR sequence contains 15 isoleucines of which at least 10 out of 15 isoleucines in bR are resolved and assigned based on their connectivities. Typical linewidths in this area is 0.55 ppm. The spectrum was processed with sinebell apodisation in both dimensions. B) Isoleucine structural formula with the statistics on the ^{13}C chemical shifts denoted in red numbers

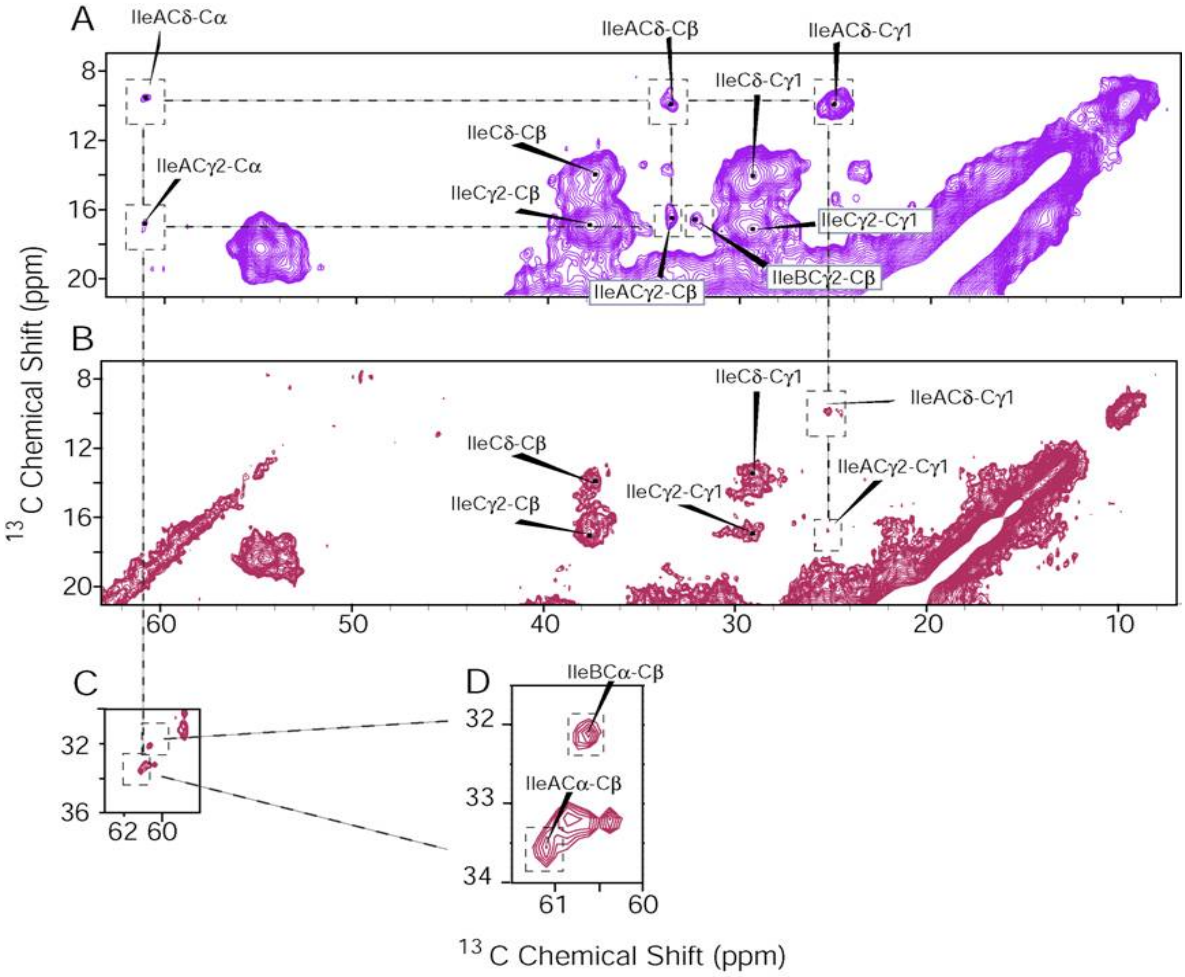

Figure 5.24 Isoleucine connectivity observed in the aliphatic region of the 2D ^{13}C-^{13}C DARR spectra of >50 % deuterated U-^{13}C, ^{15}N bR. (A) is a section of a 2D DARR spectrum (15 ms mixing time) acquired on a 500 MHz Varian/Magnex Infinity + NMR spectrometer. Figure (B) displays the identical section of a 2D DARR (13 ms mixing time) spectrum taken on an 800 MHz Varian/Magnex Infinity + NMR spectrometer. In order to enhance signal-to-noise of weak isolated peaks, 0.25 ppm and 0.16 ppm exponential line broadening were applied in both dimensions of spectrum (A) and (B) respectively. The isoleucine residue labelled IsoA is an isoleucine outlier, whose connectivity can be observed. The IsoACγ2-Cγ1 crosspeak is only visible in the DARR spectrum collected on the 800 MHz Varian/Magnex Infinity + and connects to the IsoACδ-Cγ1. The IsoACδ-Cα connects well with the IleA Cα-Cβ cross peak in section (C) of the 800 MHz spectrum, which is enlarged in section (D). With the combination of the 500 MHz and 800 MHz data sets most of the isoleucine A connectivities can be resolved. For additional experimental details see Materials and Methods section.

5.5.2.2.b Assignment studies based on heteronuclear 2D ^{15}N-^{13}C correlation spectra

Part of the assignment studies are 2D heteronuclear correlation NCA and NCO spectra, which facilitate backbone walk. However, only NCA (Figure 5.25) and NCO (Figure 5.26) spectra of the highly deuterated sample were collected and these spectra are not resolved well enough to do the backbone walk. The resolution of the NCO and NCA spectra of the fully deuterated U-^{13}C, ^{15}N bR sample is poor. In the NCA spectrum (Figure 5.25) assignment efficiency was further limited by particularly weak peaks in regions with ^{15}N chemical shifts lower than 115 ppm or higher than 130 ppm. Usually these are the regions where outliers are found which often facilitate the assignment process. For the identification of peaks in these regions, the spectra had to be processed with exponential line broadening. In the NCA spectrum in Figure 5.26 tentative assignments are shown. Residues with chemical shift less than 115 ppm in the ^{15}N dimension most likely belong to serine, glycine or threonine. The NCO and NCA spectra will be used together with future 3D experiments for assignment. In the 3D spectra, the ^{15}N dimension dramatically should improve resolution for some of the very congested regions of the 2D ^{13}C-^{13}C spectrum.

For the protonated bR sample the experiments are still in progress. Similar peak congestion is expected for the protonated sample as for the deuterated sample, even with the better resolution due to the absence of peak doubling. The reason why greater improvement in the resolution for the protonated sample is not expected is because bR is a large protein, 248 amino acids, the NCO and NCA spectra will still be congested. The carbonyl region is approximately 8 ppm wide and most ^{15}N peaks are located within 18 ppm. Over 250 peaks in this region (248 amino acids plus side chain ^{15}N) will result in a

crowded spectrum. The Cα region is 27 ppm wide, consequently the resolution for the NCA spectrum should be better than for the NCO. To resolve the congestion it will be necessary to do selective labelling, or acquire 3D experiments, as planned.

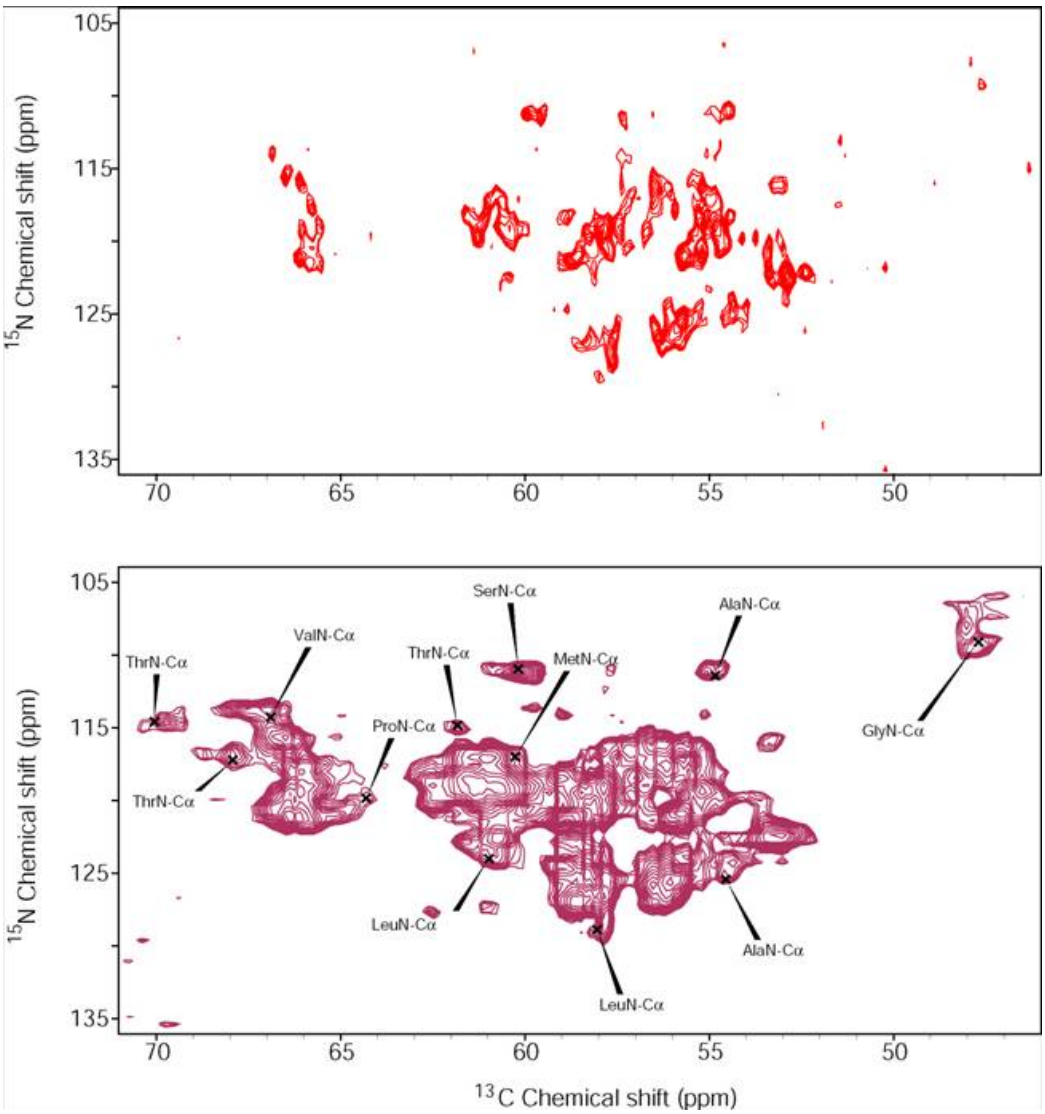

Figure 5.25 2D ^{15}N-^{13}C NCA correlation spectrum of 28.4 mg more than 50% deuterated U-^{13}C, ^{15}N, enriched purple membrane packed into a 3.2 mm thin wall rotor. The spectrum was acquired on an 800 Varian/Magnex MHz Infinity + spectrometer at 253 K probe temperature and MAS was 8.33 kHz. 192 scans were acquired and the total experimental time was 29 h. The two spectra in the figure are the same but with different processing: the top spectrum is processed without, and the bottom spectrum with the tentative amino acid assignments is processed with 0.5 ppm line broadening to increase signal-to-noise ratio.

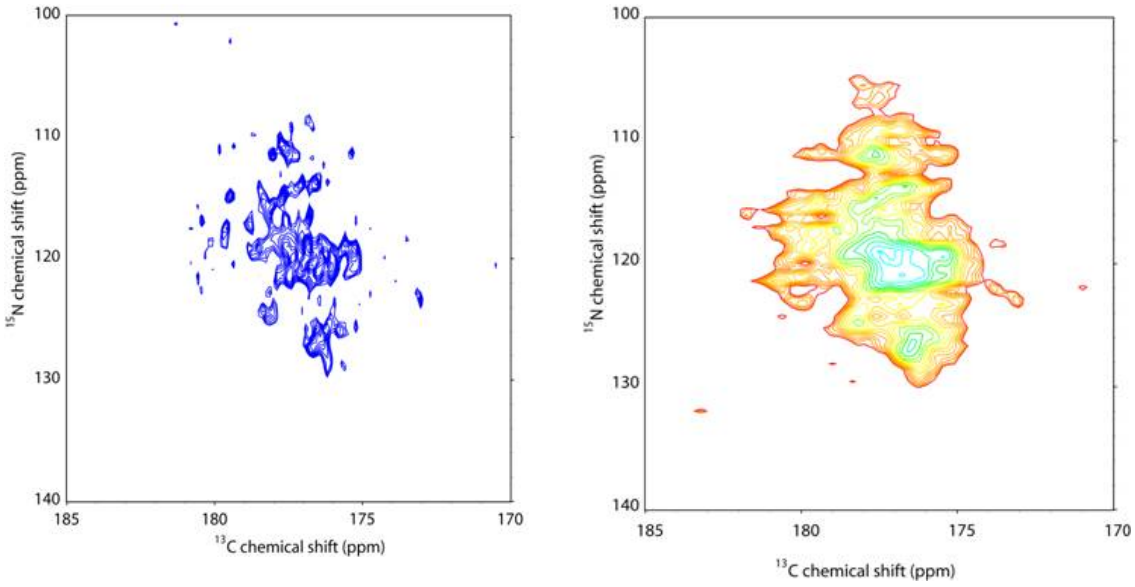

Figure 5.26 2D ^{15}N-^{13}C NCO correlation spectrum of 28.4 mg >50% U-^{13}C, ^{15}N enriched purple membrane packed into a 3.2 mm thin wall rotor. The spectrum was acquired on an 800 MHz Infinity + spectrometer at 253 K probe temperature and MAS was 8.33 kHz. 192 scans were acquired, over a total experimental time of 30 h. The two spectra in the figure are the same but with different processing: left spectrum without, and right spectrum processed with 0.5 ppm line broadening to increase signal to noise.

5.5.3 Conclusions

From the initial ^{13}C solid state NMR crystallography studies of bR it has been found that deuteration does not improve the resolution, however it may be beneficial for samples in which low decoupling powers are needed. Line widths of ^{13}C are sufficient for structural analyses (0.5-0.6 ppm) using multidimensional approaches and are little affected by covalent deuteration. The known deuterium isotope effect on ^{13}C solid state NMR spectra complicates analysis between differently deuterated samples. As a result of the sensitivity of the chemical shifts to local differences in electronic field effects, sample homogeneity can be readily detected. The 2D ^{13}C-^{13}C DARR spectrum of the highly deuterated U-^{13}C, ^{15}N bR sample exhibited peak doubling which resulted in lower resolution than the

protonated bR. This can be attributed to inherent sample inhomogeneity. The 2D ^{13}C-^{13}C DARR spectrum of the fully protonated U-^{13}C, ^{15}N bR sample on the other hand had good signal-to-noise and no peak-doubling was observed, which suggests the sample is homogenous. Finally, structural studies are possible for membrane-embedded receptors although spectral crowding may need to be relieved by selective labelling.

The preliminary data collected towards assignment of bR structure shows the feasibility of the assignment on this large membrane protein. However, more multidimensional experiments will be needed to make site-specific assignments based on backbone walk. The connectivities in the 2D DARR spectra, such as the isoleucine region, look very promising. Most of the assignment in this chapter is residue type assignment, and the groundwork for the assignment of bR has been laid.

It is necessary to acquire 3D experiments such as NCOCX for inter-residue backbone-backbone and backbone-sidechain correlations and NCACX for intra residue correlations, to improve resolution. Backbone walk will be necessary for the obtaining sequential assignments.

During the assignment process, peaks identified in the 3D spectra will be cross-checked against peaks observed in 2D ^{13}C-^{13}C DARR spectra. Close agreement is expected for the peaks in the 2D and 3D spectra. Residue type identification will be achieved by 3D experiments in which many residue types can be identified based on the backbone and side-chain chemical shifts. Sequential assignment will be accomplished by 3D experiments as well. Further data collection and analysis of spectra are necessary to accomplish the assignment of bR. It is remarkable that for a membrane protein of its size the resolution in

the 2D DARR spectra is of good quality. The most obvious improvement will be to collect the 3D experiments at the highest available magnetic field, 18.8 T in our case. Sample availability is not a limiting factor. 3D pulse sequences implemented with homonuclear ^{13}C J decoupling during evolution in the indirect dimension could also significantly improve resolution [249].

Here it has been demonstrated that solid-state NMR crystallography provides a promising approach which may have potential for application to large biological systems which may, themselves, not be amenable to X-ray crystallography.

Chapter 6 Conclusions

The work presented in this thesis demonstrates that it is possible to study large membrane proteins with solid state NMR, and that sample preparation of membrane proteins is crucial, often taking most of the experimental time.

mGluR4

As described in Chapters 2, a homology model of the truncated ligand binding domain (LBD) of mGluR4 was created and the ligand itself, L-glutamic acid, was characterised by ^{13}C, ^{15}N and ^{17}O solid state NMR. The full length mGluR4 protein was expressed in the neurotensin receptor plasmid. The level of expression was very low and had to be improved by co-expressing a plasmid which provides rare bacterial tRNAs. At that stage expression was very toxic and inhibited cell growth when induced. The temperature was reduced down to as low as 15 °C, using none or low amounts of inducer but the result was the same in that a plateau of expression was reached which then stopped the cell growth. The expression of the full length 'taste' version of mGluR4 between the MBP and TrxA fusions was also tried. It resulted in same low level expression. Removal of the TrxA tag from the C-terminus and replacing it with no tag or His-tag had no great effect on the overall expression levels.

The ligand binding domain of mGluR4 with various fusions to the periplasmic and with various fusions for expression in the cytoplasm were used. For the expression in the cytoplasm, Origami™ competent cells were used. For expression in the periplasm, helper pTum4 was used, which codes for a molecular chaperon. The most promising result was obtained with the periplasmic construct for which the western blot indicated that the protein gets into the periplasmic space but the protein could not be isolated and purified.

For the cytoplasmic expression constructs with maltose binding protein and Thiorodoxin A were made, which resulted in insoluble mGluR4. The yeast *Pichia pastoris* was used to express the full length mGluR4 without success, possibly due to codon difference of the recombinant mGluR4 with the host *P. pastoris*.

In *E.coli* the yield of the LBD of mGluR4 was always high, but the protein was mainly insoluble. Solubilisation of the LBD from inclusion bodies was not achieved despite the several different approaches to cloning and different *in vitro* refolding conditions employed. The *in vitro* refolding and screening conditions used, even though there were indications that the conditions in which the protein was soluble in the refolding buffer might be suitable, it was not possible to dialyse the protein in assay buffer, possibly because it was not properly solubilised. There was never enough protein in solution to concentrate and continue with binding assays. The *in vitro* refolding of the inclusion bodies of mGluR4 did not result in a properly soluble and active receptor, despite the extensive screening for refolding conditions and dialysis buffers. The results of the refolding screening looked promising as there was a pattern of solubility of the protein in similar refolding conditions. When the protein was

dialysed out of the refolding conditions with most soluble protein into an assay buffer it precipitated which indicates that it was either not properly solubilised or that more additives in the activity buffer should be tested. Since solubilisation and then purification of the LBD from inclusion is still under way, no crystals of mGluR4 were grown for possible solid state NMR studies with bound glutamate, both to unlabelled and labelled receptor, which was the original aim of the project.

Future work for mGluR4

The cloning and expression of different constructs of mGluR4 in *Pichia pastoris* will be continued. Use of rare codons in *P. pastoris* will be looked into as it may improve expression. Use of additives in the activity buffer will be tested.

Bacteriorhodopsin

Optimal conditions for producing spectra suitable for spectral assignment were tried as an initial step towards spectral resolution. Three dimensional crystallisation trials of bR of the monomeric, delipidated form and the PM in bicelles were tried. The first crystallisation trial of the monomeric, delipidated bR did not result in 3D crystals, only in the purple membrane in bicelles produced 3D crystals. Their resolution was compared by solid state NMR with that of bacteriorhodopsin in the purple membrane. The purple membrane was more homogeneous than the 3D bR crystals and this sample form was used for subsequent assignment experiments.

Three differently labelled samples of bacteriorhodopsin were prepared: highly deuterated >50% deuterated, 50% deuterated and fully protonated U-^{13}C, ^{15}N bR in purple membrane for two purposes, one was to test the applicability of the various assignment strategies and other one was to test the effects of deuteration on quality of solid state NMR spectra of a large, crystalline membrane protein. Comparison of the ^{13}C linewidth of the three samples by solid state NMR was done and showed that the fully deuterated bR sample did not have better linewidth than the fully protonated U-^{13}C, ^{15}N bR as expected, mainly due to peak doubling. This indicates sample inhomogeneity. The fully protonated bR spectrum gave the best resolution and sensitivity, and the CP transfer efficiency was the best in this sample. A notable upfield isotropic shift for ^{13}C resonance was observed in the deuterated samples, which complicates spectral analysis between differently deuterated samples.

The preliminary assignment studies show the feasibility of the assignment of this large membrane protein and potentially structural studies. However, more multidimensional experiments will be needed to make site-specific assignments and then resolution of the structure of membrane embedded bR.

Future work for bacteriorhodopsin

Three dimensional experiments on the U-^{13}C, ^{15}N bR will be carried out to do site-specific assignment. A backbone walk will be necessary for the sequential assignment.

Appendix

Bacterial growth media

SOC medium

Per litre: 20 g bacto-tryptone, 5 g yeast extract, 0.5 g NaCl were added to 950 ml of MilliQ H_2O and stirred until all solutes dissolved. Then 10 ml of a 250 mM KCl solution was added and the pH was adjusted to 7.0 and the volume made up to 1 L with MilliQ H_2O. The medium was sterilised by autoclaving for 20 m at 120 °C

Luria-Bertani (LB) bacterial growth medium

Per litre: 10 g bacto-tryptone, 5 g yeast extract and 10 g NaCl were added to 950 ml of MilliQ H_2O and stirred until solutes dissolved. The pH was adjusted to 7.0 and the volume made up to 1 L with MilliQ H_2O before sterilisation by autoclaving for 20 m at 120 °C.

2x TY

Per litre: 16 g bacto-tryptone, 10 g yeast extract and 5 g NaCl were added to 950 ml of pure water and shaken well until all the solutes were dissolved. The pH was then adjusted to 7.0 and the volume made up to 1 litre with pure water before sterilisation by autoclaving for 20 m at 120 °C.

References

1. Gunther, H., *NMR spectroscopy*. 1998, Chichester: Wiley.
2. Novagen, *Novagen pET vector table*, Novagen.
3. Glaubitz, C., *Magic angle sample spinning NMR spectroscopy on biomembranes*, in *Department of Biochemistry*. 1998, University of Oxford: Oxford.
4. Toyoshima, C., and Nomura, H., *Structral changes in the calcium pump accompanying the dissociation of calcium*. Nature, 2002. **418**: p. 605-611.
5. Bockaert, J., and Pin, J. P., *Molecular tinkering of G protein-coupled receptors: evolutionary success*. EMBO J, 1999. **18**: p. 1723-1729.
6. Invitrogen. *pCRT7/NT-TOPO vector data*. 2004 [cited; Available from: http://wwww.invitrogen.com/content.cfm.
7. Patzelt, H., Simon, B., terLaak, A., Kessler, B., Kuhne, R., Schmieder, P., Osterhelt, D. and Oschkinat, H., *The structure of the active center in the dark-adapted bacteriorhodopsin by solution-state NMR spectroscopy*. PNAS, 2002. **99**(17): p. 9765-9779.
8. Faham, S., Boulting, G.L., Massey, E.A., Yohannan, S., Yang, D. and Bowie, J.U., *Crystallisation of bacteriorhodopsin from bicelle formulations at room temperature*. Protein Science, 2005. **14**: p. 836-840.
9. Jingami, H., Nakanishi, S, Morikawa, K, *Structure of the metabotropic glutamate receptor*. Current Opinion in Neurobiology, 2003. **13**: p. 271-278.
10. Seeling, J.a.G., H.U., *Investigation of phosphatidylethanolamine bilayers by deiterium and phosphorus-31 nuclear magnetic resonance*. Biochemistry, 1976. **15**: p. 5199-5204.
11. Kim, C.J., *Probing structures of membrane proteins and their inhibitors*, in *Biochemistry*. 2006, University of Oxford: Oxford. p. 202.
12. Osaka University Medical School, D.o.P. *Glutamate receptors-structure and function*. 2003 [cited; Available from: http://pharma1.med.osaka-u.ac.jp/textbook/Receptors/glutamate-recep.html.
13. Andrew, E.R., A. Bradbury, and R.G. Eades, *Nuclear magnetic resonance spectra from a crystal rotated at high speed*. Nature, 1958. **4650**: p. 1659.
14. Betlach, M., Pfeifer, F., Friedman, J. and Boyer, H.W., *Bacterio-opsin mutants of* Halobacterium halobium. Proc Natl Acad Sci USA, 1983. **80**: p. 1416-1420.
15. Varga, K., and Watts, A., *Introduction to solid state NMR and its application to membrane protein-ligand binding studies*, in *Biophysical Analysis of Membrane Proteins*, E. Pebay-Peyroula, Editor. 2008, Wiley-VCH: Weinheim.
16. Helgerson, S.L., Siemsen, S. L., and Dratz, E. A., *Enrichment of bacteriorhodopsin with isotopically labeled amino-acids by biosynthetic incorporation in* Halobacterium Halobium. Canadian Journal Of Microbiology, 1992. **38**(11): p. 1181-1185.
17. Varga, K., *Membrane Protein Secondary Structure and Spectral Assignments by Solid State NMR: S. Lividans KcsA Potassium Channel and E. coli ATP Synthase Subunit c*, in *Chemistry*. 2005, Columbia University: New York.

18. Watts, J.A., Watts, A. and Middleton, D.A., *A model of reversible inhibitors in the gastric H^+/K^+-ATPase binding site determined by rotational echo double resonance NMR*. The Journal of Biological Chemistry, 2001. **276**(46): p. 43197-43204.
19. Pauli, J., van Rossum, B., Forster, H. de Groot, H. J. M. and Oschkinat, H., *Sample optimization and identification of signal patterns of amino acid side chains in 2D RFDR spectra of the alpha-spectrin SH3 domain*. Journal of Magnetic Resonance, 2000. **143**(2): p. 411-416.
20. Heyes, C.D., and .E.-Sayed., M.A., *Proton transfer reactions in native and deionised bacteriorhodopsin upon delipidation and monomerisation*. Biophys. J., 2003. **85**: p. 426-434.
21. Aharoni, W., L., Ottolenghi, M., and Sheves, M., *Bacteriorhodopsin experiences light-induced conformational alterations in nonisomerisable C13=C14 pigments*. Journal of Biologycal Chemistry, 2000. **275**(28): p. 21010-21016.
22. Mason, A.J., Grage, S.L., Glaubitz, C., Strauss, S. K., and Watts, A., *Identifying anisotropic constraints in multiply labeled bacteriorhodopsin by ^{15}N MAOSS NMR: A general approach to structural studies of membrane proteins*. Biophysical Journal, 2004. **86**(3): p. 1610-1617.
23. Bennett, A.E., Rienstra, C. M., Griffiths, J. M., Zhen, W. G., Lansbury, P. T., and Griffin, R. G., *Homonuclear radio frequency-driven recoupling in rotating solids*. Journal of Chemical Physics, 1998. **108**(22): p. 9463-9479.
24. Patzelt, H., Ulrich, A., Egbringhoffa, H., Düxb, P., Ashurstb, J., Simonb, B., Oschkinatb, H., and Oesterhelta, D., *Towards structural investigations on isotope labelled native bacteriorhodopsin in detergent micelles by solution-state NMR spectroscopy*. Journal of Biomolecular NMR, 1997. **10**: p. 95–106.
25. McDermott, A., Polenova, T., Bockmann, A., Zilm, K. W., Paulsen, E. K., Martin, R. W. and Montelione, G. T., *Partial NMR assignments for uniformly (C-13, N-15)-enriched BPTI in the solid state*. Journal of Biomolecular NMR, 2000. **16**(3): p. 209-219.
26. Grigorieff N, Ceska,T., Downing K., H., Baldwin J.,M., and Henderson R., *Electron-crystallographic refinement of the structure of bacteriorhodopsin*. Journal of Molecular Biology, 1996. **259**(3): p. 393-421.
27. Gerwert, K., Souvignier, G. and Hess, B, *Simultaneous monitoring of light-induced changes in protein side-group protonation, chromophore isomerization, and backbone motion of bacteriorhodopsin by time-resolved Fourier-transform infrared spectroscopy*. Proceedings of the National Academy of Science in the USA, 1990. **87**(24): p. 9774-9778.
28. Berman, H.M., Westbrook, J. Feng, Z., Gililand, G., Bhat, T.N., Weissig, H., Shindyalov, I.N. and Bourne, P.E., *The Protein Data Bank*. Nucleic Acids Res, 2000. **28**: p. 235-242.
29. Stevens, T.J., and Arkin, I.T., *Do more complex organisms have a greater proportion of membrane proteins in their genomes*. Proteins:Structure,Function, and Genetics, 2000. **39**: p. 417-420.
30. Torres, J., Stevens, T.J. and Samso, M., *Membrane proteins: the 'Wild West' of structural biology*. Trends in Biochemical Sciences, 2003. **28**: p. 174.
31. White, S., *Membrane proteins of known 3D structure*. 1998-2006.
32. Chill, J.H., Louis, J. M., Miller, C. and Bax, A., *NMR study of the tetrameric KcsA potassium channel in detergent micelles*. Protein Science, 2006. **15**(4): p. 684-698.
33. Hwang, P.M., Choy, W. Y., Lo, E. I., Chen, L., Forman-Kay, J. D., Raetz, C. R. H., Prive, G. G., Bishop, R. E., and Kay, L. E., *Solution structure and dynamics of the outer membrane enzyme PagP by NMR*. Proceedings of the National Academy of Sciences of the United States of America, 2002. **99**(21): p. 13560-13565.

34. Hwang, P.M., Bishop,R. E., and Kay, L. E., *The integral membrane enzyme PagP alternates between two dynamically distinct states.* Proceedings of the National Academy of Sciences of the United States of America, 2004. **101**(26): p. 9618-9623.
35. Hwang, P.M., and Kay, L.E.,, *Solution structure and dynamics of integral membrane proteins by NMR: A case study involving the enzyme PagP*, in *Nuclear Magnetic Resonance Of Biological Macromolecules, Part C*. 2005. p. 335-+.
36. Arora, A., Abildgaard, F., Bushweller, J. H., and Tamm, L. K., *Structure of outer membrane protein A transmembrane domain by NMR spectroscopy.* Nature Structural Biology, 2001. **8**(4): p. 334-338.
37. Tamm, L.K., Abildgaard, F., Arora, A., Blad, H., and Bushweller, J. H., *Structure, dynamics and function of the outer membrane protein A (OmpA) and influenza hemagglutinin fusion domain in detergent micelles by solution NMR.* FEBS Letters, 2003. **555**(1): p. 139-143.
38. Fernandez, C., Adeishvili, K., and Wuthrich, K., *Transverse relaxation-optimized NMR spectroscopy with the outer membrane protein OmpX in dihexanoyl phosphatidylcholine micelles.* Proceedings of the National Academy of Sciences of the United States of America, 2001. **98**(5): p. 2358-2363.
39. Fernandez, C., and Wuthrich, K., *NMR solution structure determination of membrane proteins reconstituted in detergent micelles.* FEBS Letters, 2003. **555**(1): p. 144-150.
40. Rastogi, V.K. and M.E. Girvin, *Structural changes linked to proton translocation by subunit c of the ATP synthase.* Nature, 1999. **402**(6759): p. 263-268.
41. Ahn, H.C., Juranic, N., Macura, S., and Markley, J. L., *Three-dimensional structure of the water-insoluble protein crambin in doidecylphosphocholine micelles and its minimal solvent-exposed surface.* Journal of the American Chemical Society, 2006. **128**(13): p. 4398-4404.
42. Downing, K.A., *Protein NMR Techniques*. 2004: Humana Press.
43. Watts, A., *Solid-state NMR in drug design and discovery for membrane-embedded targets.* Nature Reviews Drug Discovery, 2005. **4**(7): p. 555-568.
44. Watts, A., *Solid-state NMR approaches for studying the interaction of peptides and proteins with membranes.* Biochimica et Biophysica Acta, 1998. **1376**: p. 297-318.
45. Nussberger, S., Dorr, K., Wang, D. N., and Kuhlbrandt, W., *Lipid-Protein Interactions in Crystals of Plant Light-Harvesting Complex*. Journal of Molecular Biology, 1993. **234**(2): p. 347-356.
46. Fyfe, P.K., Hughes, A. V., Heathcote, P., and Jones, M. R., *Proteins, chlorophylls and lipids: X-ray analysis of a three-way relationship.* Trends In Plant Science, 2005. **10**(6): p. 275-282.
47. van den Brink-van der Laan, E., Chupin, V., Killian, J. A. and de Kruijff, B., *Stability of KcsA tetramer depends on membrane lateral pressure.* Biochemistry, 2004. **43**(14): p. 4240-4250.
48. Sternberg, B., Lhostis, C., Whiteway, C. A. and Watts, A.,, *The Essential Role Of Specific Halobacterium-Halobium Polar Lipids In 2d-Array Formation Of Bacteriorhodopsin.* Biochimica Et Biophysica Acta, 1992. **1108**(1): p. 21-30.
49. Sternberg, B., Watts, A. and Cejka, Z., *Lipid-Induced Modulation Of The Protein Packing In 2-Dimensional Crystals Of Bacteriorhodopsin.* Journal Of Structural Biology, 1993. **110**(3): p. 196-204.
50. Sabra, M.C., Uitdehaag, J. C. M., and Watts, A., *General model for lipid-mediated two-dimensional array formation of membrane proteins: Application to bacteriorhodopsin.* Biophysical Journal, 1998. **75**(3): p. 1180-1188.

51. Gil, T., Ipsen, J. H., Mouritsen, O. G., Sabra, M. C., Sperotto, M. M., and Zuckermann, M. J., *Theoretical analysis of protein organization in lipid membranes*. Biochimica Et Biophysica Acta-Reviews on Biomembranes, 1998. **1376**(3): p. 245-266.
52. Hong, M., *Solid-state NMR determination of C-13 alpha chemical shift anisotropies for the identification of protein secondary structure*. Journal of the American Chemical Society, 2000. **122**(15): p. 3762-3770.
53. Huster, D., Yao, Y. L., Jakes, K., and Hong, M., *Conformational changes of colicin Ia channel-forming domain upon membrane binding: a solid-state NMR study*. Biochimica Et Biophysica Acta-Biomembranes, 2002. **1561**(2): p. 159-170.
54. Luca, S., Filippov, D. V., van Boom, J. H., Oschkinat, H., de Groot, H. J. M. and Baldus, M.,, *Secondary chemical shifts in immobilized peptides and proteins: A qualitative basis for structure refinement under Magic Angle Spinning*. Journal of Biomolecular NMR, 2001. **20**(4): p. 325-331.
55. Huster, D., S. Yamaguchi, and M. Hong, *Efficient beta-sheet identification in proteins by solid-state NMR spectroscopy*. Journal of the American Chemical Society, 2000. **122**(46): p. 11320-11327.
56. Gether, U., Lin, S., Ghanouni, P., Ballesteros, J.A., Weinstein, H., and Kobilka, B.K., *Agonists induce conformational changes in transmembrane domain III and VI of the beta2 adrenoceptor*. EMBO J, 1997. **16**: p. 6737-47.
57. Palczewski, K., Kumasaka, T.,Hori, T., Behnke, C.,A., Motoshima, H., Fox, B., A., Le Trong, I., Teller, D.,C., Okada, T., Stenkamp, R., E., Yamamoto, M. and Miyano, M., *Crystal structure of rhodopsin: A G protein-coupled receptor*. Science, 2000. **277**: p. 687-690.
58. Pin, J.P., and Bockaer, J., *Get receptive to metabotropic glutamate receptors*. Curr Opin Neurobiol, 1995. **5**: p. 342-349.
59. Hermit, M.B., Greenwood, J.R., and Brauner-Osborne, H., *Mutation-induced quisqualic acid and ibotenic acid affinity at the metabotropic glutamate receptor subtype 4-ligand selectivity results from a synergy of several amino residues*. Journal of Biological Chemistry, 2004(Manuscript in press).
60. Kaupmann, K., Huggel, K., Heid., Flor, P.J., Bishoff, S., Mickel, S.J., McMaster, G., Angst, C., Bittiger, H., Froestl, W. and Bettler, B., *Expression cloning of $GABA_B$ receptors uncovers similarity to metabotropic glutamate receptors*. Nature, 1997. **386**: p. 575-80.
61. Caudihari, N., Landin, A.M. and Roper S.D., *A metabotropic glutamate receptor variant functions as a taste receptor*. Nature, 2000. **3**(2): p. 113-117.
62. Kunishima, N., Shimada, Y., Tsuji,Y., Sato, T., Yamamoto, M., Kumasaka, T., Nakanishi, S., Jingami, K. and Morikawa, K., *Structural basis of glutamate recognition by a dimeric metabotropic glutamate receptor*. Nature, 2000. **407**: p. 971-977.
63. Tsuchiya, D., Kunishima,N., Kamiya, N., Jingami, H, and Morikawa, K, *Structural views of the ligand-binding cores of a metabotropic glutamate receptor complexed with an antagonist and both glutamate and Gd3+*. Proceedings of National Academy of Science of the United States of America, 2002. **99**: p. 2660-2665.
64. Sato, T., Shimada, Y., Nagasawa, N., Nakanishim, S. and Jingama, H, *Amino acid mutagenesis of the ligand binding site and the dimmer interface of the metabotropic receptor*. Journal of Biological Chemistry, 2003. **278**(6): p. 4314-4321.
65. Cavanagh, J., Fairbrother,W.J., and Palmer,A.G., *Protein NMR spectroscopy. Principles and Practice* 1996, San Diego: Academic Press.

66. Watts, A., *Direct studies of ligand-receptor interactions and ion channel blocking (Review).* Mol Membrane Biol, 2002. **19**(4): p. 267-75.
67. Castellani, F., van Rossum, B., Diehl, A., Schubert, M., Rehbein, K. and Oschkinat, H., *Structure of a protein determined by solid-state magic-angle-spinning NMR spectroscopy.* Nature, 2002. **420**(6911): p. 98-102.
68. Castellani, F., van Rossum, B. J., Diehl, A., Rehbein, K. and Oschkinat, H., *Determination of solid-state NMR structures of proteins by means of three-dimensional N-15-C-13-C-13 dipolar correlation spectroscopy and chemical shift analysis.* Biochemistry, 2003. **42**(39): p. 11476-11483.
69. Zimmermann, J., Jarchau, T., Walter, U.,Oschkinat, H., and Ball, L.J., *1H,13C and 15N resonance assignment of the human Spred2 EVH1 domain.* J Biomol NMR, 2004. **29**: p. 435-436.
70. Watts, A., *Structural resolution of ligand-receptor interactions in functional, membrane-embedded receptors and proteins using novel, non-perturbing solid state NMR methods.* Pharmacy and Pharmacology Communications, 1999. **5**: p. 7-13.
71. Middleton, D.A., Rankin, S., Esmann, M., and Watts, A., *Structural insights into the binding of cardiac glycosides to the digitalis receptor revealed by solid-state NMR.* Proceedings of the National Academy of Sciences of the United States of America, 2000. **97**(25): p. 13602-13607.
72. Spooner, P.J.R., Sharples, J. M., Verhoeven, M. A., Lugtenburg, J.,Glaubitz, C., and Watts, A., *Relative orientation between the beta-ionone ring and the polyene chain for the chromophore of rhodopsin in native membranes.* Biochemistry, 2002. **41**: p. 7549-7555.
73. Verdegem, P.J., Bovee-Geurts, P.H., de Grip, W.J., Lugtenburg,J., and de Groot,H.J.,, *Retinylidene ligand structure in bovine rhodopsin, metarhodopsin-I, and 10-methylrhodopsin from internuclear distance measurements using ^{13}C-labeling and 1-D rotational resonance MAS NMR.* Biochemistry, 1999. **38**(35): p. 11316-11324.
74. Watts, J.A., Watts, A., and Middleton, D.A., *A model of reversible inhibitors in gastric H^+/K^+-ATPase binding site determined by rotational echo double resonance NMR.* Journal of Biological Chemistry, 2001. **276**: p. 43197-43204.
75. Zeri, A.C., Mesleh, M. F., Nevzorov, A. A. , and Opella, S. J., *Structure of the coat protein in fd filamentous bacteriophage particles determined by solid state NMR spectroscopy.* Proc. Natl. Acad. Sci., 2003. **100**(11): p. 6458-6463.
76. Watts, A., Straus, S. K., Grage, S., Kamihira, M., Lam, Y-H., and Xhao, Z., *Membrane protein structure determination using solid state NMR.* Methods in Molecular Biology – Techniques in Protein NMR, ed. K. Downing. Vol. 278. 2004, New Jersey: Humana Press. 403-474.
77. Kovacs, F., Quine, J. and Cross, T.A., *Validation of the single-stranded channel confirmation of gramicidin A by solid-state NMR.* Proc Natl Acad Sci USA, 1999. **96**: p. 7910.
78. Opella, S.J., Marassi, F. M., Gesell, J. J., Valente, A. P., Kim, Y., Oblatt-Montal, M. and Montal, M., *Structures of the M2 channel-lining segments from nicotinic acetylcholine and NMDA receptors by NMR spectroscopy.* Nature Structural Biology, 1999. **6**(4): p. 374-379.
79. Park, S.H., Mrse, A. A., Nevzorov, A. A., Mesleh, M. F., Oblatt-Montal, M., Montal, M. and Opella, S. J., *Three-dimensional structure of the channel-forming trans-membrane domain of virus protein "u" (Vpu) from HIV-1.* Journal of Molecular Biology, 2003. **333**(2): p. 409-424.

80. Fu, R., Cotten, M. and Cross, T.A., *Inter- and intramolecular distance measurements by solid-state MAS NMR: determination of gramicidin A channel dimer structure in hydrated phospholipid bilayers*. J Biomol NMR, 2000. **16**: p. 261.
81. Tischmack, P.A., Bugay, D.E. and Byrn, S.R., *Solid-state nuclear magnetic resonance spectroscopy- pharmaceutical applications*. J Pharm Sci, 2003. **92**: p. 441.
82. McDermott, A.E., *Structural and dynamic studies of proteins by solid-state NMR spectroscopy: rapid movement forward*. Current Opinion in Structural Biology, 2004. **14**(5): p. 554-561.
83. Hong, M., *Oligomeric structure, dynamics, and orientation of membrane proteins from solid-state NMR*. Structure, 2006. **14**(12): p. 1731-1740.
84. Baldus, M., *Molecular interactions investigated by multi-dimensional solid-state NMR*. Current Opinion in Structural Biology, 2006. **16**(5): p. 618-623.
85. Bockmann, A., *Structural and dynamic studies of proteins by high-resolution solid-state NMR*. Comptes Rendus Chimie, 2006. **9**(3-4): p. 381-392.
86. De Angelis, A.A., Jones, D. H., Grant, C. V., Park, S. H., Mesleh, M. F., and Opella, S. J., *NMR experiments on aligned samples of membrane proteins*, in *Nuclear Magnetic Resonance Of Biological Macromolecules, Part C*. 2005, Elsevier Academic Press Inc: San Diego. p. 350-382.
87. Glaubitz, C. and A. Watts, *Magic angle-oriented sample spinning (MAOSS): A new approach toward biomembrane studies*. Journal of Magnetic Resonance, 1998. **130**: p. 305-316.
88. Ramamoorthy, A., C.H. Wu, and Opella, S.J. *Experimental aspects of multidimensional solid-state NMR correlation spectroscopy*. Journal Magnetic Resonance, 1999. **140**: p. 131-140.
89. Marassi, F.M. and S.J. Opella, *A solid-state NMR index of helical membrane protein structure and topology*. Journal of Magnetic Resonance, 2000. **144**: p. 150-155.
90. Andrew, E.R., A. Bradbury, and R.G. Eades, *Removal of dipolar broadening of nuclear magnetic resonance spectra of solids by specimen rotation*. Nature, 1959. **183**(4678): p. 1802-1803.
91. Lowe, I.J., *Free induction decay of rotating solids*. Physics Review Letters, 1959. **2**(7): p. 285-287.
92. Watts, A., *Solid state NMR on biological systems*. Magnetic resonance in chemistry, 2004. **42**(2): p. 87.
93. Watts, A., *NMR of drugs and ligands bound to membrane receptors*. Current Opinion in Biotechnology, 1999. **10**: p. 48-53.
94. Watts, A., Burnett, I.J., Glaubitz, C., Groebner, G., Middleton, D.A., Spooner, P.J.R., and Williamson, P.T.F., *Structural descriptions of ligands in their binding site of integral membrane proteins at near physiological conditions*. European Biophysics Journal, 1998. **28**: p. 84-90.
95. Mason, A.J., Grage, S.L., Straus, S.K., Glaubitz, C. and Watts, A., *Identifying anisotropic constraints in multiply labeled bacteriorhodopsin by ^{15}N MAOSS NMR: a general approach to structural studies of membrane proteins*. Biophysical journal, 2004. **86**: p. 1610-1617.
96. Spooner, P.J.R., Sharples, J.M., Goodall, S.L., Seedorf, H., Verhoeven, M.A., Lugtenburg, J., Bovee-Geiurts, P.H.M., de Grip, W.J., and Watts, A., *Conformational similarities in the ß-ionone ring region of the rhodopsin chromophore in its ground state and after photoactivation to the metarhodopsin-I intermediate*. Biochemistry, 2003. **42**: p. 13371-13378.

97. Williamson, P.T.F., Watts, J.A., Addona, G.H. Miller, K.W. and Watts, A., *Dynamics and orientation of N+(CD3)3-bromoacetylcholine bound to its binding site on the nicotinic acetylcholine receptor.* Proc. Natl. Acad. Sci. U.S.A, 2001. **98**: p. 2346-2351.
98. Williamson, P.T.F., Gröbner, G., Spooner, P.J.R., Miller, K.W., and Watts, A., *Probing the agonist binding pocket on the nicotinic acetylcholine receptor: a high resolution solid state NMR approach.* Biochemistry, 1998. **37**: p. 10854-10859.
99. Middleton, D.A., Robins, R., Feng, X., Levitt, M., Spiers, I.D., Schwalbe, C., Reid, D.G., and Watts, A., *The conformation of an inhibitor bound to the gastric proton pump.* FEBS Letters, 1997. **410**: p. 269-274.
100. Auger, M., *Biological membrane structure by solid-state NMR.* Current Issues in Molecular Biology, 2000. **2**(4): p. 119-124.
101. Siminovitch, D.J., *Solid-state NMR studies of proteins: the view from static ^{2}H NMR experiments.* Biochemistry and Cell Biology, 1998. **76**(2-3): p. 411-422.
102. Ernst , R.R., Bodenhausen, G., and Wokaun, A, *Principles of nuclear magnetic resonance in one and two dimensions.* 1990: Oxford Univeristy Press.
103. Bloch, F., *Theory of line narrowing by double-frequency irradiation.* Physical Review, 1958. **111**: p. 841-853.
104. Pines, A., Waugh, J.S., and Gibby, M. G., *Proton-enhanced nuclear induction spectroscopy-method for high-resolution NMR of dilute spins in solids.* J. Chem.Phys, 1972. **56**: p. 1776-1977.
105. Schaefer, J., and Stejskal, E.O., *Nuclear magnetic resonance of polymers spinning at magic angle.* J.Am.Chem.Soc, 1976. **98**: p. 1031-1032.
106. Andrew, E.R., Bradbury, A. and Eades, R.G., *Removal of dipolar broadening of nuclear magnetic resonance spectra of solids by specimen rotation.* Nature, 1959. **183**(4678): p. 1802-1803.
107. Lowe, I.J., *Free induction decay of rotating solids.* Physical review letters, 1959. **2**(7): p. 285-287.
108. Metz, G., X.L. Wu, and S.O. Smith, *Ramped-amplitude cross-polarization in magic-angle-spinning Nmr.* Journal of Magnetic Resonance Series A, 1994. **110**(2): p. 219-227.
109. Hediger, S., Meier,B. H., Kurur, N. D. Bodenhausen,G. and Ernst, R. R., *NMR cross polarization by adiabatic passage through the Hartmann-Hahn condition (APHH),.* Chem. Phys. Letters, 1994. **223** p. 283-288.
110. Bennett, A.E., Rienstra,C. M., Auger, M., Lakshmi,K. V., and Griffin, R.G., *Heteronuclear decoupling in rotating solids.* Journal of Chemical Physics, 1995. **103**(16): p. 6951-6958.
111. Ernst, M., Zimmerman, H. and Meir, B. H., *A simple model for heteronuclear spin decoupling in solid-state NMR.* Chemical Physics Letters 2000. **317**: p. 581-588
112. Detken, A., Hardy, E. H., Ernst, M., Kainosho, M., Kawakami, T., Aimoto, S., and Meier, B. H., *Methods for sequential resonance assignment in solid, uniformly C-13, N-15 labelled peptides: Quantification and application to antamanide.* Journal of Biomolecular Nmr, 2001. **20**(3): p. 203-221.
113. Tycko, R., and Dabbagh, G , *Measurement of nuclear magnetic dipole—dipole couplings in magic angle spinning. NMR* Chemical Physics Letters, 1990. **173**(5-6): p. 461-465.

114. Bennett, A.E., Ok, J. H., Griffin, R.G., and Vega, S., *Chemical-shift correlation spectroscopy in rotating solids - radio frequency-driven dipolar recoupling and longitudinal exchange.* Journal of Chemical Physics, 1992. **96**(11): p. 8624-8627.
115. Kunwar, A.C., Turner, G.L. and Oldfield, E., *Solid-state spin-echo Fourier transform NMR of ^{39}K and ^{67}Zn salts at high field.* Journal of Magnetic Resonance, 1986. **69**: p. 124-127.
116. Koeppe, R.E., Killian J. A., and Greathouse, D. V , *Orientations of the tryptophan 9 and 11 side chains of the gramicidin channel based on deuterium nuclear magnetic resonance spectroscopy.* Biophysical Journal, 1994. **66**: p. 14-24.
117. Watts, A., Ulrich,A.S., and Middleton,D.A., *Membrane protein structure: the contribution and potential of novel solid state NMR approaches.* Molecular Membrane Biology, 1995. **12**(3): p. 233-246.
118. Prosser, R.S., and Davis,J.H., *Dynamics of an integral membrane peptide: a deuterium NMR relaxation study of gramicidin.* Biophysical Journal, 1994. **66**(5): p. 1429-1440.
119. Prosser, R.S., Daleman,S.I., and Davis,J.H., *The structure of an integral membrane peptide: a deuterium NMR study of gramicidin.* Biophysical Journal, 1994. **66**(5): p. 1415-1428.
120. Hu, J.G., Sun, B. Q., Bizounok, M., Hatcher, M. E., Lansing, J. C., Raap, J., Verdegem, P. J. E., Lugtenburg, J., Griffin, R. G., and Herzfeld, J., *Early and Late M intermediates in the bacteriorhodopsin photocycle: A solid-state NMR study.* Biochemistry, 1998. **37**: p. 8088-8096.
121. Ulrich, A.S., Wallat, I., Heyn, M. P., and Watts, A., *Re-orientation of retinal in the M-photointermediate of bacteriorhodopsin.* Nature Structural Biology, 1995. **2**(3): p. 190-192.
122. Downing, K.A., *Protein NMR Techniques.* 2004, Humana Press.
123. Seelig, J., *31 P nuclear magnetic resonance and the head group structure of phospholipids in membranes.* Biochem. Biophys. Acta, 1978. **515**: p. 105-140.
124. Gröbner, G., Taylor, A., Williamson, P.T.F., Choi, G., Glaubitz, C., Watts, J.A., de Grip, W.J., and Watts, A., *Macroscopic orientation of natural and model membranes for structural studies.* Analytical Biochemistry, 1997. **254**: p. 132-136.
125. Brown, J.M., Evenson, K.M. and Zink, L.R., *Laser magnetic-resonance measurement of the $^3P_1$-$^3P_2$ fine-structure splittings in ^{17}O and ^{18}O.* Physical Review, 1993. **48**(5): p. 3761-3763.
126. MacKenzie, K., and Smith, M.E. , *Multinuclear solid state NMR of inorganic materials.* 2002, Oxford: Pergamo-Elsevier.
127. Howes, A.P., Anupõlde, T., LemaitreV., Kukold, A., Watts, A., Samosone, A., Smith, M.E., and Dupree, R. , *Enhancing resolution and sensitivity of 17O solid-state NMR through combining double rotation, 1H decoupling and satellite modulation for biomolecular applications.* Chemical Physics Letters, 2006. **421**(1-3): p. 42-46.
128. Lemaitre, V., Smith, M.E. and Watts, A., *A review of oxygen-17 solid-state NMR of organic materials-towards biological applications.* Solid State NMR, 2004. **26**(3-4): p. 215-235.
129. Arêas, J.A.G., Cassiano, M.M., Glaubitz, C., and Watts, A., *Interaction of ß-casein at an emulsion interface studied by 2H NMR and molecular modeling.* Magnetic Resonance in Food Science: A view to the future, 2000, Royal Society of Chemistry: Cambridge, UK. 193-201.
130. Marti-Renom, M.A., Stuart, A.C., Fiser, A., Sanchez, R.,Melo, F., and Sali A, *Comparative Protein Structure Modeling of Genes and Genomes.* Annual Review of Biophysics and Biomolecular Structure, 2000. **29**: p. 291-325.

131. Sanchez, R., and Sali, A, *Advances in comparative protein-structure modelling.* Current Opinion in Structural Biology, 1997. **7**: p. 206-214.
132. Okamoto, T., Sekiyama, N., Otsu, M., Shimada, Y., Sato, A., Nakanishi, S., Jingami, H., *Expression and purification of the extracellular ligand binding region of metabotropic glutamate receptor subtype 1.* Journal of Biological Chemistry, 1998. **273**: p. 13089-13096.
133. Harding, P.J., Attrill, H., Ross, S., Koeppe, J.R., Kapanidis, A.N. and Watts, A., *Neurotensin receptor type 1:* Escherichia coli *expression, purification, characterization and biophysical studies.* Biochemical Society Transactions, 2007. **35**(4): p. 760-763.
134. Detken, A., Hardy, E.H., Ernst, M., and Meier, B.H., *Simple and efficient decoupling in magic-angle spinning solid-state NMR: the XiX scheme.* Chemical Physics Letters, 2002. **356**(3-4): p. 298-304.
135. Pike, K.J., Lemaitre, V., Kukol, A., Anupold, T., Samoson, A., Howes, A.P., Watts, A., Smith, M.E. and Dupress, R., *Solid-state ^{17}O NMR of amino acids.* Journal of Physical Chemistry, 2004. **108**: p. 9256-9263.
136. Lemaitre, V., Pike, K.J., Watts, A., Anupold, T., Samson, A., Smith, M.E. and Dupree, R., *New insigths into the bonding arrangement of L- and D-glutamates from solid state ^{17}O NMR.* Chemical Physics Letters, 2003. **371**: p. 91-97.
137. Laskowski, R.A., MacArthur, M.W., Smith, D.K., Jones, D.T., Hutchinson, E., Morris, A.L., Moss, D.S. and Thornton, J.M. *Programs to check the stereochemical quality of protein structure.* 1998 [cited 2004; Available from: http://www.biochem.ucl.ac.uk/%7Eroman/procheck/manual/index.html#.
138. Keesey, J., *Epitope tagging: Basic Laboratory Manual.* 1996, Mannheim: Boehringer Manheim.
139. Grisshammer, R., R. Duckworth, and H. Henderson, *Expression of a rat neurotensin receptor in E.coli.* Biochemical Journal, 1993. **317**: p. 891-899.
140. Kajava, A.V., Zolov, S.N., Kalnin, A.E. and Nesmeyanova, M.A., *The net charge of the first 18 residues of the mature sequence affects protein translocation across the cytoplasmic membrane of gram-negative bacteria.* Journal Of Bacteriology, 2000. **182**(8): p. 2163-2169.
141. Kunishima, N., Shimada, Y., Tsuji, Y., Sato, T., Yamamoto, M., Kumasaka, T., Nakanishi, S., Jingami, H., and Morikawa, K., *Structural basis of glutamate recognition by a dimeric metabotropic glutamate receptor.* Nature, 2000. **407**: p. 971.
142. Zhang, X.Z., Schwartz, J-C.D., Almo, S.C. and Nathenson, S.G., *Expression, refolding, purification, molecular characterisation, crystallisation, and preliminary X-ray analysis of the receptor binding domain of human B7-2.* Protein Expression and Purification, 2002. **25**(1): p. 105-113.
143. Nie, Y., Hobbs, J.R., Vigues, S., Olson, W.J., Conn, G.L. and Munger, S.D., *Expression and purification of functional ligand-binding domains of T1R3 taste receptors.* Chemical Senses, 2006. **31**: p. 505-513.
144. Lee, H.C., and Bernstein, H.D., *The target pathway of* Escherichia coli *presecretory and integral membrane proteins is specified by the hydrophobicity of the targeting signal.* PNAS, 2001. **98**(6): p. 3471-3476.
145. Thompson, J.D., Gibson, T.J., Plewniak, F, Jeanmougin, F. and Higgins, D.C., *The CLUSTAL_X windows interface: flexible strategies for multiple sequence alignment aided by quality analysis tools.* Nucleic Acids Research, 1997. **2**(24): p. 4876-82.

146. Sambrook, J., Fritsch, E.F., Maniatis, T., *Molecular Cloning: A Laboratory Manual.* 2nd ed. 1989: Cold Spring Harbor Laboratory Press.
147. Wu, X., Jornvall, H., Berndt, K.D. and Oppermann, U., *Codon optimisation reveals critical factors for high level expression of two rare codon genes in Escherichia coli:RNA stability and secondary structure but not tRNA abundance.* Biochemical and Biophysical Research Communications, 2004. **313**: p. 89-96.
148. de Marco, A., Vigh, L., Diamant, S. and Goloubinoff, P., *Native folding of aggregation-prone recombinant proteins in Escherichia coli by osmolytes, plasmid- or benzyl alcohol- overexpressed molecular chaperones.* Cell Stress Chaperones, 2005. **10**(4): p. 329-339.
149. Nasreen, A., Vogt, M., Kim, H.J., Eichinger, A. and Skerra, A., *Solubility engineering and crystallisation of human apolipoprotein D.* Protein Science, 2007. **15**: p. 190-199.
150. Sandee, D., Tunspadabku, S., Kurokawa, Y., Fukui, K. and Takasi, M., *Combination of Dsb coexpression and an addition of sorbitol markedly enhanced soluble expression of single-chain Fv in Escherichia coli.* Biotechnology and Bioengineering, 2005. **91**: p. 418-424.
151. Griffin, R.G., *Dipolar recoupling in MAS spectra of biological solids.* Nature Structural Biology, 1998. **5**: p. 508-512.
152. Spera, S., and Bax, A., *Empirical correlation between protein backbone conformation and C-alpha and C-beta C-13 nuclear-magnetic-resonance chemical shifts.* Journal of the American Chemical Society, 1991. **113**(14): p. 5490-5492.
153. Case, D.A., *Interpretation of chemical shifts and coupling constants in macromolecules.* Current Opinion in Structural Biology, 2000. **10**: p. 197-203.
154. Middleberg, A.P.J., *Preparative protein refolding.* Trends in Biotechnology 2002 **20**(10): p. 437-443.
155. Swietnicki, W., *Folding aggregated proteins into functionally active forms.* Current Opinion in Biotechnology, 2006. **17**: p. 367-372.
156. Clark, E.B., *Protein refolding for industrial processes.* Current opinion Biotechnology, 2001. **12**: p. 202-207.
157. Singh, S.M., and Panda, A. K., *Solubilisation and refolding of bacterial inclusion body proteins.* Journal of Bioscience and Bioengineering, 2005. **99**(4): p. 303-310.
158. Raman, B., Ramakrishna T., and Rao, C. M., *Refolding of denatured and denatured/reduced lysozyme at high concentration.* The Journal of Biological Chemistry, 1996. **271**: p. 17067-1707.
159. Mitraki, A., Fane, B., Haase-Pettingell, C., Sturtevant, J. and King, J., *Global suppression of protein folding defects and inclusion body formation.* Science, 1991. **253**: p. 54-58.
160. Taylor, G., Hoare, M., Gray, D.R. and Marston, F.A.O., *Size and density of protein inclusion bodies.* BioTechnology, 1986. **4**: p. 553-557.
161. Georgiou, G., and Valax, P., *Isolating inclusion bodies from bacteria.* Methods Enzymology, 1999. **309**: p. 48-58.
162. Carrio, M.M., Cubarsi, R., and Villaverde, A., *Fine architecture of bacterial inclusion bodies.* FEBS Lett, 2000. **471**: p. 7-11.
163. Valax, P., and Georgiou, G., *Molecular characterisation of beta-lactamase inclusion bodies produced in* Eschericia coli. Biotechnol Prog, 1993. **9**: p. 539-547.
164. Rinas, U., and Baily, J.E., *Protein composition analysis of inclusion bodies produced in recombinant* E.coli. Applied Environ. Microbiol, 1992. **59**: p. 561-566.

165. Villacerde, A., and Carrio, M.M, *Protein aggregation iin recombinant bacteria: biological role of inclusion bodies*. Biotechnol Lett, 2003. **25**: p. 1385-1395.
166. Lillie, H., Schwarz, E., and Rudolph, R., *Advances in refolding of proteins produced in* E.coli. Current Opinion Biotechnology, 1998. **9**: p. 497-501.
167. Khan, R.H., AppaRao, K.B.C., Eshwari, A.N.S., Totey, S.M. and Panda, A. K., *Solubilisation of recombinant ovine growth hormone with retention of native-like secondary structure and its refolding from the inclusion bodies in* Escherichia. Biotechnol Prog, 1998. **14**(722-728).
168. Maachupalli-Reddy, J., Kelly, B.D. and De Bernardez Clark E., *Effect of inclusion body contaminants on the oxidative renaturation of hen egg white lysozyme*. Biotechnology Progress, 1997. **13**: p. 144-150.
169. Puri, N.K., and Cardamone, M., *A relationship between the starting secondary structure of recombinant porcine growth hormone solubilised from inclusion bodies and the yield of native (monomeric) protein after in vitro refolding*. FEBS Lett, 1992. **305**(3): p. 177-180.
170. Rudolph, R., Bohm, G. Lilie,H. and Jaenicke, R., *Folding proteins*, in *Protein function, a practical approach*. 1997, IRL-Press, Oxford University Press:
Oxford. p. 57-99.
171. Rudolph, R.a.L., H., In vitro *folding of inclusion body proteins*. FASEB, 1996. **10**: p. 49-56.
172. Rudolph, R., Engelhard, M. and Jaenicke, R., *Kinetics of refolding and reactivation of rabbit-muscle aldolase after acid dissociation*. European Journal of Biochemistry, 1976. **67**: p. 455-462.
173. Jaenicke, R., Rudolph, R. and Feingold, D.S, *Dissociation and in vitro reconstitution of bovine liver uridine diphosphoglucose dehydrogenase. The paired subunit nature of the enzyme*. Biochemistry, 1986. **25**(23): p. 7283-7287.
174. Goldberg, M.E., Rudolph, R. and Jaenicke, R., *A kinetic study of the competition between renaturation and aggregation during the refolding of denatured-reduced egg white lysozyme*. Biochemistry, 1991. **30**(11): p. 2790-7.
175. Clark, E., *Refolding of recombinant proteins*. Current Biology, 1998. **9**: p. 157-163.
176. Li, M., Su, Z., and Janson. J., In vitro *protein refolding by chromatographic procedures*. Expression and Purification, 2004. **33**: p. 1-10.
177. Gasteiger E., G.A., Hoogland C., Ivanyi I., Appel R.D., Bairoch A., *ExPASy: the proteomics server for in-depth protein knowledge and analysis* Nucleic Acids Res, 2003. **31**: p. 3784-3788.
178. Hoogerheide, J.G., and Campbell, C.M., *Determination of cysteine plus half-cystine in protein and peptide hydrolysates: use of dithiodiglycolic acid and phenylisothiocyanate derivatisation* Analytical Biochemistry, 1992(201): p. 146-151.
179. Hamspon, D.R., Huang, X., Pekhleski, R., Peltekova, V., Hornby, G., Thomasen, C., and Thogersen, H., *Probing the ligand-binding domain of the mGluR4 subtype of metabotropic glutamate receptor*. J Biomol Chemistry, 1999. **274**: p. 33488-33495.
180. Guangming, H., and Hampson D.R., *Ligand binding to the amino-terminal domain of the mGluR4 subtype of metabotropic glutamate receptor*. J Biomol Chemistry, 1999. **274**: p. 1008-10013.
181. Jakeman, D.L., Mitchell, D.J., Shuttleworth, W. A., and Evans, J.N.S., *Effects of sample preparation conditions on biomolecular solid-state NMR lineshapes*. Journal of Biomolecular Nmr, 1998. **12**(3): p. 417-421.

182. Martin, R.W., and Zilm, K. W., *Preparation of protein nanocrystals and their characterization by solid state NMR.* Journal of Magnetic Resonance, 2003. **165**(1): p. 162-174.
183. Gregory, R.B., Gangoda, M., Gilpin, R. K., and Su, W., *The influence of hydration on the conformation of lysozyme studied by solid-state C-13-NMR spectroscopy.* Biopolymers, 1993. **33**(4): p. 513-519.
184. Gregory, R.B., Gangoda,M., Gilpin, R. K., and Su, W., *The influence of hydration on the conformation of bovine serum-albumin studied by solid-state C-13-NMRr spectroscopy.* Biopolymers, 1993. **33**(12): p. 1871-1876.
185. Lorch, M., Fahem, S., Kaiser, C., Weber, I., Mason, A. J., Bowie, J. U., and Glaubitz, C., *How to prepare membrane proteins for solid-state NMR: A case study on the alpha-helical integral membrane protein diaglycerol kinase from* E. coli. ChemBioChem, 2005. **9**(6): p. 1693-1700.
186. Hiller, M., Krabben, L., Vinothumar, K. R., Castellani, F., van Rossum, B. J., Kuhlbrandt, W., and Oschkinat, H., *Solid-state magic-angle spinning NMR of outer membrane protein G from* Escherichia coli. ChemBioChem, 2005. **6**(9): p. 1679-1684.
187. Igumenova, T.I., McDermott, A. E., Zilm, K. W., Martin, R. W., Paulson, E. K. and Wand, A. J., *Assignments of carbon NMR resonances for microcrystalline ubiquitin.* Journal of the American Chemical Society, 2004. **126**(21): p. 6720-6727.
188. Polenova, T., *Homonuclear 13C solid-state MAS spectroscopy of the uniformly (13C, 15N)-enriched* E. coli *thioredoxin at 17.6 Tesla. Spin system identification and sidechain resonance assignments.* 45th ENC, talk, 2004.
189. Martin, R.W., Paulson, E. K., and Zilm, K. W., *Design of a triple resonance magic angle sample spinning probe for high field solid state nuclear magnetic resonance.* Review of Scientific Instruments, 2003. **74**(6): p. 3045-3061.
190. Igumenova, T., Wand, J.A., and McDermott, A., *Assignment of the backbone resonances for microcrystalline ubiquitin.* Journal of American Chemical Society, 2004. **126**(16): p. 5323-5331.
191. Ernst, M., Detken, A., Bockmann, A., and Meier, B. H., *NMR spectra of a microcrystalline protein at 30 kHz MAS*. Journal of the American Chemical Society, 2003. **125**(51): p. 15807-15810.
192. Henderson, R.E., *The purple membrane from Halobacterium halobium.* Annu. Rev. Biophys. Bioeng, 1977. **6**: p. 87-109.
193. Lanyi, K., *Bacteriorhodopsin.* Annual Review of Physiology, 2004. **66**: p. 665-688.
194. Matsubara, T., Iada-Tanaka, N., Kamekura, M., Moldoveanu, N., Ishuzuka, I., Onishi, H., Hayashi, A. and Kates, M., *Polar lipids of a non-alkaliphilic extremely halophilic archaebacterium strain 172: a novel bis-sulfated glycolipid.* Biochem. Biophys. Acta, 1994. **1214**: p. 97-108.
195. Osterhelt, D., and Stoekenius, W., *Functions of a new photoreceptor membrane.* Proceedings of the National Academy of Science in the USA, 1973. **70**: p. 2853-2857.
196. Lanyi, J.K., *Mechanism of ion transport across membrane. Bacteriorhodopsin as a prototype for proton pump.* Journal of Biological Chemistry, 1997. **272**: p. 31209-31212.
197. Massotte, D., Boucher, F. and Aghion, J., *Light adaptation of bacteriorhodopsin in the presence of valinomycin and potassium. pH-dependence.* Photosynthesis Research, 1988. **18**: p. 307-315.
198. Stoeckenius, W., Lozier, R.H., and Niederberg, W., *Photoreactions of bacteriorhodopsin.* Biophysical Structure Mechanisms, 1977. **3**: p. 65-68.

199. Taneva, S. *Bacteriorhodopsin*. 2004 5 June 2004 [cited 2004 7 July 2004]; Available from: http://www.bioc21.bg/ibf/bR2.gif.
200. Essen L.O., S., R., Lehmann,W.D., and Oeserhelt, D., *Lipid patches in membrane protein oligomers: Crystal structure of the bacteriorhodops in lipid complex*. Proceedings of the National Academy of Science in the USA, 1998. **95**: p. 11673-11678.
201. Hirai, T., and Subramaniam, S., *Structural insights into the mechanism of proton pumping by bacteriorhodopsin* FEBS Letters, 2003. **545**(1): p. 2-8
202. Patzelt, H., Ulrich, A.S., Egringhoff, H., Dux, P., Ashurst, J., Simon, B., Oschkinat, H. and Oesterhelt, D., *Towards structural investigations on isotope labelled native bacteriorhodopsin in detergent micelles by solution-state NMR spectroscopy*. Journal of Biomolecular NMR, 1997. **10**: p. 95-106.
203. Mason, A.J., Grage, S. L., Glaubitz, C., Strauss, S. K., and Watts, A., *Identifying anisotropic constraints in multiply labelled membrane proteins by ^{15}N MAS NMR*. Biophysical Journal, 2003. **86**: p. 1610-1617.
204. Oesterhelt, D. and W. Stoeckenius, *Isolation of the cell membrane of* Halobacterium halobium *and its fractionation into red and purple membrane*. Methods in Enzymology, 1974. **31**: p. 667-678.
205. Schertler, G.F.X., Bartunik, H.D., Michel, H. and Oesterhhelt, D. *Orthorhombic crystal form of bacterhiorhodopsin nucleated on benzamidine diffracting to 3.6 A resolution*. Journal of Molecular Biology, 1993. **234**(5): p. 156-164.
206. Oesterhelt, D., and W. Stoeckenius., *Isolation of the cell membrane of* Halobacterium halobium *and its fractionation into red and purple membranes*. . Methods Enzymol. , 1974. **31**: p. 667-678.
207. Schertler, G.F.X., Bartunik, H.D., Michel, H. and Osterhhelt, *Orthorhombic crystal form of bacterhiorhodopsin nucleated on benzamidine diffracting to 3.6 A resolution*. Journal of Molecular Biology, 1993. **234**(5): p. 156-164.
208. McDermot, A.E., and Gu, Z., ed. *Carbon and nitrogen chemical shifts of solid state enzymes*. In Encyclopedia of Nuclear Magnetic Resonance, 1996, John Wiley & Sons. 113.
209. Oesterhelt, D., Brauchle, C., and Hampp, N., *Bacteriorhodopsin: a biological material for information processing*. Quarterly Reviews of Biophysics, 1991. **24**: p. 425-478.
210. Gardner, K.H. and L.E. Kay, *The use of H-2, C-13, N-15 multidimensional NMR to study the structure and dynamics of proteins*. Annual Review of Biophysics and Biomolecular Structure, 1998. **27**: p. 357-406.
211. Hologne, M., Chevelkov,V., and Reif, B., *Deuterated peptides and proteins in MAS solid-state NMR*. Progress in Nuclear Magnetic Resonance Spectroscopy, 2006. **48**(4): p. 211-232.
212. Grzesiek, S., and Bax, A., *An efficient experiment for sequential backbone assignment of medium-sized isotopically enriched proteins*. Journal of Magnetic Resonance, 1992. **99**: p. 201-207.
213. Grage, S.L., and Watts, A., *Applications of REDOR for distance measurements in biological solids*. Annual Reports in NMR, 2007. **60**: p. 192-228.
214. Paulson, E.K., Morcombe, C. R., Gaponenko, V., Dancheck, B., Byrd, R. A., and Zilm, K. W., *Sensitive high resolution inverse detection NMR spectroscopy of proteins in the solid state*. Journal of the American Chemical Society, 2003. **125**(51): p. 15831-15836.
215. Morcombe, C.R., Gaponenko,V., Byrd, A., and Zilm, K.W., *13 C CPMAS spectroscopy of deuterated proteins: CP dynamics, line shapes, and T1 relaxation*. JACS, 2005. **127**: p. 397-404.

216. Bockmann, A., Juy, M., Bettler, E., Emsley, L., Galinier, A., Penin, F. and Lesage, A., *Water-protein hydrogen exchange in the micro-crystalline protein Crh as observed by solid state NMR spectroscopy*. Journal of Biomolecular NMR, 2005. **32**: p. 195-207.
217. Agarwal, V., Diehl, A., Skrynnikov, N., and Reif, B., *High resolution H-1 detected H-1,C-13 correlation spectra in MAS solid-state NMR using deuterated proteins with selective H-1,H-2 isotopic labeling of methyl groups*. Journal of The American Chemical Society, 2006. **128**(39): p. 12620-12621.
218. Lesage, A., and Bockmann, A., *Water-protein interactions in microcrystalline crh measured by ^{1}H-^{13}C solid-state NMR spectroscopy*. Journal of American Chemical Society, 2003. **125**(44): p. 13336-13337.
219. Schubert, M., Kolbe, M., Kessler, Osterhelt, D and Schmieder P., *Heteronuclear multidimensional NMR spectroscopy of solubilized membrane proteins: resonance assignment of native bacteriorhodopsin*. Chembiochem 2002. **3**(10): p. 1019-23.
220. Wagner, G., and Wutrich, K, *Sequential resonance assignments in protein 1H nuclear magnetic resonance spectra. Basic pancreatic trypsin inhibitor*. Journal of Mol Biol, 1982. **155**: p. 347-366.
221. Clore, G.M., and Gronenborn, A.M., *Applications of 3-dimensional and 4-dimensional heteronuclear NMR-spectroscopy to protein-structure determination*. Prog Nucl Magn Reson Spectrosc, 1991. **23**: p. 43-92.
222. Bax, A., *Multidimensional nuclear-magnetic-resonance methods for protein studies*. Current Opinion in Structural Biology, 1994. **4**: p. 738-744.
223. Ernst, R.R., Bodenhausen, G., and Wokaun, A., *Principles of nuclear magnetic resonance in one and two dimensions*. 2002, Oxford: Clarendon Press.
224. Wüthrich, K., *NMR of Proteins and Nucleic Acids*. 1986, New York: Wiley.
225. Sun, B.-Q., Costa, P. R., Kocisko, D., Lansbury Jr., P.T., and Griffin, R. G., *Internuclear distance measurements in solid state nuclear magnetic resonance: Dipolar recoupling via rotor synchronized spin locking*. Journal of Chemical Physics, 1995. **102**(2): p. 702-707.
226. Gregory, D.M., Mitchell, D.J., Stringer, J.A., Kihne, S., Shiels, J.C., Callahan, J., Mehta, M.A., and Drobny, G. P, *Windowless dipolar recoupling the detection of weak dipolar couplings between spin 1/2 nuclei with large chemical shift anisotropies*. Chemical Physics Letters, 1995. **246**: p. 654-663.
227. Lee, Y.K., Kurur, N.D., Helmele, M., Johannessen, O.G., Nielesen, N.C., and Levitt, M.H., *Efficient dipolar recoupling in the nmr rotating solids- a sevenfold symmetrical radiofrequency pulse sequence* Chem. Phys. Letters, 1995. **242**: p. 304-309.
228. Baldus, M., Petkova, A.T., Herzfeld, J., and Griffin R.G., *Cross polarisation in the tilted frame:assignment and spectral simplification in heteronuclear spin*. Molecular Physics, 1998. **95**(6): p. 1197-1207.
229. Takegoshi, K., Nakamura,S., and Terao, T., *C-13-H-1 dipolar-assisted rotational resonance in magic-angle spinning NMR*. Chemical Physics Letters, 2001. **344**(5-6): p. 631-637.
230. Schaefer, J., McKay, R.A., and Stejskal, E.O., *Double-cross-polarization NMR of solids*. Journal of Magnetic Resonance (1969), 1979. **34**(2): p. 443.
231. Crocker, E., Patel, A.B., Eilers, M., Jayaraman, S., Getmanova, E., Reeves, P. J., Ziliox, M., Khorana, H.G., Sheves, M. and Smith, S.O., *Dipolar assisted rotational resonance NMR of tryptophan and tyrosine in rhodopsin*. Journal of Biomolecular NMR, 2004. **29**: p. 11-20.

232. Igumenova, T., Wand, J.A., and A. McDermott, *Assignment of the backbone resonances for microcrystalline ubiquitin.* Journal of American Chemical Society, 2004. **126**(16): p. 5323-5331.
233. Sumper, M., Reitmeier, H., and Oesterhelt, D., *Biosynthesis of the purple membrane of halobacteria.* Angewandte Chemie-England Edition, 1976. **15**: p. 187-194.
234. Oesterhelt, D., and Stoeckenius, W., *Rhodopsin-like protein from the purple membrane of Halobacterium halobium.* Nature, 1971. **233**(39): p. 149-152.
235. Grzesiek, S., Anglister, J., Ren, H. and Bax, A., *13C narrowing by 2H decoupling in 2H/13C/15N-enriched proteins. Application to triple resonance 4D J connectivity of sequential amides.* Journal of American Chemical Society, 1993. **115**: p. 4369-4370.
236. Stoeckenius, W., Lozier, R.H., and Bogomolni, R.A., *Bacteriorhodopsin and the purple membrane of halobacteria.* Biochem. Biophys. Acta, 1979. **505**: p. 215-278.
237. Shand, R.F., and Betlach, M.C., *Expression of the bop gene cluster of* Halobacterium halobium *is induced by low oxygen tension and by light.* Journal of Bacteriology, 1991. **173**(15): p. 4692-4699.
238. Takegoshi, K., T. Imaizumi, and T. Terao, *One- and two-dimensional C-13-H-1/N-15-H-1 dipolar correlation experiments under fast magic-angle spinning for determining the peptide dihedral angle phi.* Solid State Nuclear Magnetic Resonance, 2000. **16**(4): p. 271-278.
239. Morcombe, C.R., and Zilm, K. W., *Chemical shift referencing in MAS solid state NMR.* Journal Of Magnetic Resonance, 2003. **162**(2): p. 479-486.
240. Delaglio, F., Grzesiek, S.., Vuister, G. W.., Zhu, G., Pfeifer, J., and Bax, A., *NMRpipe - a multidimensional spectral processing system based on Unix pipes.* Journal of Biomolecular NMR, 1995. **6**(3): p. 277-293.
241. Goddard, D.T., and Kneller, D. G., *Sparky 3.*, in *University of California.* 2002: San Francisco.
242. Saito, H., *Dynamic pictures of membrane proteins in two-dimensional crystal, lipid bilayer and detergent as revealed by site-directed solid-state 13C NMR.* Chemistry and Physics of Lipids, 2004. **132**(1): p. 101-112.
243. Ernst, T.N., Herzfeld, J., and Rothschild, K. J., *Polarised Fourier transform infrared spectroscopy of bacteriorhodopsin.* Biophysical Journal, 1990. **58**: p. 1539-1546.
244. Wisconsin, U., *http://www.bmrb.wisc.edu*, in *Biological Magnetic Resonance Data Bank.*
245. Wishart, D.S., and Sykes, B. D., *Chemical-shifts as a tool for structure determination*, in *Nuclear Magnetic Resonance, Pt C.* 1994, Academic Press Inc: San Diego. p. 363-392.
246. Wishart, D.S., Bigam, C.G., Yao, J., Abildgaard, F., Dyson, H.J., Oldfield, E., Markley, J.L., and Sykes, B. D., *H-1, C-13 and N-15 chemical-shift referencing in biomolecular NMR.* Journal of Biomolecular NMR, 1995. **6**(2): p. 135-140.
247. Etzkorn, M., Martell, S., Andronesi, O.C., Seidel, K., Engelhard, M., and Baldus, M., *Secondary structure, dynamics, and topology of a seven-helix receptor in native membranes, studied by solid-state NMR spectroscopy.* Angewandte Chemie International Edition, 2007. **46**(3): p. 459-462.
248. Jehle, S., Hiller, M., Rehbein, K., Diehl, A., Oschkinat, H., and van Rossum, B. J., *Spectral editing: selection of methyl groups in multidimensional solid-state magic-angle spinning NMR.* Journal of Biomolecular NMR, 2006. **36**(3): p. 169-177.
249. Igumenova, T.I., and A.E. McDermott, *Homo-nuclear 13C J-decoupling in uniformly 13C-enriched solid proteins.* Journal of Magnetic Resonance, 2005. **175**(1): p. 11.